198048

NHTSA-98-3588-190

# Project B.14 – Demonstration of Enhanced Fire Safety Technology – Fire Retardant Materials

## Part 1: Full Scale Vehicle Fire Tests of a Control Vehicle and a Test Vehicle Containing an HVAC Module Made from Polymers Containing Flame Retardant Chemicals

**Jeffrey Santrock**
**General Motors Corporation**

Abstract

The tests described in this report were conducted by General Motors (GM) pursuant to an agreement between GM and the U.S. Department of Transportation. The purpose of these tests was to evaluate the effects of substituting plastic resins containing flame retardant chemicals in the HVAC module on elements of fire behavior during tests in which a fire was ignited in the engine compartments of the test vehicles. Two vehicles were used in these tests. The test vehicles were 1999 Chevrolet Camaros. A control vehicle was tested as received without modifications other than those required for these tests which are described in this report. An experimental vehicle contained an HVAC module made from plastics that contained flame retardant chemicals. The Control and Experimental vehicles were crash tested using identical crash test protocols. The crash tested vehicles were then used in fire tests using identical fire test protocols. Substitution of plastic materials containing flame retardant chemicals in the HVAC module did not affect the rate of flame-spread from the engine compartment into the passenger compartment during these tests. The peak carbon monoxide concentration in the experimental vehicle was approximately 27X the peak carbon monoxide concentration in the control vehicle.

***Table of Contents***

## Appendicies

## List of Figures

**Report**

## List of Figures

### Appendicies

## List of Tables

**Report**

## 1 Introduction

The tests described in this report were conducted by General Motors (GM) pursuant to an agreement between GM and the U.S. Department of Transportation. The purpose of these tests was to evaluate the effects of substituting plastic resins containing flame retardant chemicals in the HVAC module on elements of fire behavior during tests in which a fire was ignited in the engine compartments of the test vehicles. Two vehicles were used in these tests. The test vehicles were 1999 Chevrolet Camaros with 3.8 liter sequential fuel injection V6 engines and automatic transmissions with overdrive. One of the vehicles was designated Control and the other vehicle was designated FR. The Control vehicle was tested as received without modifications other than those required for these tests which are described in this report. The HVAC module in the FR vehicle was removed and replaced with an HVAC module in which the poly(propylene) and polyester components in the HVAC assembly contained flame retardant chemicals. The Control and FR vehicles were crash tested using identical crash test protocols. The test protocols used in the crash tests described in this report were similar to crash test protocols described in an earlier report [1]. Test instrumentation was installed in the crash tested vehicles for the fire tests, and the instrumented, crash tested vehicles were then used in fire tests. The test protocol and the method of ignition were the same in both tests. Data from the fire tests of the Control and FR vehicles were analyzed to determine the effect of flame retardant chemicals in the HVAC module on flame-spread into the passenger compartment, heat transfer into the passenger compartment, and combustion byproduct concentrations in the passenger compartment.

## 2 HVAC Modules

The HVAC module used in the control vehicle was assembled from service parts components purchased from a Chevrolet dealership. None of the materials in the Control HVAC module used in these test contained active flame retardant chemicals. Poly(propylene) and polyester parts in the FR HVAC module used in these tests contained flame retardant chemicals. Table 1 lists the base polymers of components in the FR HVAC assembly that contained flame retardant chemicals. These components included the Air Inlet and Outlet Housing, Auxiliary A/C Evaporator and Blower Upper Case, Auxiliary A/C Evaporator and Blower Lower Cases, Heater Front Case, Heater Rear Case, Heater Case, Air Distribution Case, A/C Evaporator Core, Heater Core, Mode Valve, and Blower Motor.

The Air Inlet and Outlet Housing, Auxiliary A/C Evaporator and Blower Upper Case, Heater Front Case, Heater Rear Case, Heater Case, and Air Distribution Case were molded from RTP 156

(RTP Company, Winona, Minnesota) by Delphi Harrison Thermal Systems (Lockport, New York). Auxiliary A/C Evaporator and Blower Lower Cases containing flame retardant chemicals were obtained from Caine Engineering Group (Hebron, Ohio).

**Table 1**
**Base Polymer in HVAC Parts**

| Component | Material |
|---|---|
| Air Inlet and Outlet Housing | Poly(Propylene) |
| Auxiliary A/C Evaporator and Blower Upper Case | Poly(Propylene) |
| Auxiliary A/C Evaporator and Blower Lower Case | Polyester |
| Heater Front Case | Poly(Propylene) |
| Heater Rear Case | Poly(Propylene) |
| Heater Case | Poly(Propylene) |
| Air Distribution Case | Poly(Propylene) |

Table 2 summarizes the chemical additives in the poly(propylene) and polyester in the control and two FR HVAC modules used in these tests. The inert fillers [$Ca(CO_3)$ in the polypropylene components, and glass fiber and clay in the polyester component] reduced the combustible content of the finished polymer, and thus reduced the heat output per gram of material burned when compared to the pure base polymer.

**Table 2**
**Additives in the Poly(propylene) and Poly(ester) Parts in the Control and FR HVAC Modules**

| | Poly(Propylene)[1] | Polyester |
|---|---|---|
| **Control** | $Ca(CO_3)$ | glass fiber<br>clay<br>cissel |
| **FR** | decabromodiphenyleneoxide<br>$SbO_3$<br>Zn-compounds | glass fiber<br>$SbO_3$<br>$Al_2O_3 \bullet (SiO_2)$ |

[1]The resin used to make poly(propylene) parts in the HVAC module used in the FR vehicle had a V-0 rating in UL-94 [2].

Thermocouples were installed in the HVAC modules of the Control and FR vehicles before the crash tests. The instrument panels and HVAC modules were removed from the Control and FR vehicles. Thermocouples were installed in identical locations in the Control and FR HVAC modules (see **Appendix H**). These HVAC modules and instrument panels were reinstalled in the test vehicles.

## 3 Crash Tests

The Control and FR vehicles were crash tested using identical frontal impact, vehicle-into-pole crash test protocols. The crash test of the Control Vehicle was C12730 and occurred on October 27, 1999. The crash test of the FR Vehicle was C12731 and occurred on October 13, 1999. A schematic representation of the crash test protocol used in these tests is shown in Figure 1.

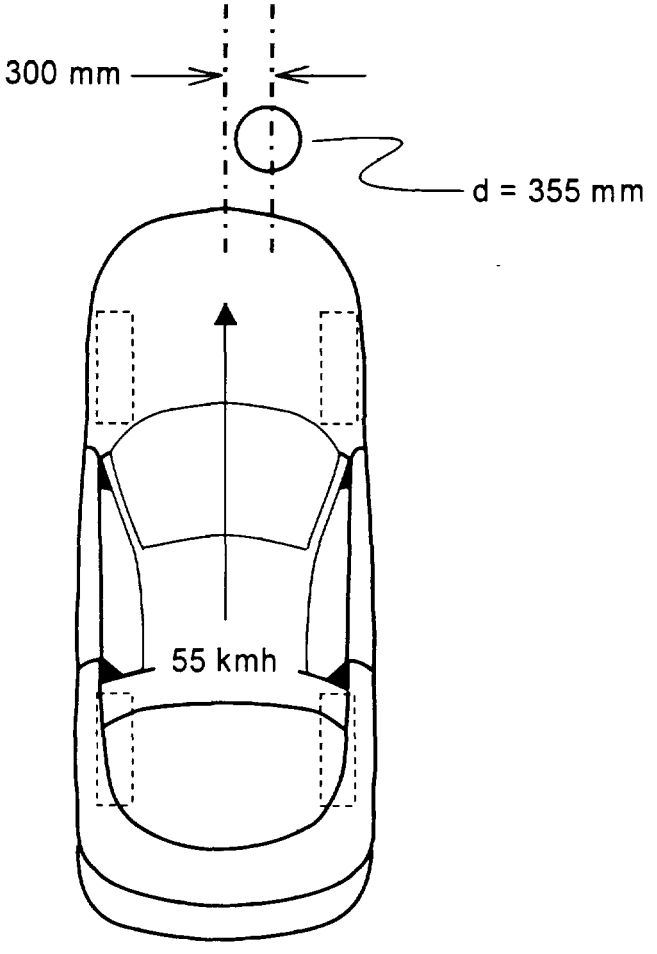


Figure 1. Schematic representation of crash test protocol used in these tests.

The test vehicles were towed into a steel pole (diameter = 355 mm). The lateral offset between the vehicle longitudinal centerline and the pole center was 300 mm, with the point of impact to the right of the vehicle centerline. Vehicle speed at impact was approximately 55 kmh (34.3 mph). Vehicle mass as tested was 1848 kg. Each test vehicle contained two 50$^{th}$ percentile adult male anthropomorphic body forms in the front outboard seating positions for ballast. The mass of each ATD was 75.7 kg. The anthropomorphic body forms were belted and the supplemental restraint systems in each vehicle were active and deployed during both tests. No data was recorded from the anthropomorphic body forms during these tests.

The test vehicles contained the factory fills of motor oil (4.3 L), transmission fluid (4.7 L), engine coolant (10.8 L), brake fluid (0.78 L), power steering fluid (0.72 L), and windshield washer fluid. The fuel tanks in each of the test vehicle contained 60.4 L of Stoddard solvent. Gasoline for the engines was supplied from a secondary fuel tank with a capacity of 8 L mounted in the rear compartment area for these tests. The secondary fuel tank was fitted with a new service parts fuel pump for a 1999 Chevrolet Camaro. The wiring harness and fuel lines were connected to the fuel pump in the secondary fuel tank.

The engines in the Control and FR Vehicles were run for approximately 3 and 1 hours, respectively, before impact, and were running at the time of impact. A static (vehicle stationary) engine warm-up procedure was used to achieve underhood temperatures greater than ambient in the test vehicles for these crash tests (Table 3).

### 3.1 Crash Test Data

Data recorded from accelerometers located on the rocker panels is in **Appendix A**. Data recorded from the flammable vapor sensors is in **Appendix B**. Data from analysis of gas samples from the engine compartment is in **Appendix C**. Data recorded from the thermocouples on the exhaust system is in **Appendix D**. Data recorded from the throttle position sensor and engine speed sensor are in **Appendix E**. Sensing and diagnostic module event data recorder data is in **Appendix F**.

Figures 2 and 3 show photographs of the Control and FR vehicles before and after the crash test, respectively. Table 4 summarizes the vehicle mass, vehicle speed at impact, engine speed at impact, location of impact, average change in velocity, and maximum dynamic crush for the Control and FR Vehicles as tested. The velocities at impact differed by < 0.1 kmh (< 0.2%). The masses of the two test vehicles were identical (1848.0 kg). The impact locations were identical

(300 mm right of center). The average change in velocity was 60.5 kmh for the control vehicle and 63.1 kmh for the FR vehicle, a difference of 4.3%. The maximum dynamic crush was 1309 mm at 128 milliseconds in the control vehicle and 1224 mm at 119 milliseconds in the FR vehicle, a difference of 6.5%. Although the average change in velocity of the FR vehicle was 4.3% greater than that of the control vehicle, the maximum dynamic crush of the FR vehicle was 6.5% less than that of the control vehicle. Delta-V or average change in velocity is often regarded as the most important measured variable used to characterize crash severity in real world or crash test settings. One might, therefore, expect more damage (e.g., as measured by dynamic crush)

**Table 3**
**Pre-Impact Vehicle Warm-Up Timing for the Control and FR Vehicles**

| | Time (hr:min:sec) | |
|---|---|---|
| | **Control** | **FR** |
| **Start Engine** | 00:00:00 | 00:00:00 |
| **Increase Engine Idle Speed to 1,800 rpm** | 00:00:30 | 00:01:00 |
| **Turn on Radio / Heater / High Fan / High Beam Head Lamps** | 00:10:18 [1] | 00:01:00 |
| **Start Background Vapor Sampling** | 00:09:28 | 00:02:00 |
| **End Background Vapor Sampling** | 00:19:34 | 00:13:00 |
| **Scan Pre-Crash ECM and EDR Data** | 2:45:00 [2] | 00:12:00 |
| **Power-Down Vapor Sensors / shut Engine** | 00:44:00 | 00:40:00 |
| **Begin Instrumentation Calibration** | 00:45:00 | 00:41:00 |
| **Instrumentation Calibration Complete** | 00:45:30 | 00:51:00 |
| **Restart Engine** | 00:46:00 | 00:52:00 |
| **Increase Engine Idle Speed to 1,800 rpm** | 00:46:00 (02:40:00 [2]) | 00:52:00 |
| **Power-Up Vapor Sensors** | 00:47:30 | 00:52:00 |
| **Impact** | 03:09:15 [2] | 01:03:00 |

[1] This step was delayed approximately 10 minutes because of an intermittent fault in the instrument panel ground circuit, which was diagnosed and corrected at this time.

[2] This step was delayed between 2 and 2 ½ hours because of a delay at the crash test facility unrelated to this test. For the control vehicle, the engine idle speed was set to 1,800 rpm when engine was restarted after instrumentation calibration and adjusted to 1,800 rpm after drifting to 1,500 rpm during the delay.

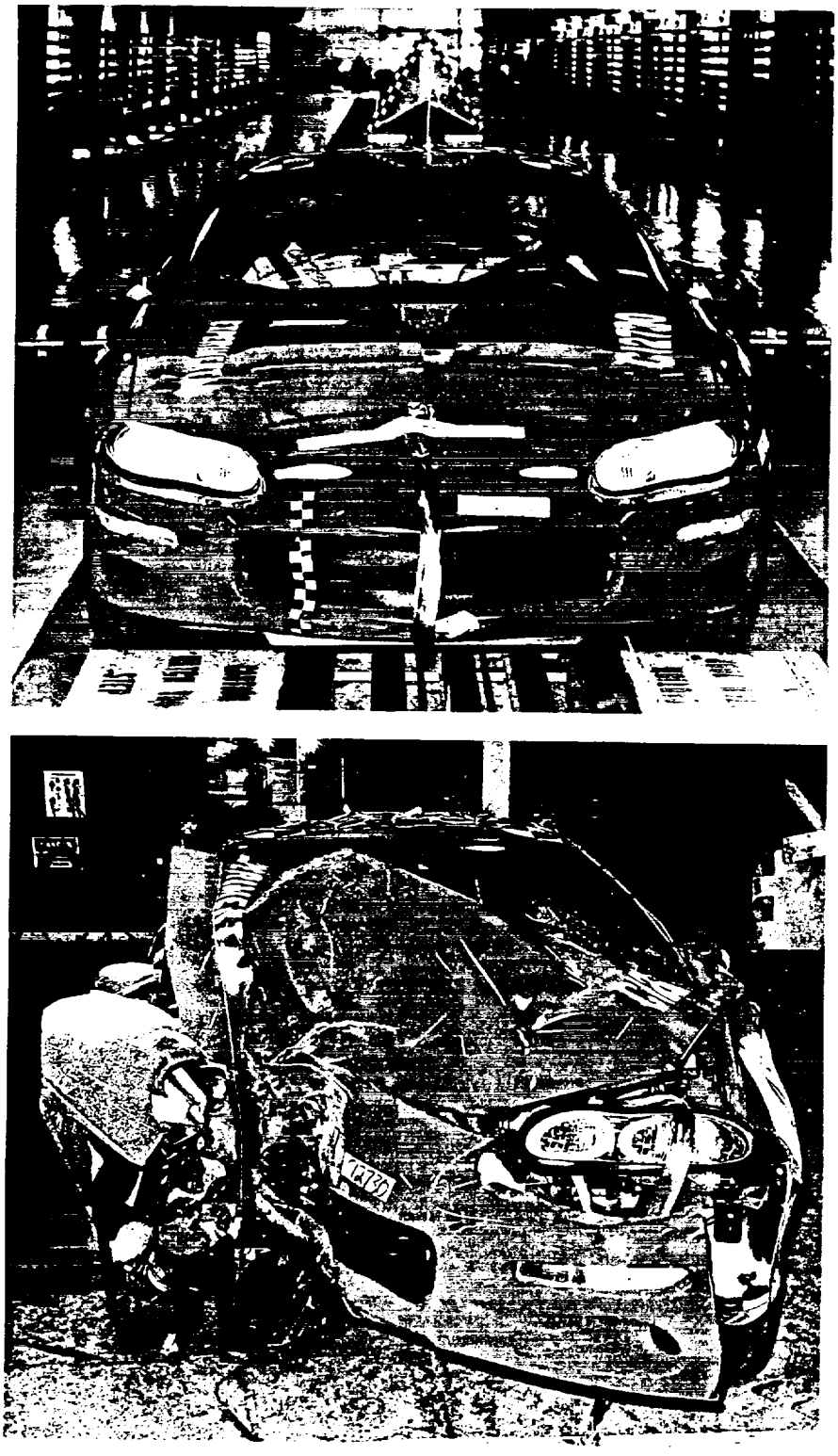

Figure 2. Crash Test C12730. Photographs of the Control Vehicle before (upper) and after (lower) the crash test.

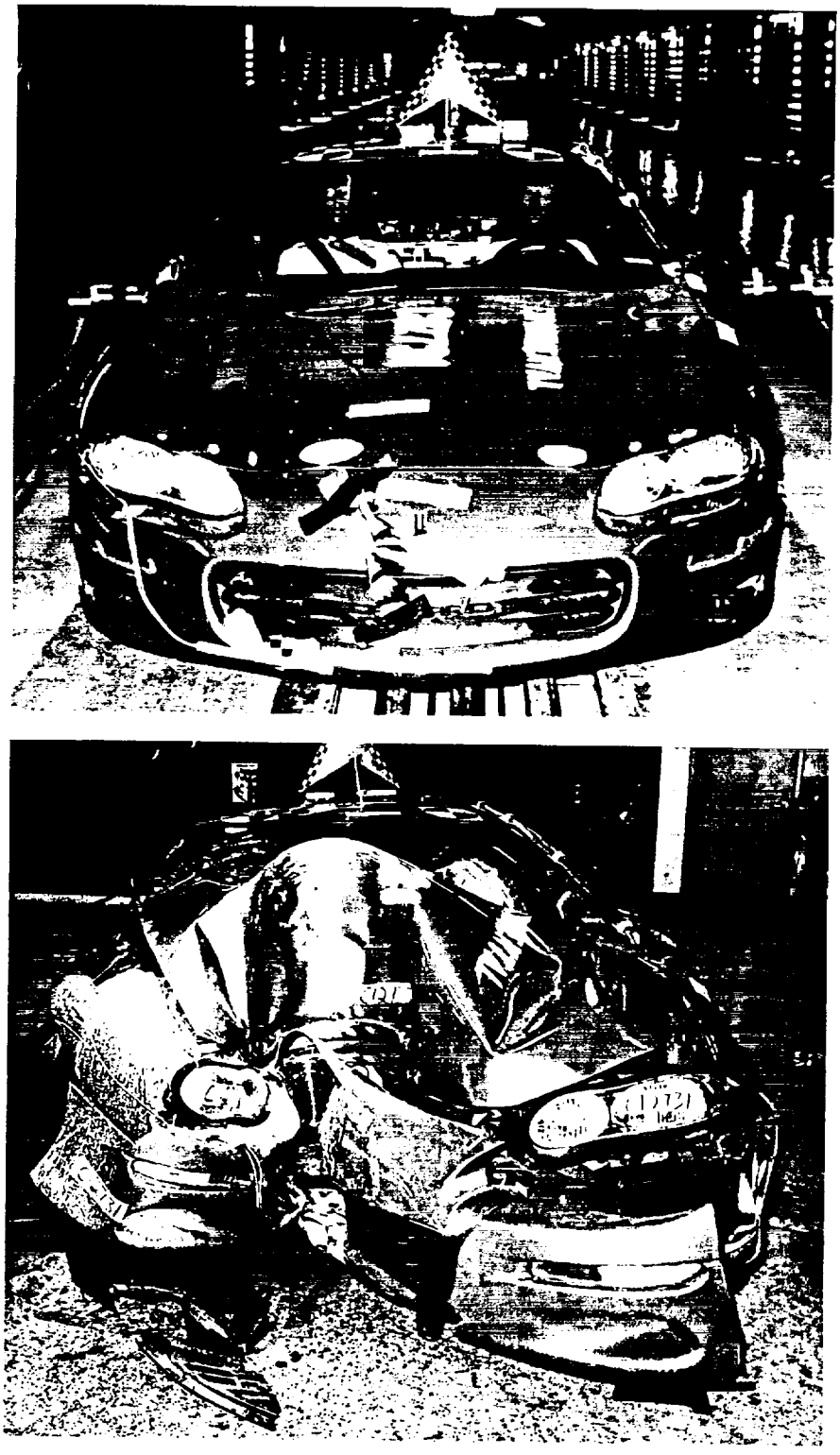

Figure 3. Crash Test C12731. Photographs of the FR Vehicle before (upper) and after (lower) the crash test.

in the vehicle with the higher measured Delta-V, other things being equal. These data underscore the possible variability associated with crash tests performed under tightly controlled conditions, with essentially identical vehicles.

**Table 4**

**Summary of Vehicle Mass, Vehicle Speed at Impact, Engine Speed at Impact, Location of Impact, Average Change in Velocity, and Maximum Dynamic Crush for the Control and FR Vehicles**

| | Control | FR |
|---|---|---|
| **Vehicle Test Mass - Front** | 934.0 kg | 932.0 kg |
| **Vehicle Test Mass – Rear** | 914.0 kg | 916.0 kg |
| **Vehicle Test Mass – Total** | 1848.0 kg | 1848.0 kg |
| **Throttle Position at Impact[1]** | 7% | 7% |
| **Engine Speed at Impact[2]** | 2,160 ± 120 rpm | 1,920 ± 120 rpm |
| **Vehicle Speed at Impact[3]** | 55.1 kmh | 55.0 kmh |
| **Location of Impact** | 300 mm Rt. of Center | 300 mm Rt . of Center |
| **Average Change in Velocity[4]** | 60.5 kmh | 63.1 kmh |
| **Maximum Dynamic Crush[5]** | 1309 mm @ 129 ms | 1224 mm @ 119 ms |

[1] Throttle Position at Impact was percentage of full throttle determined from the average throttle position sensor output during the 1-second period prior to time zero (Plots E1 and E2, Appendix E) and the nominal electronic throttle calibration for the engine type in the test vehicles.

[2] Engine Speed at Impact was determined from the camshaft position sensor timing pulse rate for the 1-second period prior to time zero (Plots E3 and E4, Appendix E). The uncertainty in these values represents an uncertainty of ± 1 timing pulse in a one-second interval.

[3] Vehicle Speed at Impact was determined by the radar speed measurement at time zero.

[4] Average Change in Velocity was determined from the difference between the maximum and minimum average velocities in the direction of the X-axis calculated from the accelerometers on the left and right rear rockers (Plots A25 and A26, Appendix A).

[5] Maximum Dynamic Crush was determined the average maximum displacement in the direction of the X-axis calculated from the accelerometers on the left and right rear rockers (Plots A25 and A26, Appendix A).

### 3.2 Sensing and Diagnostic Module Event Data Recorder Data

The Sensing and Diagnostic Modules (SDM) of the Supplemental Inflatable Restraint (SIR) systems were removed from the test vehicles. Data stored in the SDM's removed from the test vehicles after these crash tests was downloaded and translated using a Vetronix Crash Data Retrieval system tool (Software version 1.3241, Vetronix, Santa Barbara, CA). Table 5 shows comparisons of throttle position, engine speed, vehicle speed at 1-second intervals for 5 seconds prior to impact, brake switch circuit status, and driver's seatbelt switch circuit status determined from the crash test data and from the SDM data.

**Table 5**
**Comparison of Crash Test Data to SDM Data**

| | C12730 | | C12731 | |
|---|---|---|---|---|
| | **Crash Test** | **SDM** | **Crash Test** | **SDM** |
| **Throttle Position** | 7% | 5%[1] | 7% | 6%[1] |
| **Engine Speed** | 2,160 ± 120 rpm | 2,112 rpm[1] | 1,920 ± 120 rpm | 1,792 rpm[1] |
| **Vehicle Speed** | | | | |
| **- 5 seconds** | --- | 43.5 kmh | --- | 43.5 kmh |
| **- 4 seconds** | --- | 48.3 kmh | --- | 48.3 kmh |
| **- 3 seconds** | --- | 53.1 kmh | --- | 53.1 kmh |
| **- 2 seconds** | --- | 53.1 kmh | --- | 53.1 kmh |
| **- 1 seconds** | --- | 53.1 kmh | --- | 54.7 kmh |
| **0 seconds** | 55.1 kmh | --- | 55.0 kmh | --- |
| **Brake Switch** | no braking | 0%[1] | no braking | 0%[1] |
| **Seat Belt** | buckled | unbuckled[1] | buckled | unbuckled[2] |

[1]Throttle position, engine speed, brake switch circuit status, and driver's seat belt switch circuit status were written to the crash record in the SDM starting a minimum of 100 milliseconds after impact.

The Vetronix SDM Crash Data Retrieval report indicated throttle positions of 5% in C12730 and 6% in C12731 (**Appendix F**). Throttle positions of 7% were calculated from the average voltages recorded from the throttle positions sensors for the 1 second interval before impact in both tests (**Appendix E**)

The Vetronix SDM Crash Data Retrieval report indicated engine speeds of 2,112 rpm in C12730 and 1,792 rpm in C12731 (**Appendix F**). Engine speeds determined from the number of pulses in the camshaft position sensor timing output in the 1 second interval prior to impact were 2,160 ± 120 rpm in C12730 and 1,920 ± 120 rpm in C12731 (**Appendix E**).

The Vetronix SDM Crash Data Retrieval report indicated vehicle speeds increased during the 5 seconds prior to impact in both crash tests (**Appendix F**), showing final vehicle speeds of 53.1 kmh in C12730 and 54.7 kmh in C12731. Vehicle speeds at impact determined from the radar speed measurement at the crash test facility were 55.1 kmh in C12730 and 55.0 kmh in C12731 (Appendix E).

The Vetronix SDM Crash Data Retrieval report indicated brake switch status as OFF (0%) in both tests (**Appendix F**). The brake pedals in both test vehicles were not depressed in either test.

The Vetronix SDM Crash Data Retrieval report indicated unbuckled for the driver's seat belt switch circuit status in both crash tests. The driver's seat belts were buckled in both crash tests. The discrepancy between the actual driver's seat buckle status during these tests and the driver's seat belt switch circuit status recorded by the SDM was caused by loss of vehicle electrical power during impact in both tests. The drivers seat belt switch circuit status recorded in the SDM's indicated unbuckled in both test vehicles. The SDM modules in the test vehicles (Model SDM-G, software version SDG99FXZ04) record a driver's status from the normally closed switch input to the SDM. A voltage input of less than 3.72 V indicates that the switch is closed and the seat belt latch plate has not been inserted into the buckle (interpreted as unbelted by the SDM-G). A voltage input of greater than 3.9 V indicates that the switch is open and the seat belt latch plate has been inserted into the buckle (interpreted as belted by the SDM-G).

In both test vehicles, penetration of the pole into the right side of the engine compartments of the test vehicles crushed the batteries, which were in the right front corners of the engine compartment, and resulted in loss of vehicle electrical system power at approximately 40 milliseconds post-impact. (The white powder on the right fenders in the lower photographs in Fig.'s 2 and 3 is baking soda used to neutralize acid expelled from the batteries during these crash tests). In the SDM-G's in the test vehicles, the crash record is stored in the Electrically

Erasable Programmable Read Only Memory (EEPROM). During a crash event, data from Random Access Memory (RAM) is written to the crash record in EEPROM after the sensing algorithm in the SDM-G, which occurs after both of the following conditions are satisfied: 10 to 15 Delta V samples are collected and the acceleration falls below a preset value for a preset number of samples (typically 5 to 10 milliseconds). The SDM's in the test vehicles (SDM-G, software version SDG99FXZ04) writes the crash record to EEPROM at the rate of 1 byte every 10 milliseconds, and driver's seat belt switch circuit status is the 20$^{th}$ byte written to EEPROM. Therefore, driver's seat belt circuit switch circuit status is written to EEPROM a minimum of 300 milliseconds after the algorithm enabled (100 to 150 milliseconds to write Delta V samples + 200 milliseconds to write bytes 1 though 19 into the crash record). The data stored in RAM is updated if a change in driver's seat belt switch circuit status occurs during the interval from algorithm enable to the time driver's seat belt switch circuit status in written from RAM to EEPROM. In both crash tests, the voltage input from the seat belt switch circuit to the SDM became zero (less than 3.72 V) after the loss of vehicle electrical system power at approximately 40 milliseconds, causing the driver's seat belt switch circuit status stored in RAM to change from buckled to unbuckled at least 260 milliseconds before the driver's seat belt switch circuit status was written from RAM to the crash record in the EEPROM.

Figures 4 and 5 show plots of longitudinal velocity calculated from the average filtered longitudinal acceleration data recorded from the accelerometers on the left and right rear rockers of the test vehicles during C12730 and C12731, respectively. Post-impact velocity for each test vehicle was calculated from data down-loaded from the SDM's and also plotted on these figures. The error bars on the SDM velocity data represent 10% relative uncertainty in the recorded change in velocity, which has been determined to be the maximum potential error in this data [2]. These data show that the true change in velocity for the vehicle may be higher than that recorded by the SDM if the duration of the crash is longer than the time the SDM records post-impact velocity data.

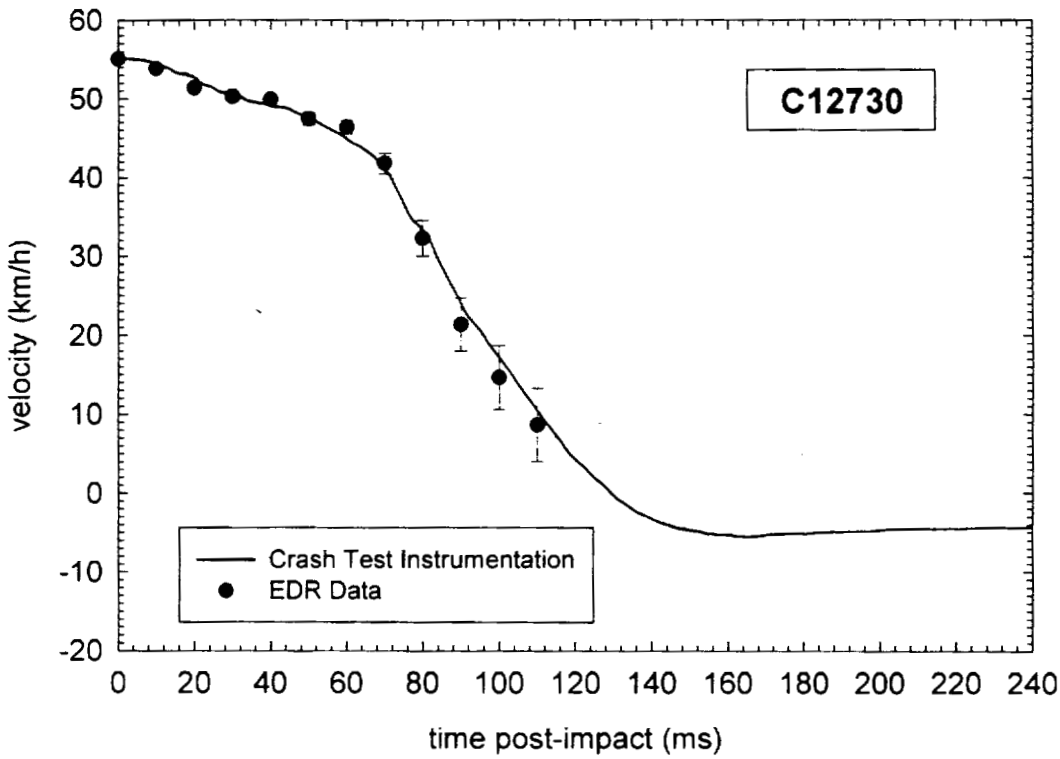


Figure 4. Crash Test 12730. Longitudinal velocity calculated from the average longitudinal acceleration data recorded from the accelerometers on the left and right rear rockers and velocity data down-loaded from the SDM in the test vehicle. The error bars on the SDM data indicate 10% relative uncertainty [3].

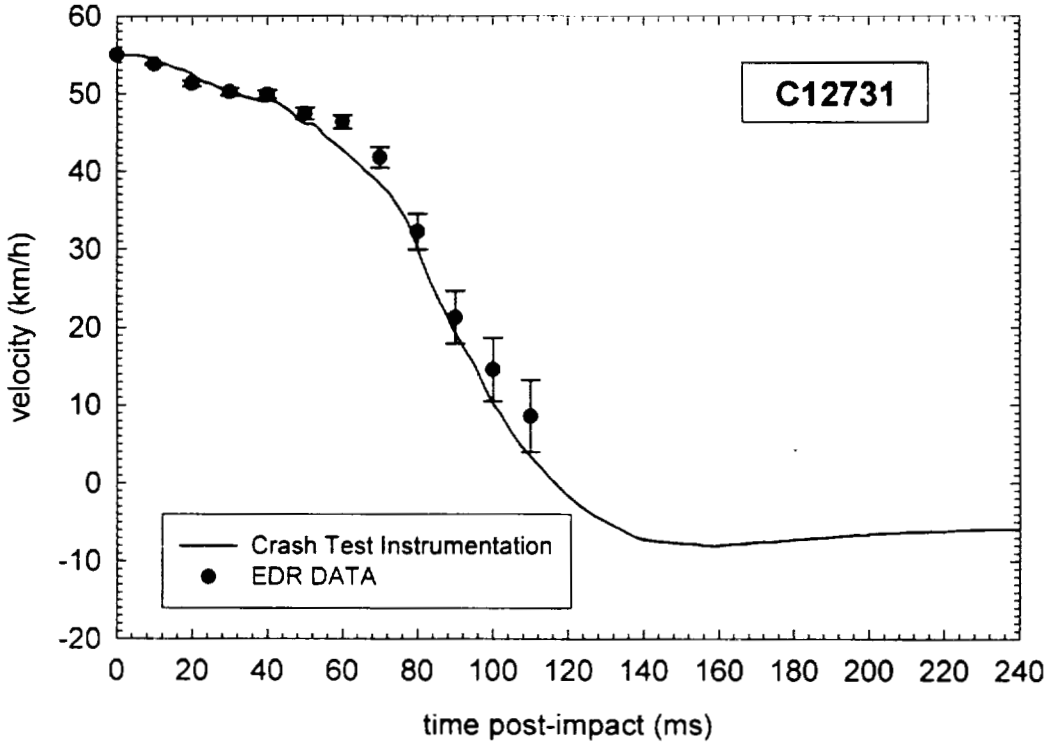


Figure 5. Crash Test 12731. Longitudinal velocity calculated from the average longitudinal acceleration data recorded from the accelerometers on the left and right rear rockers and velocity data down-loaded from the SDM in the test vehicle. The error bars on the SDM data indicate 10% relative uncertainty [3].

# 4 Fire Tests

The fire test of the Control Vehicle (F99B1401) occurred on February 17, 2000. The fire test of the FR Vehicle (F99B1402) occurred on February 21, 2000. Both tests were conducted at the Factory Mutual Global Test Center in West Glocester, Rhode Island

## 4.1 Vehicle Condition and Test Protocol

The crash-tested vehicles were prepared for the fire tests at the General Motors Research and Development Center in Warren, Michigan, and shipped to the Factory Mutual Global Test Center in West Glocester, Rhode Island for these fire tests. The test vehicles were returned to the General Motors Research and Development Center after the fire tests, where they were systematically disassembled to permit closer inspection of the fire damage and identification of fire spread paths that were not obvious during the tests.

A description of the video cameras used in during these fire tests is in **Appendix G**. A description of the thermocouples installed in the test vehicles and data from these thermocouples are in **Appendix H**. A description of the aspirated thermocouples used in these tests and data from the aspirated thermocouples are in **Appendix I**. A description of the heat flux transducer/radiometer assemblies installed in the test vehicles and data from these devices are in **Appendix J**. Description of the pressure measurement equipment and analysis procedures, and data from these measurements are in **Appendix K**. A description of the Fire Products Collector (FPC) at the Factory Mutual Global Test Center and analysis procedures, and data from this device are in **Appendix L**. A description of the Fourier Transform Infrared Gas Analysis System used to measure gases in the passenger compartment during these tests and FTIR gas analysis results are in **Appendix M**.

The vehicle was placed in a rectangular steel pan (length = 25 ft., width = 15 ft., height = 4 in.) to prevent spilled and leaking automotive fluids from spreading in the test facility. This fluid containment pan was fabricated from two sheets of carbon steel. Angle-braces were welded to the under-side of the pan to keep it from flexing under the weight of the vehicle. The corners of the support frame rested on load cells. Mass loss was determined from data acquired from the load cells during the test.

A layer of fiberglass-reinforced cement construction board (DuraRock, USG Corporation) was placed on the bottom of the fluid containment pan. A thin layer of sand was used to level the concrete board so that the grade of the surface measured from the center to the edges along the major and minor axes was no greater than 1%. The joints between boards were sealed with latex caulking.

The test vehicles were placed in the center of the pan (Fig. 6). All doors were closed, and the door window glasses were raised to the fully closed position in each door. The glass outer-layers in the windshields of both the Control and FR Vehicles were broken in the crash tests. The windshields remained attached to the frames of the test vehicles, with the windshield inner-layer supporting the glass fragments. The right window glasses (passenger's door) in both the Control and FR Vehicles were broken during the crash tests, and were not replaced for the fire test.

Three signals were used to synchronize the videos and the data acquisition systems used in these tests: (1) the video lights were switched off and on before the test, (2) an air horn was sounded to signal electrical power to the igniter ON, and (3) the end of the test and start of fire suppression. The horn soundings were audible on the videos. For videos that did not record sound, the lights switching off and on was used for timing. One channel of the data acquisition system for vehicle instrumentation monitored a normally open switch, which was depressed at each sounding. The real-time clock in the FTIR data system was synchronized to the real-time clock in the vehicle instrumentation data system. The horn soundings are audible on the audio

### 4.2 Ignition

Electrical igniters similar to that shown in Figure 7 were installed in the air cleaner housings in the engine compartments of the test vehicles.[1] The electrical igniters consisted of nichrome heating wire wrapped around several pieces of poly(propylene) sheet. Electrical power was supplied to the igniters from a variable tap transformer with a maximum output of 120 VAC. These igniters produced approximately 1.2 kW of heat, estimated from the resistance of the heating wire and the applied voltage. Table A shows the timing of igniter electrical power on, ignition, and igniter electrical power off.

The exact time of ignition was determined from review of videos from Camera 4 for F99B1401 and Camera 8 for F99B1402, which show flames in the areas around the air cleaner housings in the engine compartments of the test vehicles (Fig. 8). During Fire Test F99B1402, the transformer malfunctioned and did not supply electrical power to the igniter for approximately the first 3 minutes of the test. The malfunction was repaired without restarting this test.

[1] The igniter was made by winding Nichrome wire (24 AWG, length = 350 cm, resistance ≅ 12 Ω) around four pieces of poly(propylene) sheet (0.1 x 10 x 15 cm, mass ≅ 110 g).

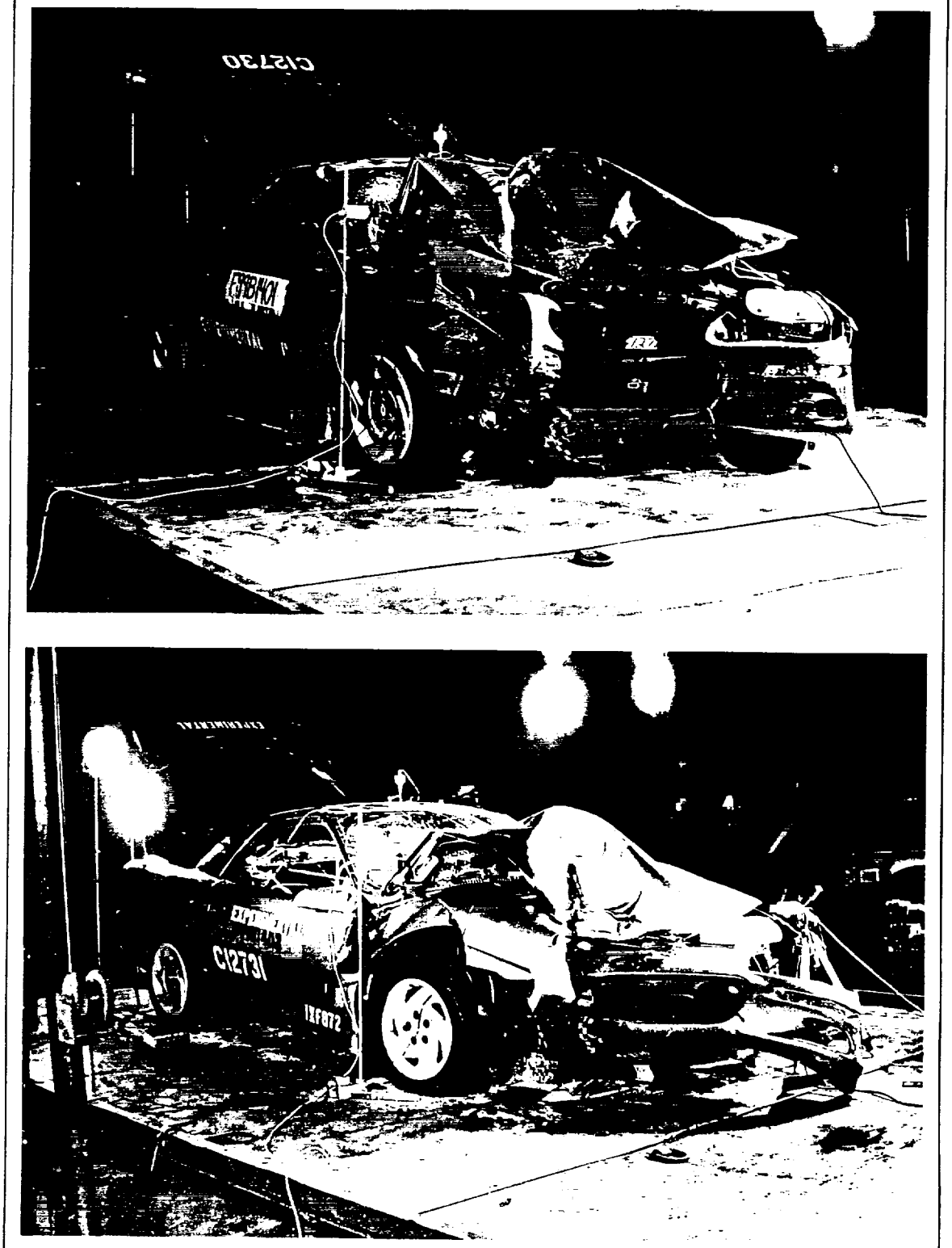

Figure 6. Photographs of the test vehicle in the fluid containment pan before the fire tests: Fire Test F99B1401 (upper photograph); and Fire Test F99B1402 (lower photograph).

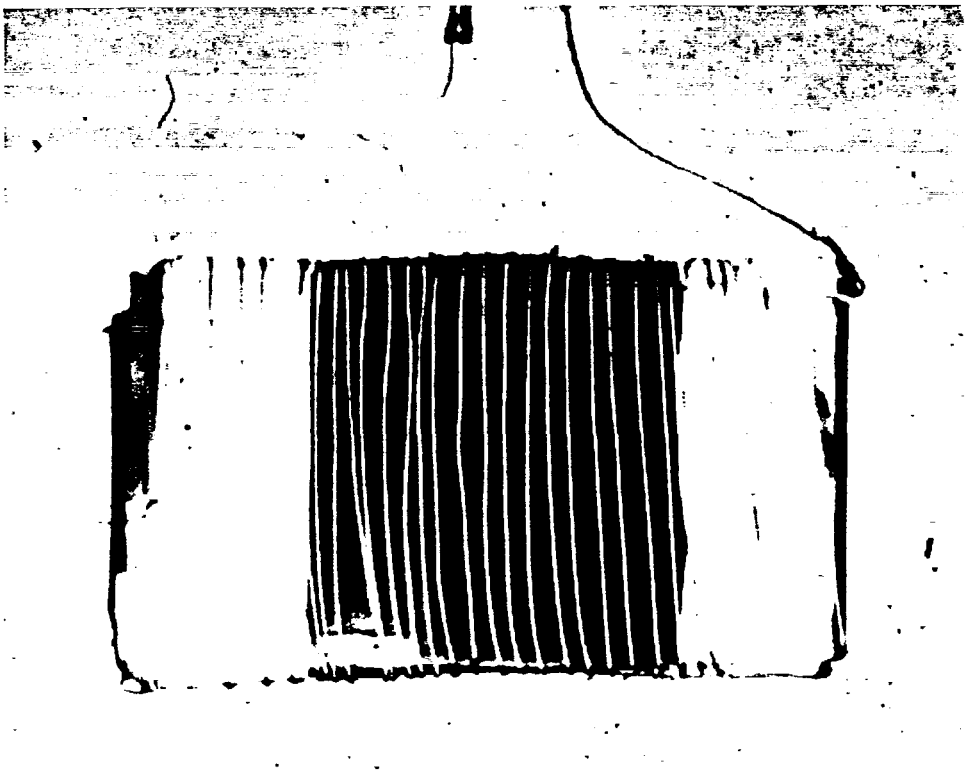

Figure 7. Photograph of an igniter similar to the one used in Fire Tests F99B1401 and F99B1402.

**Table 6**
**Ignition Timing**

| | Time Post-Ignition (min:sec) | |
|---|---|---|
| | **F99B1401** | **F99B1402** |
| **Electrical Power ON** | - 1:39 | -5:18 [1] |
| **Ignition** | 0:00 | 0:00 |
| **Electrical Power OFF** | + 1:10 | +1:00 |

[1] The transformer control malfunctioned and did not supply electrical power to the ignitor for approximately the first 3 minutes of this test. This malfunction was repaired without restarting this test.

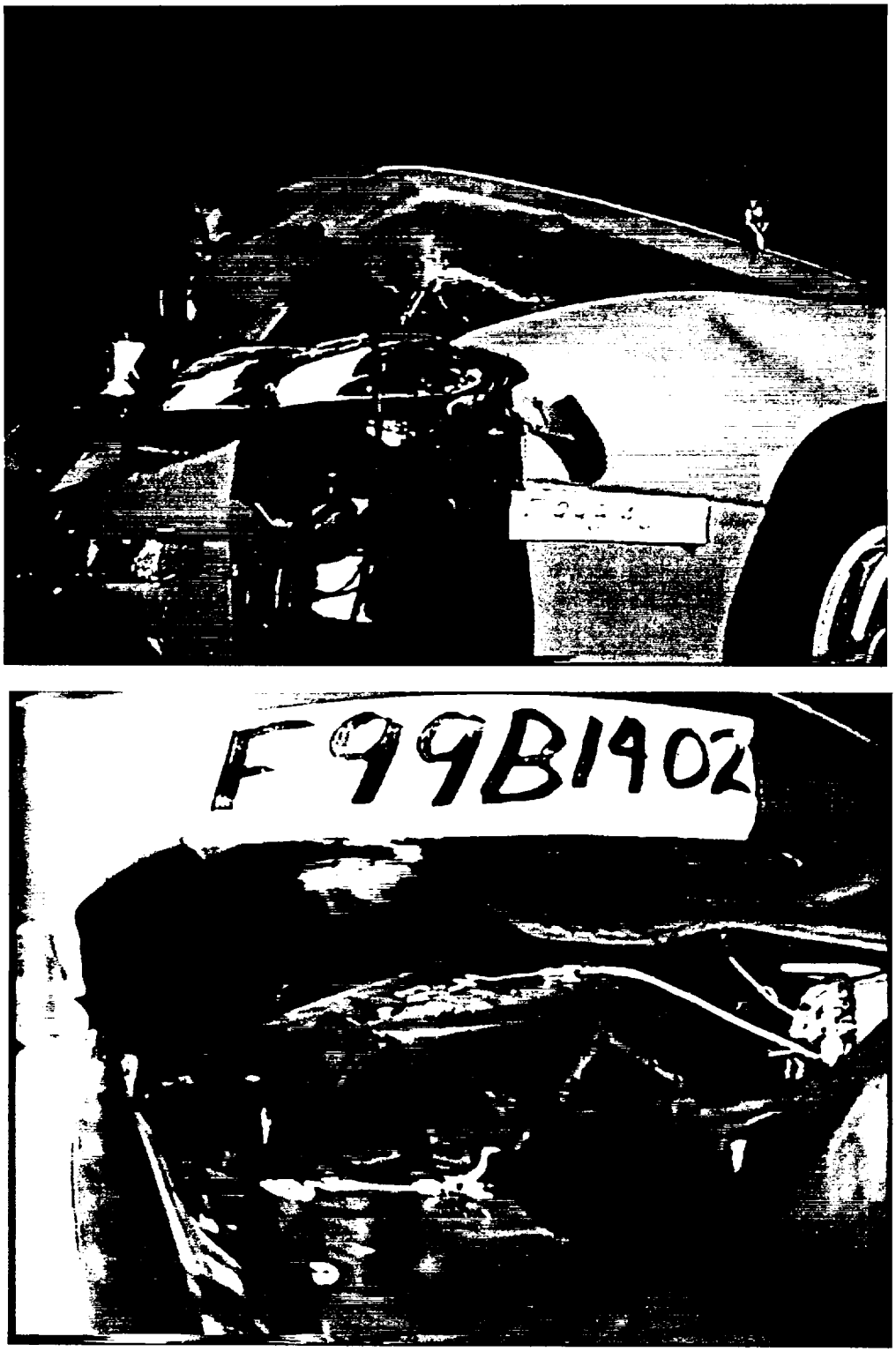


Figure 8. Video stills at the time of ignition 00:00 min:sec post-ignition from Camera 5 during F99B1401 (upper video still) and from Camera 8 during F99B1402 (lower video still).

### 4.3 Flame-Spread in the Engine Compartment

Video Camera 5 provided views into the engine compartments of the test vehicles under the right side of the deformed hood. The initial fuel for these fires was the pieces of poly(propylene) sheet in the igniters and the filter element in the air cleaner. Flames spread from the air cleaner housing rearward to the air inlet screen along the lower edge of the windshield, then laterally along the air inlet screen toward the right side of the engine compartment. Differences in the shapes of the deformed hoods, the geometries of the engine compartments, and the arrangement of components within the engine compartments appeared to have affected the timing of flame-spread in the engine compartments of the test vehicles. For example, the air cleaner housing covers were dislodged from the air cleaner housings during the crash tests of both test vehicles. The gap between the air cleaner housing cover and the air cleaner housing was larger in F99B1402 than in F99B1401, allowing flames to emerge from the air cleaner approximately 150 seconds sooner in F99B1402 than in F99B1401.

The difference in the timing of flame-spread in the engine compartments of the test vehicles can be seen in the videos from Camera 5. Figures 9 through 11 show a series of video stills from Camera 5, where the video stills have been paired to show approximately the same extent of flame-spread along the air inlet screen. Flames from the burning igniter and air cleaner element started to emerge from the rear of the air cleaner housing by 03:30 min:sec in F99B1401, compared to 01:00 min:sec in F99B1402 (Fig. 9). The air inlet screen had ignited and flames had started to spread laterally along the hood lace seal on the air inlet screen by 04:40 min:sec in F99B1401 and 03:00 min:sec in F99B1402 (Fig. 10). Camera 5 was moved away from the test vehicles 7:50 min:sec post-ignition in F99B1401 and 4:30 min:sec post-ignition in F99B1402. Video stills from Camera 5 just before these times show that the right edge of the HVAC air inlet screen, a section of wiring harness on top of the right front wheelhouse, and the inner edge of the right fender had ignited by 05:40 min:sec in F99B1401 and 04:00 min:sec in F99B1402, (Fig. 11).

Figure 12 compares estimated temperature distributions in the upper parts of the engine compartments of the test vehicles at 1-minute intervals from the time of ignition through 13 minutes post-ignition. The estimated temperature distributions in this figure are isothermal contours estimated from temperature data recorded from the E- and C-Thermocouples.[2] The isothermal contours in Figure 12 indicate approximate temperatures along an imaginary surface with boundaries roughly defined by the upper radiator support member in front, the inside top edges of the front fenders on the sides, and the air inlet screen in the rear.

[2] Isothermal contours of the temperature in the upper engine compartment were estimated from recorded temperature data using a three-dimensional interpolation algorithm available in SigmaPlot for Windows Version 4.00 [3]. This algorithm uses an inverse distance method to generated temperature values for points on a uniformly spaced Cartesian grid from input [x,y,t] triple data. Data recorded from thermocouples E1, E2, E3, E4, E5, E6, E7, E8, E9, E12, C1, C2, C3, C4, and C5 were used in these calculations.

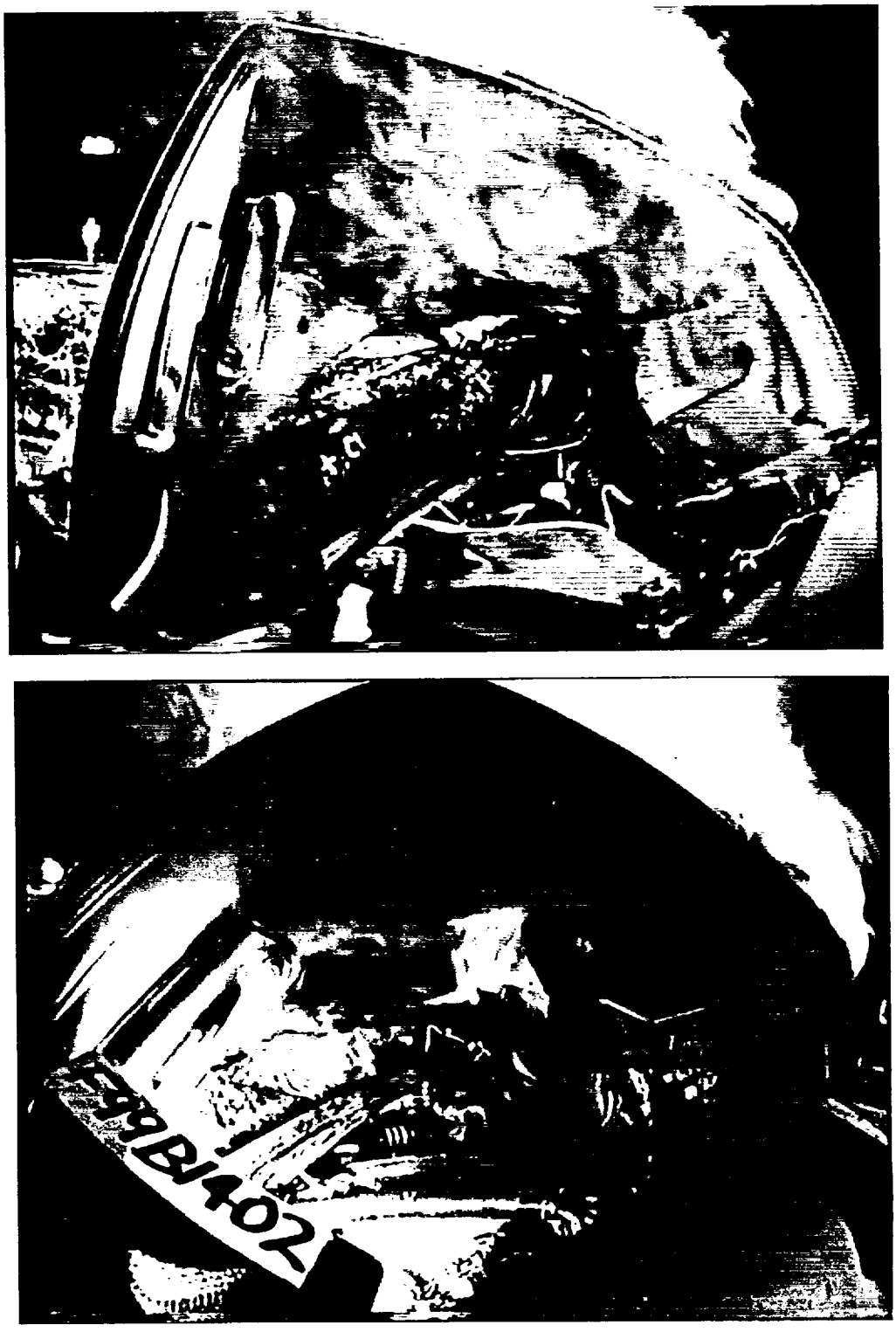


Figure 9. Video stills from Camera 5 at the time of ignition 03:30 min:sec post-ignition during F99B1401 (upper video still) and 01:00 min:sec post-ignition during F99B1402 (lower video still).

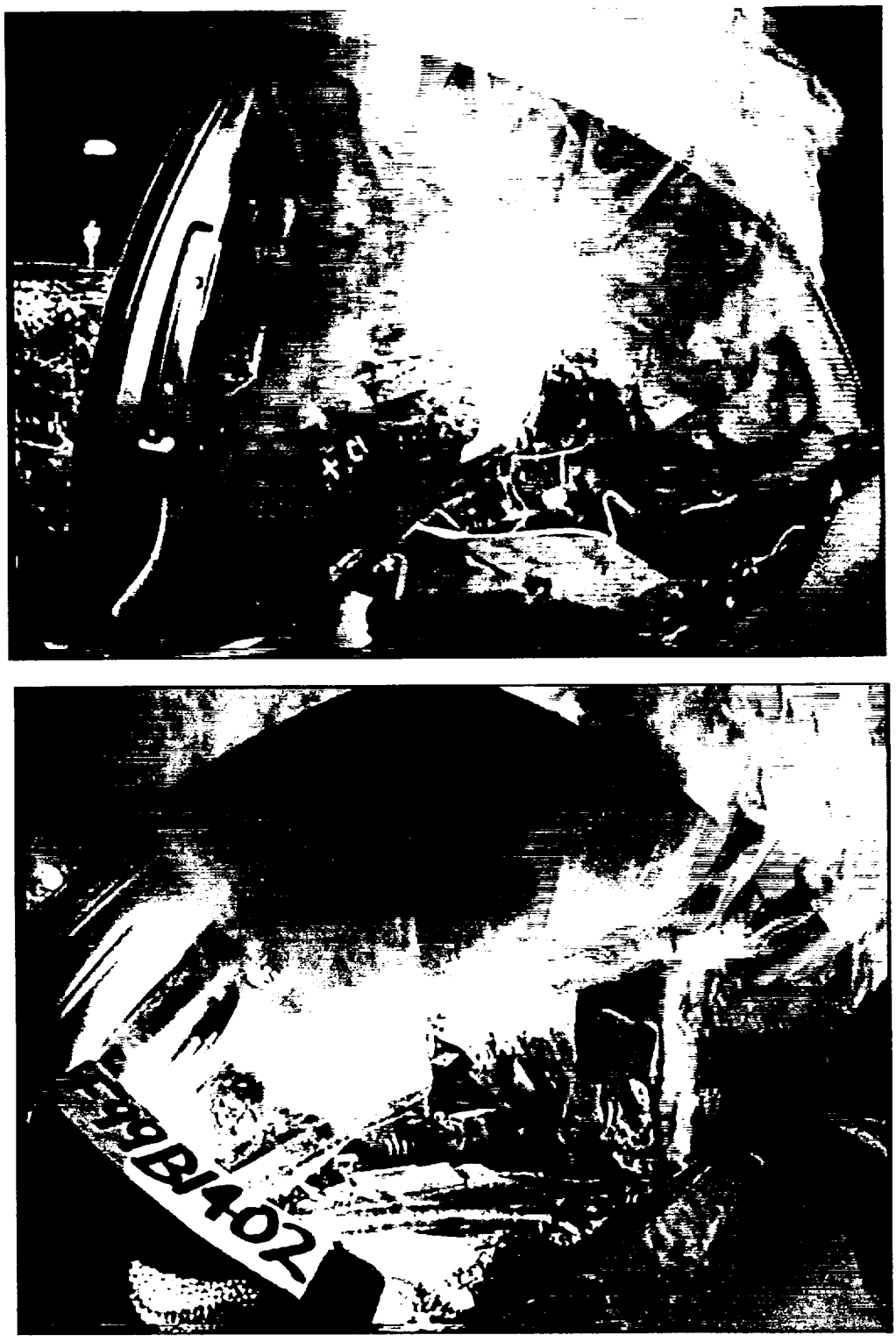


Figure 10. Video stills from Camera 5 at the time of ignition 04:40 min:sec post-ignition during F99B1401 (upper video still) and 03:00 min:sec post-ignition during F99B1402 (lower video still).

Figure 11. Video stills from Camera 5 at the time of ignition 05:40 min:sec post-ignition during F99B1401 (upper video still) and 04:00 min:sec post-ignition during F99B1402 (lower video still).

These estimated isothermal contours provide no information about flame-spread downward in the engine compartment, or flame-spread outside of the engine compartment. The timing of flame-spread inferred from the estimated isothermal contours in Figure 12 is consistent with the timing of flame spread observed in the videos from Camera 5 (Fig.'s 9 through 11).

The temperature data indicate that the air cleaner housing cover ignited between 3 and 4 minutes post-ignition in F99B1401 and between 1 and 2 minutes post-ignition in F99B1042.[3] Flames had spread rearward to a section of the air inlet screen directly behind the air cleaner housing between 4 and 5 minutes post-ignition in F99B1401 and between 3 and 4 minutes post-ignition in F99B1402. Flames had spread to the right side of the air inlet screen by 7 minutes post-ignition in F99B1401 and 5 minutes post-ignition in F99B1402. By 7 minutes post-ignition, estimated temperatures along the right section of the air inlet screen exceeded 800°C. Most of the combustible materials in the upper section of the right side of the engine compartment appeared to be burning and flames started to spread to the left side of the engine compartment around the brake fluid reservoir. Combustible materials in the front of the left side of the engine compartment ignited between 7 and 9 minutes post-ignition in F99B1401 and between 9 and 11 minutes post-ignition in F99B1402.

Heat release rates of the fires in both tests were determined from data acquired using the fire products collector at the test facility (**Appendix M**). Figure 13 shows plots of the heat release rate curves for F99B1401 and F99B1402. The heat release rate curves for both tests were nearly identical. The major difference was the timing of the initial increases in the heat release rates during the early stages of the fires. The heat release curve for F99B1401 showed an initial deflection starting between 4 and 5 minutes post-ignition, and the heat release curve for F99B1402 showed an initial upward deflection starting between 3 and 4 minutes post-ignition (Fig. 13). The heat release rates of the fires were approximately the same from about 5 ½ minutes post-ignition to the ends of these tests. The difference in heat release rates of the fires during the early stages of the fires is consistent with the difference in flame spread in the engine compartments of the test vehicles noted in Figure 12.

The tests were ended when flame-spread into the passenger compartment through the windshield opening had progressed to the rear of the instrument panel upper trim panel and pieces of burning windshield started to fall inward. This was at 12:47 min:sec for F99B1401 and 12:50 min:sec for F99B1402. Fire suppression began at about 13 minutes post-ignition in both tests (**Section 4.4**).

[3] As in previous reports, a value of 600°C was used in this report as the threshold to indicate the presence of flame. Using this criterion, the 600°C isothermal contour indicated the approximate boundary of the flame front in the engine compartment.

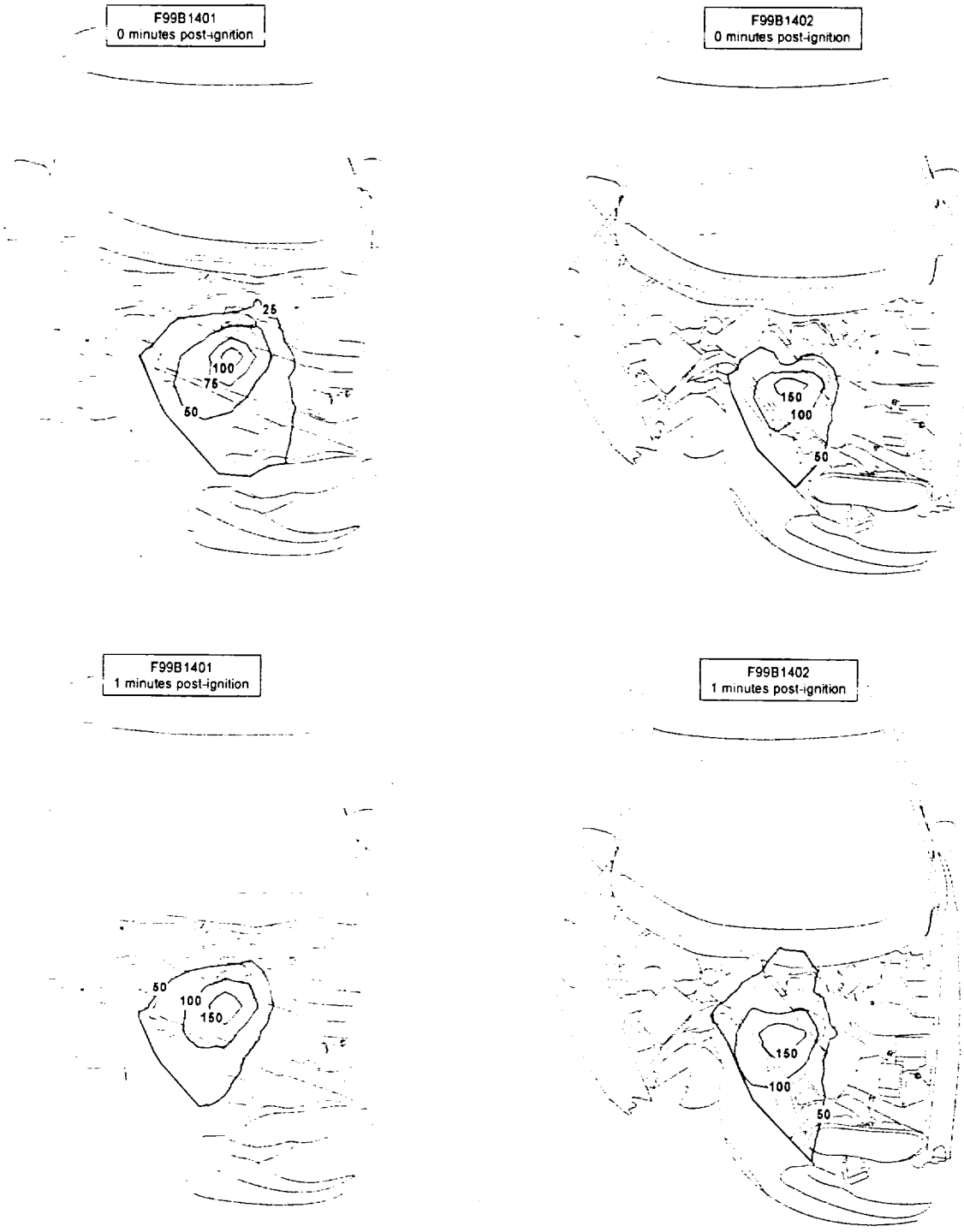


Figure 12. Estimated isothermal contour plots of temperatures on the engine compartments of the test vehicles 0, 1, 2, 3, 4, 5, 6, 7, 8, 9, 10, 11, 12, and 13 minutes post-ignition.

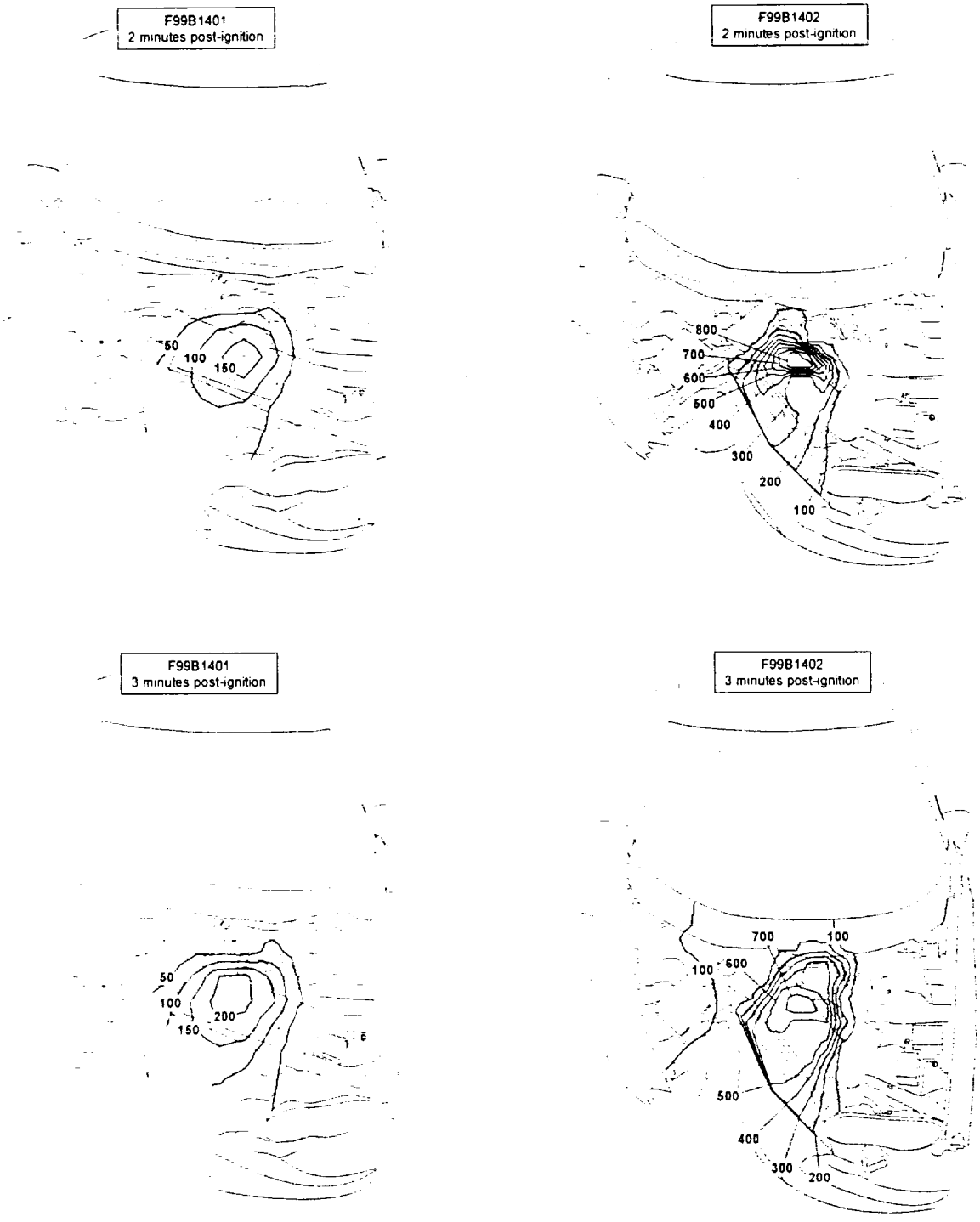


Figure 12, continued. Estimated isothermal contour plots of temperatures on the engine compartments of the test vehicles 0, 1, 2, 3, 4, 5, 6, 7, 8, 9, 10, 11, 12, and 13 minutes post-ignition.

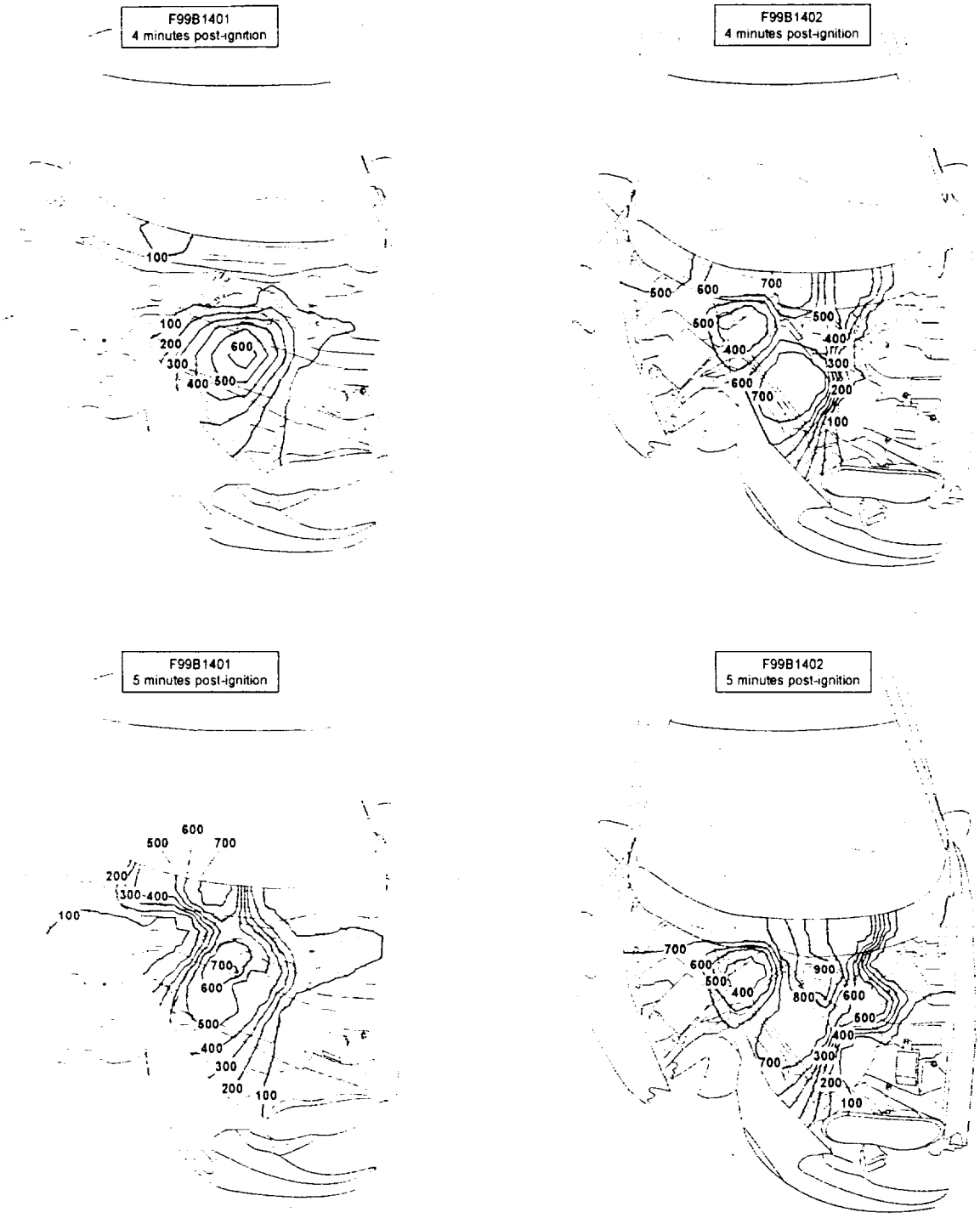


Figure 12, continued. Estimated isothermal contour plots of temperatures on the engine compartments of the test vehicles 0, 1, 2, 3, 4, 5, 6, 7, 8, 9, 10, 11, 12, and 13 minutes post-ignition.

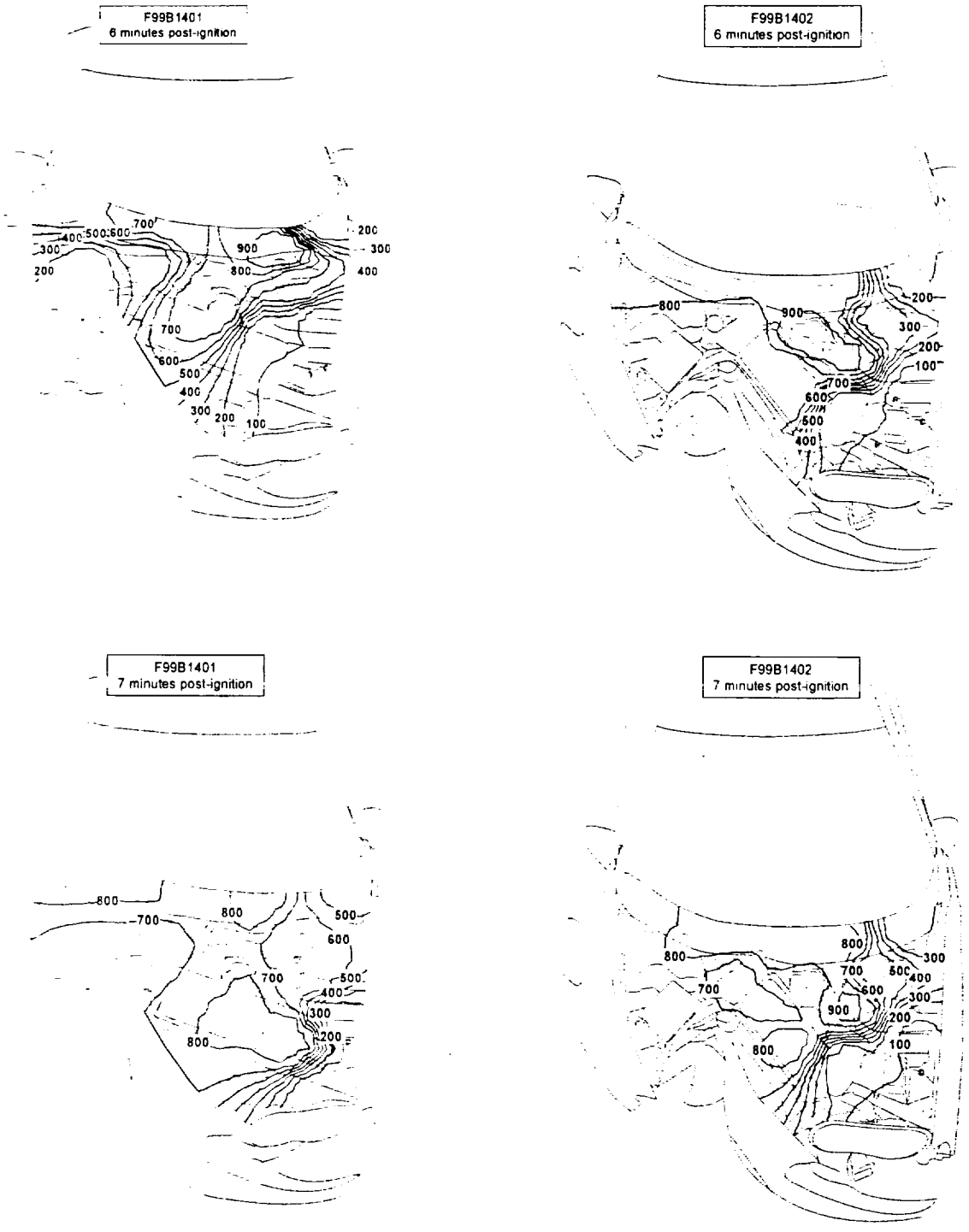


Figure 12, continued. Estimated isothermal contour plots of temperatures on the engine compartments of the test vehicles 0, 1, 2, 3, 4, 5, 6, 7, 8, 9, 10, 11, 12, and 13 minutes post-ignition.

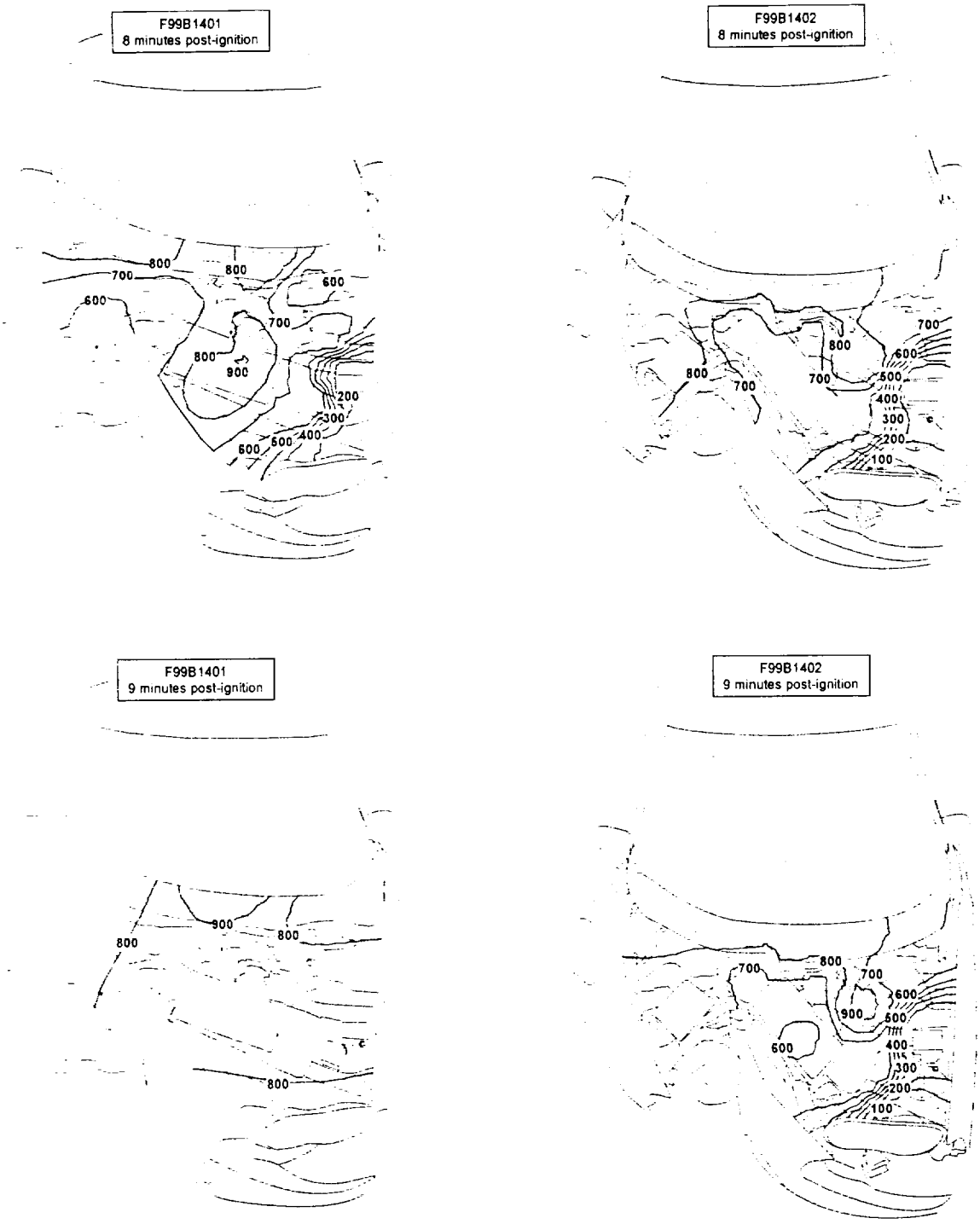


Figure 12, continued. Estimated isothermal contour plots of temperatures on the engine compartments of the test vehicles 0, 1, 2, 3, 4, 5, 6, 7, 8, 9, 10, 11, 12, and 13 minutes post-ignition.

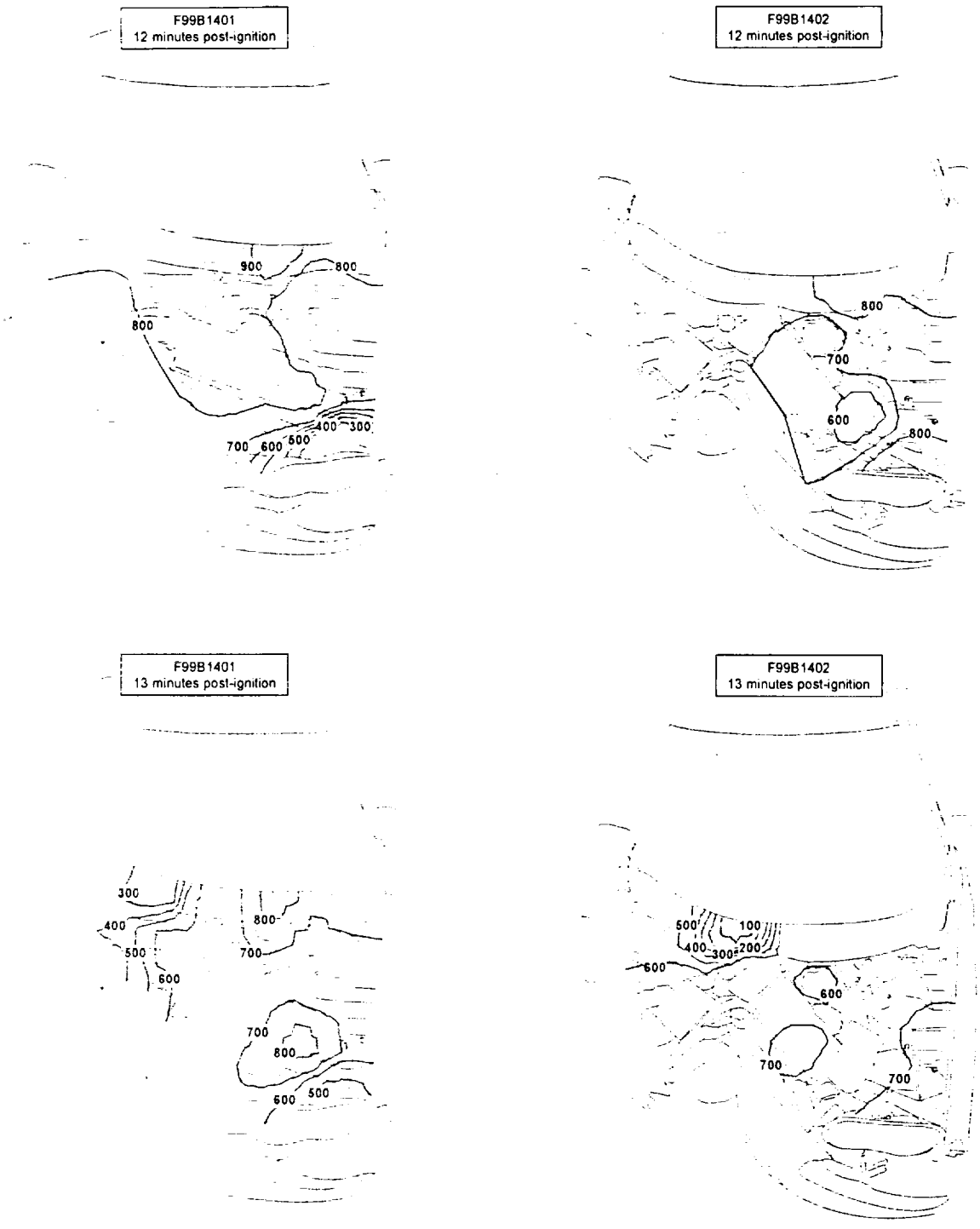


Figure 12, continued. Estimated isothermal contour plots of temperatures on the engine compartments of the test vehicles 0, 1, 2, 3, 4, 5, 6, 7, 8, 9, 10, 11, 12, and 13 minutes post-ignition.

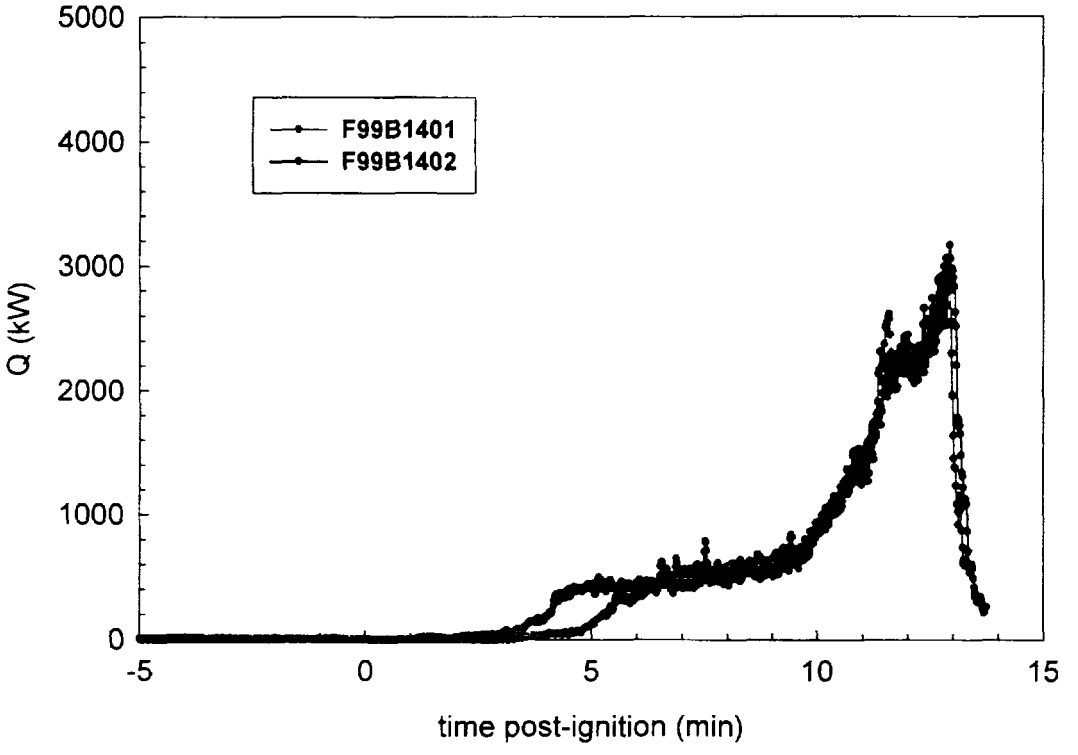


Figure 13. Plots of heat release curves for F99B1401 and F99B1402.

The patterns of burn damage observed in and around the engine compartments of the test vehicles were similar. Figure 14 shows photographs of the test vehicles after these tests. Combustible materials in the upper sections of the engine compartments were largely consumed by fire. Sections of glass fiber mat from the hood silencer pad had detached from the hood and were observed on top of the left side of the engine, the generator, the HVAC module, and the left wheelhouse panel. The left and right outer fender panels[4] had ignited and burned during both tests. During both tests, pieces of the fender panels fell off of the test vehicles and were visible on the ground near the test vehicles after each test. The front bumper fascia and front bumper energy absorber ignited and were largely consumed by fire.

[4] The fenders in the test vehicles were a styrene-cross-linked-polyester-glass-fiber composite (Sheet Molding Compound).

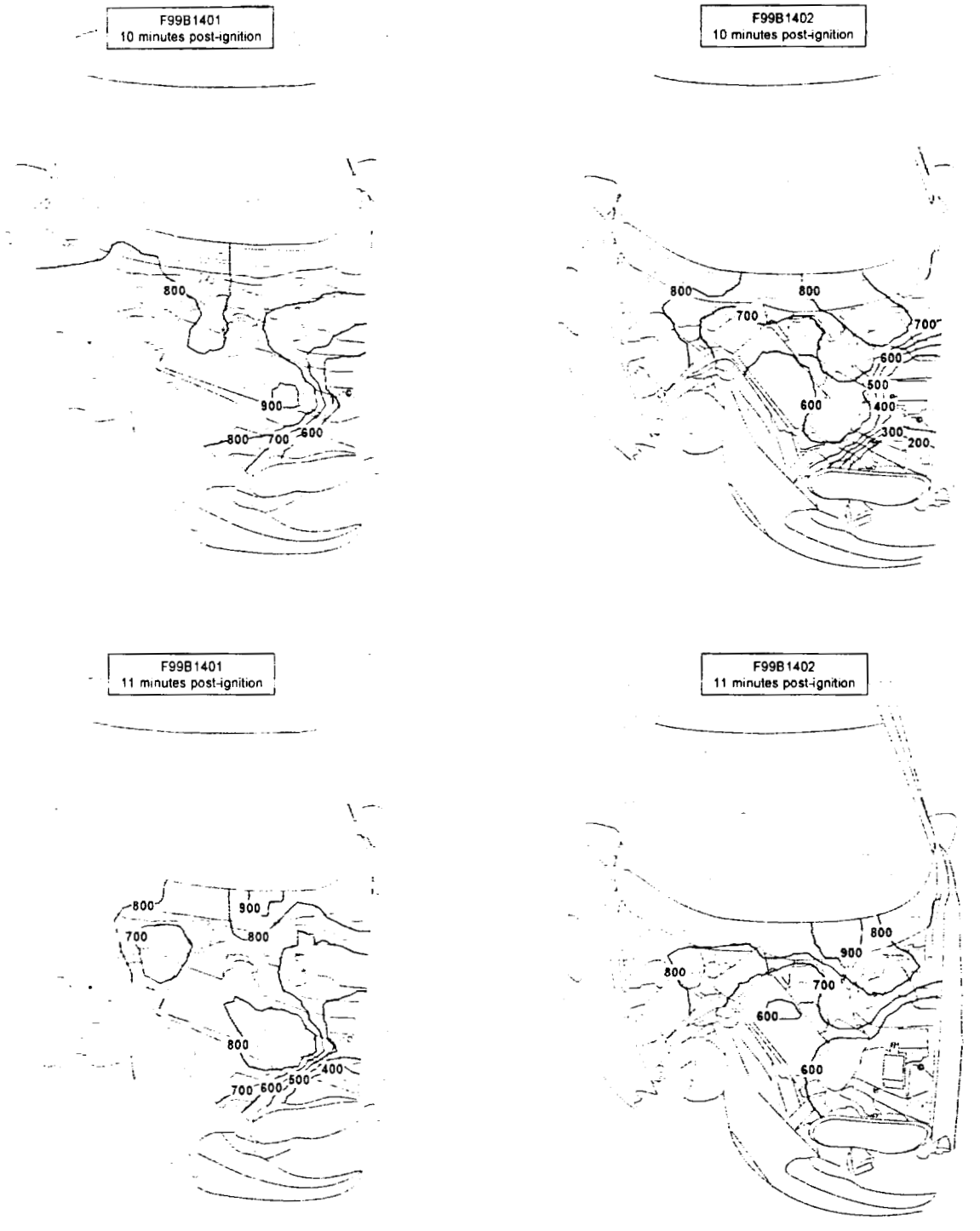


Figure 12, continued. Estimated isothermal contour plots of temperatures on the engine compartments of the test vehicles 0, 1, 2, 3, 4, 5, 6, 7, 8, 9, 10, 11, 12, and 13 minutes post-ignition .

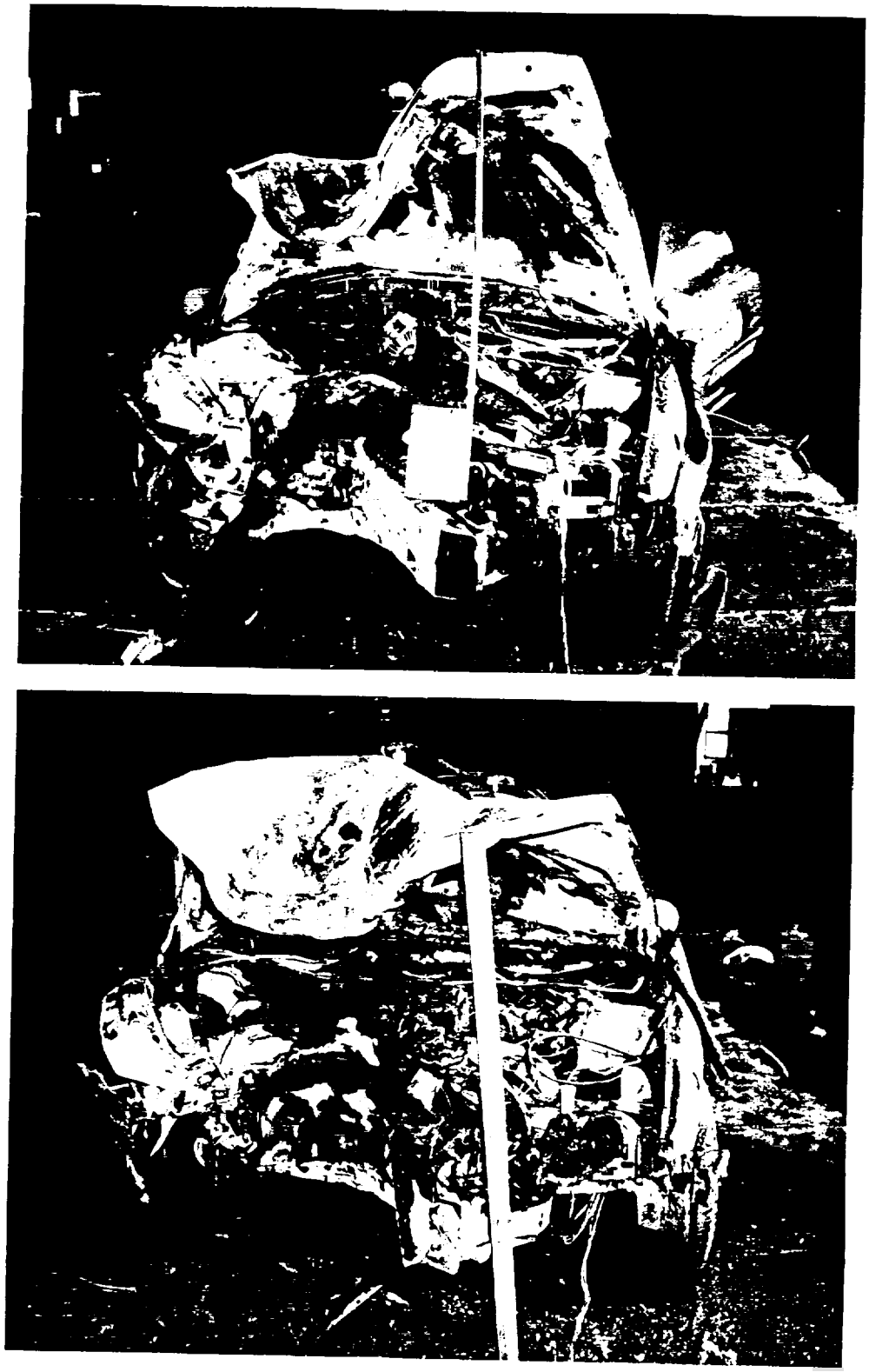

Figure 14. Photographs of the engine compartments of the test vehicles after Fire Test F99B1401 (upper photograph) and Fire Test F99B1402 (lower photograph).

### 4.4 Flame-Spread into the Passenger Compartment

The data collected during these tests and the patterns of fire damage observed during inspection of the test vehicles after these tests indicated that flame-spread into the passenger compartments of both test vehicles was progressing along two pathways concurrently when the tests were ended. These pathways include flame-spread through the windshield onto the instrument panel top cover and the flame-spread through the HVAC module in the dash panel. At the time flames were extinguished in both tests, flames had spread through the windshield onto the instrument panel upper trim panel. During these tests, pieces of windshield fell inward sporadically igniting the deployed passenger air bags and the right front seat cushions. Sections of the auxiliary A/C evaporator and blower upper cases that were exterior to the dash panel ignited before these tests were ended. Flames had not spread into sections of the HVAC modules that were interior to the dash panel. There was no evidence of flame-spread through any of the other front-of-dash pass-through openings.

The diagram below shows a top-view of the dash panel and windshield support panel.

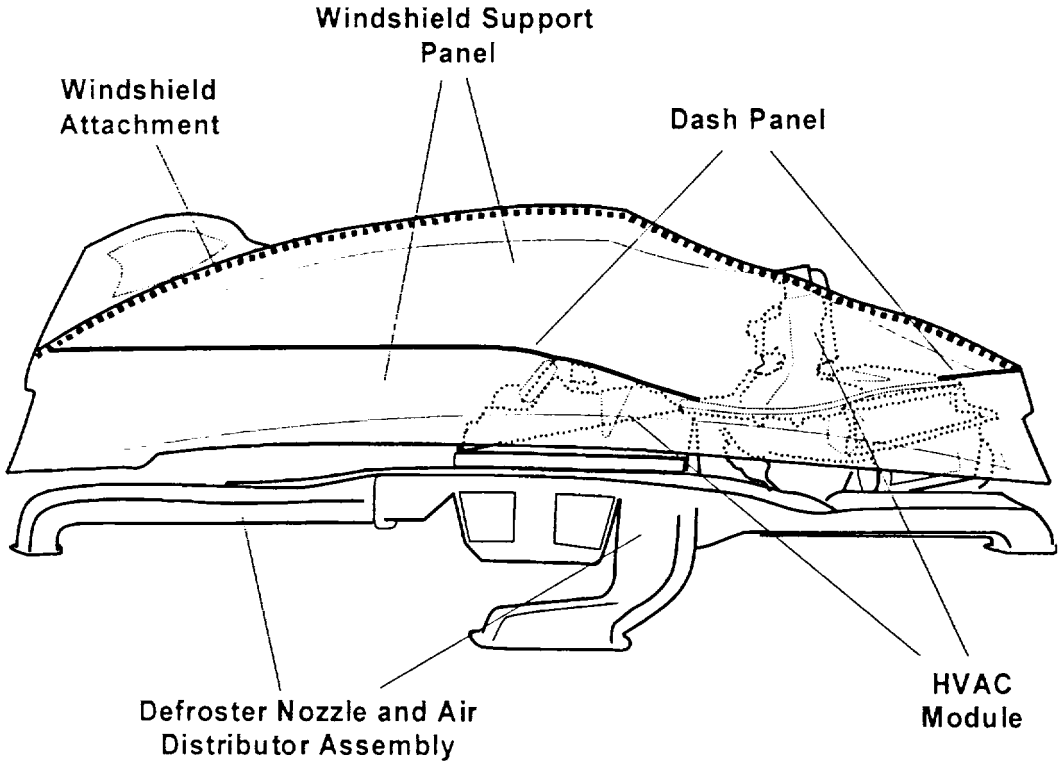


The dashed line indicates where the lower edge of the windshield was attached to the lower windshield support panel. This diagram also shows the approximate locations of the HVAC module, and defroster nozzle and air distributor assembly.

In both test vehicles, the glass outer layers of the windshields[5] shattered during the crash tests. The right side of the dash panels deformed and were displaced rearward. The right sides of the upper dash extension panels and windshield support panels were deformed, with the broken windshield partially detaching from deformed sections of windshield support panels. The sides and top of the windshields remained attached to the A-pillars and roof. The front section of the broken windshields sagged onto the instrument panel upper trim panel.

The diagram below shows a face-view of the dash panel in the test vehicle. The HVAC module pass-through was located on the right side of the dash panel. The brake linkage pass-through and steering column pass-through were located on the left side of the dash panel.

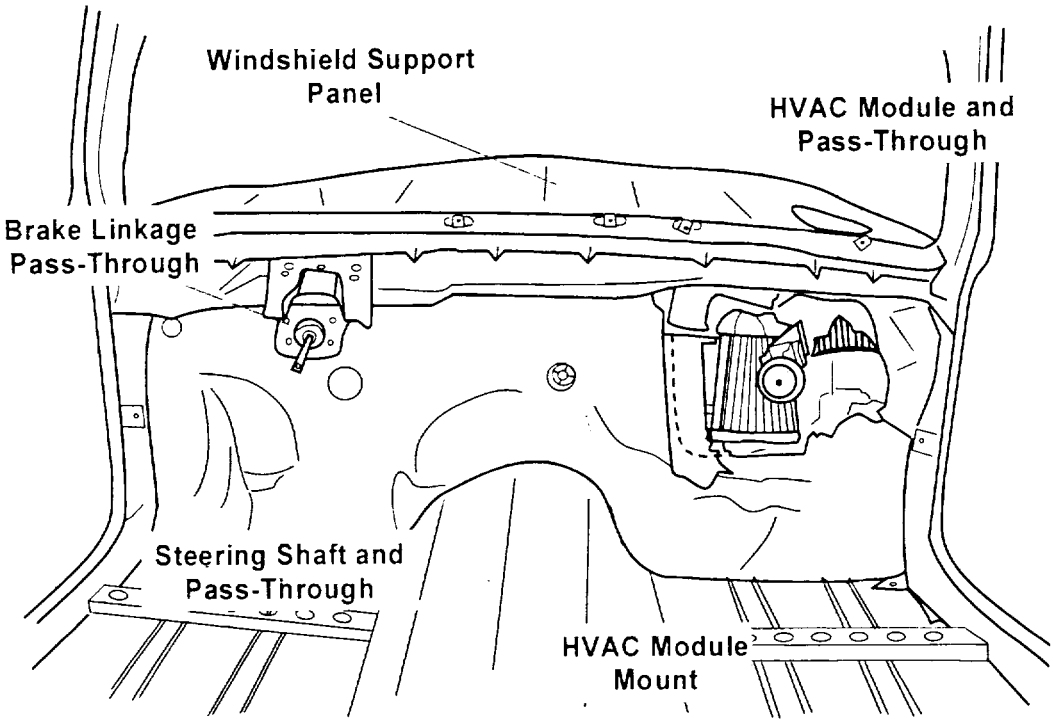


In the analysis that follows, flame-spread through the windshield was characterized by analysis of the video records from exterior and interior cameras that showed the windshield, the recorded thermocouple data, and the burn patterns observed in the test vehicles after these tests. In both test vehicles, the exterior surfaces of the dash panels were obscured by the engines and other components that were pushed to the rear of the engine compartments during the crash tests. The instrument panel storage compartments (glove box) were removed and video cameras were

[5] Motor vehicle windshields generally are composite structures, consisting of two outer layers of annealed glass and an inner layer of a vinyl butyral/vinyl alcohol copolymer. The inner layer in the windshield of the test vehicle contained dihexyl adipate (plasticizer) and 2-(2H-benzotriazol-2-yl)-4-methylphenol (UV-inhibitor).

mounted on the seat cushions of the right front seats in both test vehicles to obtain views of the interior sections of the HVAC modules during these tests. Video cameras were mounted in lower sections of the rear of the engine compartments to obtain views of the lower portions of the exterior sections of the HVAC modules. Flame-spread through the HVAC module was characterized by analysis of these video records, the recorded thermocouple data, and burn patterns observed in the test vehicles after these tests.

### 4.4.1 Flame-Spread through the Windshield

Figure 15 compares estimated temperature distributions on the windshields of the test vehicles at 1-minute intervals from the time of ignition through 9 minutes post-ignition. The isothermal contours in this figure were calculated from temperature data recorded from the C- and W-Thermocouples using a three-dimensional interpolation algorithm.[6] These thermocouples were located approximately 5 mm away from (in front of) the exterior surface of the windshield or below the air inlet screen just above the leading edge of the windshield. These thermocouples were heated by convection and radiation from hot gases and flames venting from the engine compartment along the rear edge of the deformed hood. Thus, the estimated temperature profiles shown in Figure M indicate the approximate distribution of heated gases and flames along the exterior surface of the windshield. This analysis cannot be used to estimate the temperature of the exterior surface of the windshield because the thermocouples used to acquire the data for these calculations were not in contact with the windshield.

The estimated temperature profiles in Figure 15 indicate that as flames spread laterally to the right along the rear of the engine compartment, the exterior surfaces of the windshields in both test vehicles were exposed to heated gases and flames from the burning air inlet screens. In F99B1401, estimated temperatures on the air inlet screen and sections in the windshield just above the air inlet screen first exceeded 600°C between 4 and 5 minutes post-ignition. In F99B1402, estimated temperatures on the air inlet screen and sections of the windshield just above the air inlet screen first exceeded 600°C between 3 and 4 minutes post-ignition. Radiation from the flames heated the windshields and caused the windshield inner layers to soften and stretch and the lower portions of the windshield to sag onto the instrument panel top covers.

---

[6] Isothermal contours of the temperature in the upper engine compartment were estimated from temperature data recorded from Thermocouples C1, C2, C3, C4, C5, W1, W2, W3, W4, W5, W6, W7, W8, W9, and W10 using a three-dimensional interpolation algorithm available in SigmaPlot for Windows Version 4.00 [3]. This algorithm uses an inverse distance method to generated temperature values for points on a uniformly spaced Cartesian grid from input [x,y,t] triple data.

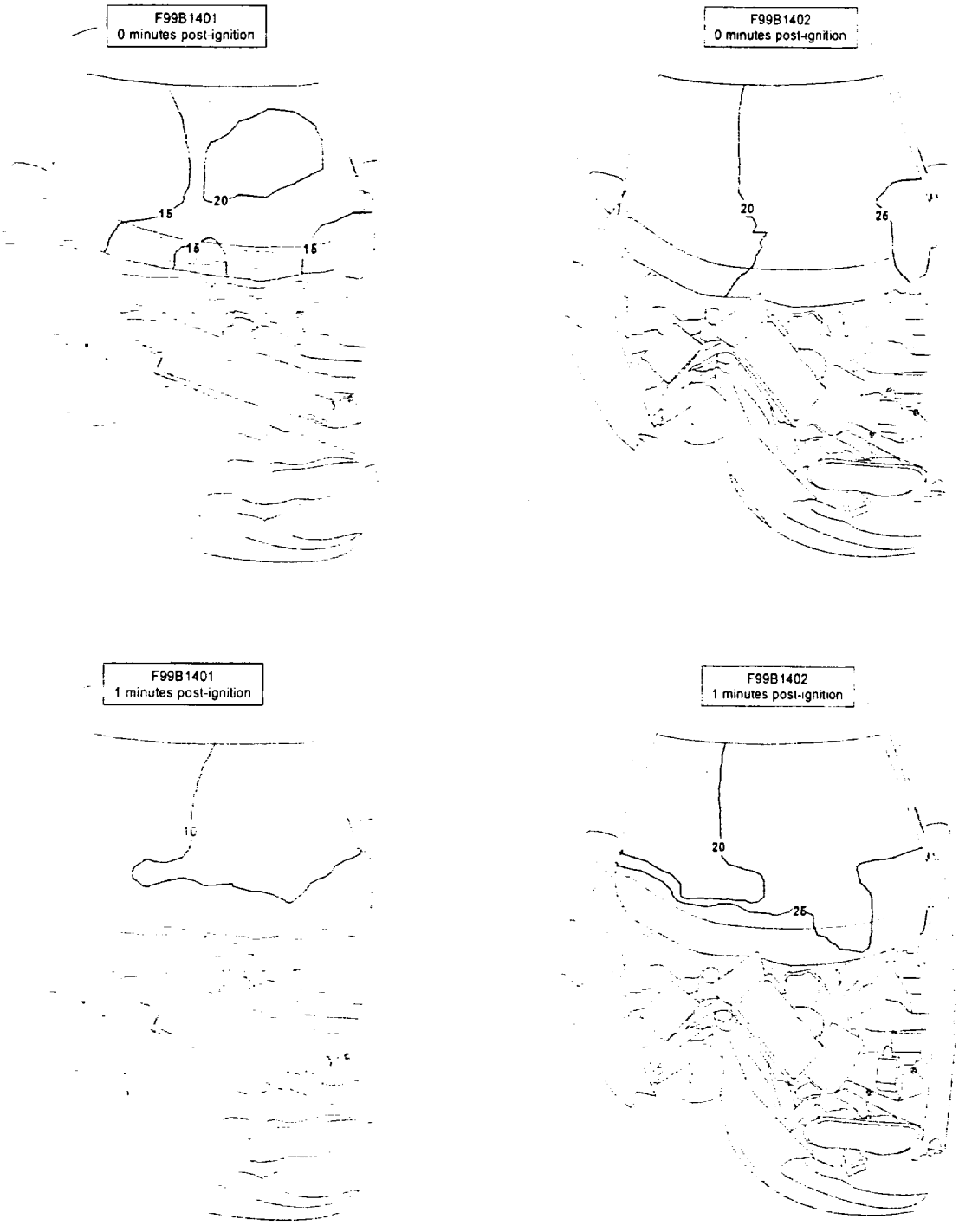


Figure 15 Estimated temperature distributions on the windshields of the test vehicles 0, 1, 2, 3, 4, 5, 6, 7, 8, and 9 minutes post-ignition.

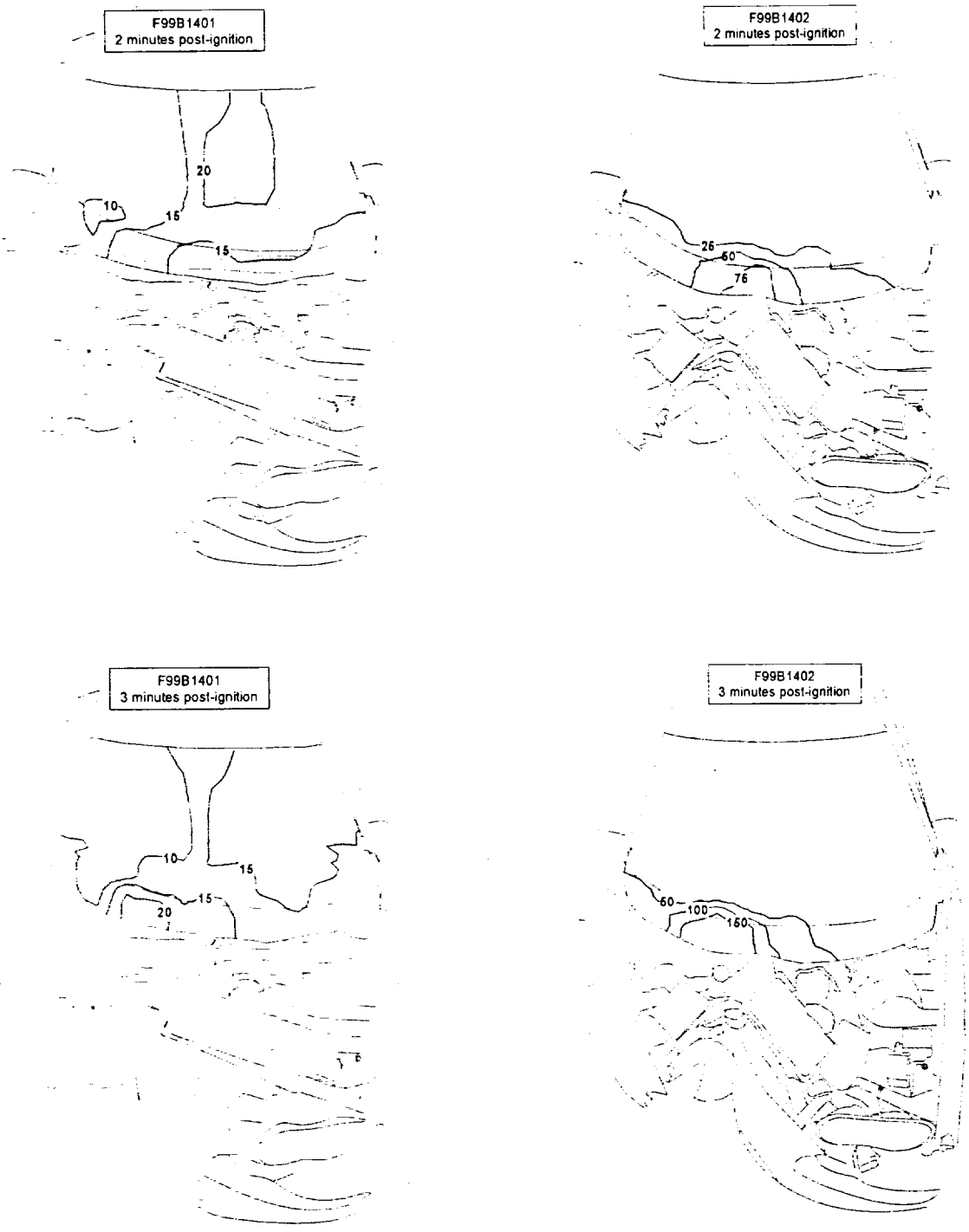


Figure 15, continued. Estimated temperature distributions on the windshields of the test vehicles 0, 1, 2, 3, 4, 5, 6, 7, 8, and 9 minutes post-ignition.

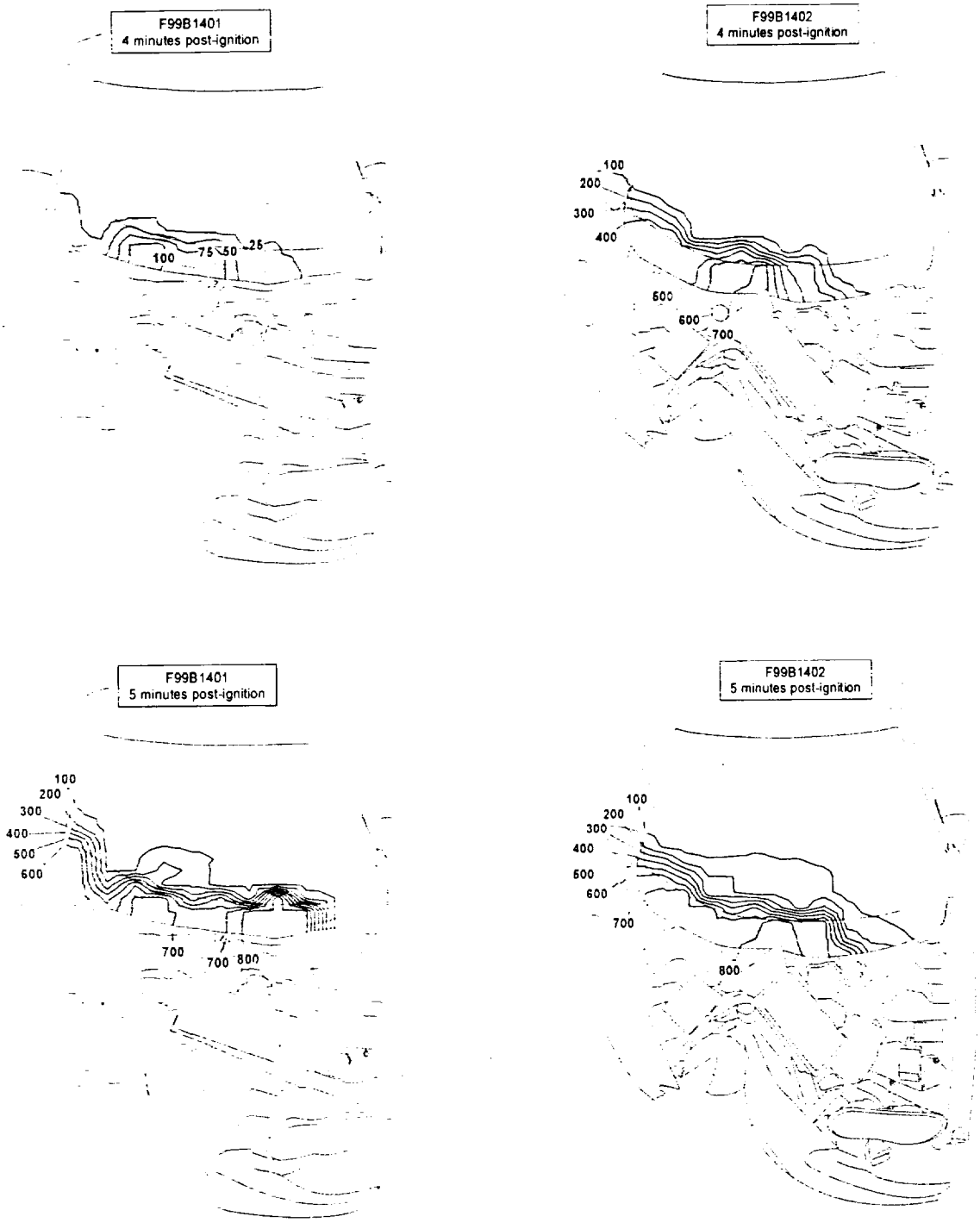


Figure15, continued. Estimated temperature distributions on the windshields of the test vehicles 0, 1, 2, 3, 4, 5, 6, 7, 8, and 9 minutes post-ignition.

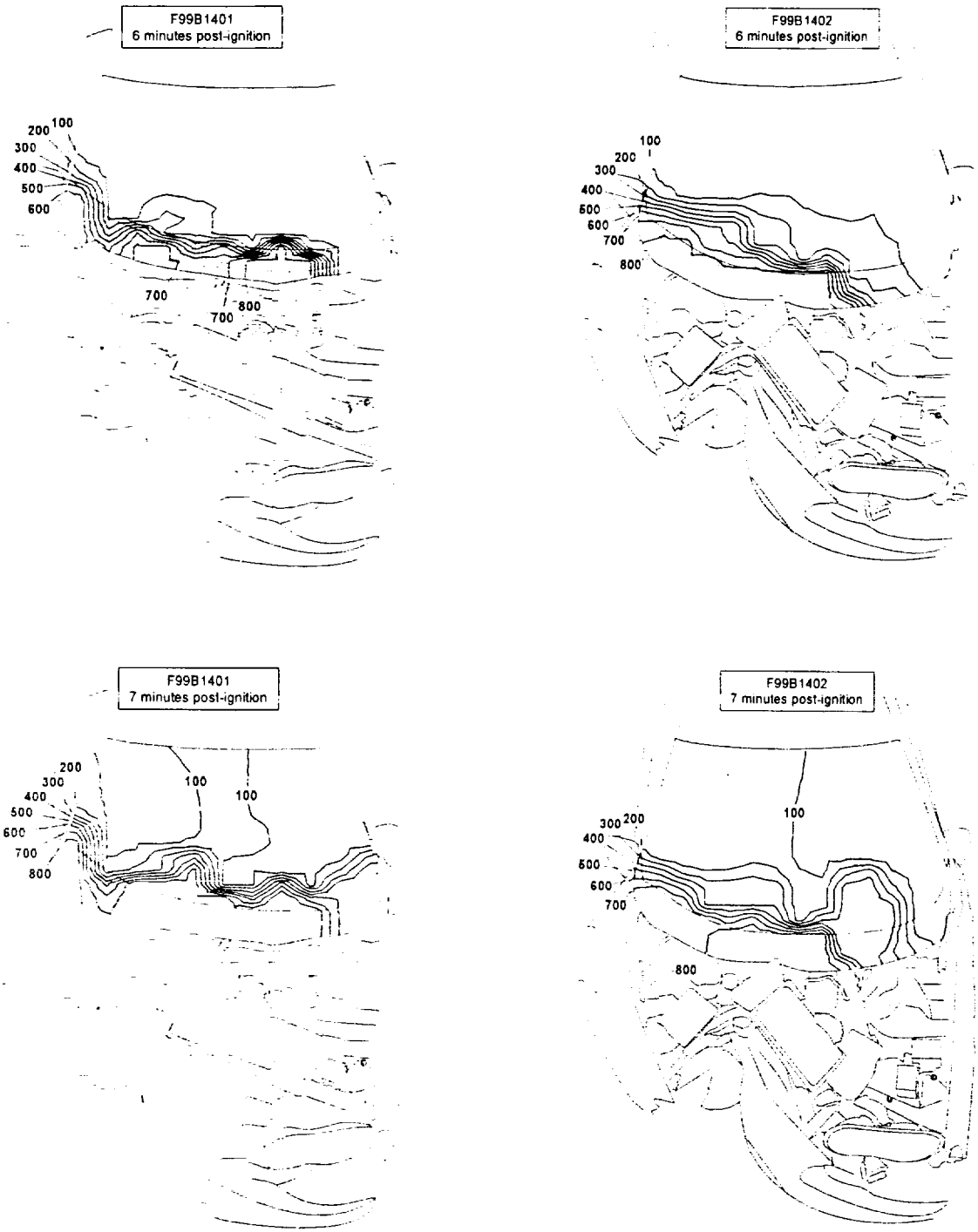


Figure 15, continued. Estimated temperature distributions on the windshields of the test vehicles 0, 1, 2, 3, 4, 5, 6, 7, 8, and 9 minutes post-ignition.

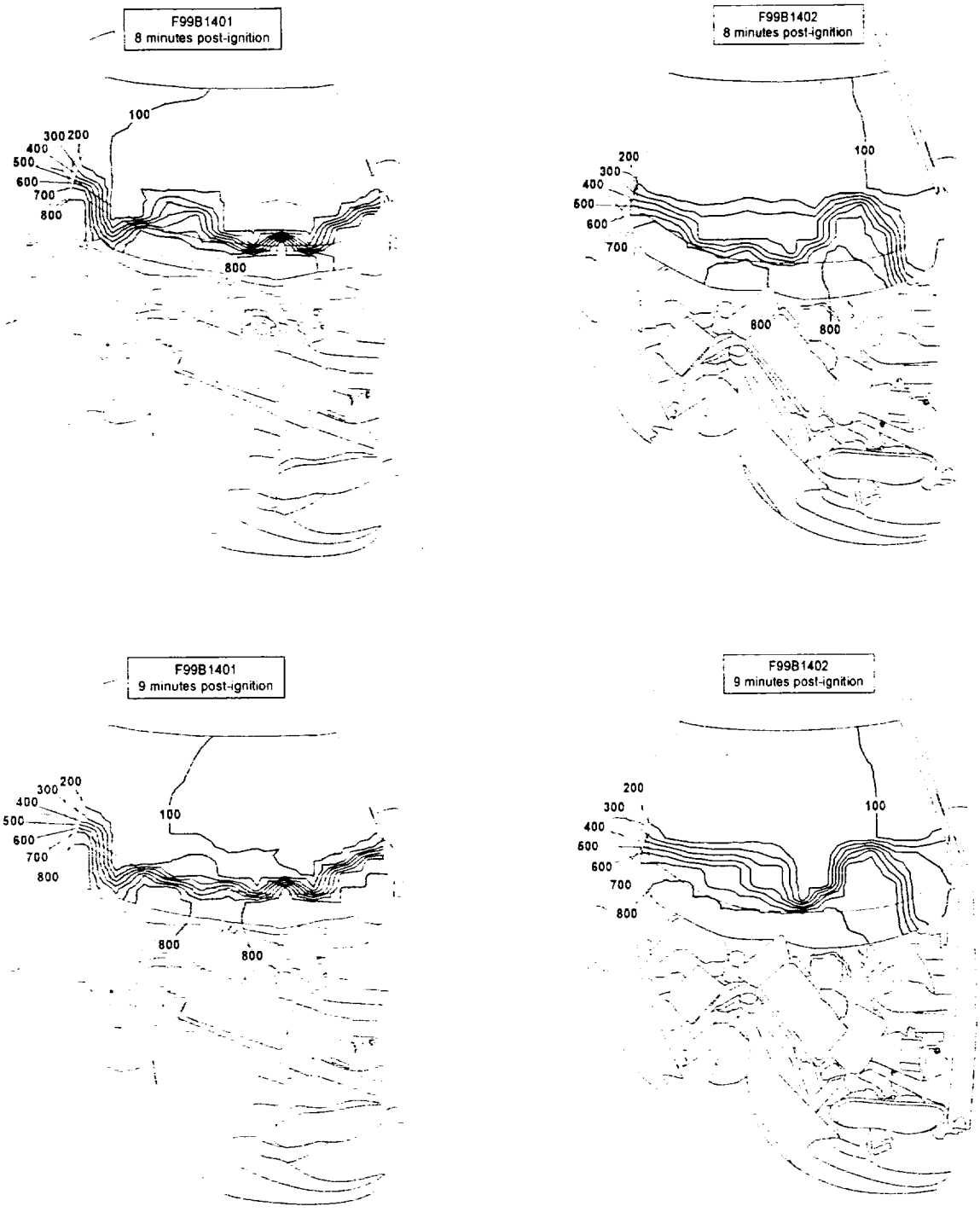


Figure 15, continued. Estimated temperature distributions on the windshields of the test vehicles 0, 1, 2, 3, 4, 5, 6, 7, 8, and 9 minutes post-ignition.

Figures 16 and 17 show video stills from Camera 1 at the time of ignition and at 7 minutes post-ignition in F99B1401 and F99B1402, respectively. The video stills in these figures show that in both test vehicles the windshields had sagged further onto the instrument panel top covers than at the start of these tests. The estimated temperature profiles in Figure 15 indicate that the temperature along the right sides of the windshields was >100°C at 7 minutes post-ignition in both test vehicles. Continued heating of the right sides of the windshields caused the windshield inner layers to soften further. Sections of the right sides of the windshields fell on the instrument panel top covers between 7 and 8 minutes post-ignition. Piecies of windshield had separated and fallen into the passenger compartments of both test vehicles by 8 minutes post ignition (Fig. 18). Pieces of windshield fell onto the instrument panel top cover, the passenger air bag covers, and the deployed passenger air bags (Fig. 19). Flames had spread rearward along the top of the instrument panels to the passenger air bag covers and deployed passenger air bags in both test vehicles by 12:30 min:sec post-ignition (Fig. 20). The lower sections of the right A-Pillar trim panels had ignited and were burning by this time (Fig. 20). Pieces of windshield where the innerlayer had ignited and was burning had fallen onto the right front seat cushion in F99B1401 and onto the deployed passenger air bag in F99B1402. The pieces of burning windshield extinguished before igniting the seat cushion in F99B1401 (upper video still, Fig. 20) and the deployed passenger air bag in F99B1402 (lower video still, Fig. 20).

The patterns of fire damage observed in the pasenger compartments of the test vehicles after these tests were consistent with flame-spread through the windshield. For example, the center and right of the windshields of both test vehicles had fallen into the passenger compartment (Fig. 21). Pieces of windshield were observed on the instrument panel upper trim panels, the instrument panels, the deployed passenger's airbags, and the front seat cushions (Fig. 21). The instrument panel upper trim panels in both test vehicles were melted and charred (Fig. 21). The inner layer was burned and charred in windshield fragments on the front and right side of the instrument panel upper trim panels, and on the deployed passenger air bags (Fig. 21). Pieces of windshield were observed on both of the front seat cushions in both test vehicles after these tests (Fig. 22). Sections of the right and left front seat cushions in F99B1401 and the right front seat chuhion in F99B1402 were burned and charred.

### 4.4.2 Ignition of the Auxillary A/C Evaporator and Blower Upper Case

Sections of the auxillary A/C evaporator and blower upper cases that were in the engine compartments of the test vehicles had ignited at some time before these tests were ended and flames were extinguished. The auxillary A/C evaporator and blower upper case in F99B1401 was made of 40% talc-filled poly(propylene) containing no added flame retardant chemicals and the auxillary A/C evaporator and blower upper case in F99B1402 was made of poly(propylene) that

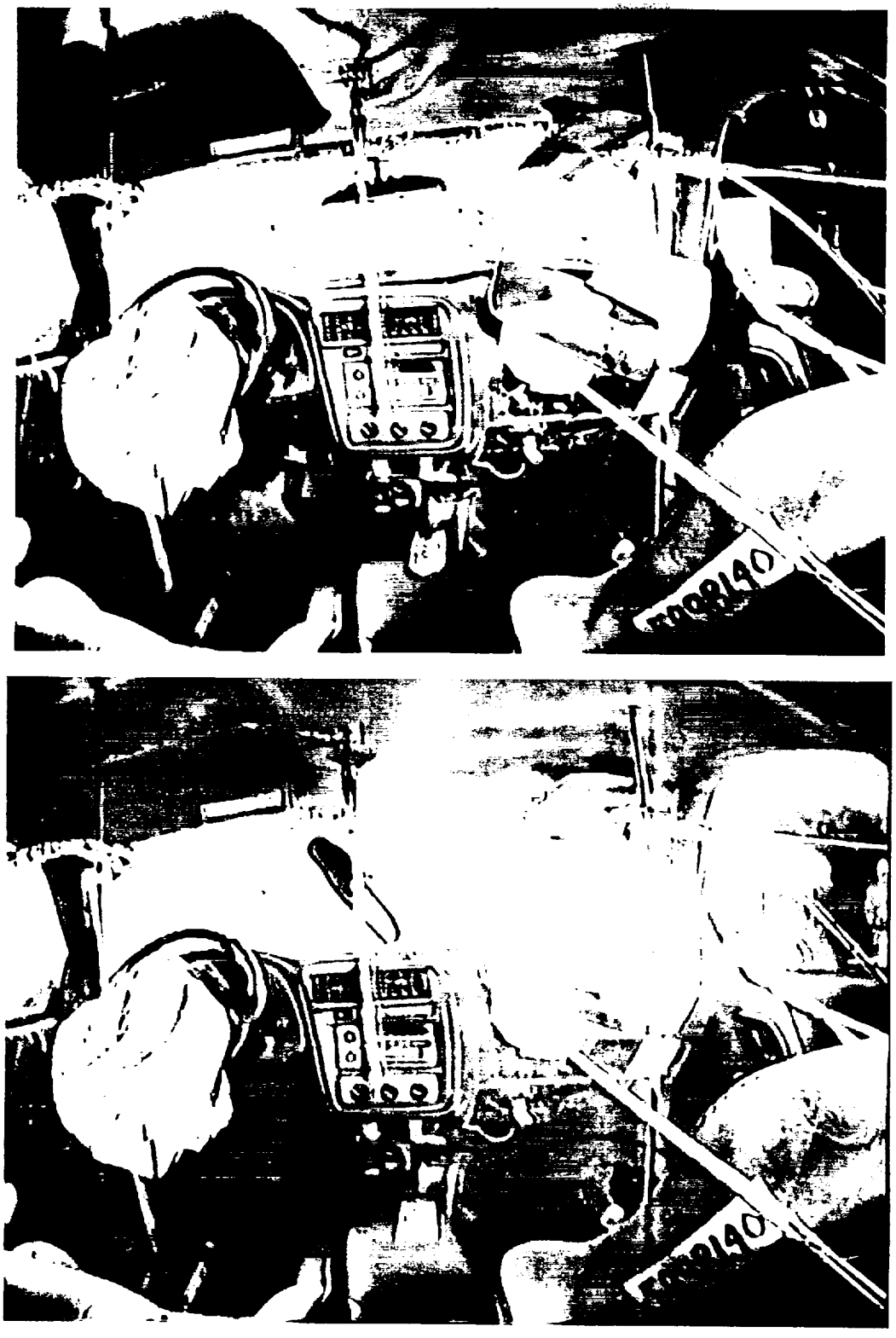

Figure 16. Fire Test F99B1401. Video Stills from Camera 1 at the time of ignition (upper video still) and at 7 minutes post-ignition. (lower video still).

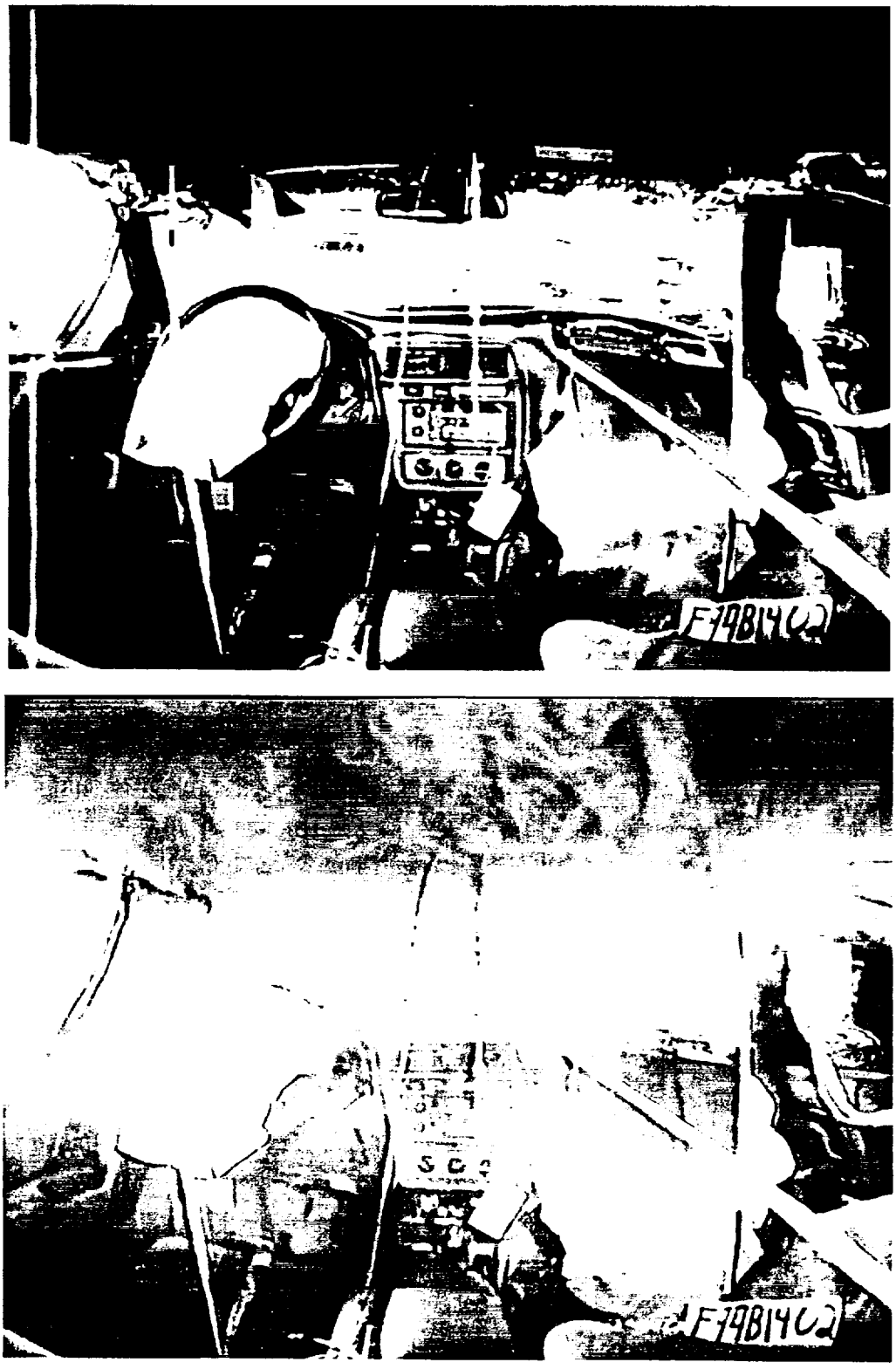


Figure 17. Fire Test F99B1402. Video Stills from Camera 1 at the time of ignition (upper video still) and at 7 minutes post-ignition (lower video still).


Figure 18. Video Stills from Camera 7 at 8 minutes post-ignition in Fire Test F99B1401 (upper video still) and in Fire Test F99B1402 (lower video still).

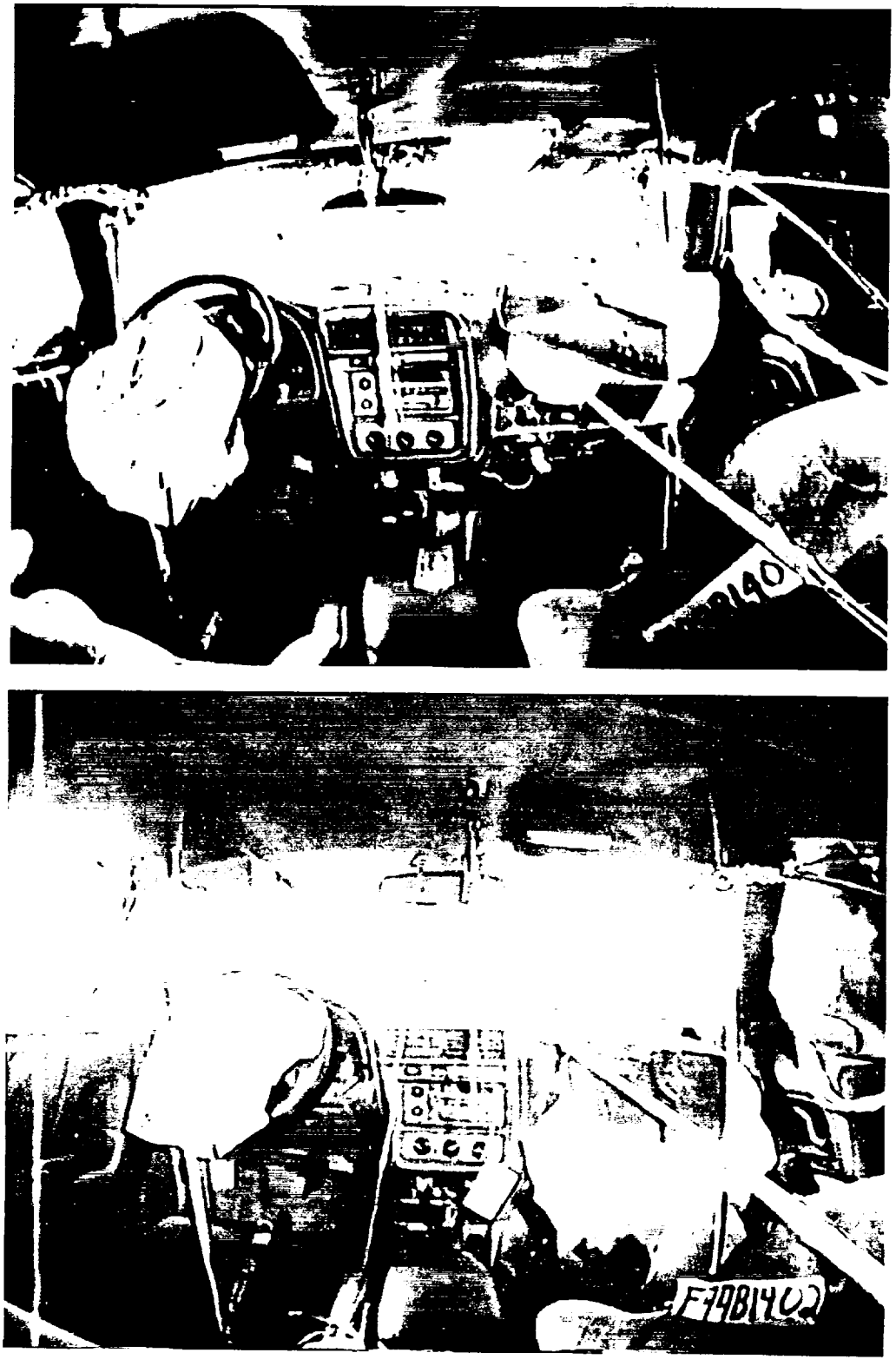

Figure 19. Video Stills from Camera 1 at 8 minutes post-ignition in Fire Test F99B1401 (upper video still) and Fire Test F99B1402 (lower video still).


Figure 20. Video Stills from Camera 1 at 12:30 min:sec post-ignition in Fire Test F99B1401 (upper video still) and in Fire Test F99B1402 (lower video still).

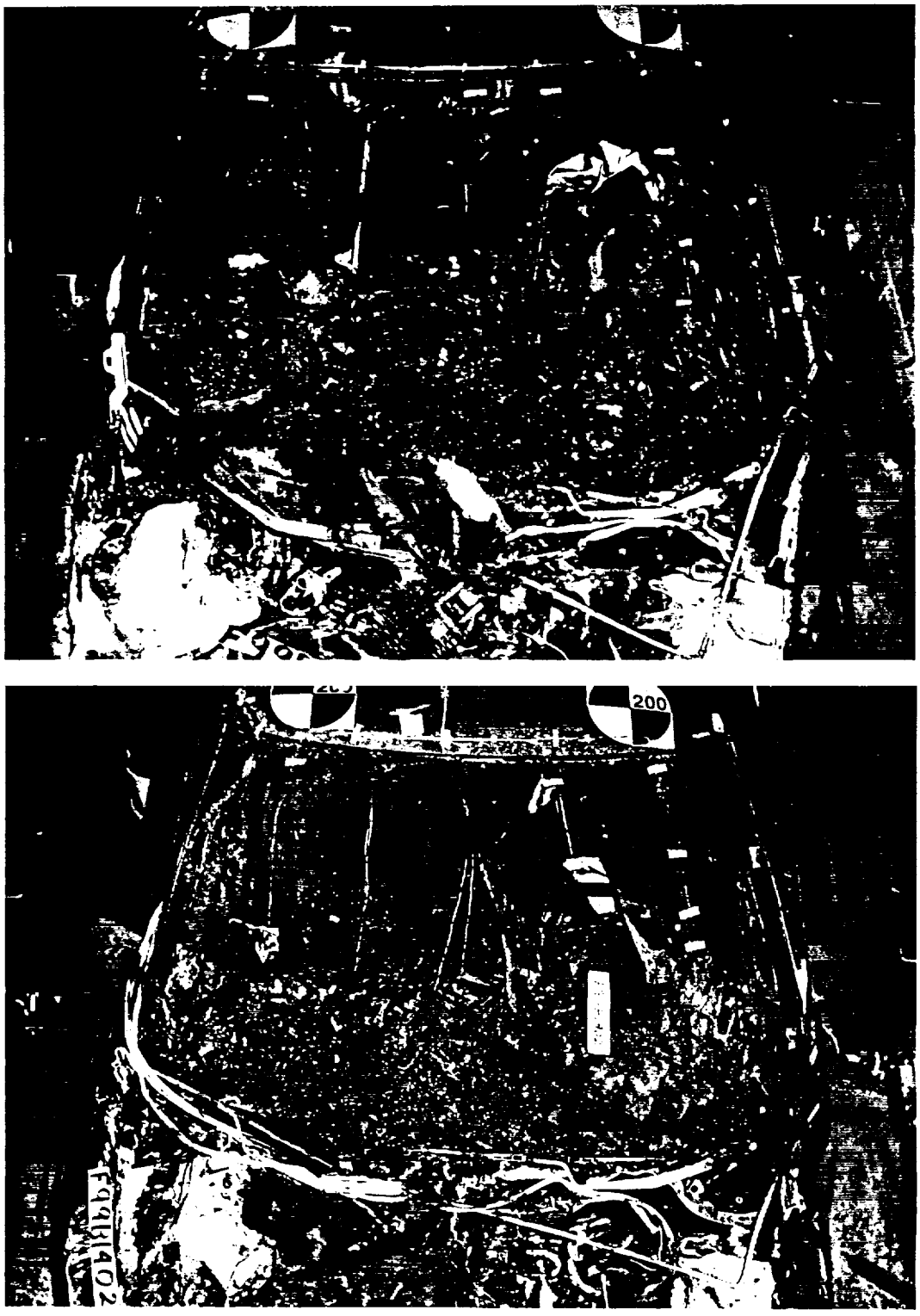


Figure 21. Photographs of the front of F99B1401 (upper photograph) and F99B1402 (lower photograph) after the fire tests. The hoods were removed for this photograph and were on the test vehicles during the fire tests.

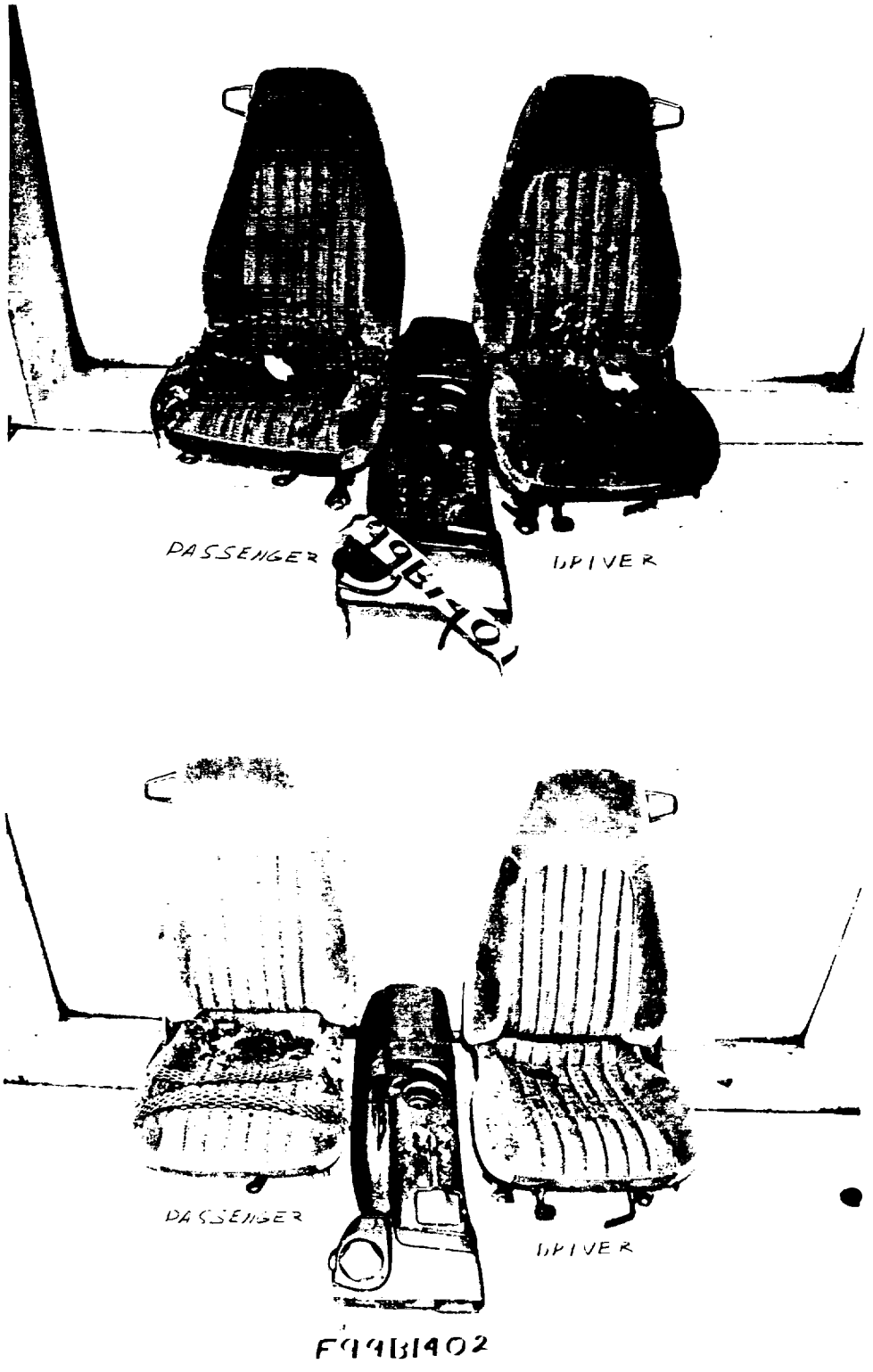


Figure 22. Photographs of the front seats and center console removed from F99B1401 (upper photograph) and F99B1402 (lower photograph) after the fire tests.

contained decabromodiphenyleneoxide, antimony trioxide, and zinc-based flame retardant chemicals (Table 2). Figure 23 shows photographs of the HVAC modules upper dash extension panel and lower windshield support panel were cut away. The section of the HVAC module that extends into the engine compartment is normally under the HVAC air intake cowl that is formed by the upper dash extension panel and lower windshield panel. In these test vehicles, the HVAC modules were fractured and pushed rearward further under the HVAC air intake cowl during the crash tests. The upper dash extension panel and lower windshield panel were partially removed to allow inspection of the HVAC modules before they were removed from the test vehicles. The photographs in Figure 23 show that the sections of the auxiliary A/C evaporator and blower upper cases that were above the A/C evaporator had burned during this test. In both test vehicles, the plastic had melted and sagged onto the A/C evaporator cores (Fig. 23). Some material in both HVAC modules was consumed by fire, and the residue on top of the A/C evaporator core was burned and charred (Fig. 23).

Figure 24 shows video stills from Camera 3 in both test vehicles at 11:30 min:sec post-ignition. Camera 3 was located in the lower part of the engine compartment under the HVAC modules looking upward. The views in Figure 24 show the exhaust manifold heat shield and right side of the engine block on the left, a section of the deformed dash panel on top, a section of the right front wheelhouse panel in the lower right corner, and the flange connecting the right exhaust manifold to the right exhaust take-down pipe in the lower left. The bottom of the auxiliary A/C evaporator and blower lower case is in the center of these video stills. These video stills show that the auxiliary A/C evaporator and blower lower cases in both test vehicles were exposed to flames in the areas above the right exhaust manifolds by 11:30 min:sec post-ignition. The views from Camera 3 in both test vehicles were obscured by smoke at later times, so the video record could not be used to accurately determine exposure of the HVAC module to flames after about 11:30 min:sec post-ignition.

Data recorded from thermocouples located inside the HVAC module indicate that both faces of the A/C evaporator core were heated by gases and flames between about 10 and 13 minutes post-ignition in F99B1401, and that the A/C evaporator core was not exposed to heated gases and flames at any time during this test in F99B1402. Figure 25 shows estimated temperature profiles on both faces of the A/C evaporator core in F99B1401 from 10 to 12:45 min:sec. The isothermal contours in this figure were calculated from temperature data recorded from the H-thermocouples using a three-dimensional interpolation algorithm.[7]

[7] Isothermal contours of the temperatures on both faces of the A/C evaporator core estimated temperature data recorded from thermocouples H1 through H18 using a three-dimensional interpolation algorithm available in SigmaPlot for Windows Version 4.00 [3]. This algorithm uses an inverse distance method to generated temperature values for points on a uniformly spaced Cartesian grid from input [x,y,t] triple data.


Figure 23. Photographs of the HVAC modules in F99B1401 (upper photograph) and F99B1402 (lower photograph) after the fire tests. The upper dash extension and lower windshield support panels were partially cut away for these photographs.

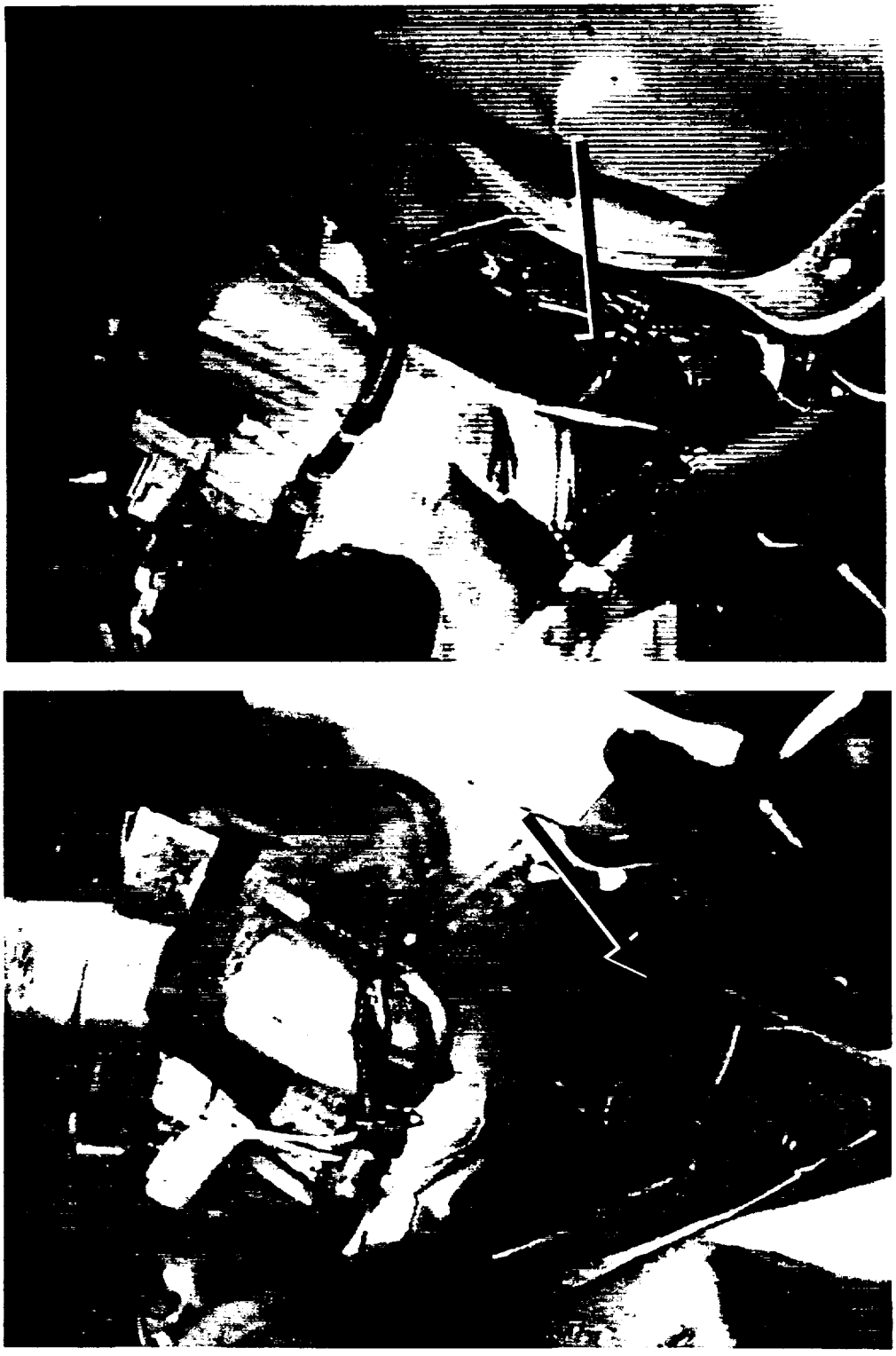

Figure 24. Video stills from Camera 3 in F99B1401 (upper photograph) and F99B1402 (lower photograph) at 11:30 min:sec post-ignition. The arrows indicate the bottom of the auxiliary A/C evaporator and blower lower case.

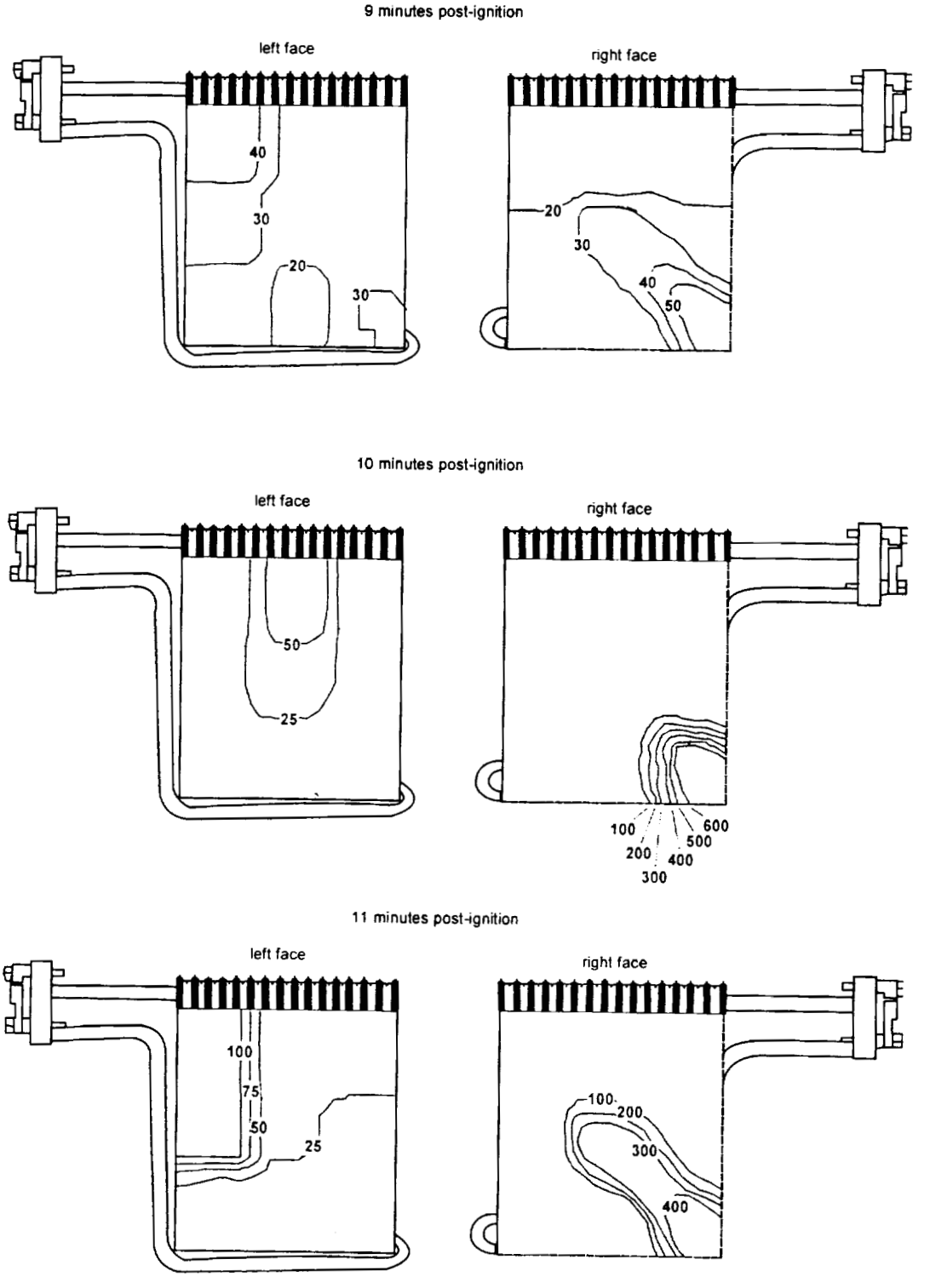


Figure 25. Fire Test F99B1401. Estimated temperature distributions on both faces of the A/C evaporator core of the test vehicles at 9, 10, 11, and 12 minutes post-ignition, and at 12:45 min:sec post-ignition.

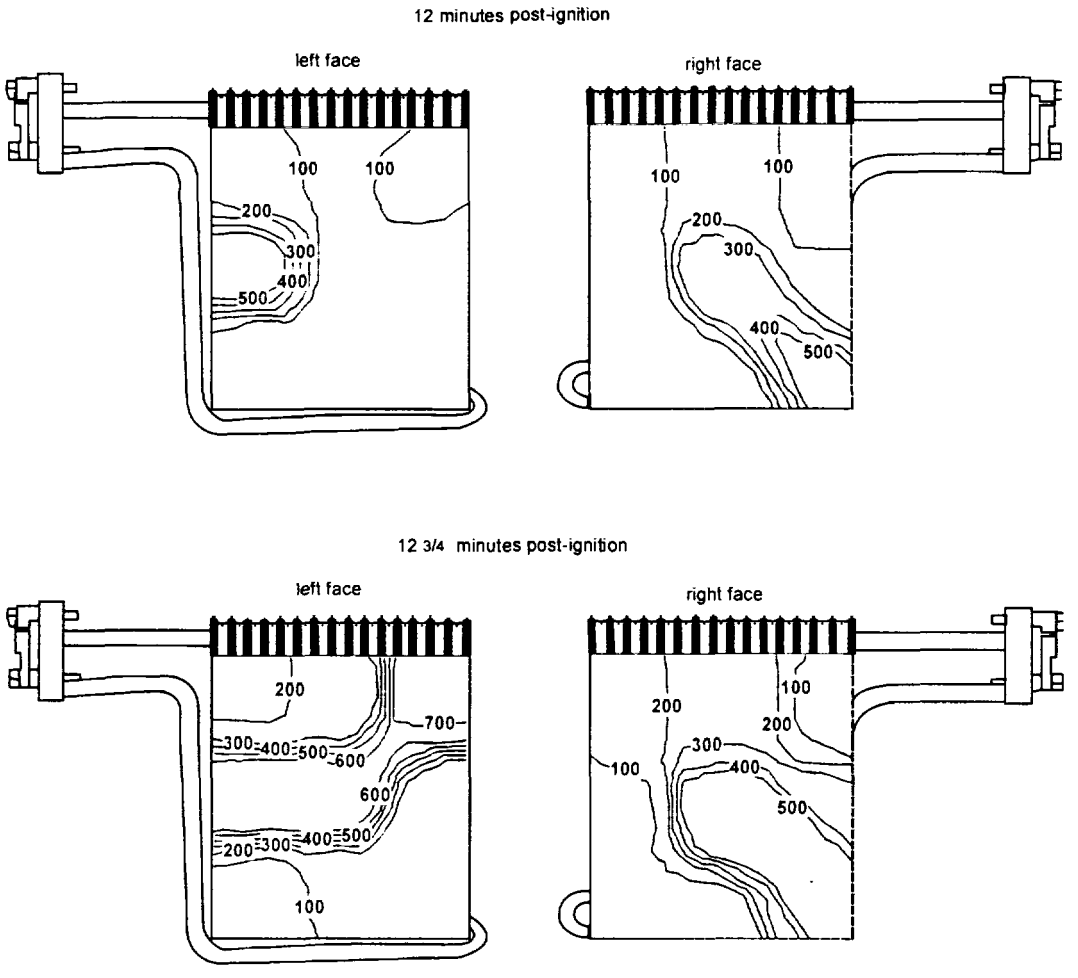


Figure 25, continued. Fire Test F99B1401. Estimated temperature distributions on both faces of the A/C evaporator core of the test vehicles at 9, 10, 11, and 12 minutes post-ignition, and at 12:45 min:sec post-ignition.

The thermocouples around the A/C evaporator core were located approximately 5 mm away from (in front of) the screens covering the right and left faces of the core. These thermocouples were heated by convection and radiation from heated gases and flames entering the broken HVAC module from the engine compartment. Thus, the estimated temperature profiles shown in Figure 25 indicate the approximate distribution of heated gases and flames along both faces of the A/C evaporator core. Data recorded from thermocouples in the HVAC module in the F99B1402 indicate that temperatures were < 400°C, therefore, estimated temperature distributions on the A/C evaporator core in F99B1402 are not shown here.

The HVAC module in the control vehicle was more extensively fractured than the HVAC module in the FR vehicle. Figure 26 shows photographs of the HVAC modules removed from the test


Figure 26. Photographs of the HVAC modules removed from F99B1401 (upper photograph) and F99B1402 (lower photograph) after the fire tests.

vehicles after these tests. Kinematic analysis of the high speed film from the crash tests indicated that the maximum dynamic pole penetrations into the test vehicles were 1309 mm in F99B1401 and 1224 mm in F99B1402 (Table 4). This resulted in approximately 85 mm more pole penetration into the right side right side of the engine compartment in F99B1401 than in F99B1402. As the principle direction of force in these crash tests was parallel to the longitudinal axes of the test vehicles and intersected the HVAC modules in the dash panels, this difference in dynamic crush resulted in more extensive breakage to the HVAC module in F99B10410 than in F99B1402 (Fig. 26). The auxiliary A/C evaporator and blower upper and lower cases in the HVAC module from F99B1402 was cracked in several places, with a section of the dash mounting flange separated from the lower case (lower photograph, Figure 26). In contrast, the HVAC module in F99B1401 was more extensively cracked, with a number of pieces separated from the auxiliary A/C evaporator and blower upper and lower cases (upper photograph, Figure 26). The estimated temperature distributions on the A/C evaporator core (Fig. 25) indicate that heated gases and flames from the engine compartment penetrated the section of the HVAC module exterior to the dash panel in F99B1401 through these openings. Inspection of the HVAC modules from the test vehicles after these tests indicted that only the sections of the auxiliary A/C evaporator and blower upper cases that were above the A/C evaporator core had burned (Fig. 23). There was no evidence of fire damage to the auxiliary A/C evaporator and blower lower cases in either of the test vehicles (Fig. 26), indicating that the polyester resin in this component did not ignite and burn during these tests.

The video records from Camera 2 indicated that flames did not spread into the section of the HVAC module in the instrument panel. Camera 2 was on the right front seat cushion focused through the instrument panel storage box opening on the HVAC modules interior to the dash panel (see **Appendix G**). Video stills from Camera 2 at 12:45 min:sec post-ignition show no flames on the sections of the HVAC modules visible in these views just before these tests were ended and fire suppression began. Quartz halogen lights placed in the test vehicles to illuminate the under-sides of the instrument panels during these tests produced the glow in the lower right corners of the video stills in Figure 27. Data recorded from thermocouples in the sections of the HVAC modules interior to the dash panel showed temperatures < 350°C throughout each test (**Appendix H**). No evidence of fire damage to the sections of the HVAC modules in the instrument panel was observed during the physical inspection of the test vehicles after these tests (Fig. 28). Thus, the video record, the thermocouple data, and burn pattern in the test vehicles indicate that flames did not spread through the HVAC modules into the instrument panels of either test vehicle during these tests.

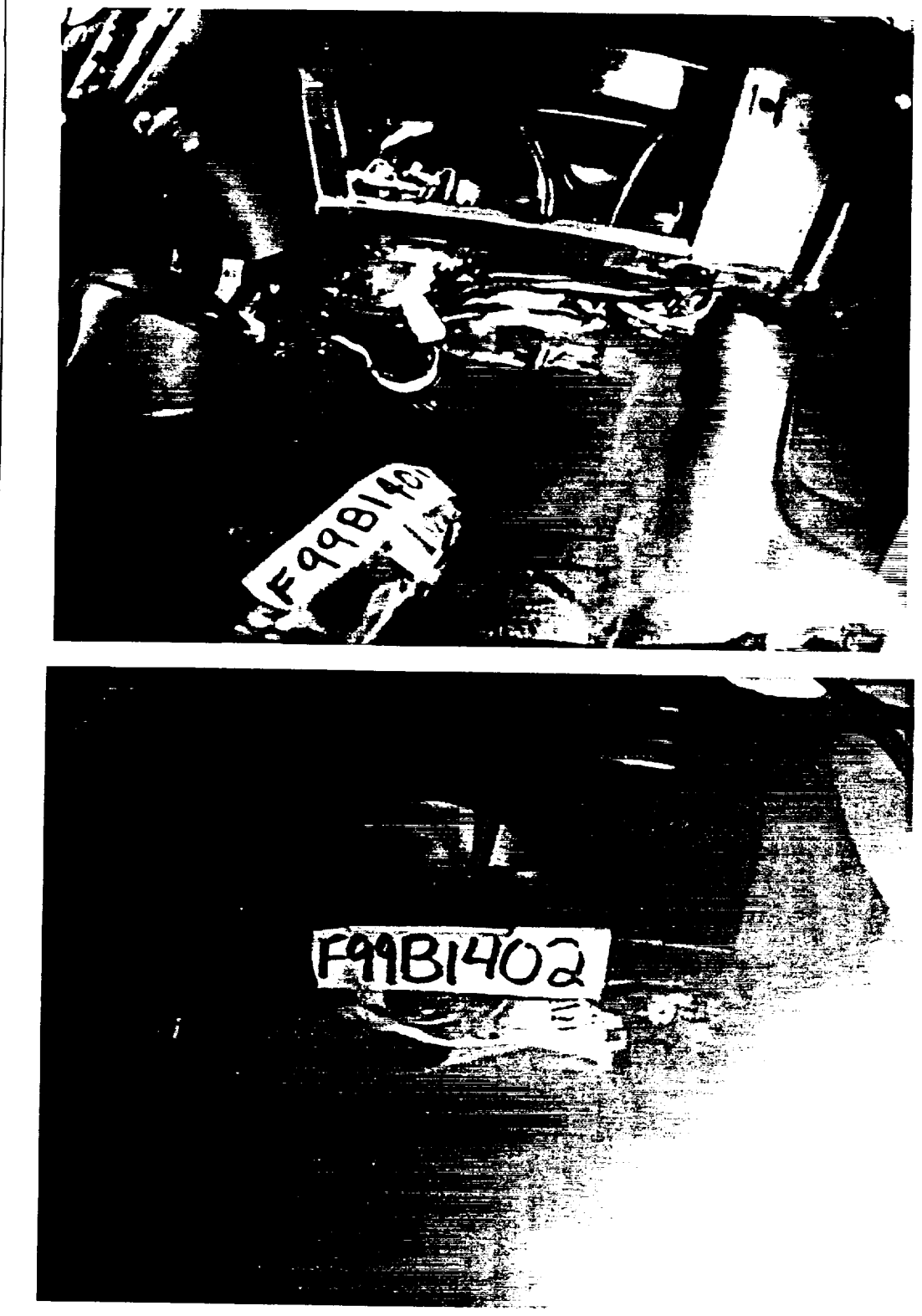


Figure 27. Video stills from Camera 2 at 12:45 min:sec post-ignition from F99B1401 (upper video still) and F99B1402 (lower video still).

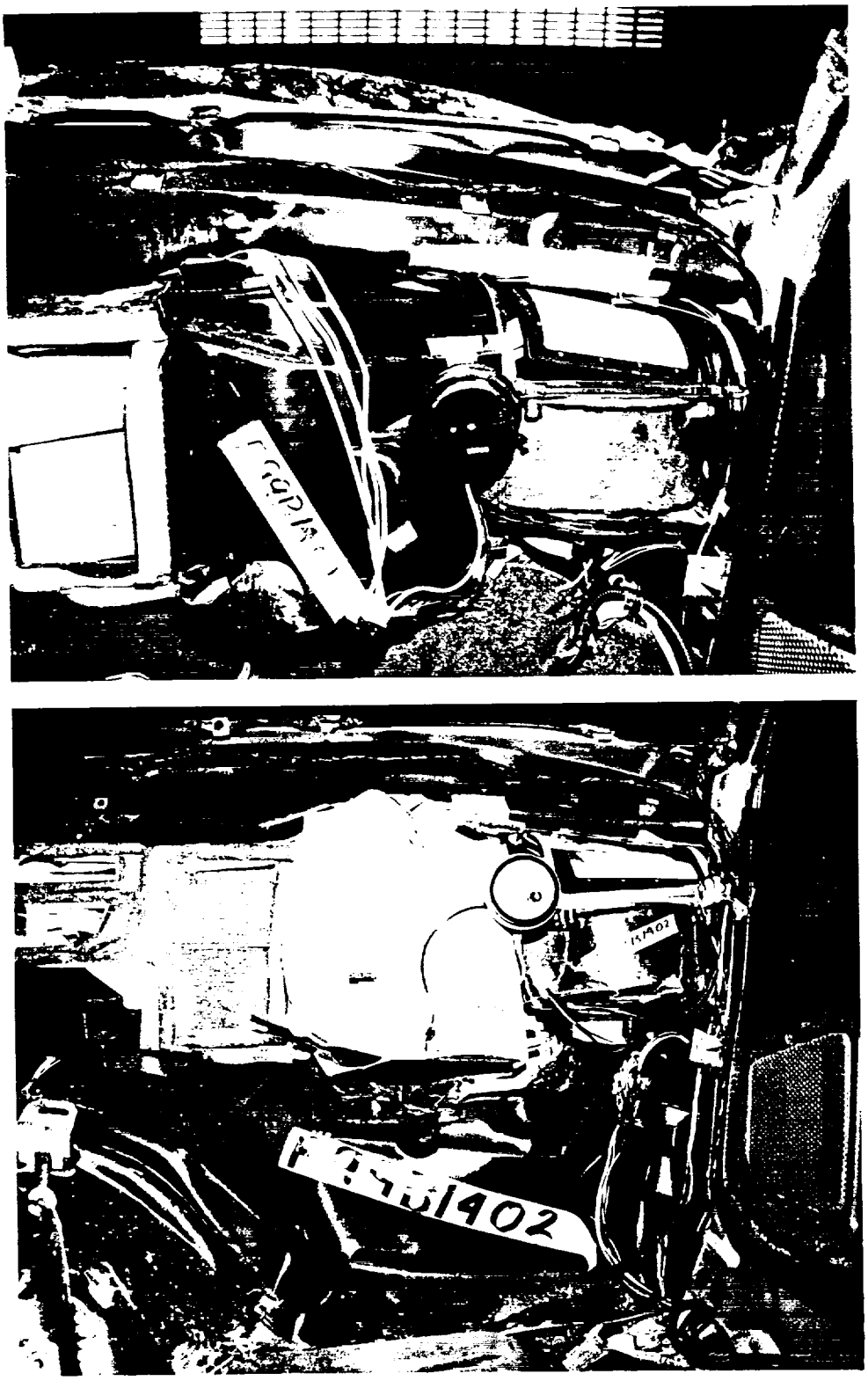

Figure 28. Photographs of the HVAC modules in F99B1401 (upper photograph) and F99B1402 (lower photograph) after these tests.

### 4.4.3 Conditions in the passenger compartment

Air temperatures in the passenger compartments of the test vehicles were measured with aspirated thermocouple assemblies (**Appendix I**). One aspirated thermocouple assembly was installed between the front seats in each of the test vehicles and was oriented vertically. The aspirated thermocouple assemblies contained 6 thermocouples each. The spacing between thermocouples was 3 inches, with the upper-most thermocouple located between ½ to 1 inch below the lower surface of the headlining trim panels. Figures 29 and 30 show plots of temperature data recorded from the aspirated thermocouples in F99B1401 and F99B1402, respectively. Air temperatures just below the headlining trim panel started to increase between 5 and 10 minutes post-ignition in both test vehicles, reaching maxima of 160°C at 12:56 min:sec post-ignition in F99B1401 and 114°C at 12:58 min:sec post-ignition in F99B1402. Air temperature decreased as distance below the headlining trim panel increased. For example, air temperatures recorded approximately 18 inches below the lower surface of the headlining trim panel reached maxima of 50°C at 13:15 min:sec post-ignition in F99B1401 and 44°C at 13:19 min:sec post-ignition in F99B1402. This data indicates that a burning upper layer did not develop in either of the test vehicles at any time during these tests.

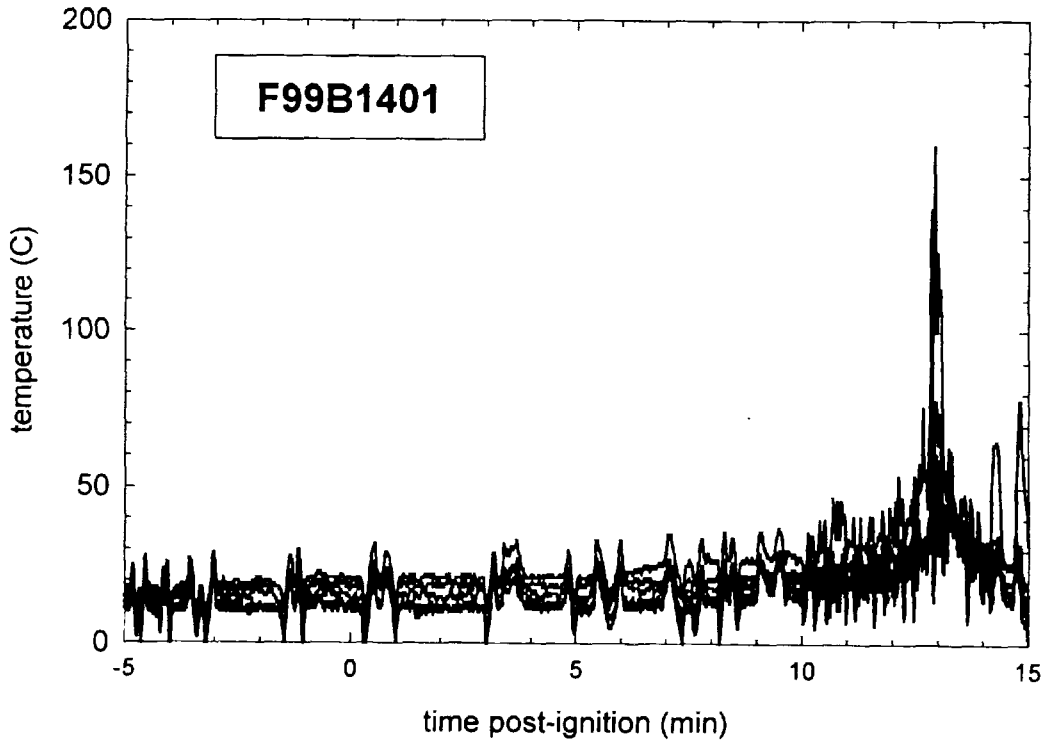


Figure 29. Fire Test F99B1401. Plots of temperature data recorded from the aspirated thermocouple assembly.

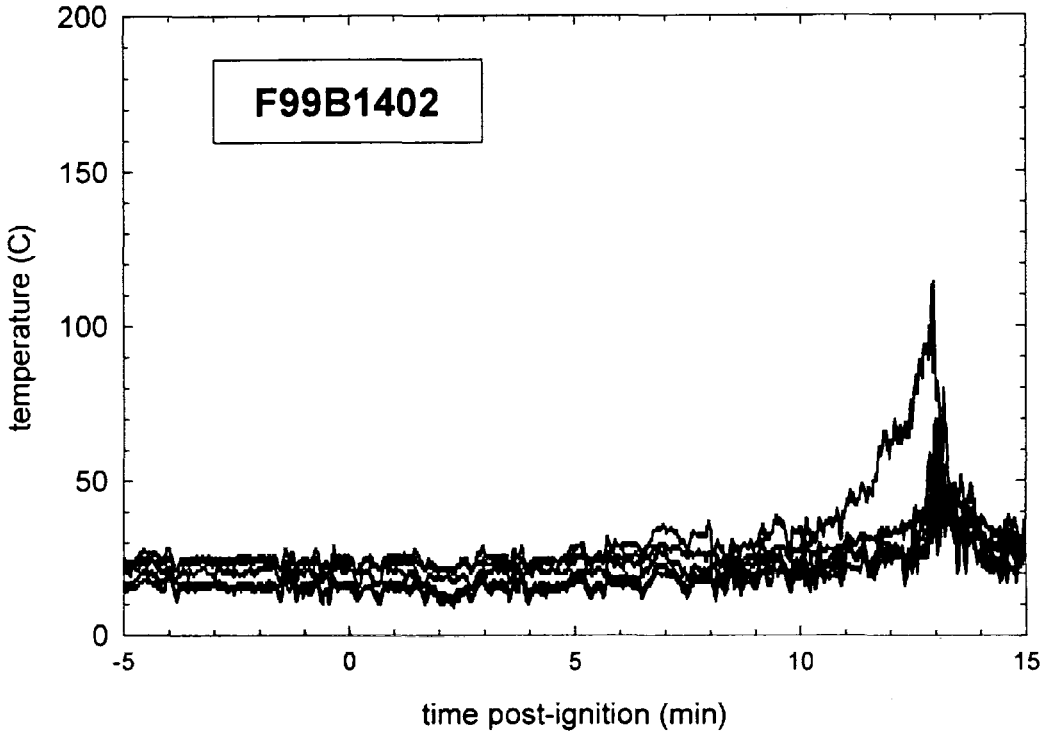


Figure 30. Fire Test F99B1402. Plots of temperature data recorded from the aspirated thermocouple assembly.

Heat flux transducer/radiometer assemblies were located above both front seats in the test vehicles (**Appendix J**). These transducers measured the convective and radiative heat fluxes to vertical, forward-facing planes approximately 30 inches above the centers of the seat cushions. Figures 31 and 32 show plots of temperature data recorded from the heat flux transducer/radiometer assemblies above the left front seats in F99B1401 and F99B1402. In both tests, the radiative heat fluxes increased from background levels at about 7 minutes post-ignition (Fig.'s 31 and 32), which was coincident with the timing of sections of the windshields first starting to fall onto the instrument panel upper trim panel and holes developing in the windshield. The radiative heat fluxes increased exponentially until the tests were ended and the fires extinguished just before 13 minutes post-ignition, (Fig.'s 31 and 32). The peak heat flux recorded during F99B1401 was 15.9 kW/m2 at 12:49 min:sec post-ignition and the peak heat flux recorded during F99B1402 was as 15.8 kW/m2 at 12:51 min:sec post-ignition (Fig.'s 31 and 32). The convective heat fluxes to these transducers did not change significantly from background levels during these tests (Fig.'s 31 and 32).

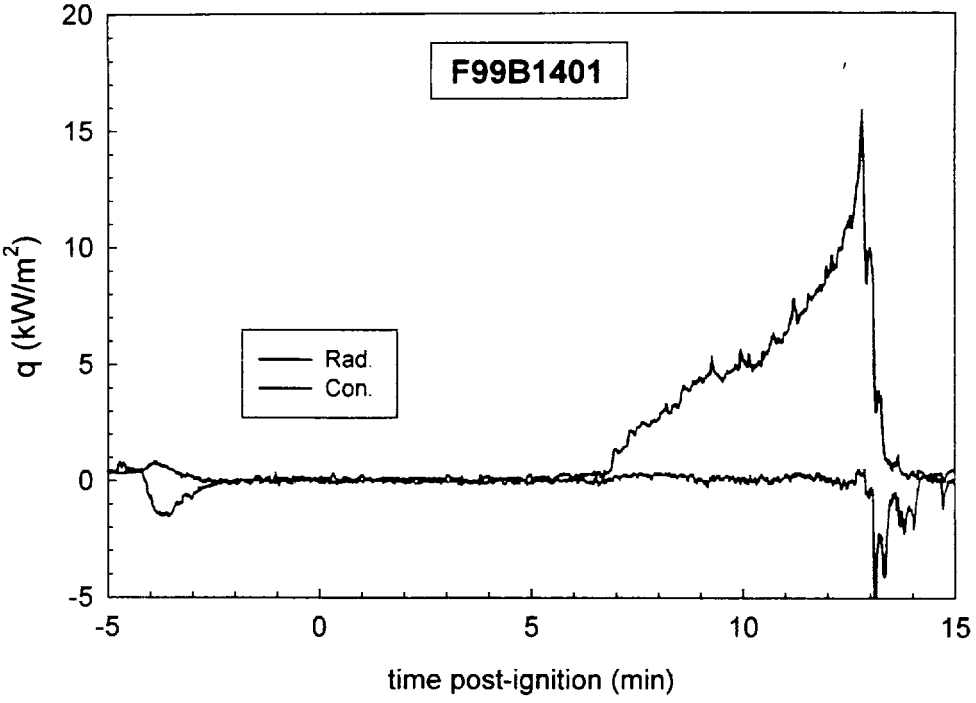


Figure 31. Fire Test F99B1401. Plots of radiative and convenctive heat fluxes measured by a heat flux transducer/radiometer assembly above the left front seat.

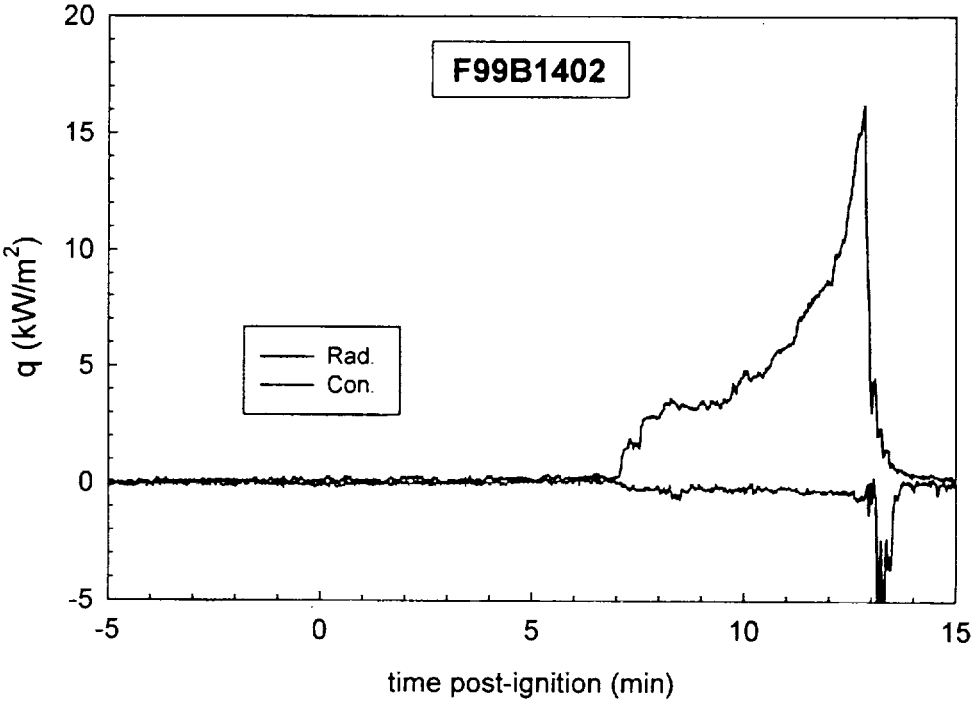


Figure 32. Fire Test F99B1402. Plots of radiative and convenctive heat fluxes measured by a heat flux transducer/radiometer assembly above the left front seat.

This heat flux data indicates that thermal radiation from the fire plume at the rear of the deformed hoods started to reach the surfaces of the heat flux transducer/radiometer assemblies when holes started to develop in the windshields of the test vehicles. The radiative heat fluxes to these transducers increased as the size of the openings in the windshields increased and the intensities of the fires in the engine compartments of the test vehicles increased. The measured convective heat fluxes remained constant from the times of ignition to the times these tests were ended. The temperatures of the transducers were maintained between 60 and 70°C by circulation of a thermostated fluid through the transducer bodies. The convective heat flux data plotted in Figures 31 and 32 indicates that the temperature of the air surrounding these transducers was not substantially greater than the temperatures of the transducer bodies themselves, resulting in no net heat exchange between the transducers and the surrounding air and no measured convective heat flux. This is consistent with air temperatures < 100°C at the elevation of the heat flux transducer/radiometer assemblies measured in the passenger compartments of the test vehicles during these tests (Fig.'s 29 and 30). The negative deflections in the convective heat flux plots occurring between 13 and 15 minutes post-ignition indicate cooling of the transducer bodies caused by the water spray used to extinguish the fires.

During these tests, combustion products such as smoke and carbon monoxide entered the passenger compartments of the test vehicles before flames spread to the instrument panel upper trim panel. The amount of smoke and the concentration of carbon monoxide in the passenger compartment of F99B1402 was substantially greater than the amount of smoke and the concentration of carbon monoxide in the passenger compartment of F99B1401. For example, a few diffuse streams of smoke were visible emanating from the broken HVAC module in F99B1401 by 7 minutes post-ignition (lower video still, Fig. 16). In contrast, smoke visible in F99B1402 at 7 minutes post-ignition almost totally obscured the headlining trim panel (lower video still, Fig. 17). Figure 33 shows plots of the carbon monoxide concentrations in the passenger compartments of F99B1401 and F99B1402 during these tests (**Appendix L**). The concentrations of carbon monoxide in the passenger compartments show peaks of 38 ppm at 7:03 min:sec in F99B1401 and 1024 ppm at 6:35 min:sec in F99B1402 (Fig. 33). Smoke and carbon monoxide cleared from the passenger compartments of both test vehicles starting at about 7 minutes post-ignition, which was coincident with the timing of the development of openings in the windshields of both test vehicles. In both test vehicles, thermal convection created by the fire plume above the engine compartment caused air to be drawn out of the passenger compartment through the opening in the windshield. Clean outside air flowed into the passenger compartment through the open right side window, which resulted in dilution of the smoke and carbon monoxide.

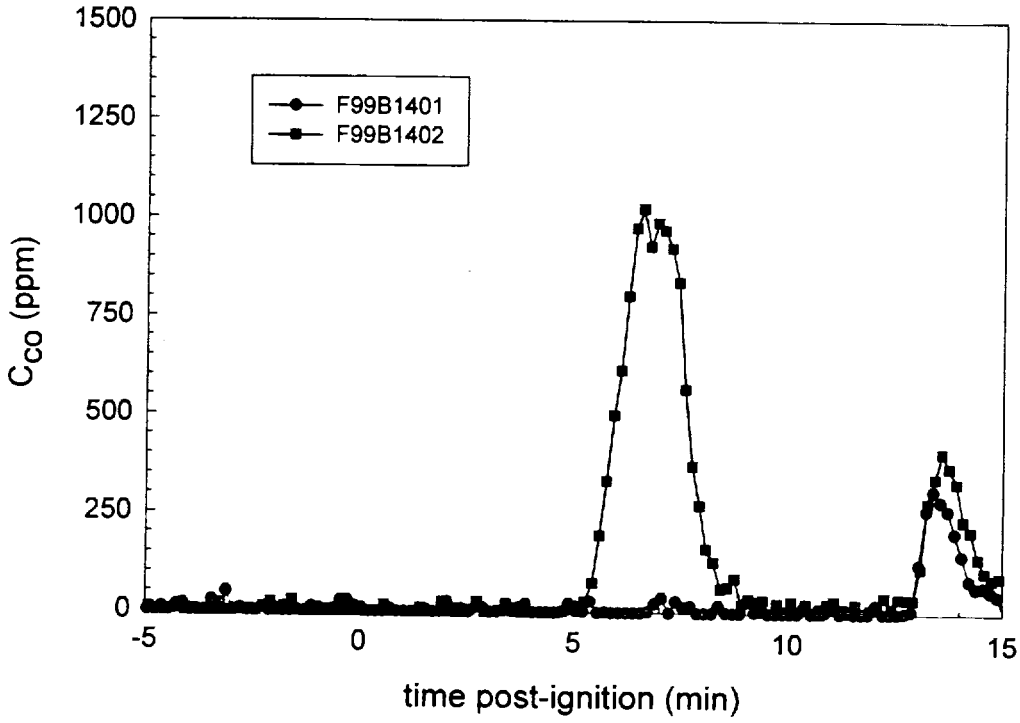


Figure 33. Plots of carbon monoxide concentration measured in the passenger compartments of the control vehicle (F99B1401) and FR vehicle (F99B1402).

## 5 Summary

The tests described here were conducted to assess the effect of substituting plastic materials containing flame retardant chemicals in the HVAC module on the path and rate of flame spread from a fire ignited in the engine compartment. The HVAC module in the control vehicle was constructed from materials typical of those found in HVAC modules in vehicles sold in 1999. The HVAC module in the FR vehicle was constructed from materials that contained flame retardant chemicals in sufficient concentration to produce a V-0 rating in UL-94 Tests for Flammability of Plastic Materials for Parts in Devices and Appliances, a vertical flammability test [2].

Both test vehicles were crash tested using identical crash test protocols. The vehicle kinematics during the crash tests were similar, as was the damage to the test vehicles. The maximum dynamic crush to the control vehicle during the crash test was approximately 85 mm greater than the maximum dynamic crush to the FR vehicle during the crash test.

The crash tested vehicles were used in fire tests. Both test vehicles were prepared identically for the fire tests. The ignition protocols were the same in both tests. Differences in the shape and orientation of the deformed hoods of the test vehicles resulted in a difference in the timing of flame-spread in the engine compartments and the heat release rates of the fires for the first 5 minutes of these tests. The distributions of flames in the engine compartments of the test vehicles were essentially the same by about 6 minutes post-ignition. The heat release rate curves were identical from about 5 ½ minutes post-ignition through the end of these tests.

The windshield opening was the principle path for flame-spread from the engine compartment into the passenger compartment in both tests. Both tests were ended when flames had spread rearward on the instrument panel upper trim panel and pieces of burning windshield were observed falling into the passenger compartment. This was at 12:47 min:sec for F99B1401 and 12:50 min:sec for F99B1402. Fire suppression began at about 13 minutes post-ignition in both tests.

Combustion products such as smoke and carbon monoxide entered the passenger compartments of the test vehicles before flames spread through the windshield opening to the instrument panel upper trim panel. Analysis of the video records from both tests indicated that the amount of smoke in the passenger compartment of FR vehicle was greater than the amount of smoke in the passenger compartment of control vehicle. The Fourier transform infrared gas analysis data indicated that the concentration of carbon monoxide in the passenger compartment of the FR vehicle was greater than the concentration of carbon monoxide in the control vehicle. The peak

carbon monoxide concentration in the FR vehicle was approximately 27X the peak carbon monoxide concentration in the control vehicle.

Inspection of the test vehicles after these tests revealed that the top sections of the auxiliary A/C and blower upper cases had ignited and burned in both test vehicles. The auxiliary A/C and blower upper case in F99B1401 was made from 40% talc-filled poly(propylene) resin. The auxiliary A/C and blower upper case in F99B1402 was made from polypropylene containing antimony trioxide, decabromodiphenyloxide, and zinc-based flame retardant chemicals. The analysis in Section 4.3 indicates that the auxiliary A/C and blower upper cases were exposed to flames starting at about 05:40 min:sec post-ignition in F99B1401 and 04:00 min:sec post-ignition in F99B1402 (Fig. F). The section of the auxiliary A/C and blower upper case above the A/C evaporator core was burned in both test vehicles (Fig.'s T1 and T4). The amount of material consumed by fire appeared to be about the same in the control HVAC module as in the FR HVAC module. Thus, substitution of plastic materials containing flame retardant chemicals in the HVAC module did not result in an observable difference in the flammability of the HVAC module in these tests.

Substitution of plastic materials containing flame retardant chemicals in the HVAC module did not affect the rate of flame-spread from the engine compartment into the passenger compartment during these tests. The auxiliary A/C and blower upper cases in both HVAC modules were burned to the same extent. The concentrations of smoke and carbon monoxide in the passenger compartment of the FR vehicles were substantially greater than the concentrations of smoke and carbon monoxide in the passenger compartment of the control vehicle.

## ACKNOWLEDGEMENTS

Dr. Archibald Tewarson of Factory Mutual Research Corporation provided the data from the Fire Products Collector at the test facility that was collected during this test.

## REFERENCES


1. Jack L. Jensen and Jeffrey Santrock. Evaluation of Motor Vehicle Fire Initiation and Propagation. Part 5: Crash Tests on a Rear Wheel Drive Passenger Car. Submitted to the National Highway Transportation Safety Administration pursuant to the Settlement Agreement between General Motors and the Department of Transportation. Submitted March 7, 2001.

2. See reference for RTP-156 on www.rtpcompany.com/info/ul/100.htm.

3. Augustus Chidester, John Hinch, Thomas C. Mercer, and Keith S. Schultz. Recording Automotive Crash Event Data. Presented at the International Symposium on Transportation Recorders, Arlington, Virginia, May 3 – 5, 1999.

4. SigmaPlot® 4.0 for Windows®, SPSS Inc., 444 North Michigan Avenue, Chicago, IL 60611. Copyright © 1997 by SPSS Inc..

## Appendix A

## Crash Tests C12730 and C12731
## Accelerometer Data

Four tri-axial (longitudinal, lateral, and vertical) accelerometers were mounted to each of the test vehicles in the following locations:

- Right front rocker panel
- Left front rocker panel
- Right Rear Rocker Panel
- Left Rear Rocker Panel

Figure A1 shows the approximate locations of the accelerometers on the test vehicles

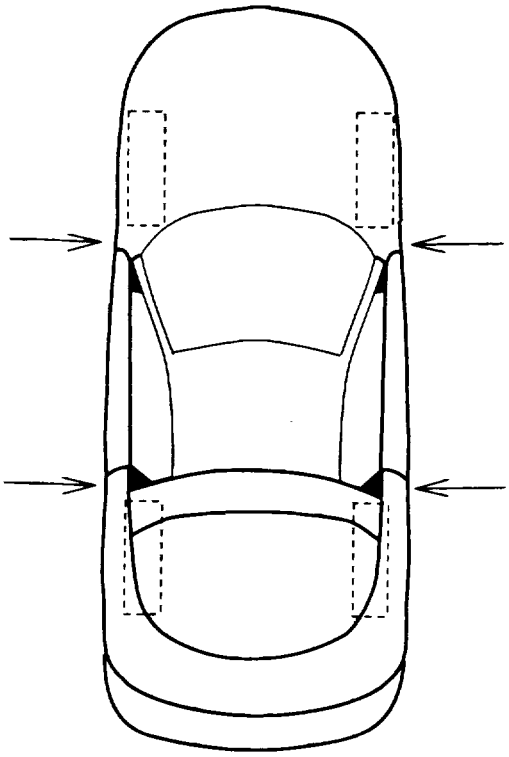

Figure A1. Diagram showing the approximate locations of the accelerometers on the test vehicles.

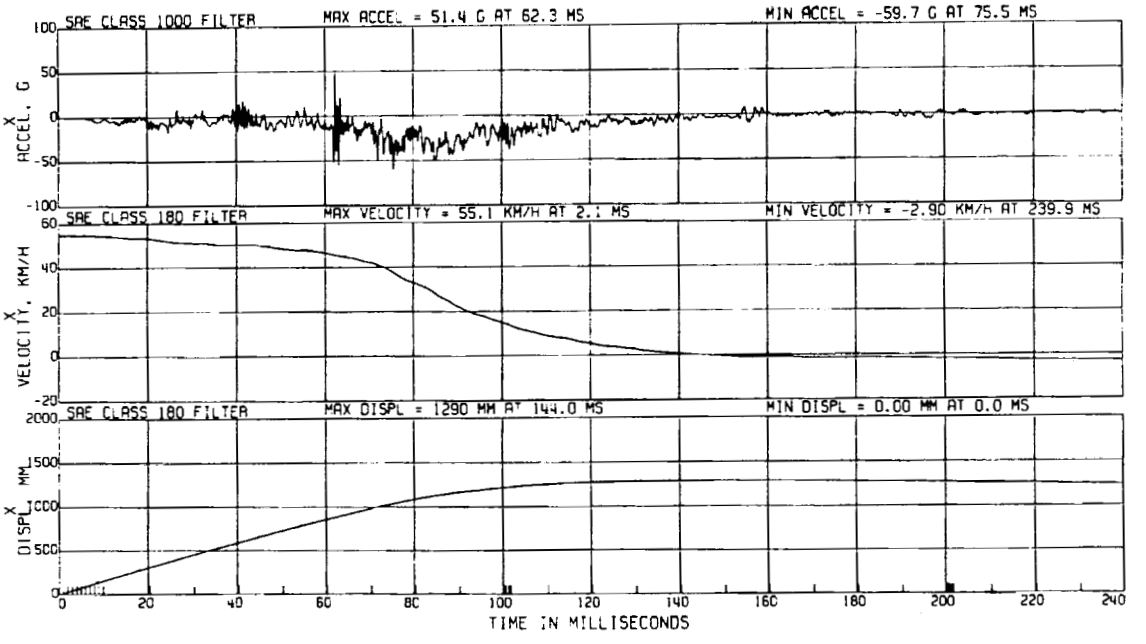


Plot A1. Crash Test C12730. Plots of acceleration, velocity, and displacement in the direction of the X-axis calculated from the accelerometer on the left front rocker.

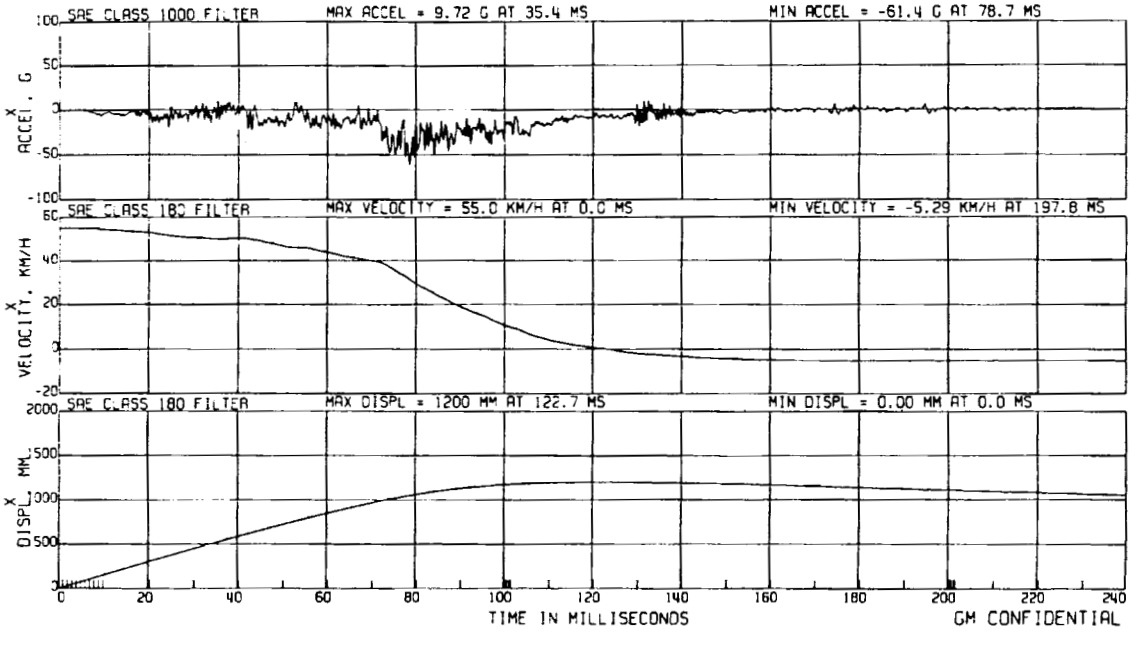


Plot A2. Crash Test C12731. Plots of acceleration, velocity, and displacement in the direction of the X-axis calculated from the accelerometer on the left front rocker

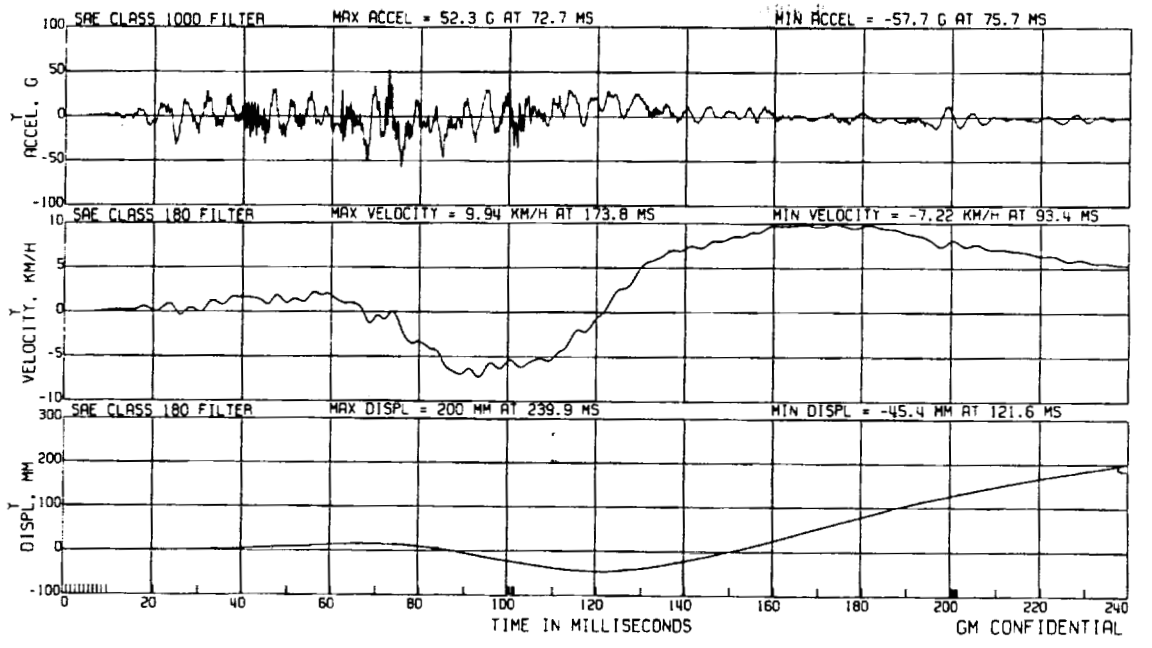


Plot A3. Crash Test C12730. Plots of acceleration, velocity, and displacement in the direction of the Y-axis calculated from the accelerometer on the left front rocker.

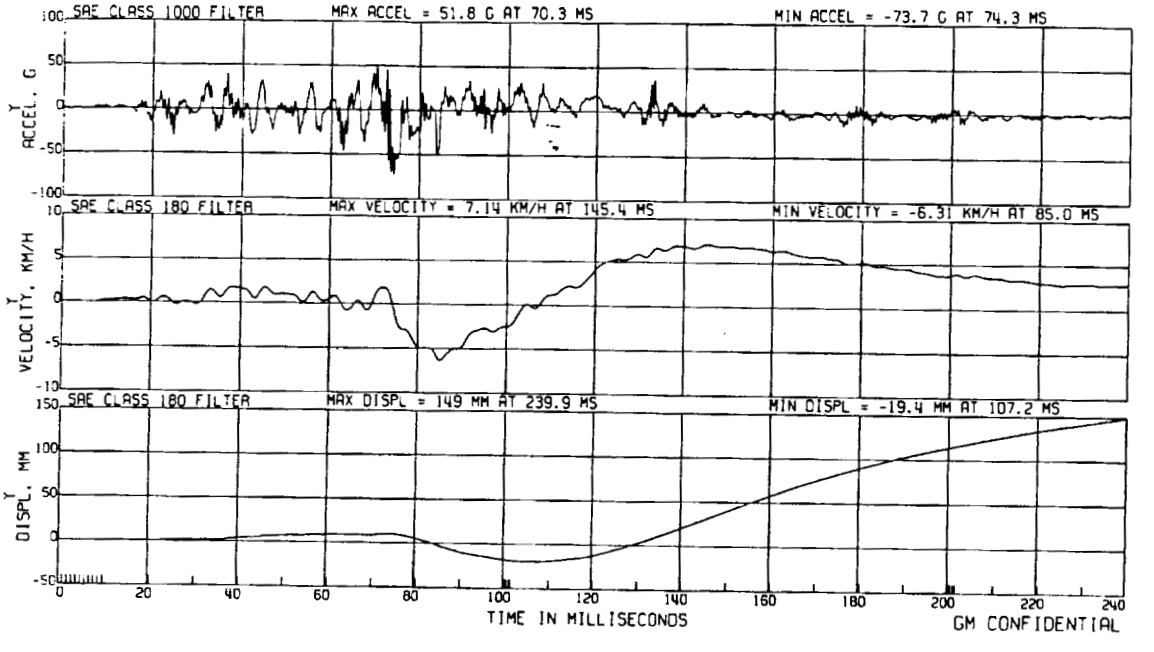


Plot A4. Crash Test C12731. Plots of acceleration, velocity, and displacement in the direction of the Y-axis calculated from the accelerometer on the left front rocker.

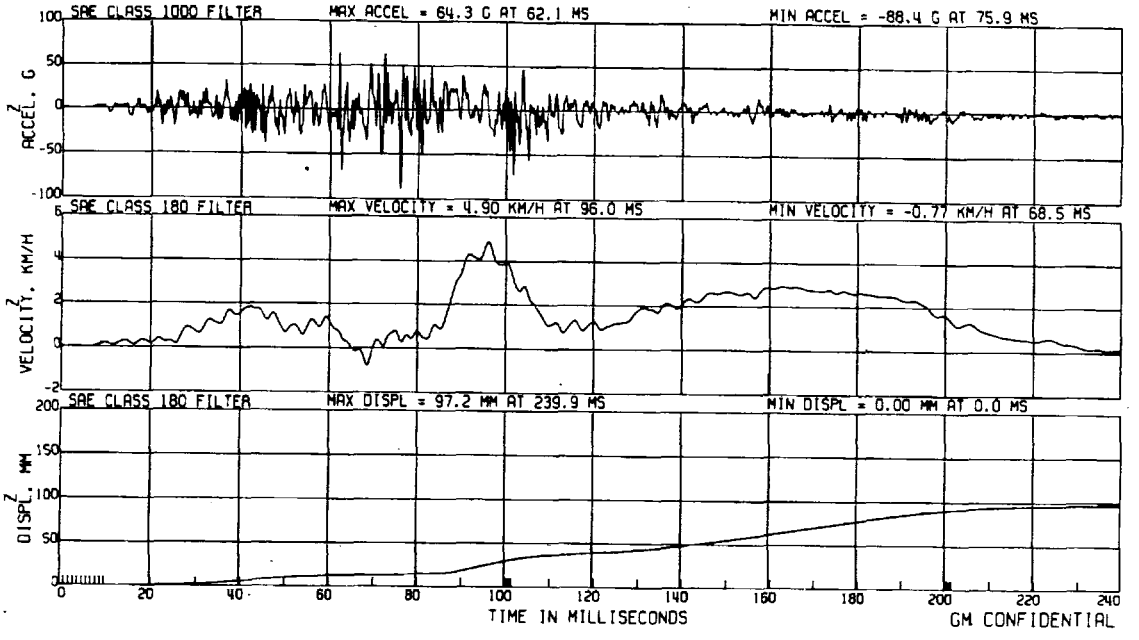


Plot A5. Crash Test C12730. Plots of acceleration, velocity, and displacement in the direction of the Z-axis calculated from the accelerometer on the left front rocker.

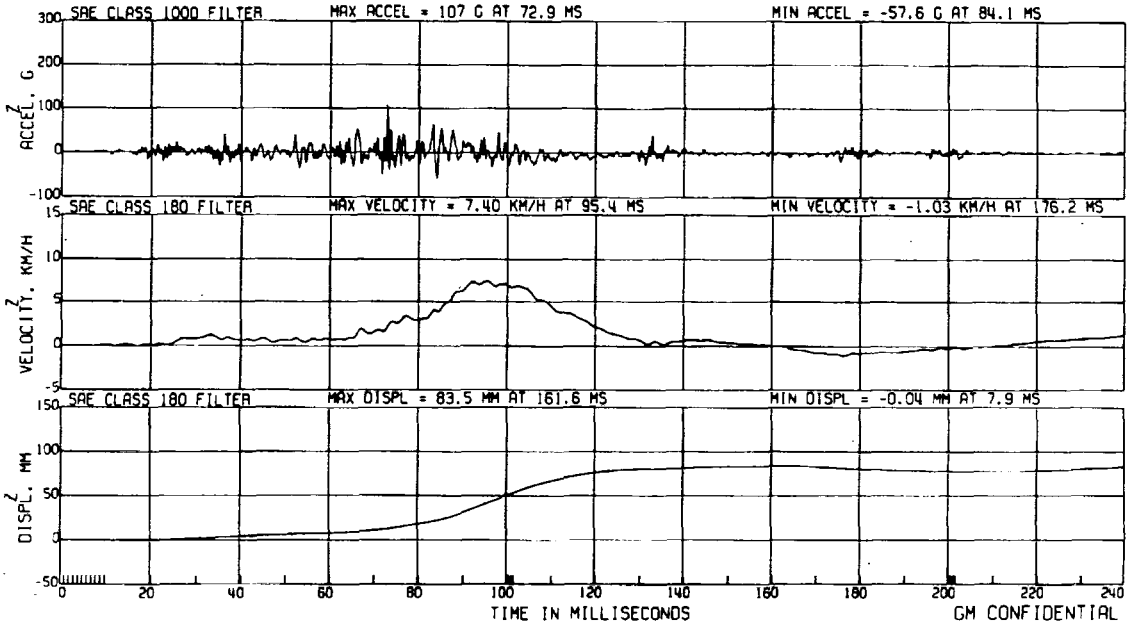


Plot A6. Crash Test C12731. Plots of acceleration, velocity, and displacement in the direction of the Z-axis calculated from the accelerometer on the left front rocker.

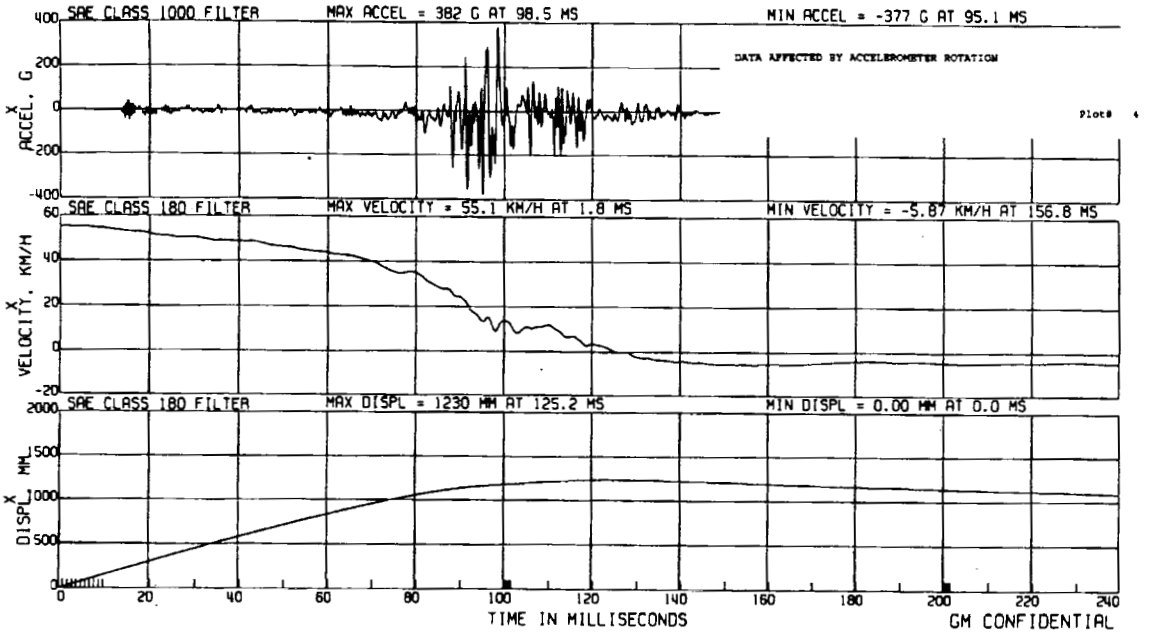


Plot A7. Crash Test C12730. Plots of acceleration, velocity, and displacement in the direction of the X-axis calculated from the accelerometer on the right front rocker.

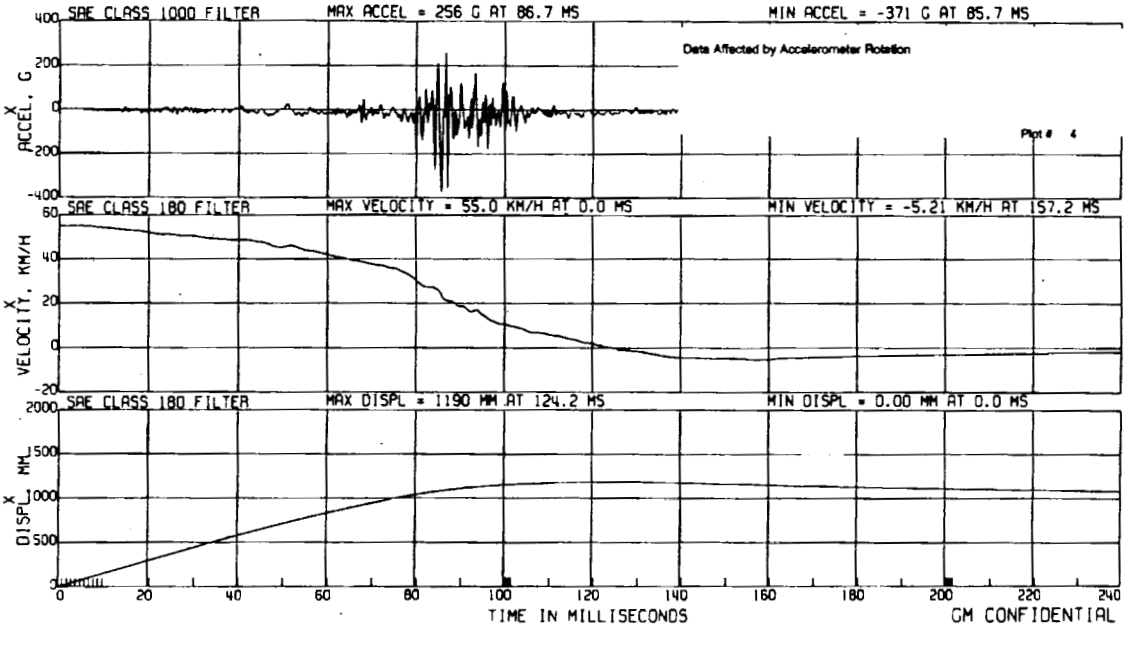


Plot A8. Crash Test C12731. Plots of acceleration, velocity, and displacement in the direction of the X-axis calculated from the accelerometer on the right front rocker.

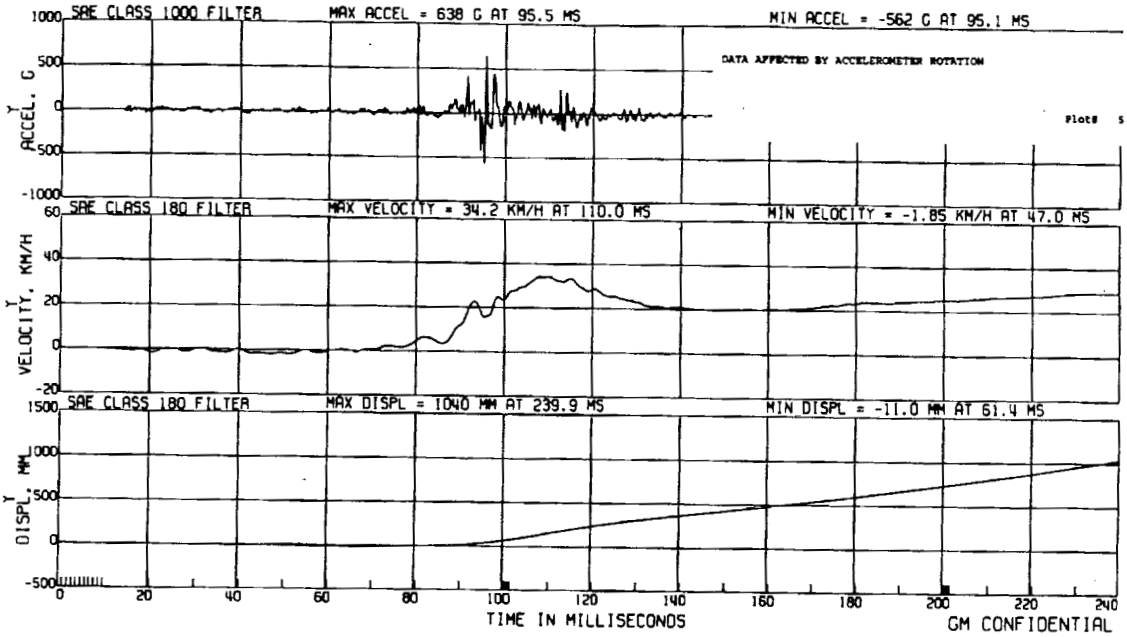


Plot A9. Crash Test C12730. Plots of acceleration, velocity, and displacement in the direction of the Y-axis calculated from the accelerometer on the right front rocker.

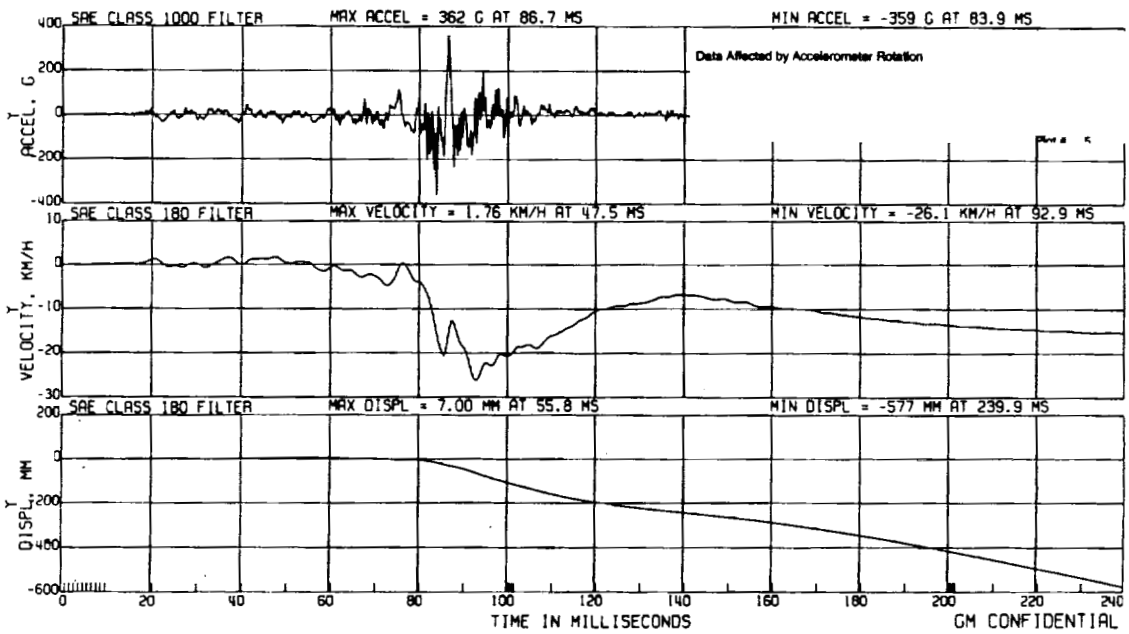


Plot A10. Crash Test C12731. Plots of acceleration, velocity, and displacement in the direction of the Y-axis calculated from the accelerometer on the right front rocker.

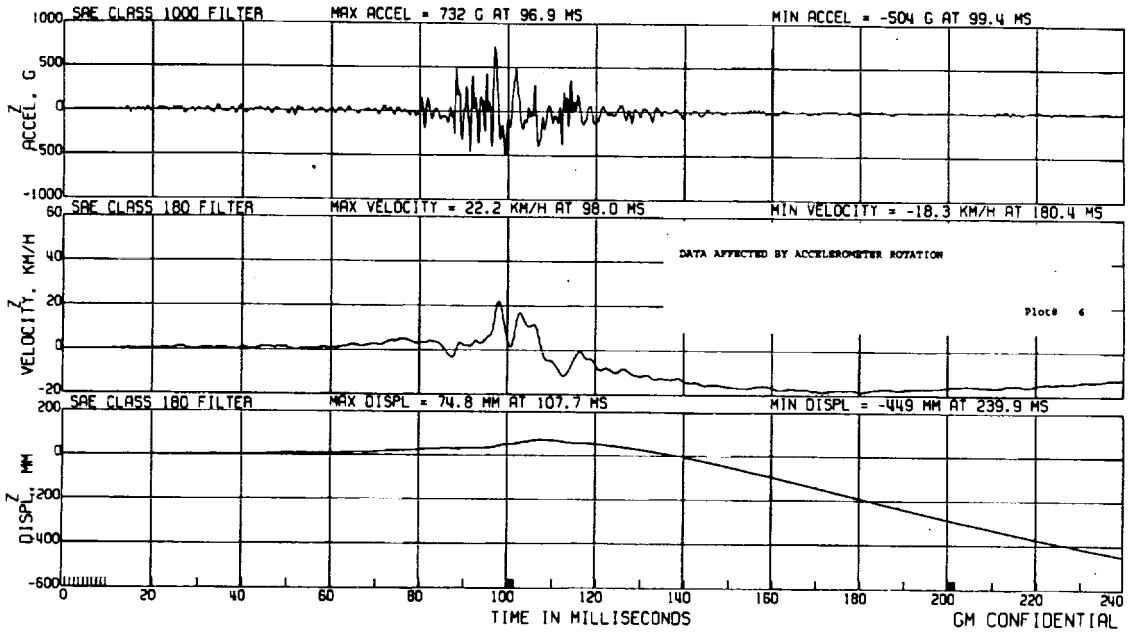


Plot A11. Crash Test C12730. Plots of acceleration, velocity, and displacement in the direction of the Z-axis calculated from the accelerometer on the right front rocker.

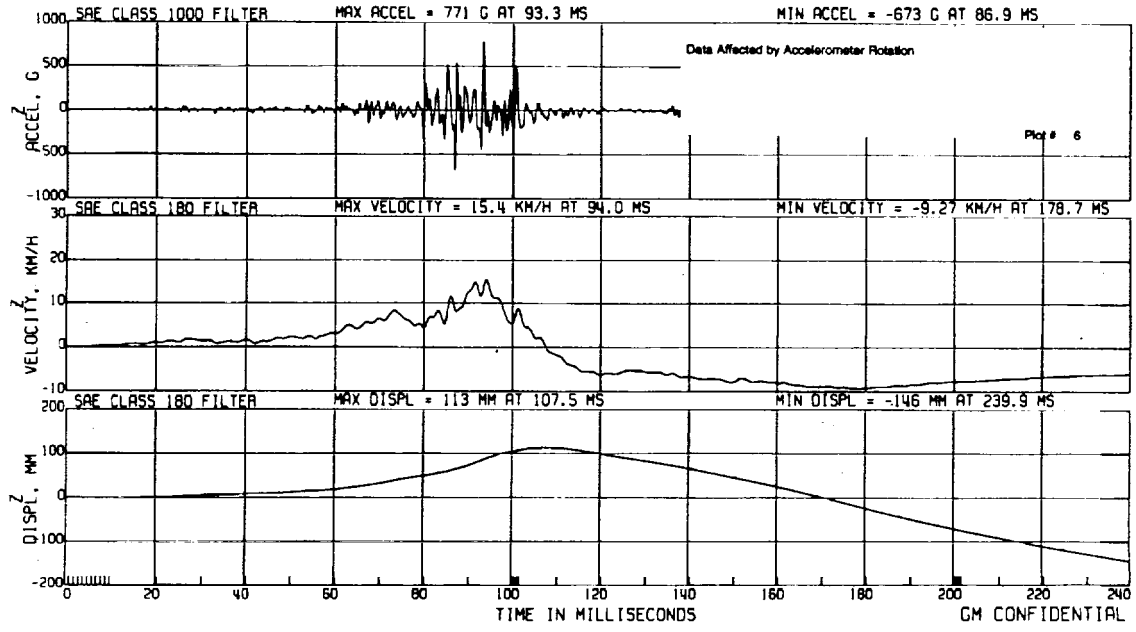


Plot A12. Crash Test C12731. Plots of acceleration, velocity, and displacement in the direction of the Z-axis calculated from the accelerometer on the right front rocker.

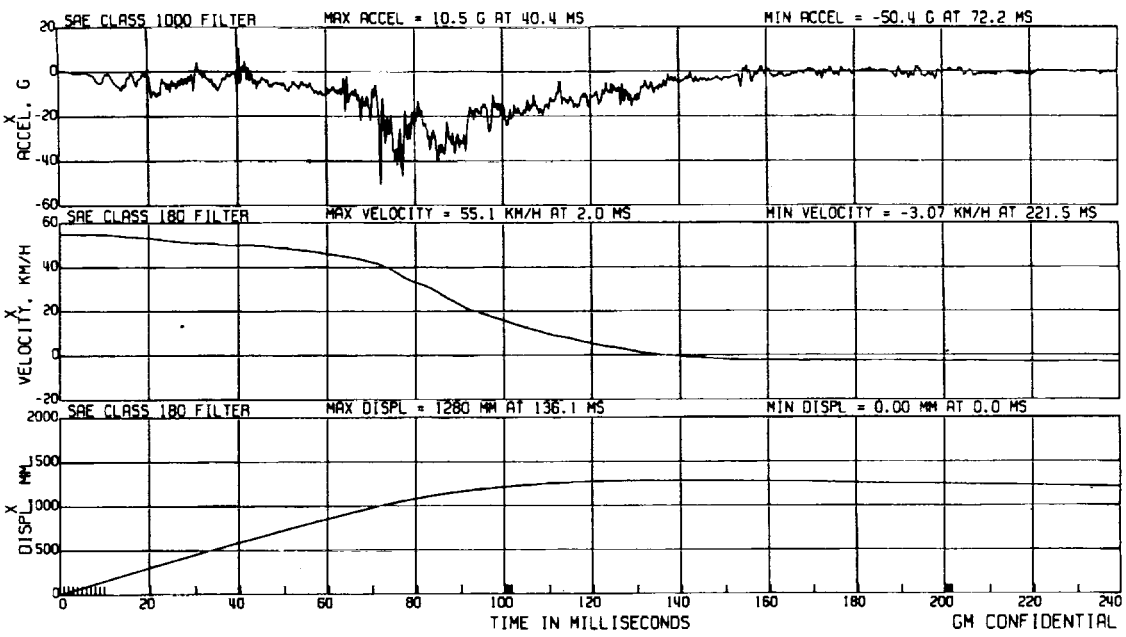


Plot A13. Crash Test C12730. Plots of acceleration, velocity, and displacement in the direction of the X-axis calculated from the accelerometer on the left rear rocker.

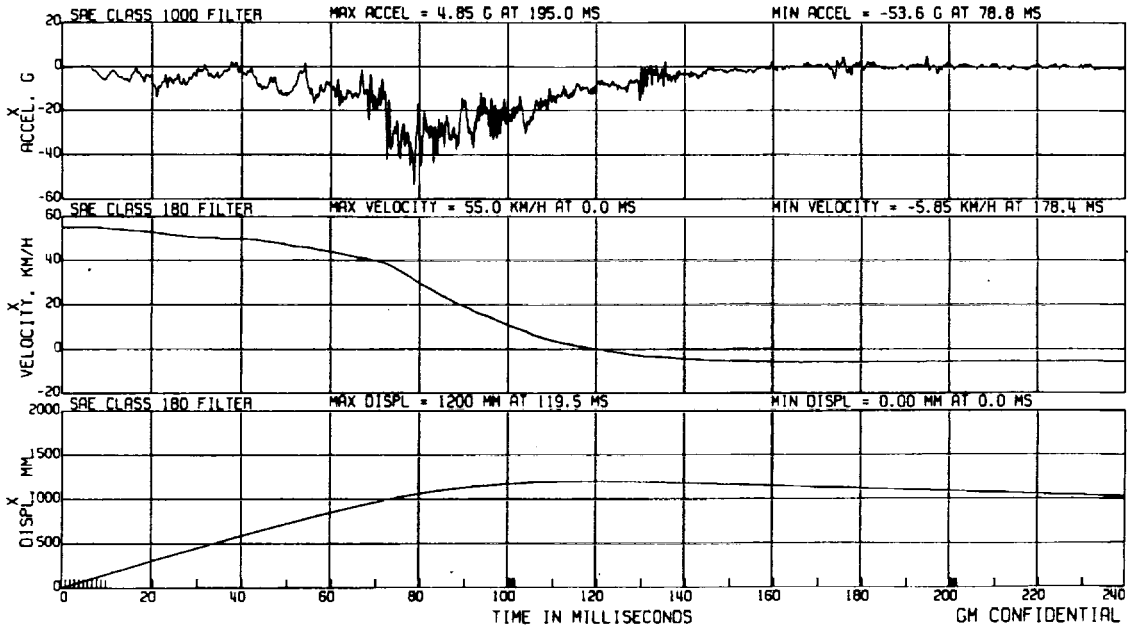


Plot A14. Crash Test C12731. Plots of acceleration, velocity, and displacement in the direction of the X-axis calculated from the accelerometer on the left rear rocker.

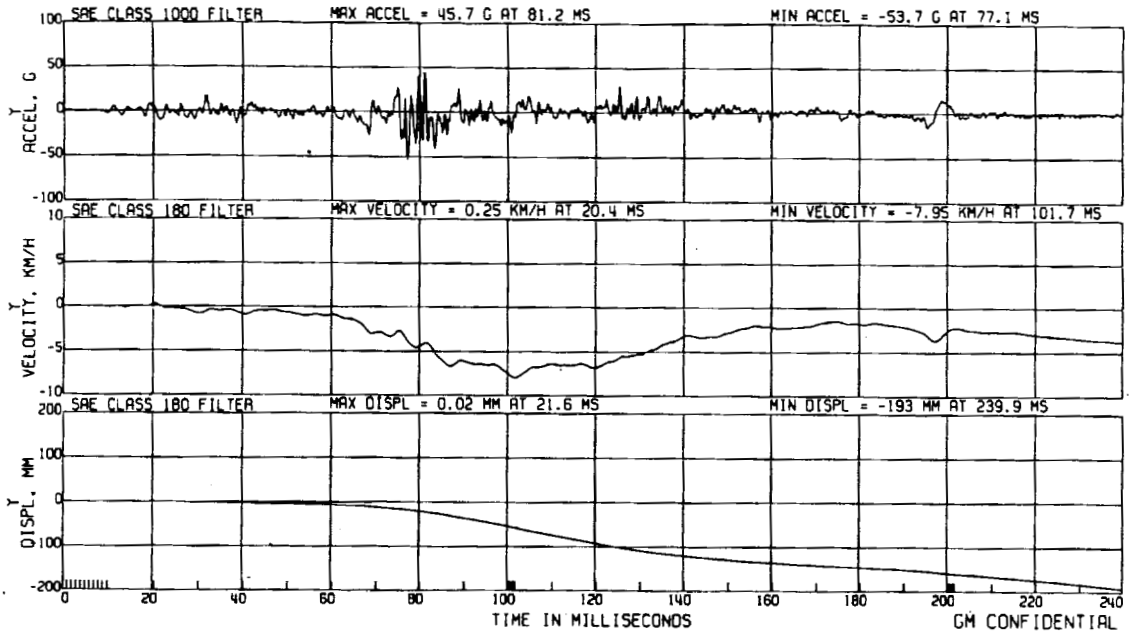


Plot A15. Crash Test C12730. Plots of acceleration, velocity, and displacement in the direction of the Y-axis calculated from the accelerometer on the left rear rocker.

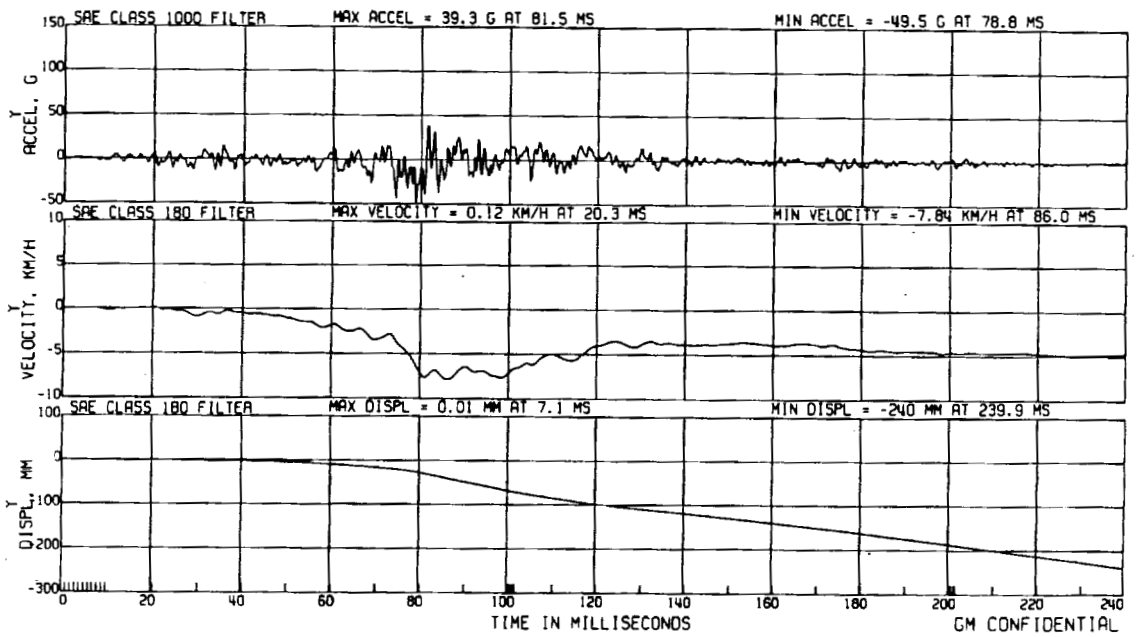


Plot A16. Crash Test C12731. Plots of acceleration, velocity, and displacement in the direction of the Y-axis calculated from the accelerometer on the left rear rocker.

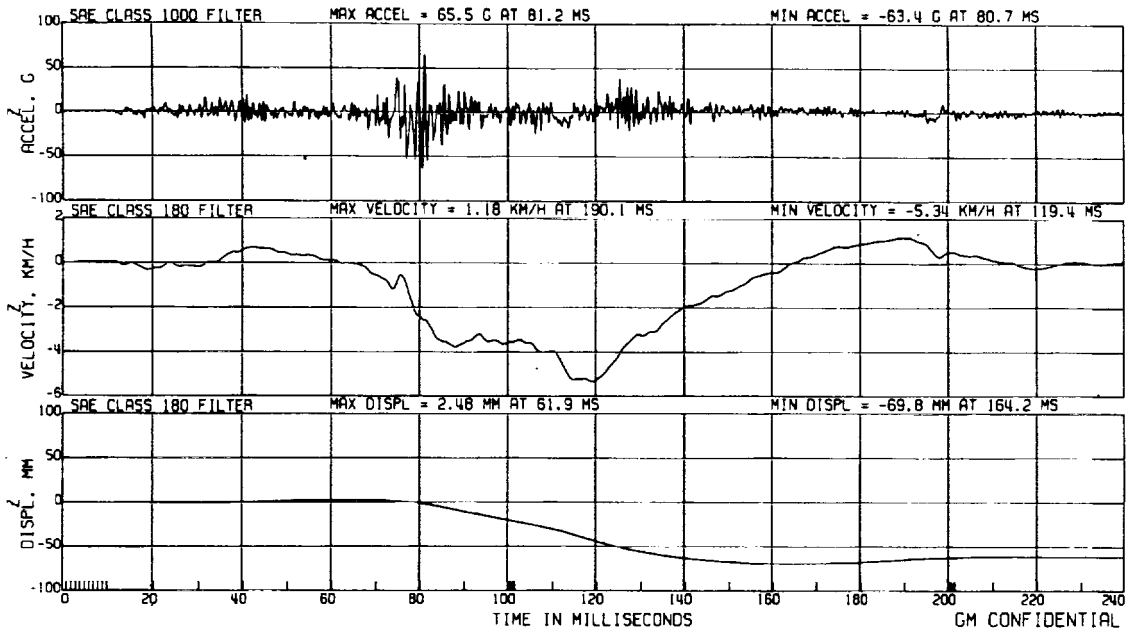


Plot A17. Crash Test C12730. Plots of acceleration, velocity, and displacement in the direction of the Z-axis calculated from the accelerometer on the left rear rocker.

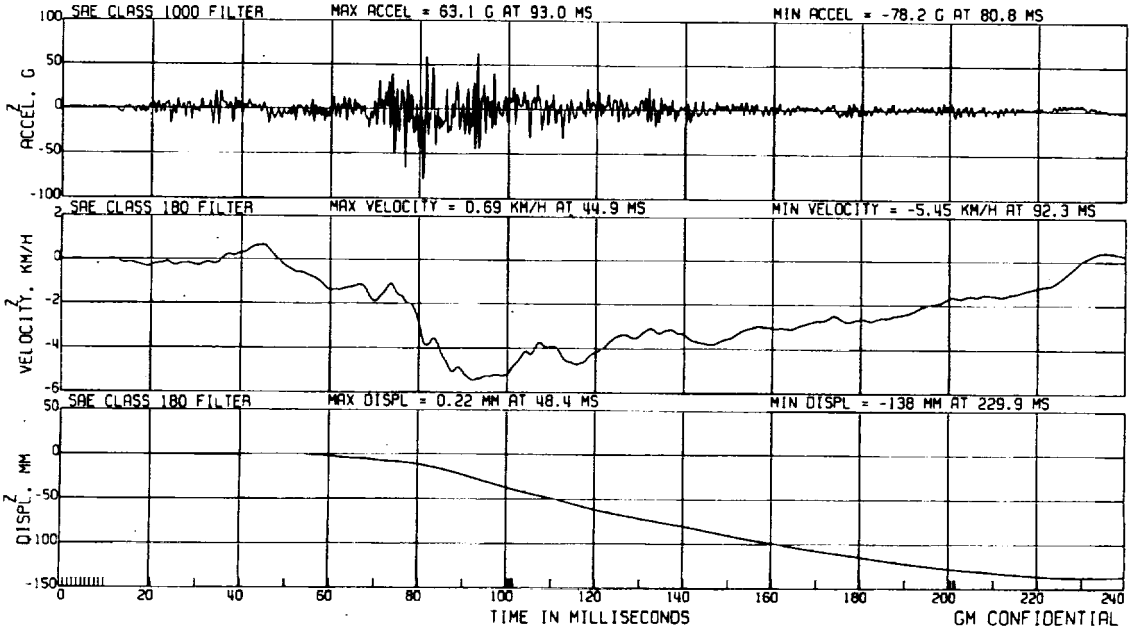


Plot A18. Crash Test C12731. Plots of acceleration, velocity, and displacement in the direction of the Z-axis calculated from the accelerometer on the left rear rocker.

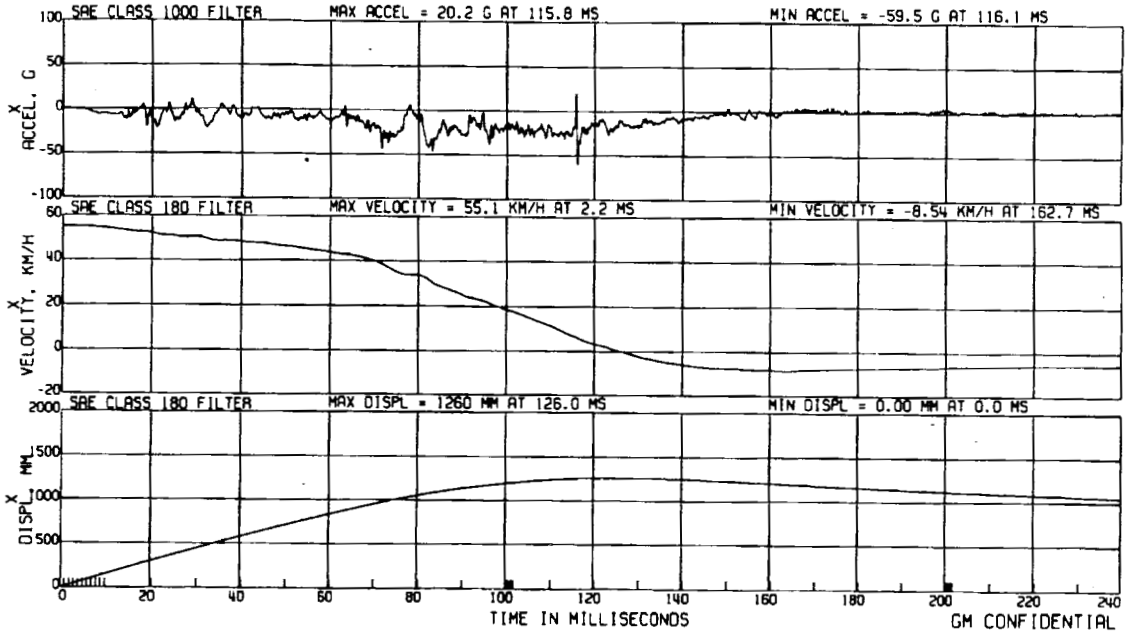


Plot A19. Crash Test C12730. Plots of acceleration, velocity, and displacement in the direction of the X-axis calculated from the accelerometer on the right rear rocker.

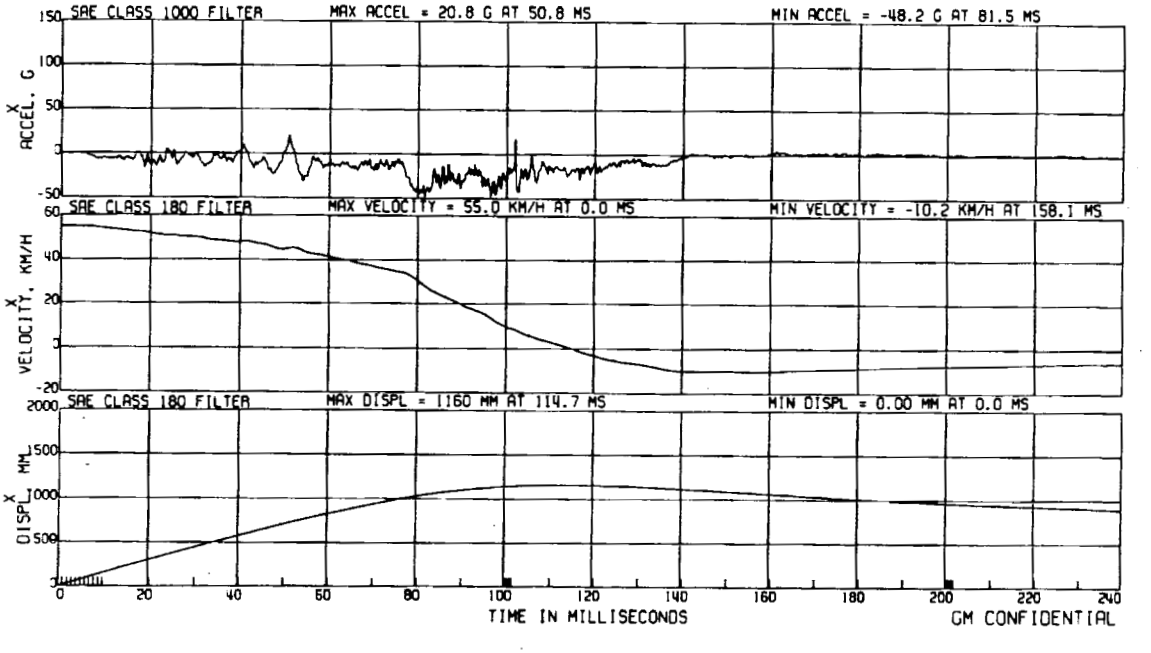


Plot A20. Crash Test C12731. Plots of acceleration, velocity, and displacement in the direction of the X-axis calculated from the accelerometer on the right rear rocker.

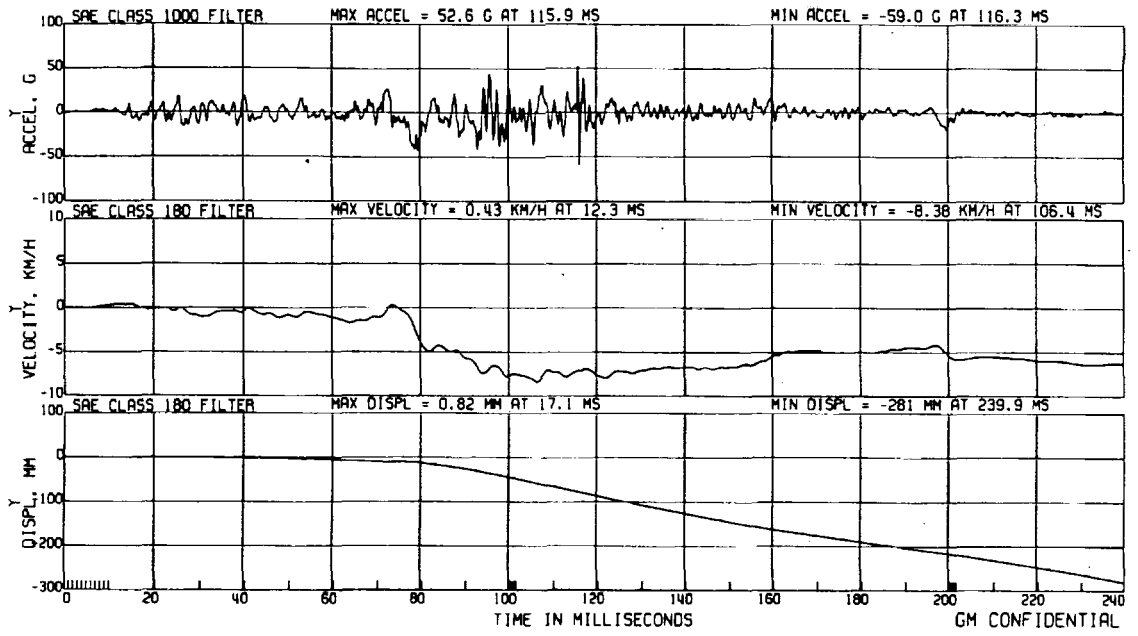


Plot A21. Crash Test C12730. Plots of acceleration, velocity, and displacement in the direction of the Y-axis calculated from the accelerometer on the right rear rocker.

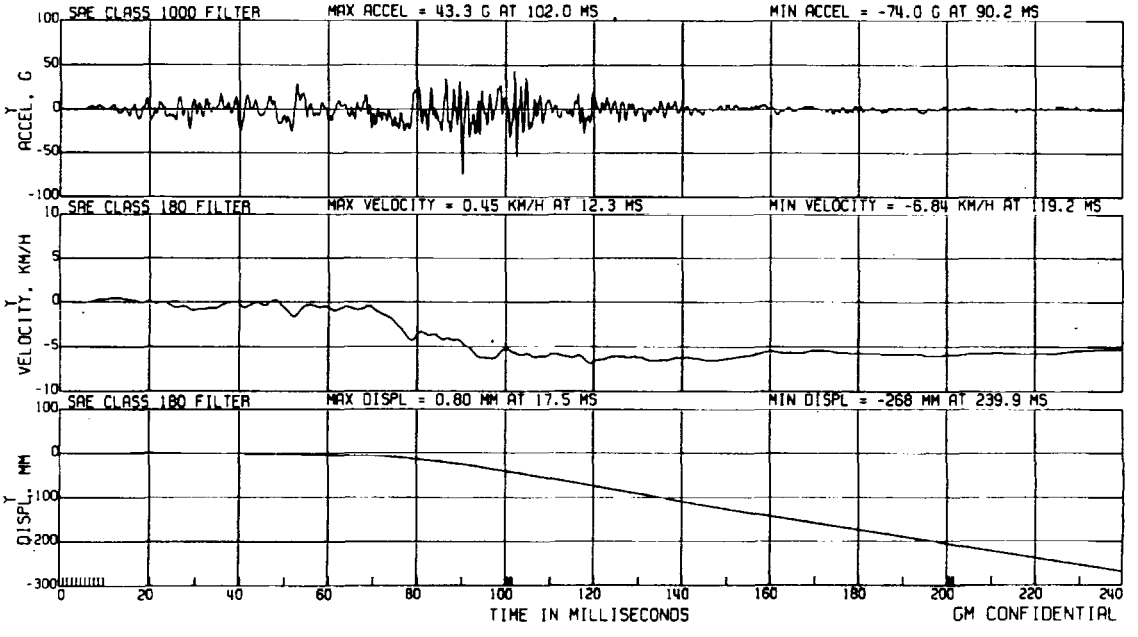


Plot A22. Crash Test C12731. Plots of acceleration, velocity, and displacement in the direction of the Y-axis calculated from the accelerometer on the right rear rocker.

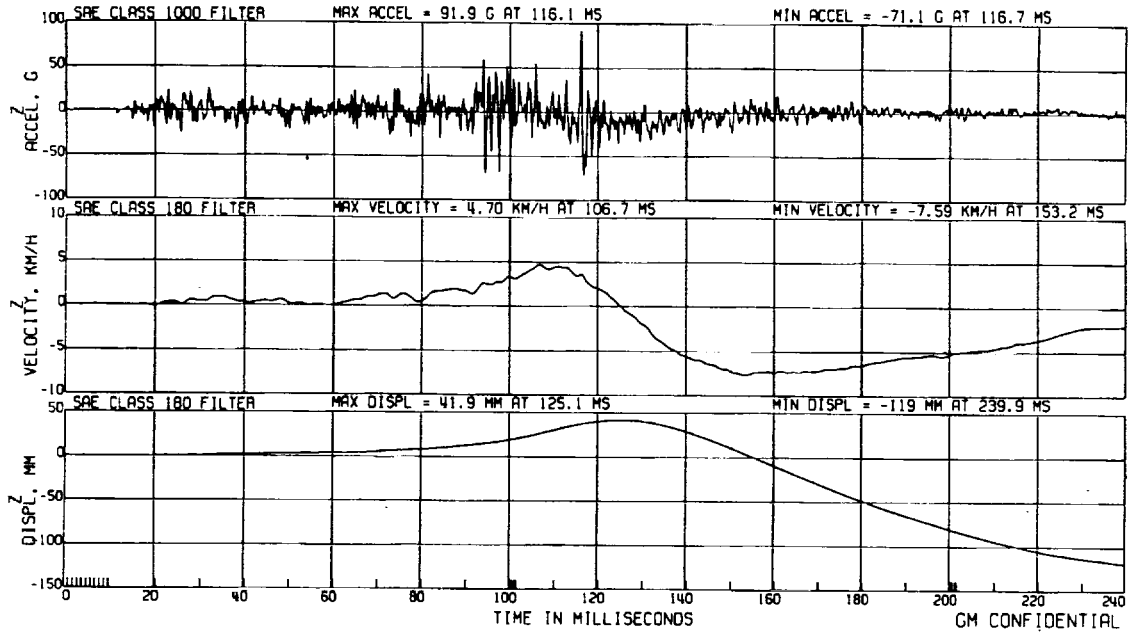


Plot A23. Crash Test C12730. Plots of acceleration, velocity, and displacement in the direction of the Z-axis calculated from the accelerometer on the right rear rocker.

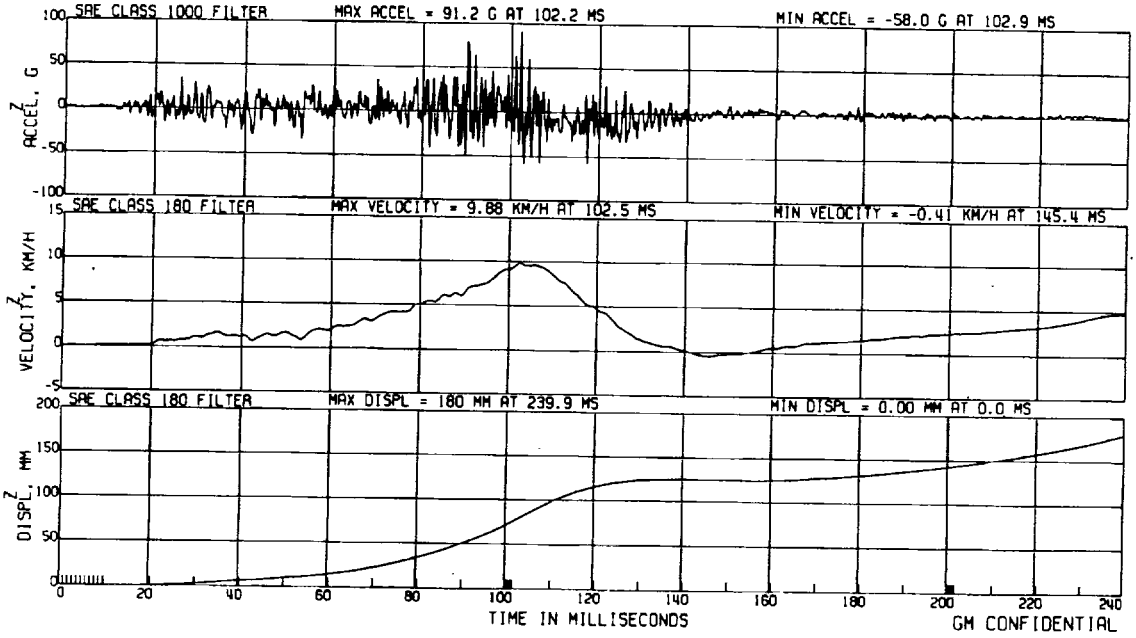


Plot A24. Crash Test C12731. Plots of acceleration, velocity, and displacement in the direction of the Z-axis calculated from the accelerometer on the right rear rocker.

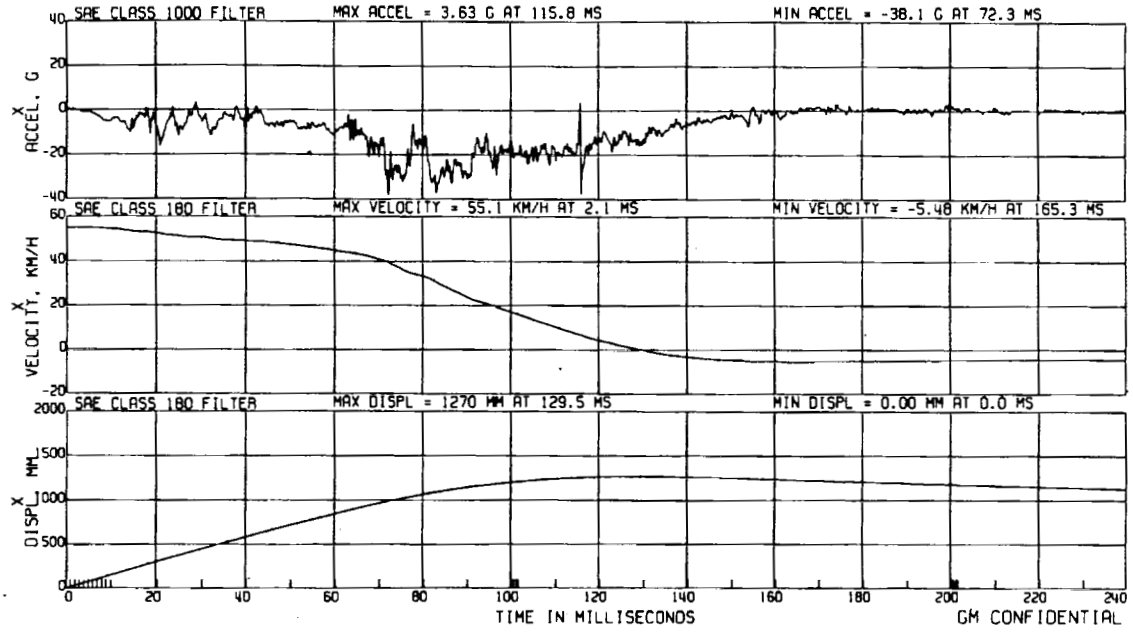


Plot A25. Crash Test C12730. Plots of the average acceleration, velocity, and displacement in the direction of the X-axis calculated from the accelerometers on the left and right rear rockers.

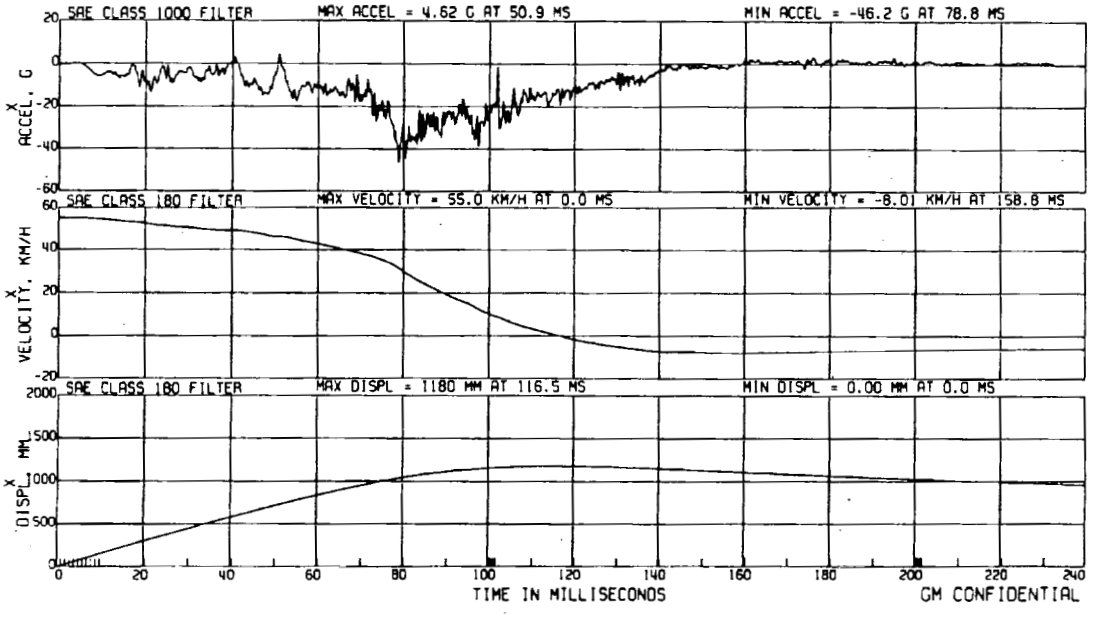


Plot A26. Crash Test C12731. Plots of the average acceleration, velocity, and displacement in the direction of the X-axis calculated from the accelerometers on the left and right rear rockers.

**Appendix B**

**Crash Tests C12730 and C12731**

**Flammable Vapor Sensor Data**

Five flammable gas sensors (TGS 813, FIGARO USA, Inc, Wilmette, IL) were installed in the engine compartments of the test vehicle in the following locations:

- Location 1: Above the left exhaust manifold
- Location 2: Above the left valve cover
- Location 3: Above the right valve cover
- Location 4: Above the engine oil fill
- Location 5: Above the right exhaust manifold

Gas phase concentration – sensor output voltage calibration data was obtained using heptane in the range of 0 to 5% (V/V). Estimates of the flammable gas concentration at each location in the engine compartment of both test vehicles using this calibration data are shown in Plots B1 through B10.

The tin oxide semiconductor elements in these sensors also respond to changes in temperature. Exposure to heated vapor or aerosol of a non-flammable fluid, such as electrolyte from the battery (20% sulfuric acid in water) expelled from a battery being crushed during the crash test, will cause the sensor output voltage to increase as if it was exposed to a flammable gas. Interpretation of the flammable sensor data therefore must include a consideration of the results of the gas chromatography/mass spectrometry analysis of gas samples acquired from these locations during the crash test shown in APPENDIX C.

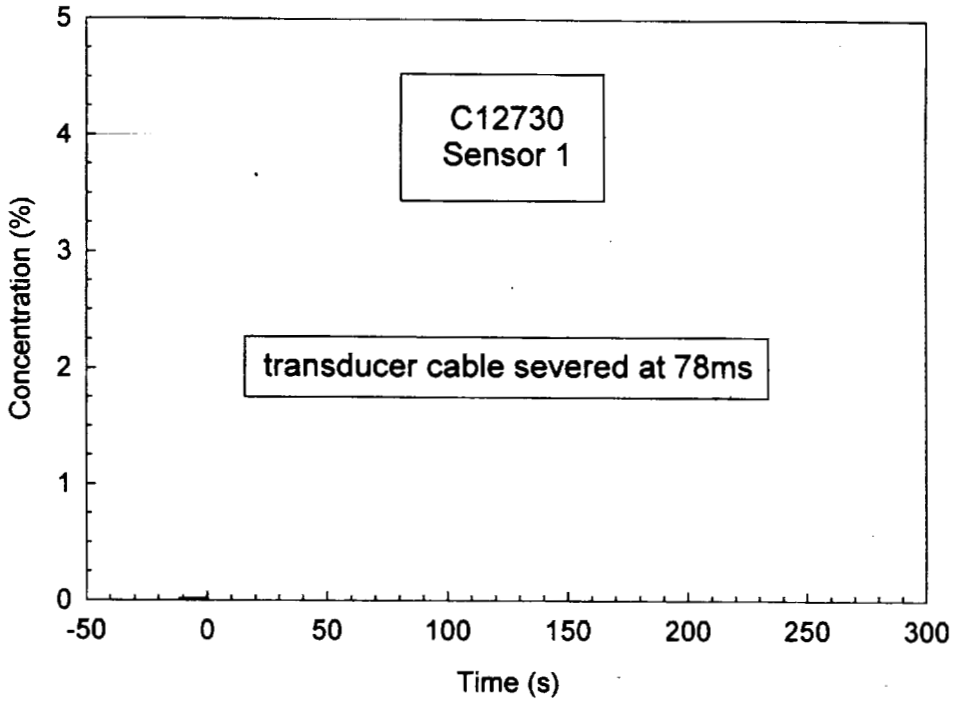


Plot B1. Crash Test C12730. Plot of flammable vapor concentration recorded by the flammable gas sensor at Location 1.flammable gas sensor at Location 1.

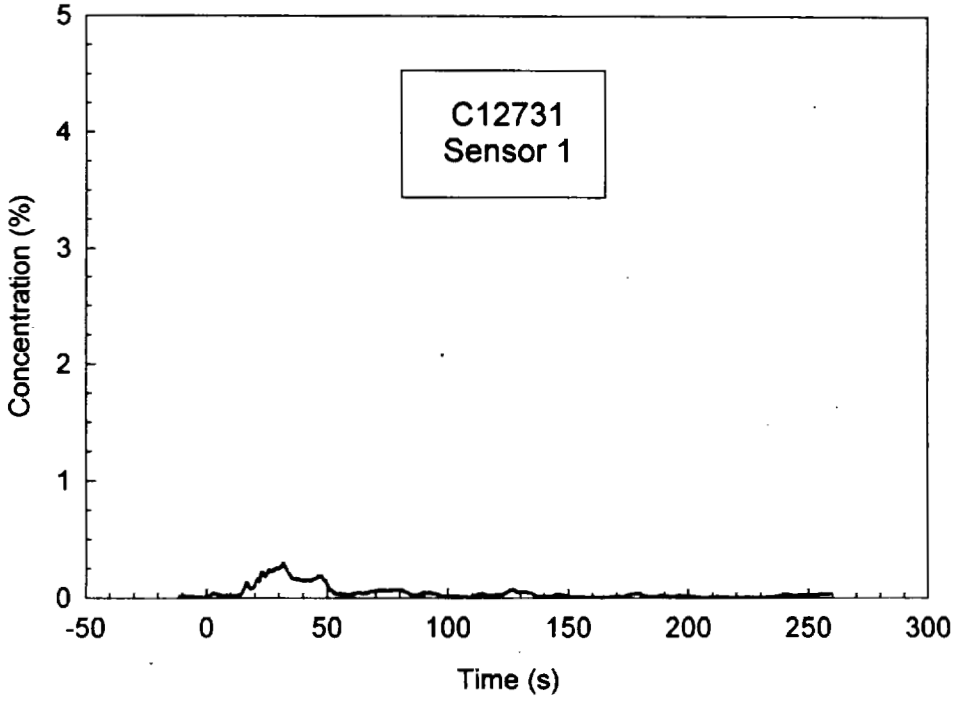


Plot B2. Crash Test C12731. Plot of flammable vapor concentration recorded by the flammable gas sensor at Location 1.

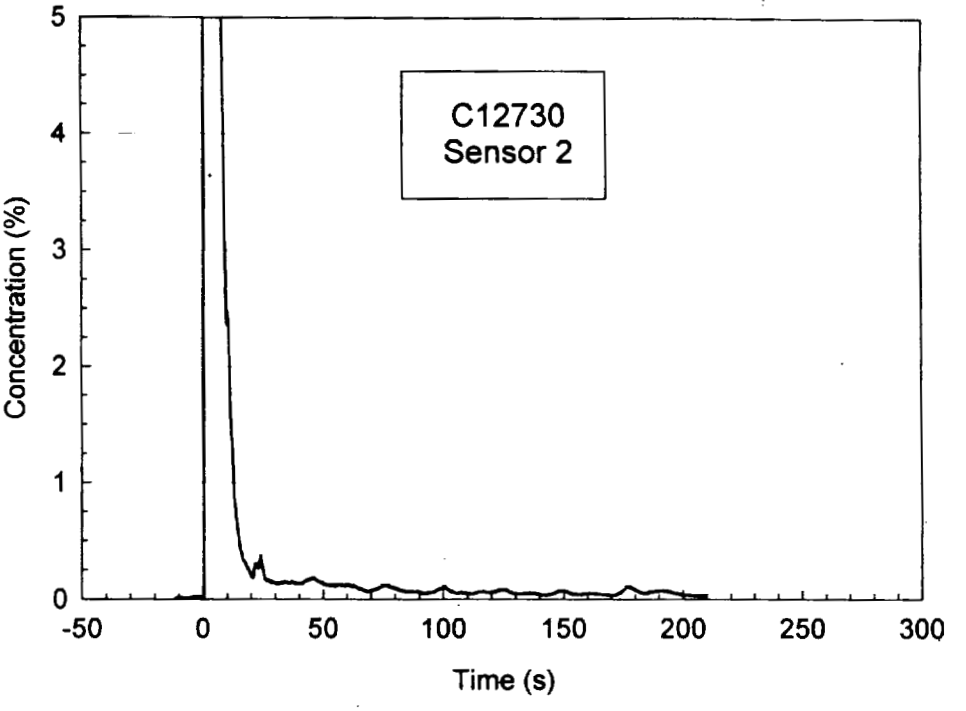


Plot B3. Crash Test C12730. Plot of flammable vapor concentration recorded by the flammable gas sensor at Location 2.

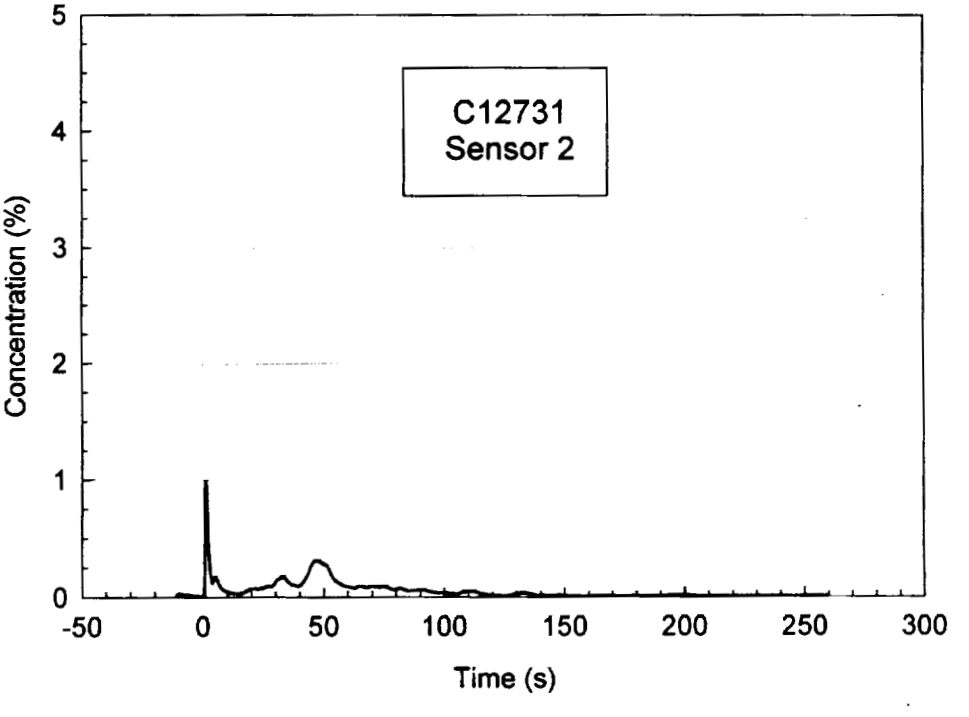


Plot B4. Crash Test C12731. Plot of flammable vapor concentration recorded by the flammable gas sensor at Location 2.

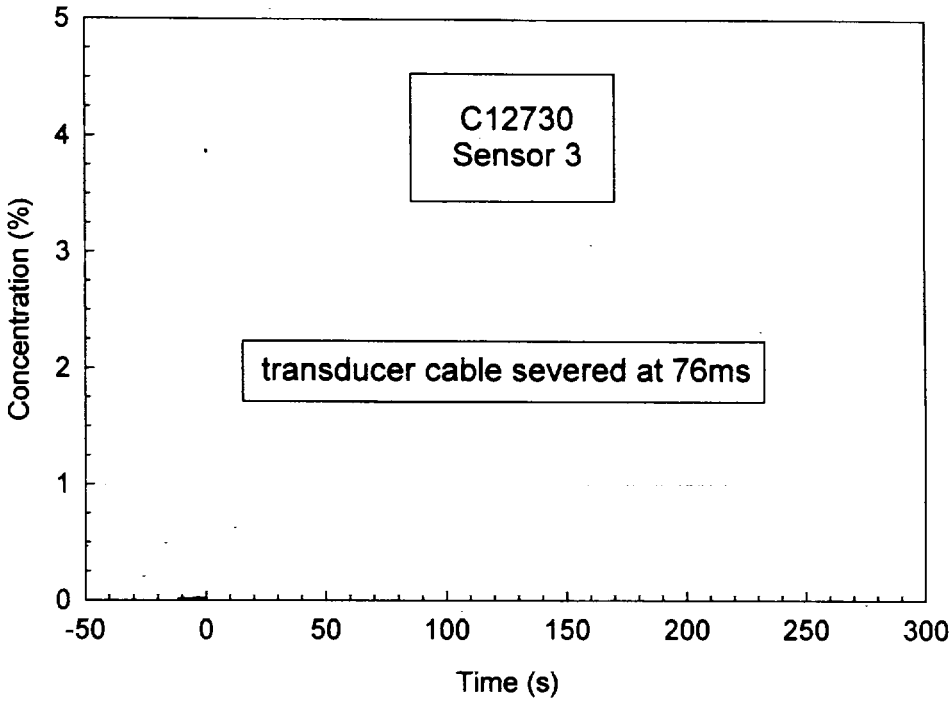


Plot B5. Crash Test C12730. Plot of flammable vapor concentration recorded by the flammable gas sensor at Location 3.

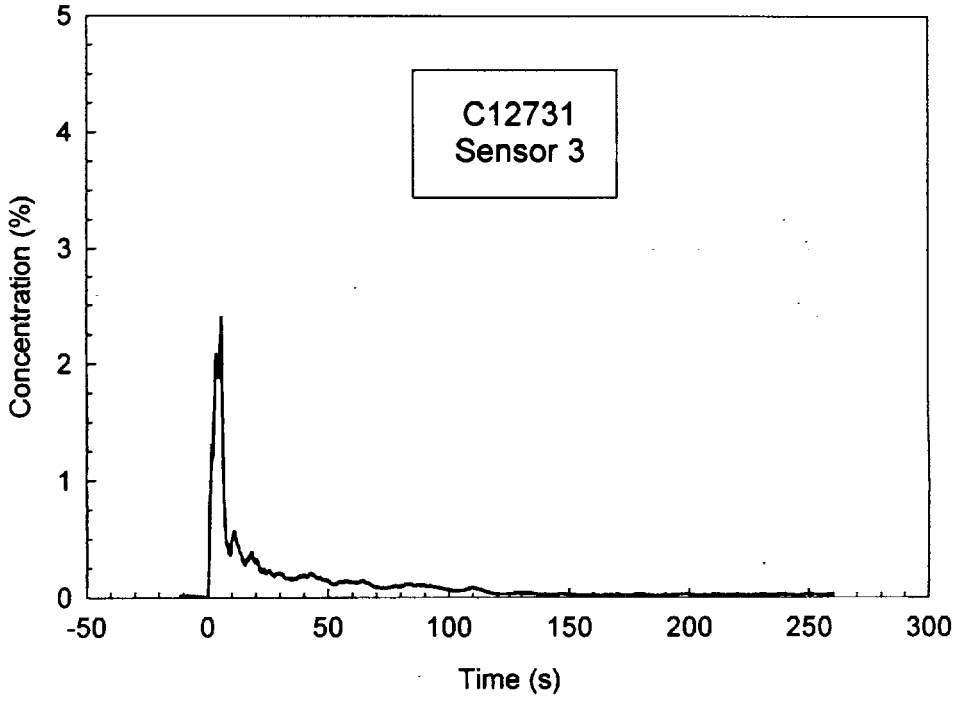


Plot B6. Crash Test C12731. Plot of flammable vapor concentration recorded by the flammable gas sensor at Location 3.

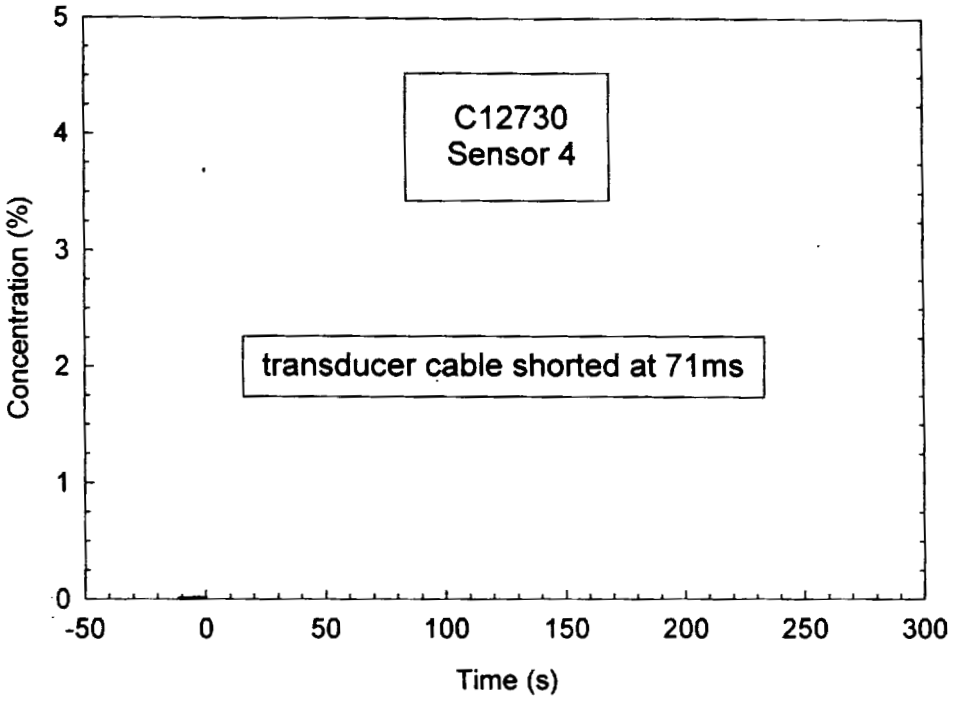


Plot B7. Crash Test C12730. Plot of flammable vapor concentration recorded by the flammable gas sensor at Location 4.

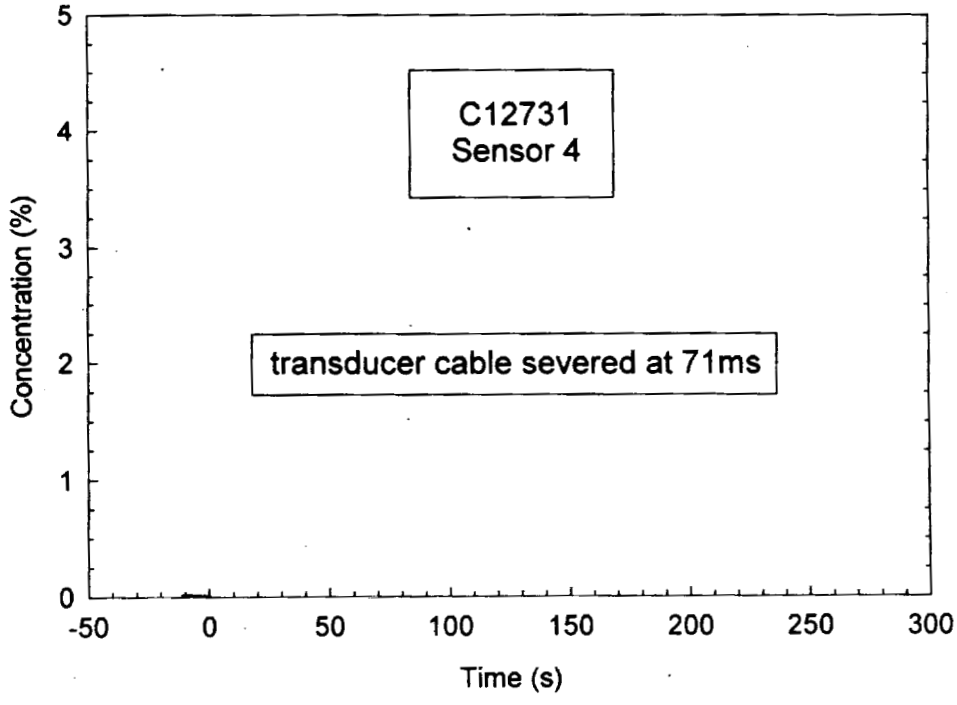


Plot B8. Crash Test C12731. Plot of flammable vapor concentration recorded by the flammable gas sensor at Location 4.

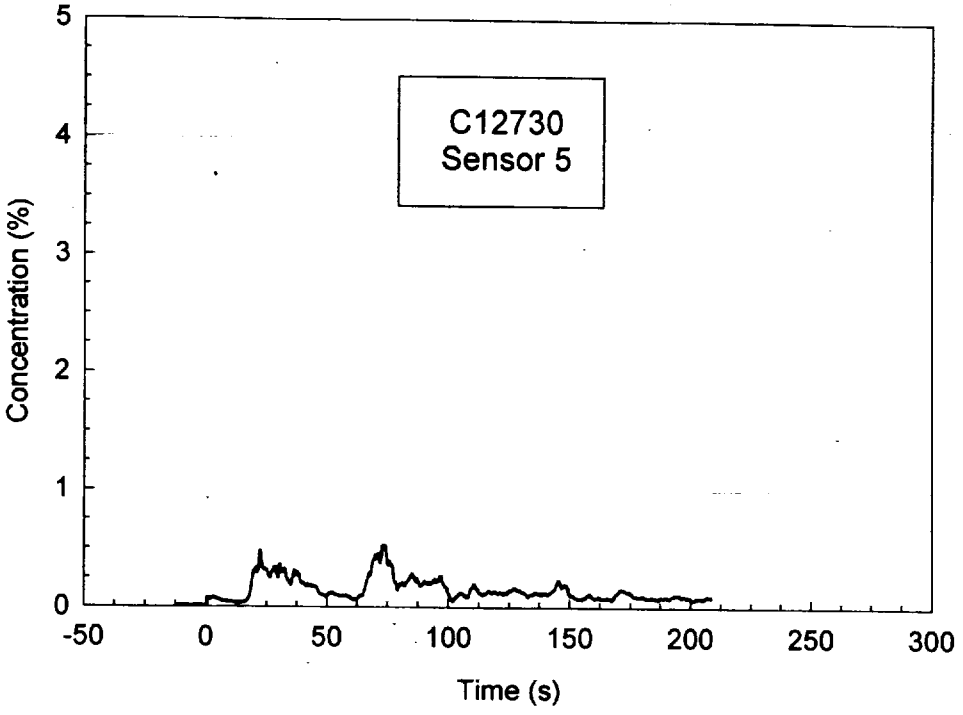


Plot B9. Crash Test C12730. Plot of flammable vapor concentration recorded by the flammable gas sensor at Location 5.

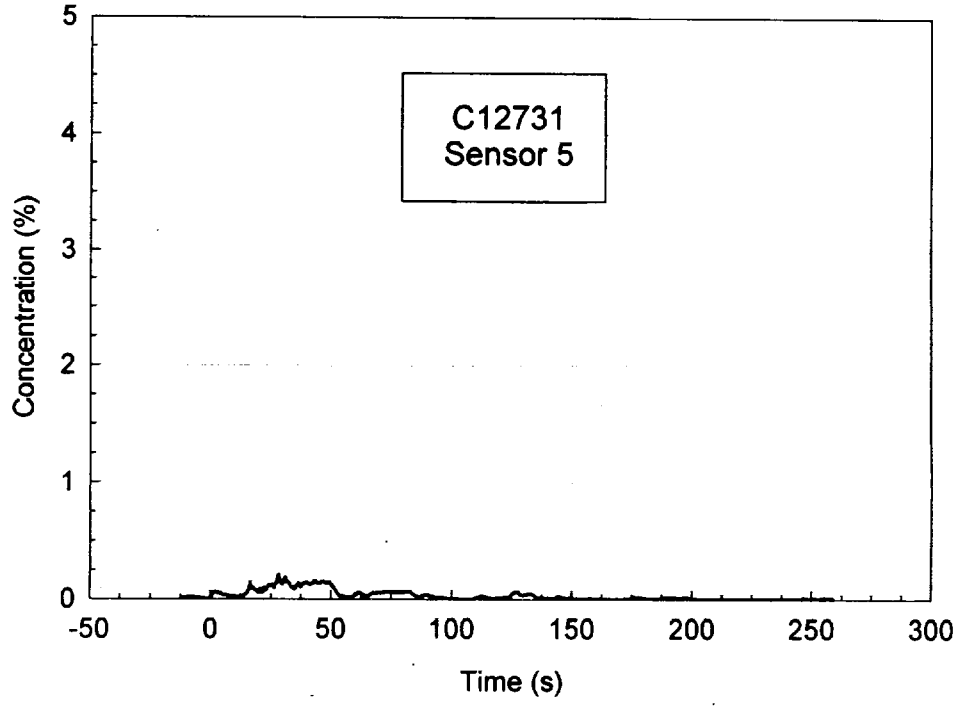


Plot B10. Crash Test C12731. Plot of flammable vapor concentration recorded by the flammable gas sensor at Location 5.

## Appendix C

## Crash Tests C12730 and C12731
## Gas Chromatography / Mass Spectroscopy Analysis of
## Engine Compartment Air Samples

Air was samples from were acquired from five locations in the engine compartments of the test vehicles during these crash tests. Sample cartridges packed with an absorbent media were connected to a pumping manifold located in the rear compartments of the test vehicles. A sample cartridge consisted of a glass-lined stainless steel tube (i.d. = 4 mm; length = 10 cm; Scientific Instrument Services, Inc, Ringoes, NJ) packed with 25 mg of Carbotrap™ C Graphitized Carbon Black (Supelco, Inc.; Bellefonte, PA) in series with 15 mg of Carbotrap™ Graphitized Carbon Black (Supelco). The inlet of each sample cartridge was connected to a stainless-steel tube (o.d. = 0.125 in. (3.18 mm), i.d. = 0.085 in. (2.16 mm)), which ran from the rear compartment into the engine compartment. The inlets of the sample tubes were located one of the flammable sensors:

- Blank / Sample 1: Above the left exhaust manifold
- Blank / Sample 2: Above the left valve cover
- Blank / Sample 3: Above the right valve cover
- Blank / Sample 4: Above the engine oil fill
- Blank / Sample 5: Above the right exhaust manifold

The airflow rate through each cartridge was adjusted to 250 $cm^3$/min with a rotometers mounted to the pumping manifold. Blank samples were acquires for a 10 minute period during the engine warm-up before the crash test. Samples during the crash test were acquires for a 15 minute period starting approximately 5 minutes before impact and ending approximately 10 minutes after impact.

Organic substances retained by the absorbent media in the sample cartridges were analyzed by thermal desorption/gas chromatography/mass spectrometry after the crash tests. Deuterated standards dissolved in deuterated methanol were added to each sorbent cartridge to monitor sample recovery. A modified purge-and-trap concentrator was used for thermal desorption (Model 600 Purge-and-Trap Concentrator, CDS Analytical, Oxford, PA). The gas chromatograph was a Model 5890 Series II Plus Gas Chromatograph (Hewlet Packard, Palo Alto, CA). The mass spectrometer was a Hewlet Packard Model 5989B Mass Spectrometer (Hewlett Packard). The thermal desorption unit was interfaced directly to the split/splitless injector of the gas chromatograph through a cryo-focusing unit. The injector was operated in the split mode with a split of approximately 10 mL/min. The chromatographic column was a fused silica capillary column coated with 100% methyl silicone (HP-1 ; length = 30 m; i.d. = 0.25 mm; film thickness = 0.25 μm).

The sample was desorbed at 320°C for 10 min, and cryofocused onto the head of the chromatographic column -80°C. The temperature of the analytical column was maintained at 0°C

while the sample was desorbed and cryo-focused. To start the chromatographic analysis, the cryo-focusing unit was heated bullistically to a temperature of 320°C. The column temperature was programmed from 0 to 325°C at a rate of 5°C/min. Mass spectra were obtained by scanning from m/z 40 to 600 at a rate of 1.2 scan/s.

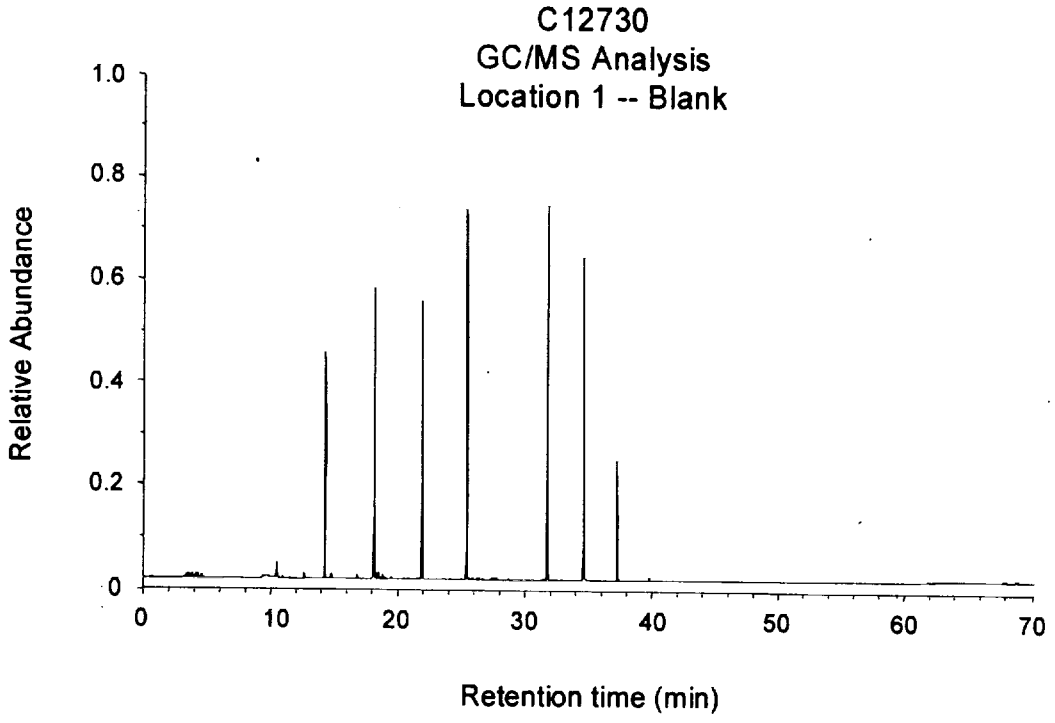


Plot C1. Crash Test C12730. Chromatogram of blank from Location 1 acquired before impact.

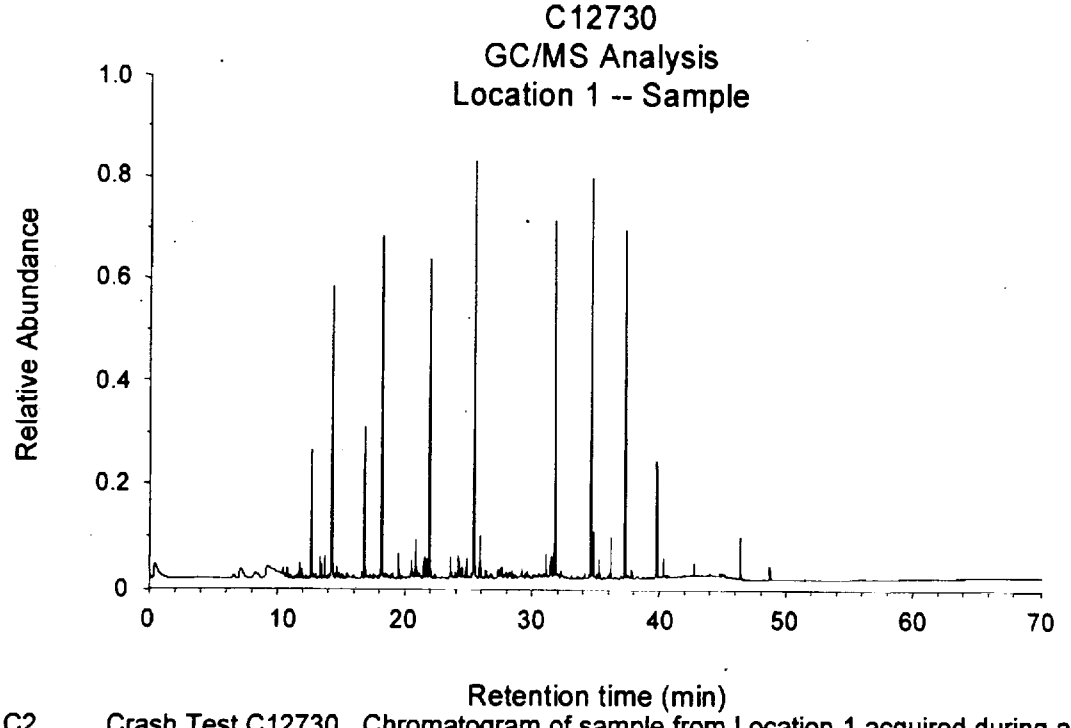


Plot C2 Crash Test C12730. Chromatogram of sample from Location 1 acquired during and after impact.

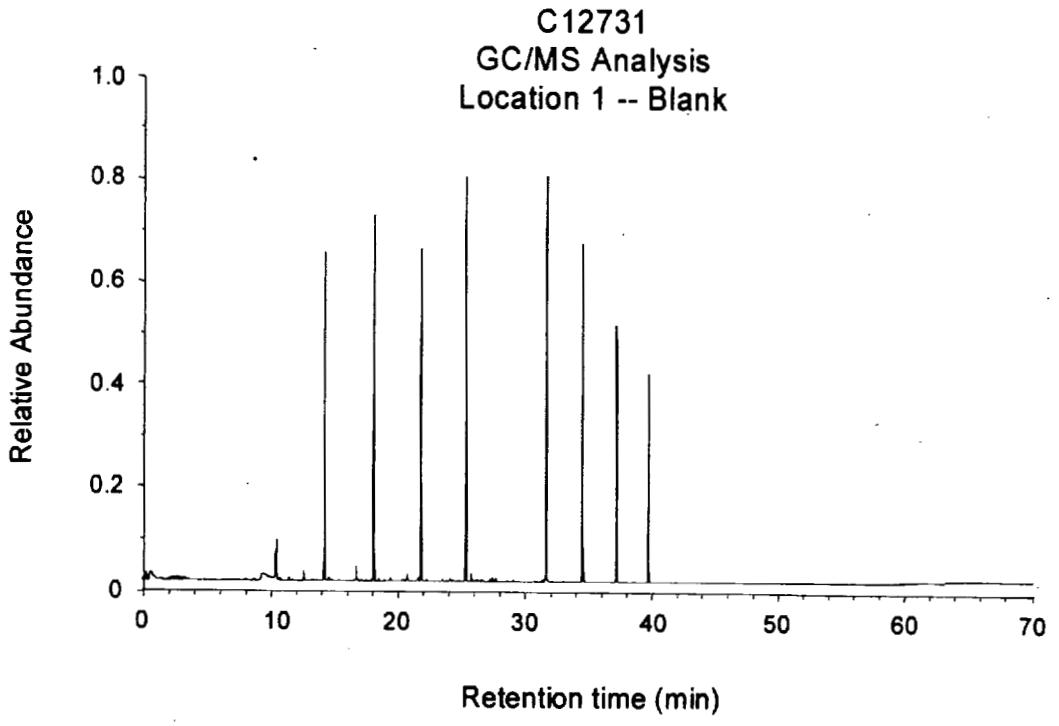


Plot C3. Crash Test C12731. Chromatogram of blank from Location 1 acquired before impact.

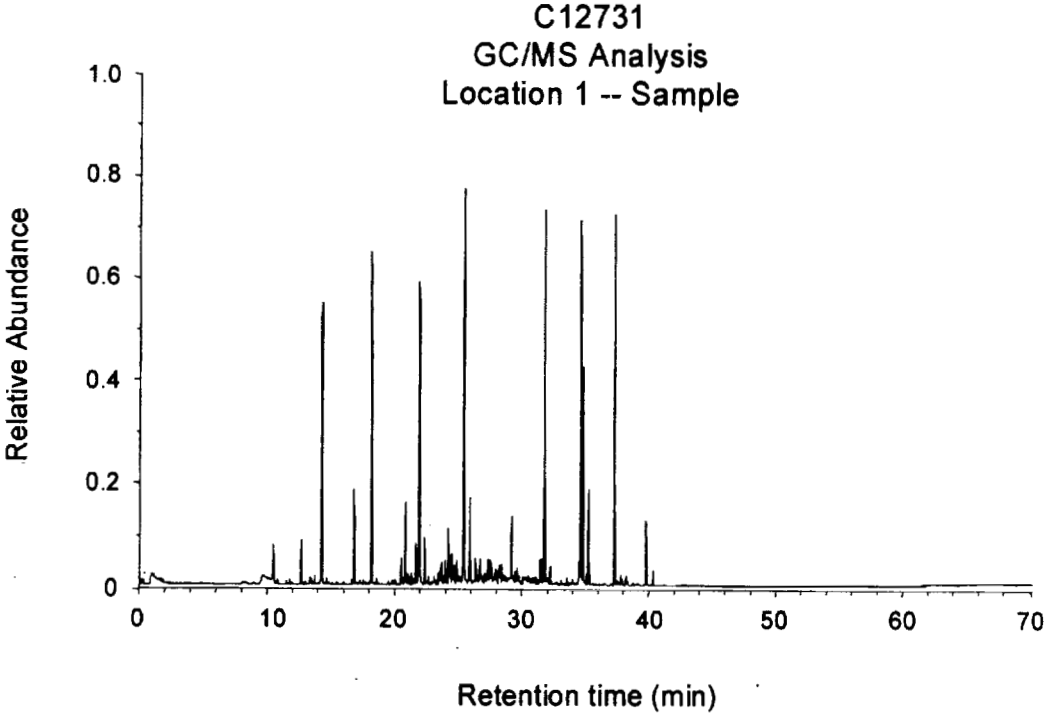


Plot C4. Crash Test C12731. Chromatogram of sample from Location 1 acquired during and after impact.

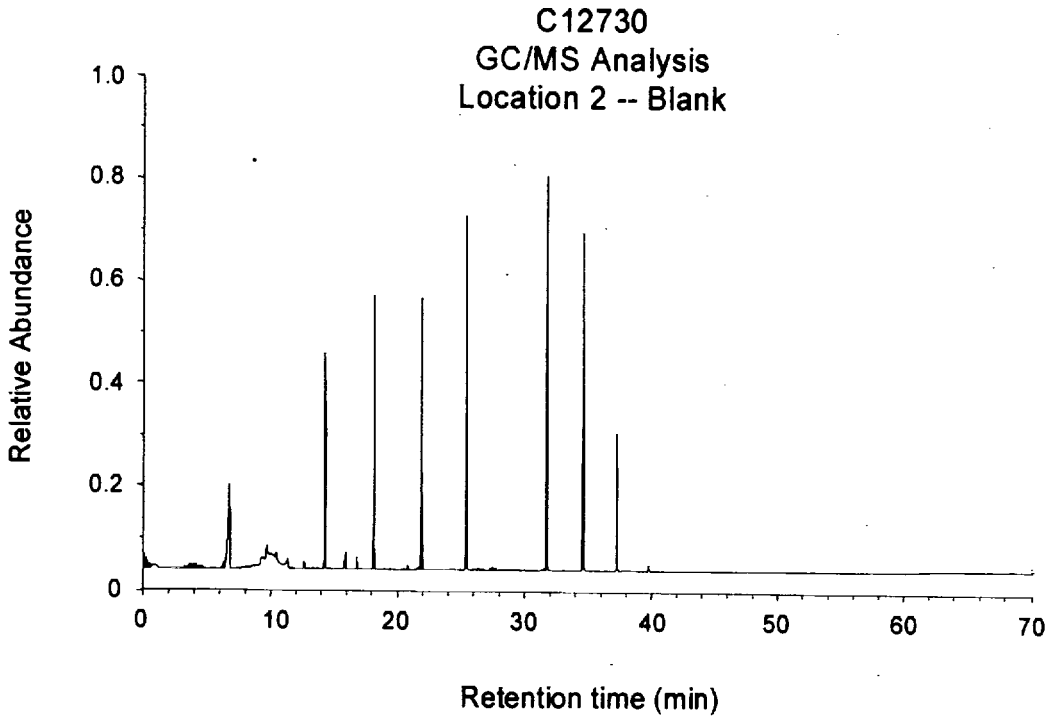


Plot C5. Crash Test C12730. Chromatogram of blank from Location 2 acquired before impact.

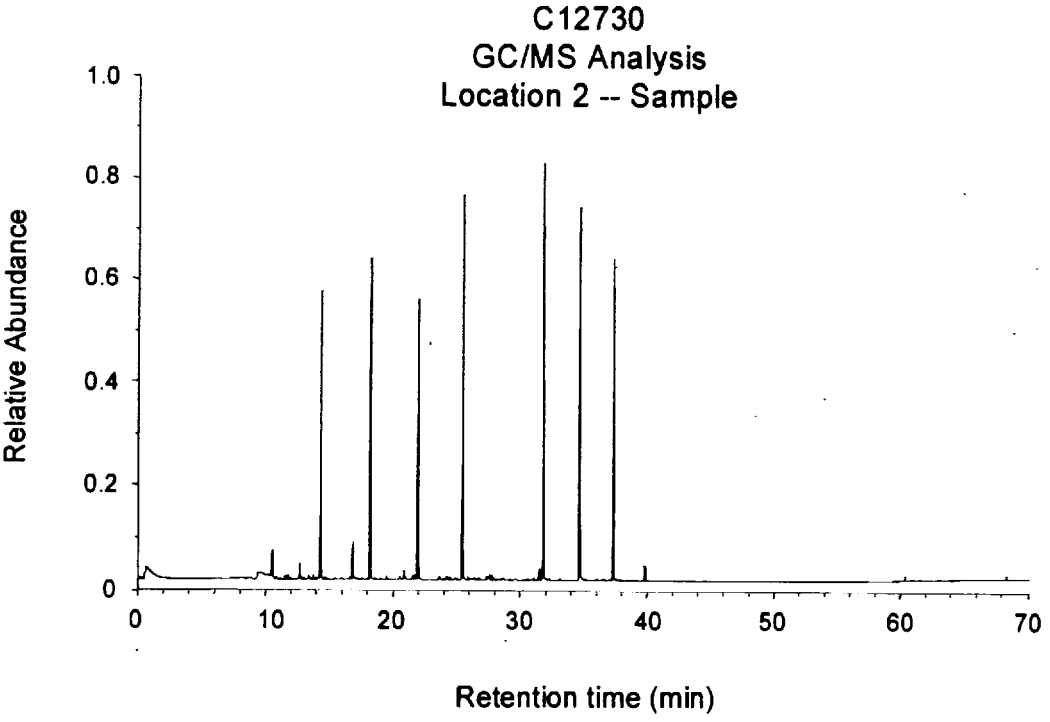


Plot C6. Crash Test C12730. Chromatogram of sample from Location 2 acquired during and after impact.

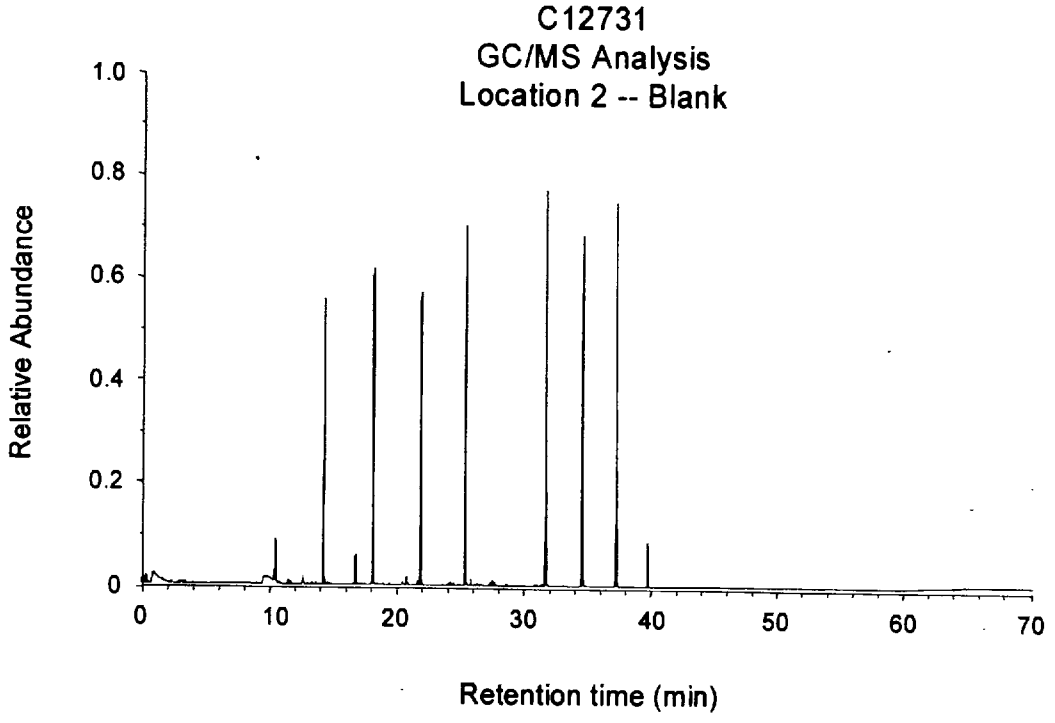


Plot C7. Crash Test C12731. Chromatogram of blank from Location 2 acquired before impact.

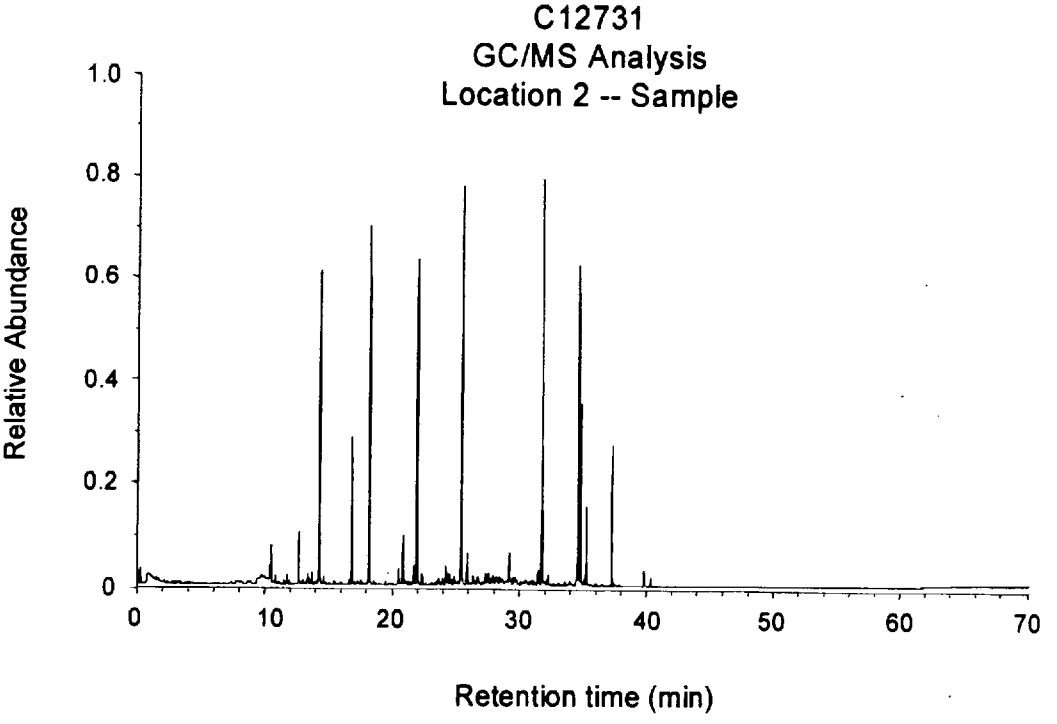


Plot C8. Crash Test C12731. Chromatogram of sample from Location 2 acquired during and after impact.

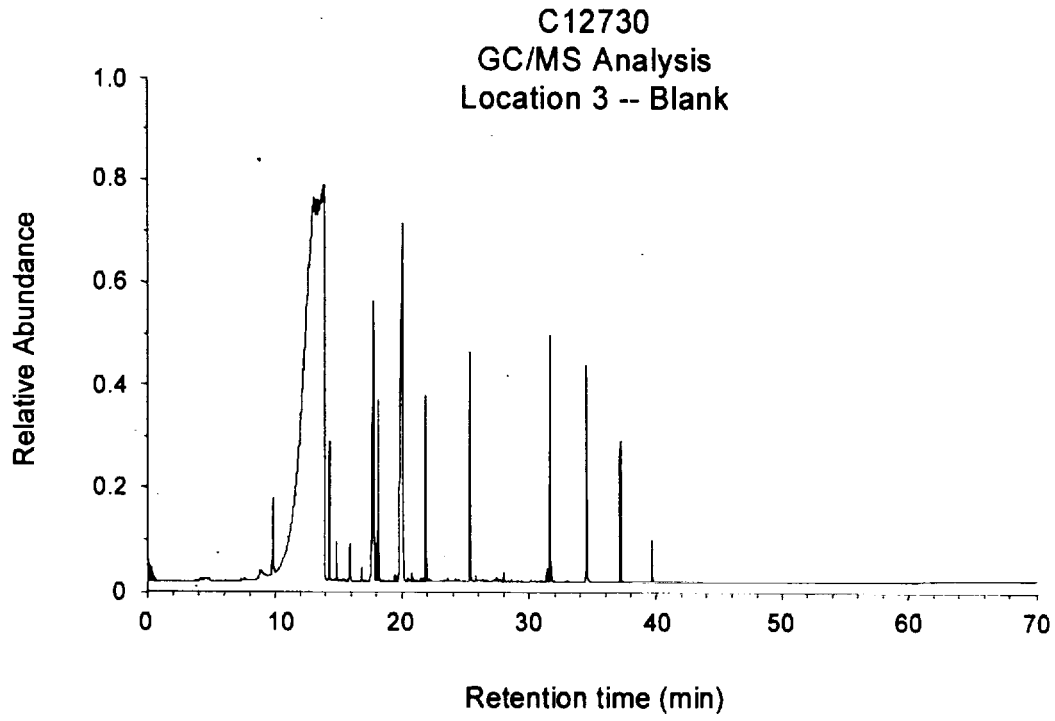


Plot C9. Crash Test C12730. Chromatogram of blank from Location 3 acquired before impact.

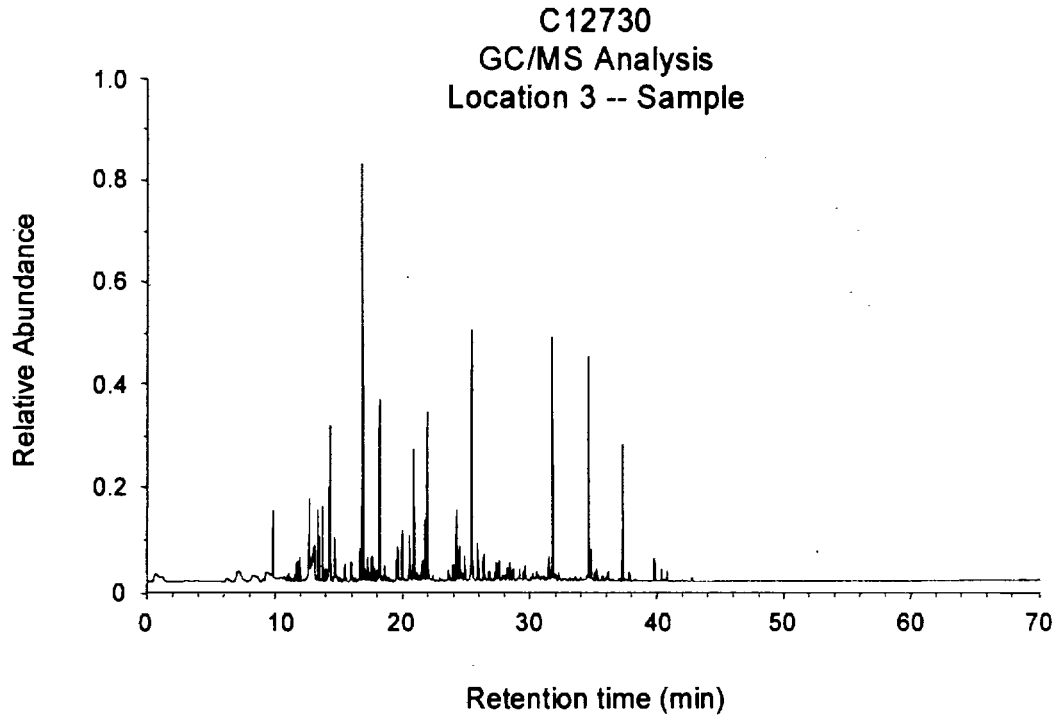


Plot C10. Crash Test C12730. Chromatogram of sample from Location 3 acquired during and after impact.

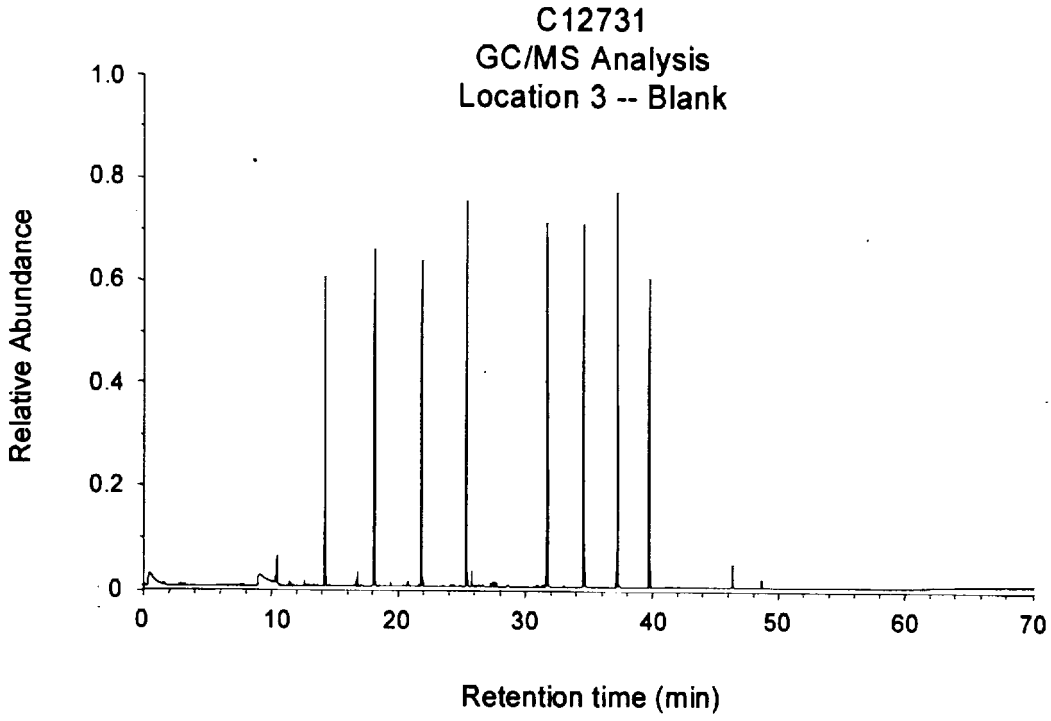


Plot C11. Crash Test C12731. Chromatogram of blank from Location 3 acquired before impact.

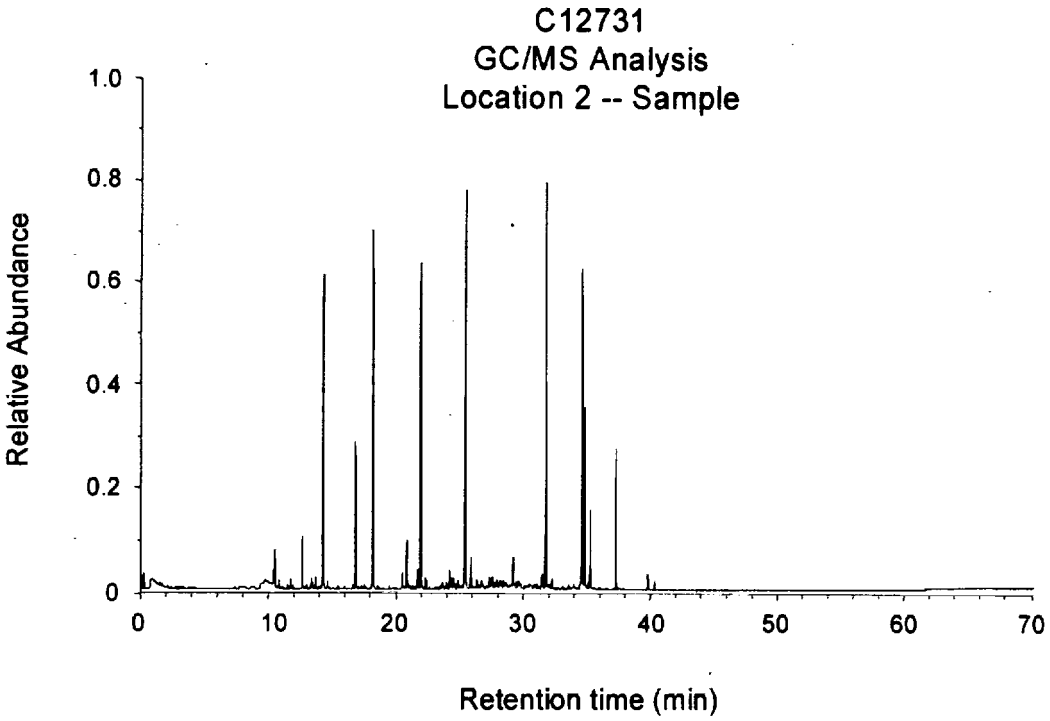


Plot C12. Crash Test C12731. Chromatogram of sample from Location 3 acquired during and after impact.

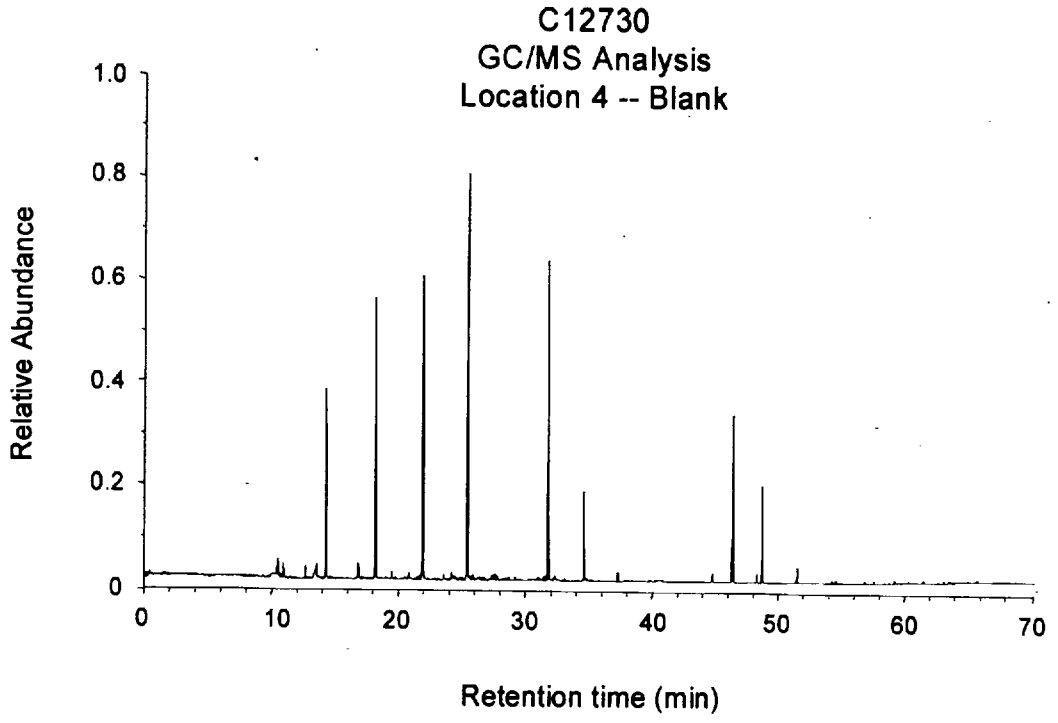


Plot C13. Crash Test C12730. Chromatogram of blank from Location 4 acquired before impact.

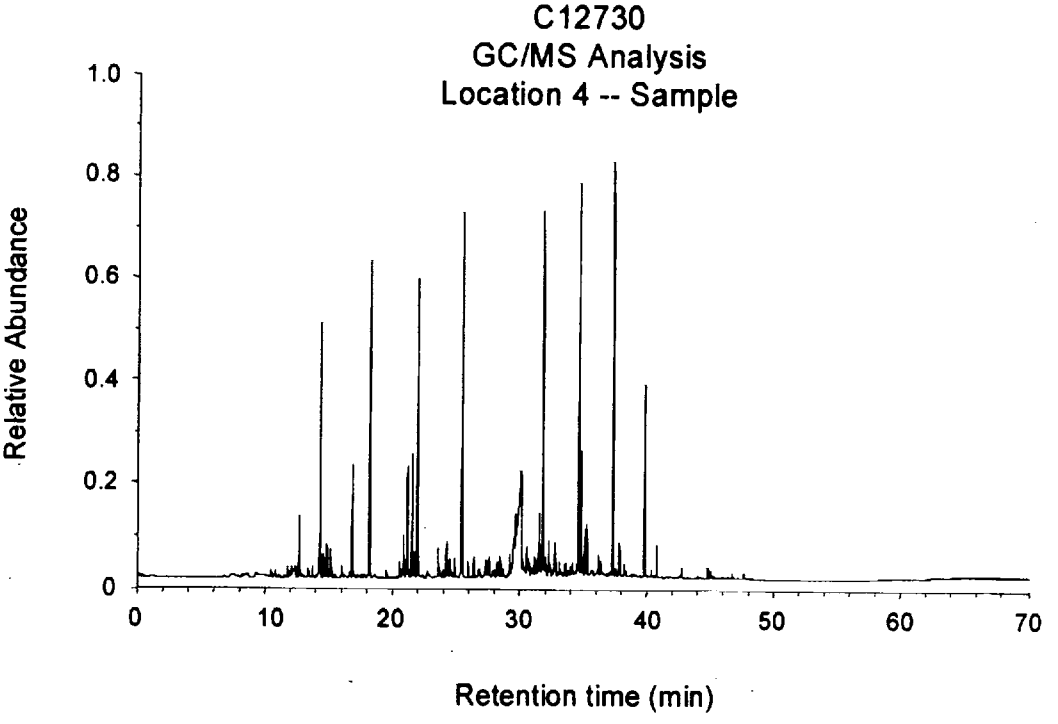


Plot C14. Crash Test C12730. Chromatogram of sample from Location 4 acquired during and after impact.

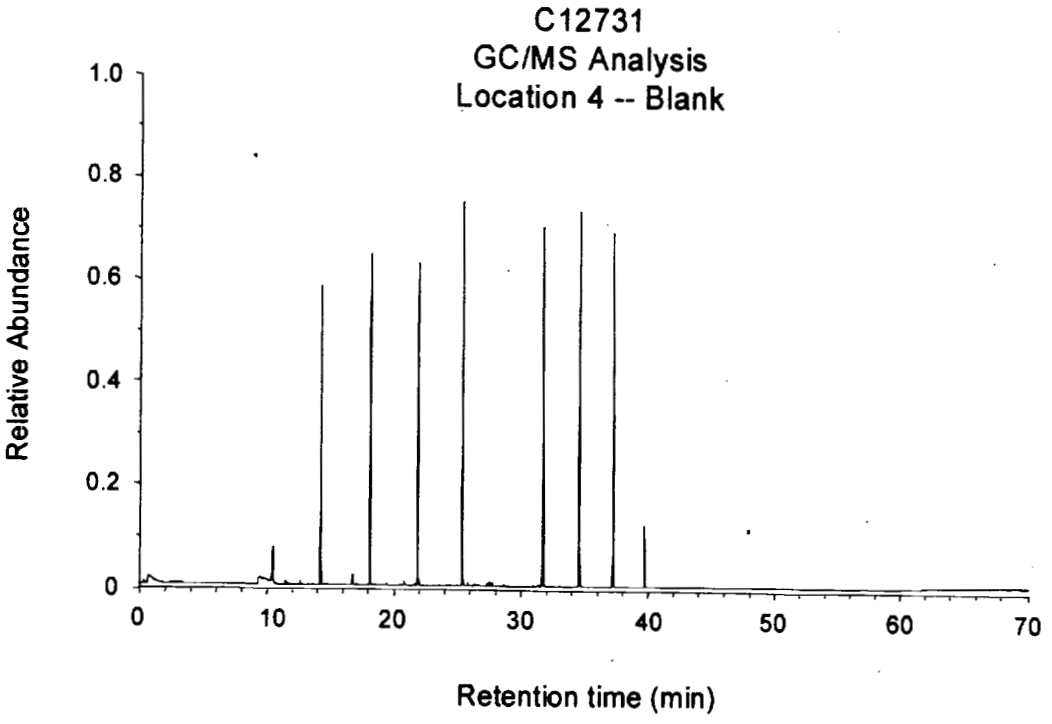


Plot C15. Crash Test C12731. Chromatogram of blank from Location 4 acquired before impact.

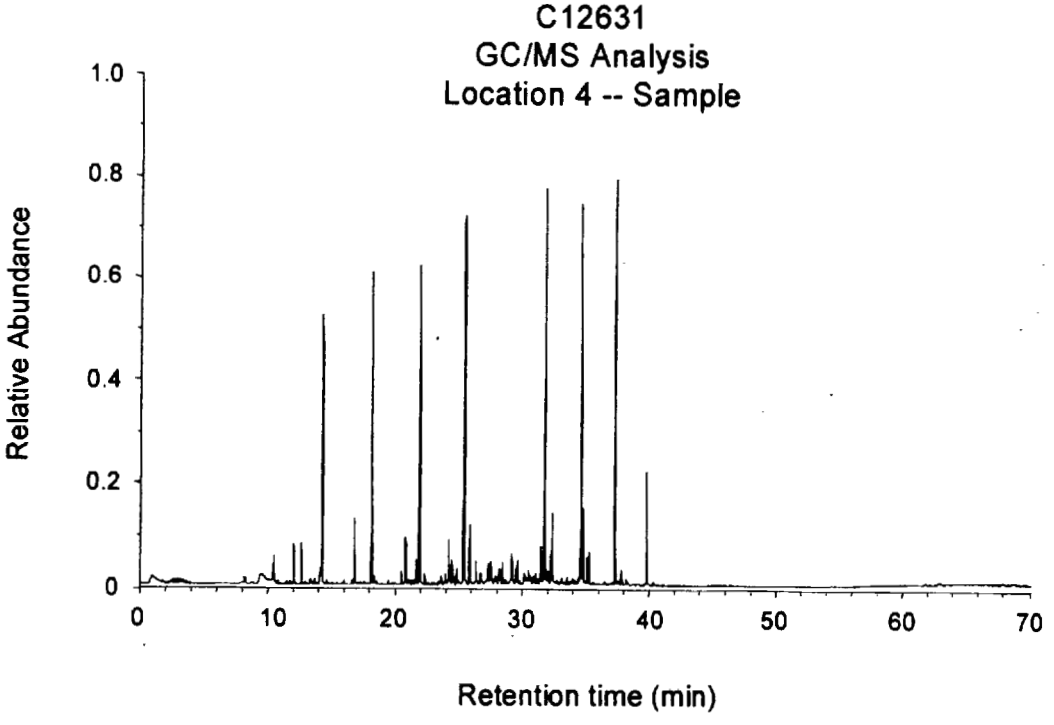


Plot C16. Crash Test C12731. Chromatogram of sample from Location 4 acquired during and after impact.

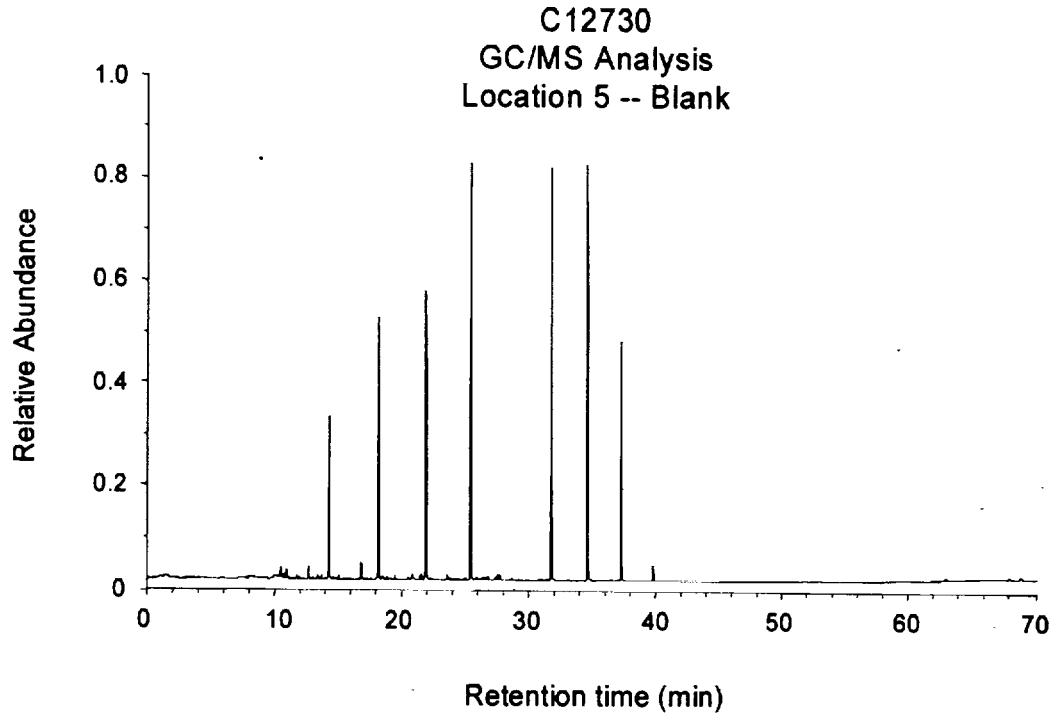


Plot C17. Crash Test C12730. Chromatogram of blank from Location 5 acquired before impact.

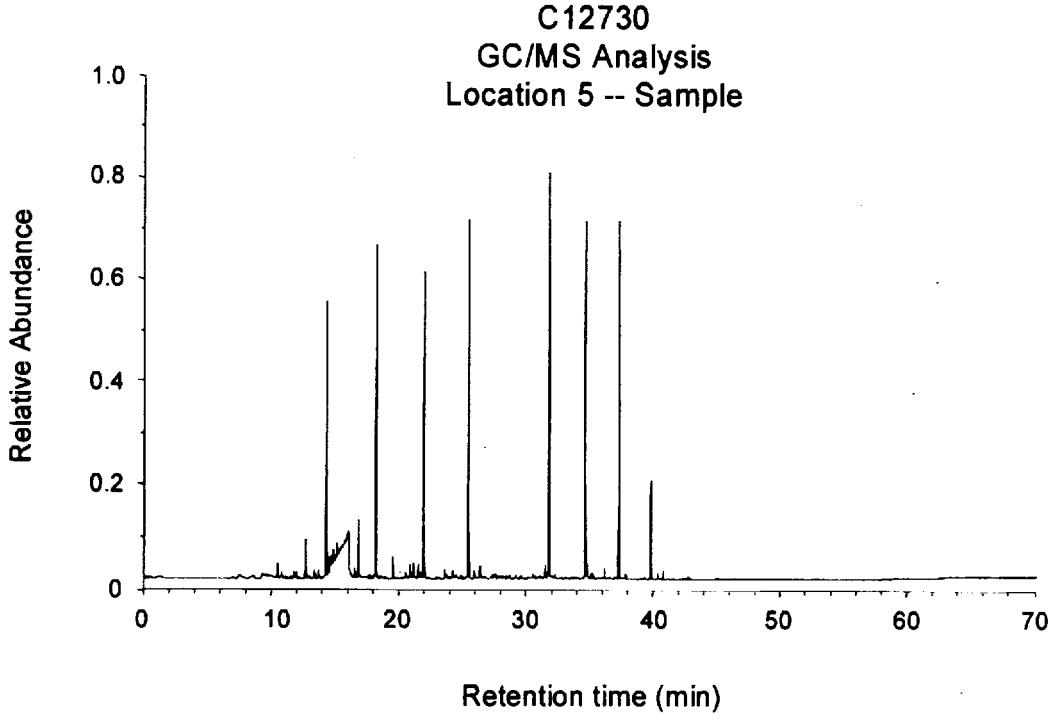


Plot C18. Crash Test C12730. Chromatogram of sample from Location 5 acquired during and after impact.

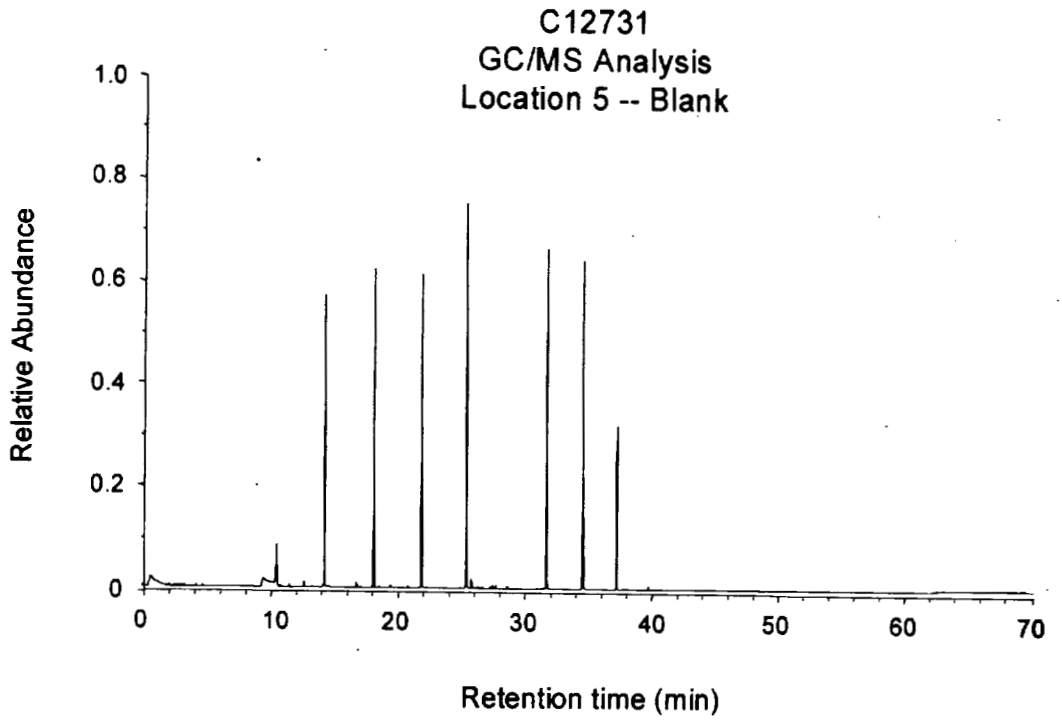


Plot C19. Crash Test C12731. Chromatogram of blank from Location 5 acquired before impact.

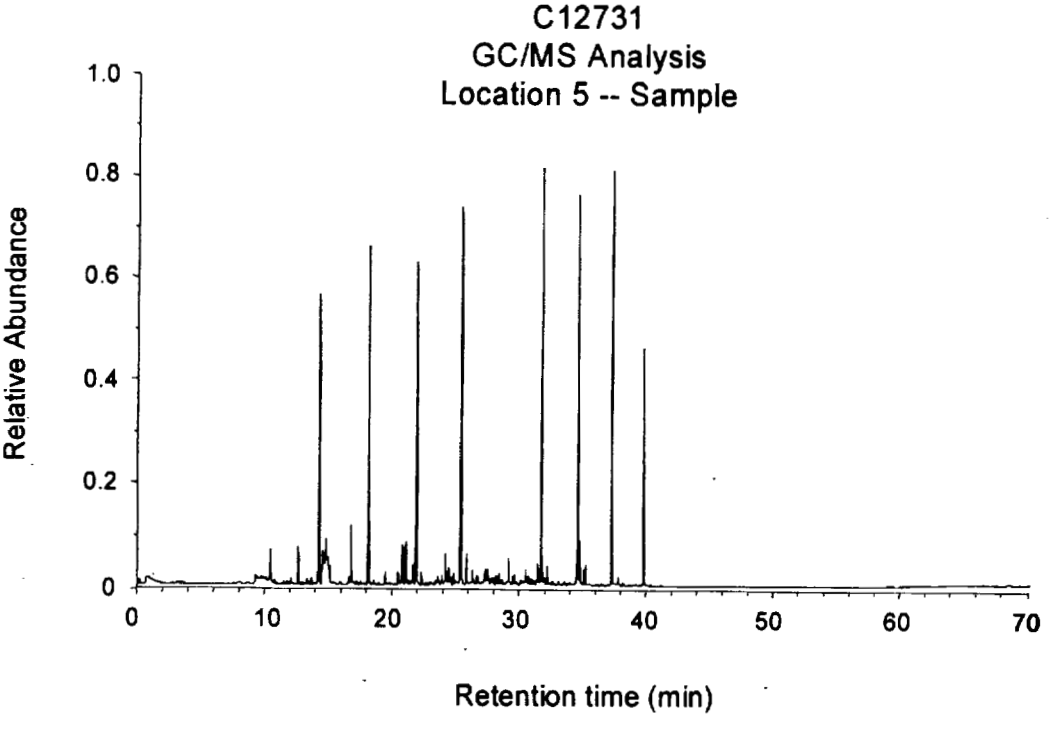


Plot C20. Crash Test C12731. Chromatogram of sample from Location 5 acquired during and

**Appendix D**

**Crash Tests C12730 and C12731**

**Exhaust manifold Temperature Data**

Type-K thermocouples were intrinsically welded to the exhaust system at the following locations:

- Thermocouple 1: Right Exhaust Take-Down Pipe
- Thermocouple 2: Exhaust Manifold Runner – Cylinder 1
- Thermocouple 3: Right Exhaust Manifold Collector
- Thermocouple 4: Exhaust Manifold Runner – Cylinder 4
- Thermocouple 5: Exhaust Manifold Runner – Cylinder 3

Each thermocouple was connected to a thermocouple amplifier (OMNI-AMP IV, Omega Engineering, Stamford, CT) calibrated using a thermocouple calibrator (Model CL27, Omega) at 0, 100, 200, 300, 400, 500, 600, 700, 800, 900, and 1000°C. The output signals from the thermocouple amplifiers were recorded by the data acquisition system at the crash test facility.

The higher exhaust system temperatures in the C12730 are attributed to the higher engine speed and longer warm-up time for the Control Vehicle (C12730) when compared to E1perimental Vehicle (C12731).

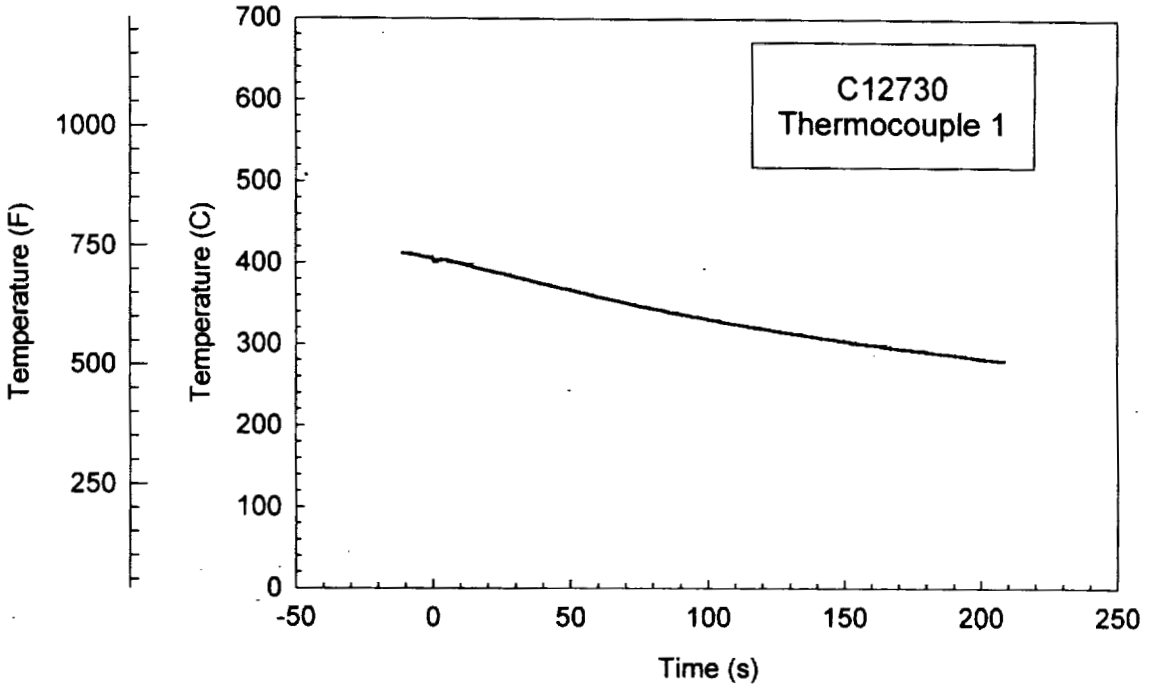


Plot D1. Crash Test C12730. Right exhaust take-down pipe temperature recorded from Thermocouple 1.

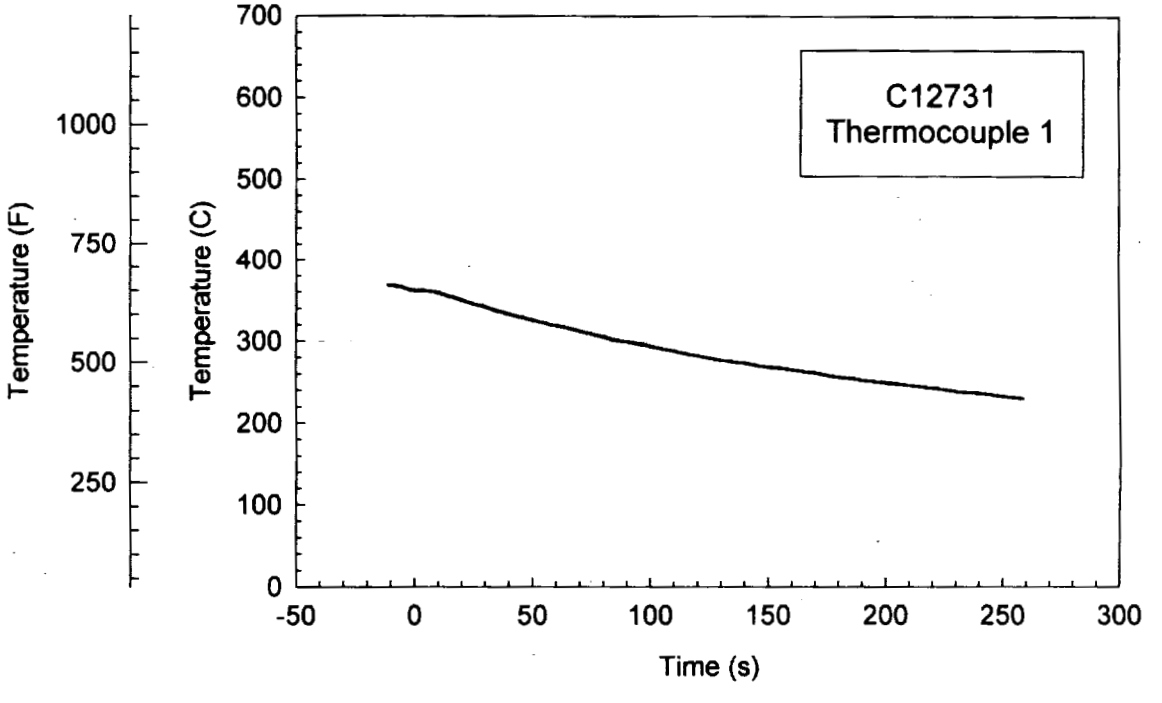


Plot D2. Crash Test C12731. Right exhaust take-down pipe temperature recorded from Thermocouple 1.

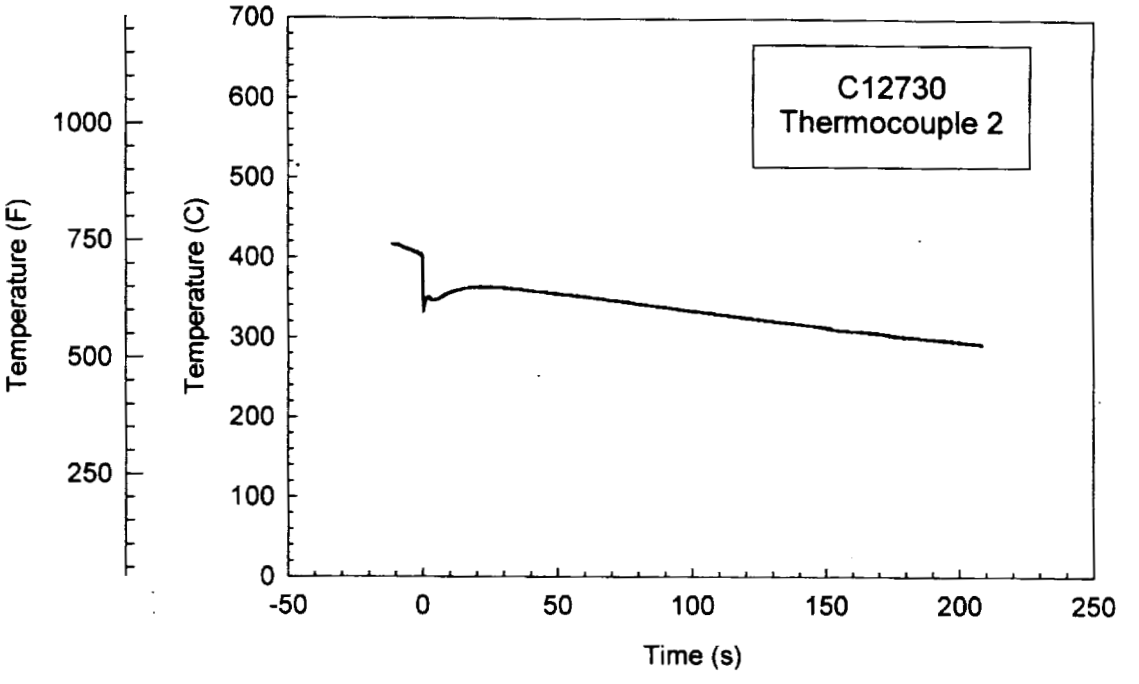


Plot D3. Crash Test C12730. Exhaust manifold runner – cylinder 1 temperature recorded from Thermocouple 2.

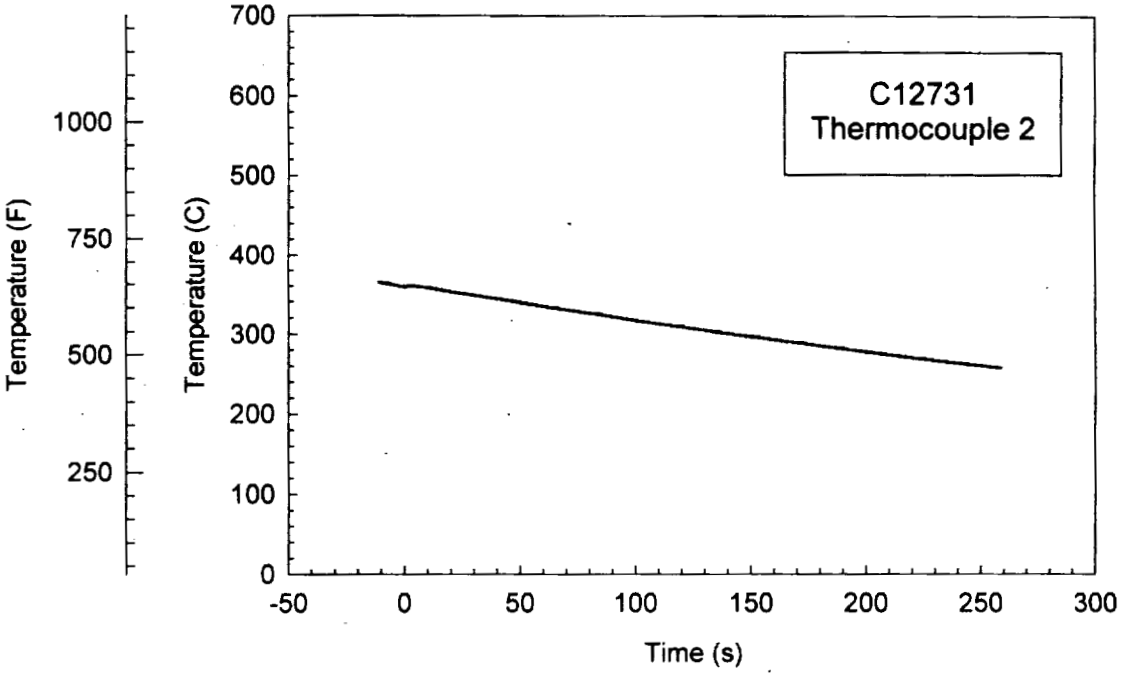


Plot D4. Crash Test C12731. Exhaust manifold runner – cylinder 1 temperature recorded from Thermocouple 2.

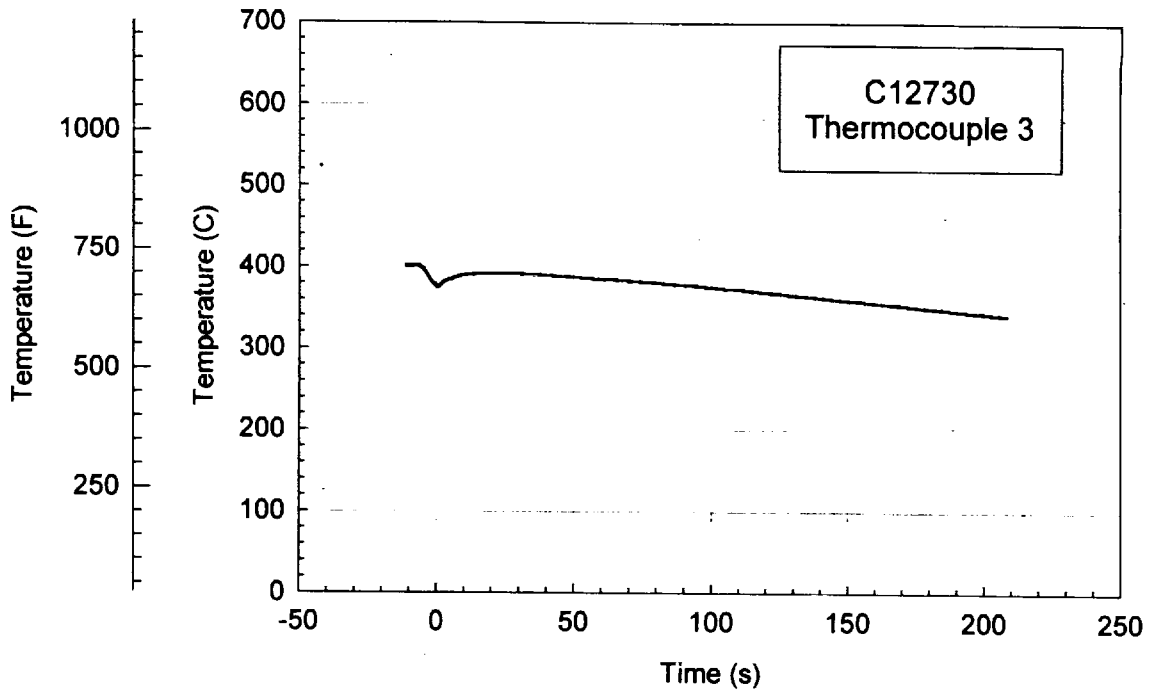


Plot D5. Crash Test C12730. Right exhaust manifold collector temperature recorded from Thermocouple 3.

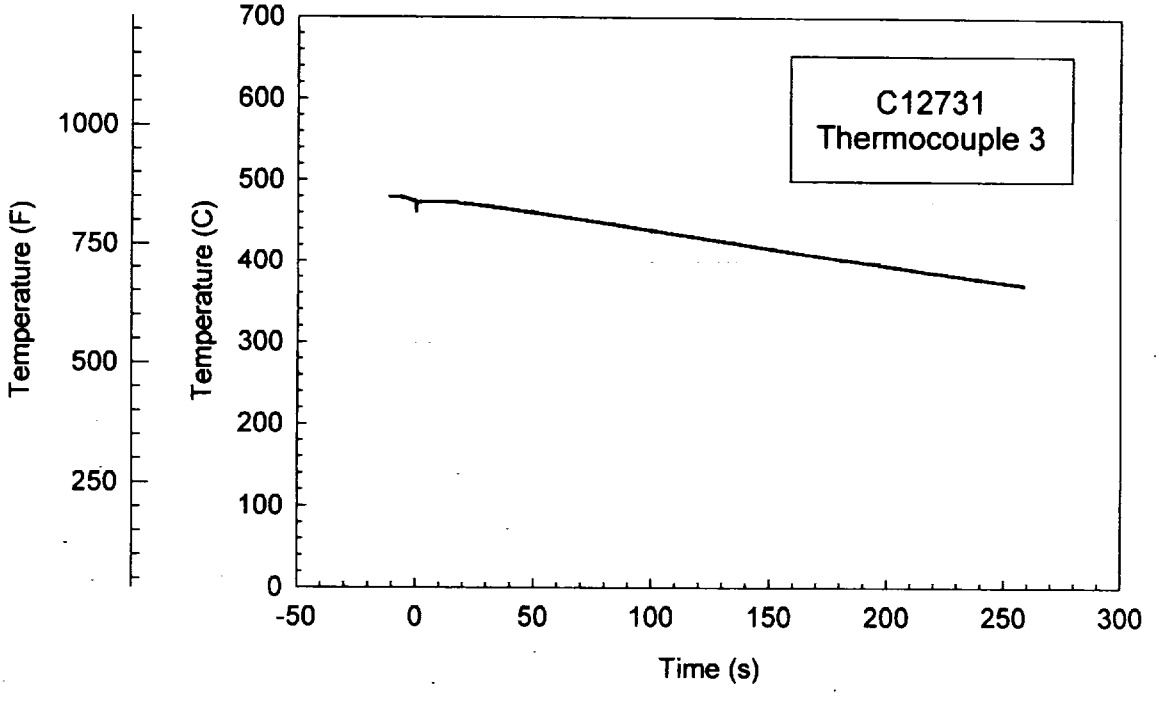


Plot D6. Crash Test C12731. Right exhaust manifold collector temperature recorded from Thermocouple 3.

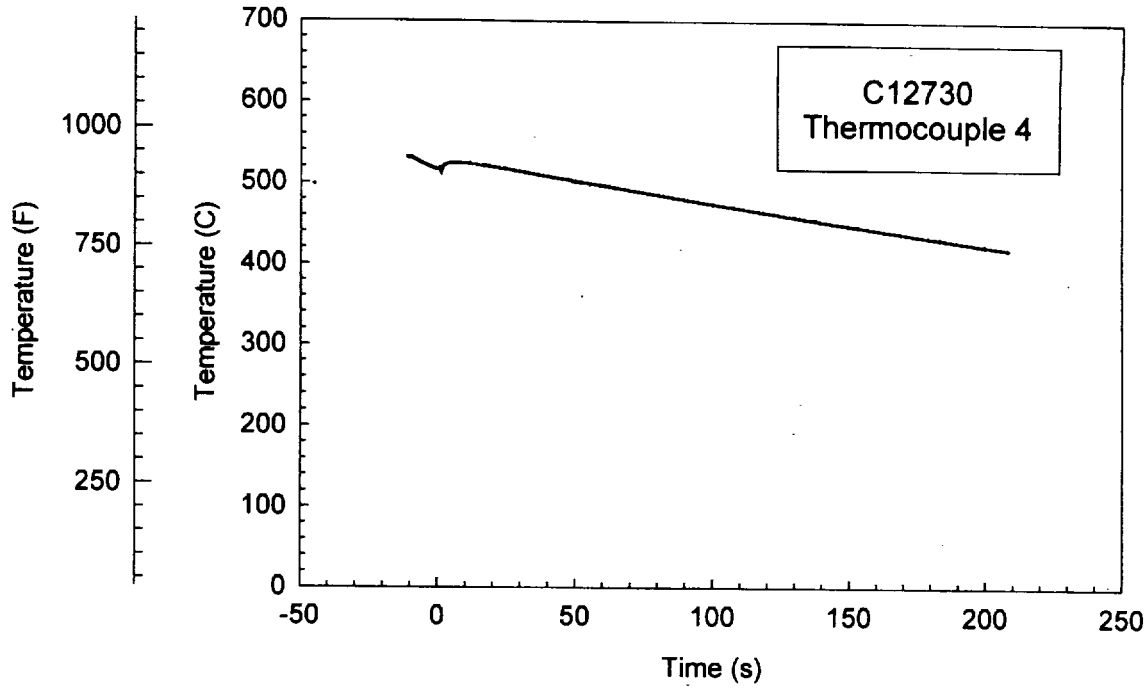


Plot D7. Crash Test C12730. Exhaust manifold runner – cylinder 4 temperature recorded from Thermocouple 4.

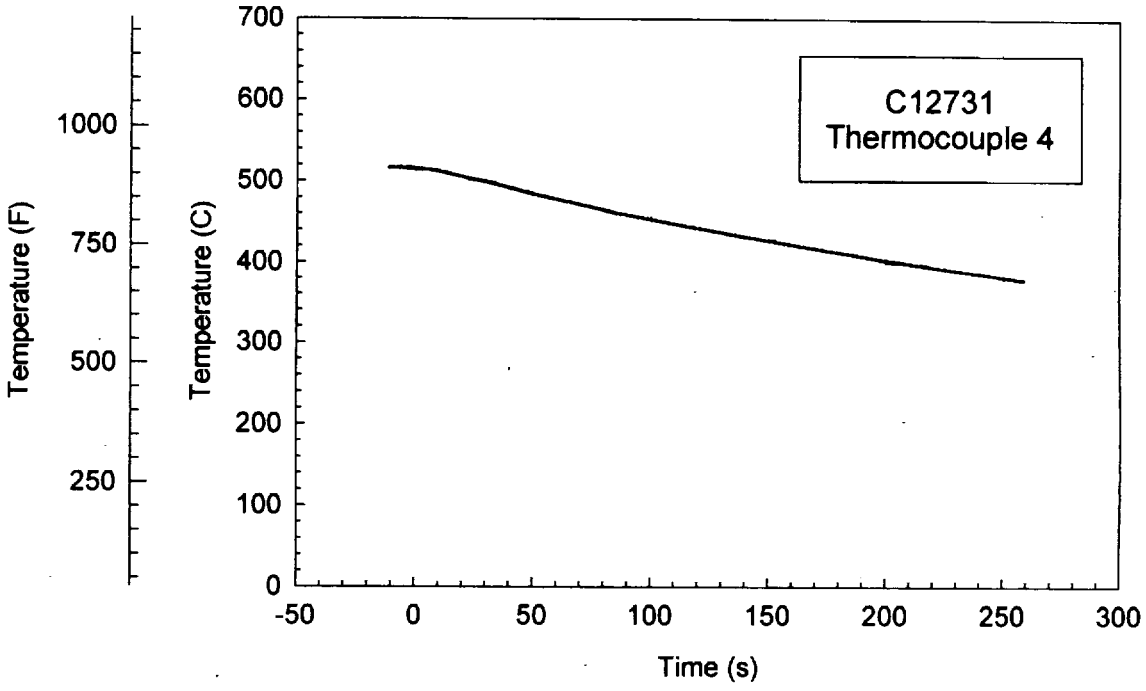


Plot D8. Crash Test C12731. Exhaust manifold runner – cylinder 4 temperature recorded from Thermocouple 4.

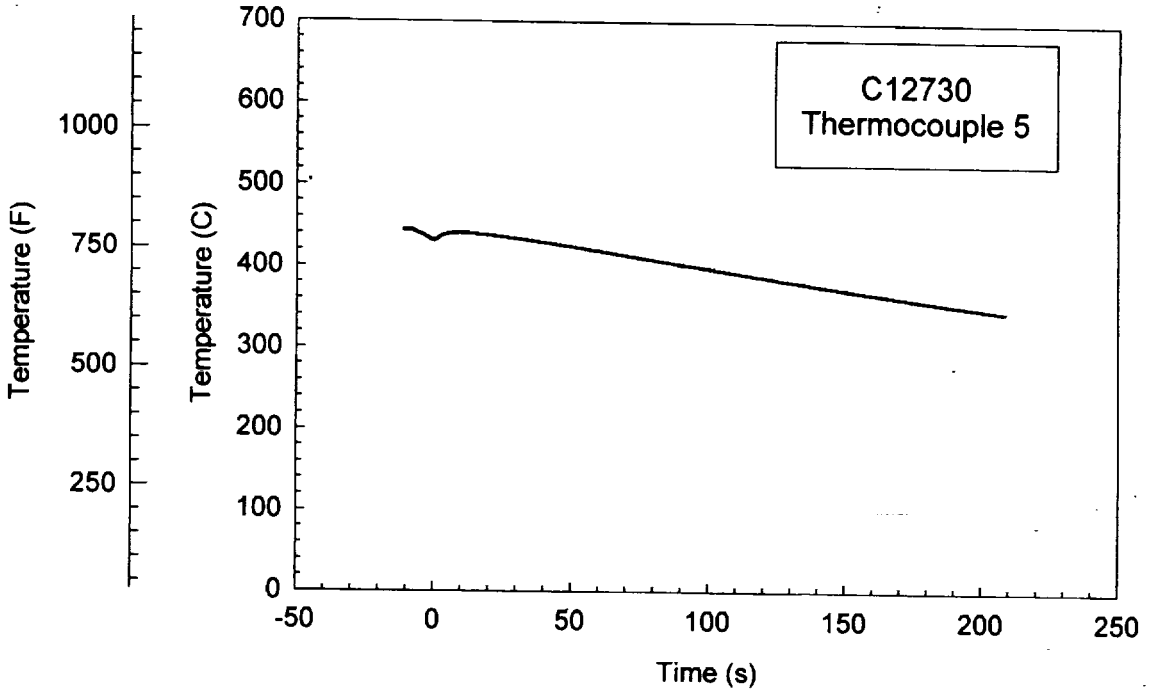


Plot D9. Crash Test C12730. Exhaust manifold runner – cylinder 3 temperature recorded from Thermocouple 5.

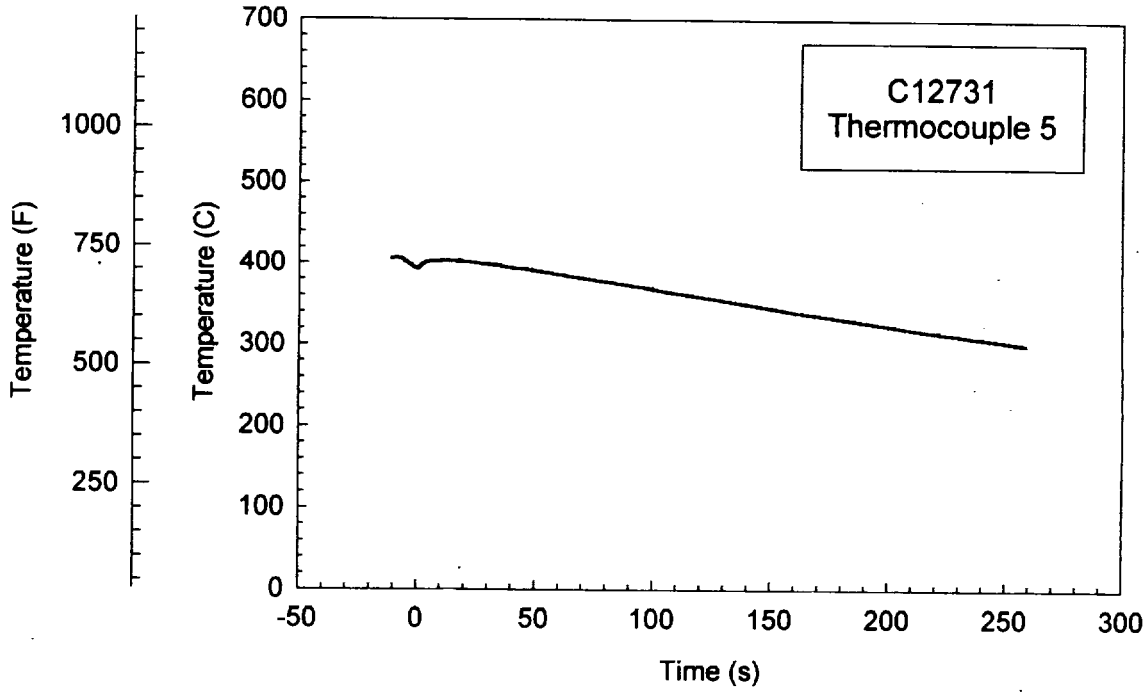


Plot D10. Crash Test C12731. Exhaust manifold runner – cylinder 3 temperature recorded from Thermocouple 5.

**Appendix E**

**Crash Tests C12730 and C12731**

**Throttle Position Sensor Data**

**Engine Speed Sensor Data**

Plots E1 and E2 show the outputs of the throttle actuator on the throttle bodies in the test vehicles for C12730 and 12731, respectively. Throttle position (% full throttle) was determined from the engine calibration for the engines in the test vehicles and the average voltage for 1 second prior to impact (Table E1).

**Table E1**
**Average Throttle Actuator Output for 1 second prior to impact and Throttle position**

| | Throttle Position Sensor (V) | Throttle Position (% Full Throttle) |
|---|---|---|
| C12730 | 0.799 | 7% |
| C12731 | 0.789 | 7% |

Plots E3 and E4 show the outputs from the camshaft position sensor in the test vehicles for C12730 and C12731, respectively. The rotation rate of the camshaft was determined from the number of timing pulses in the 1-second interval prior to impact (-1 seconds post-impact to 0 seconds post-impact). Engine speed in rotations par minute (rpm) is 2 X the camshaft rotation rate (Table E2). This method of determining engine speed has an uncertainty of ± 1 pulse per second, which results in an uncertainty in engine speed of ± 120 rpm.

**Table E2**
**Number of Camshaft Timing Pulses in the 1 second prior to impact and Engine Speed**

| | Camshaft Timing Pulses (number) | Engine Speed (rpm) |
|---|---|---|
| C12730 | 18 | 2,160 ± 120 rpm |
| C12731 | 16 | 1,920 ± 120 rpm |

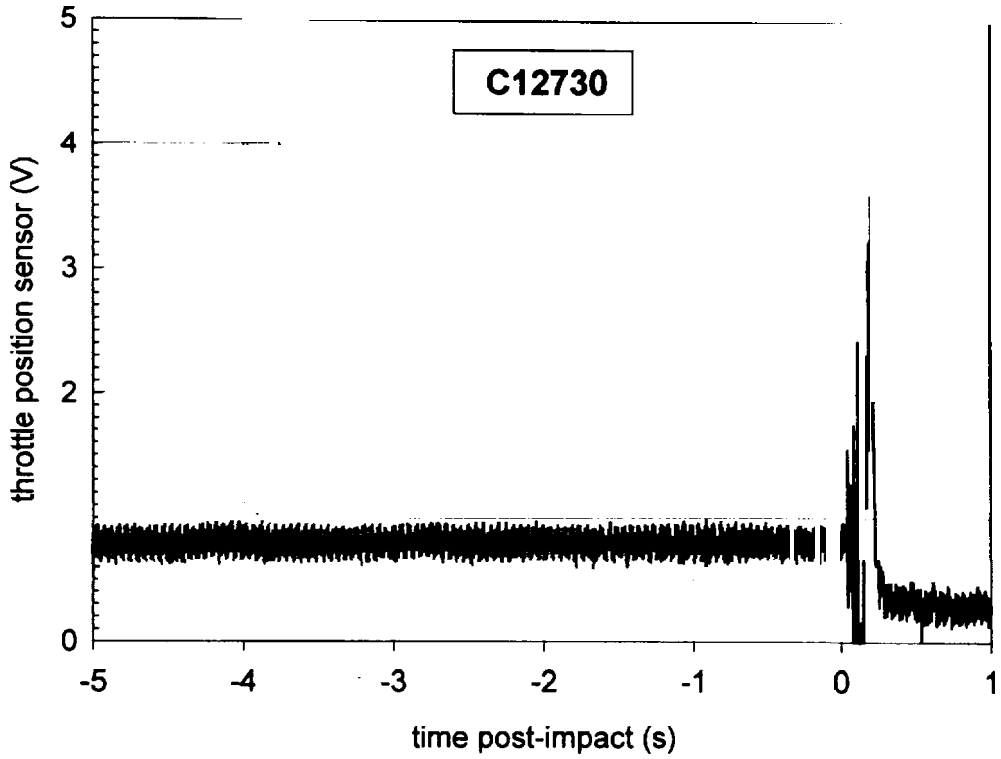


Plot E1. Crash Test C12730. Plot of throttle position sensor output

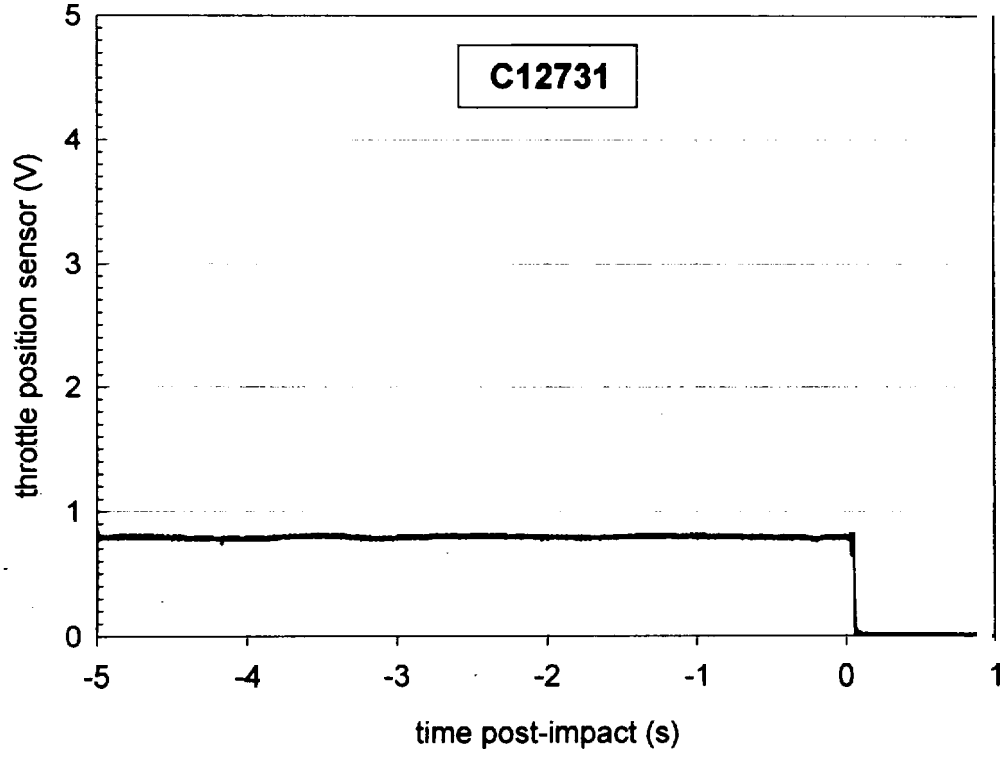


Plot E2. Crash Test C12731. Plot of throttle position sensor output.

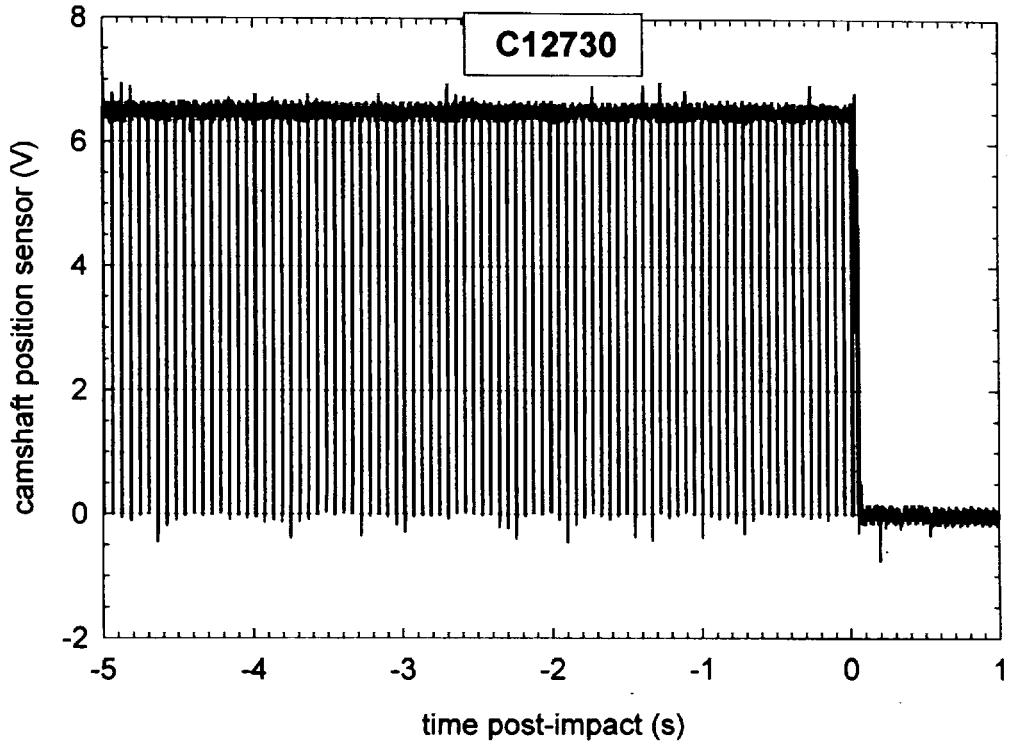


Plot E3. Crash Test C12730. Plot of camshaft position sensor output.

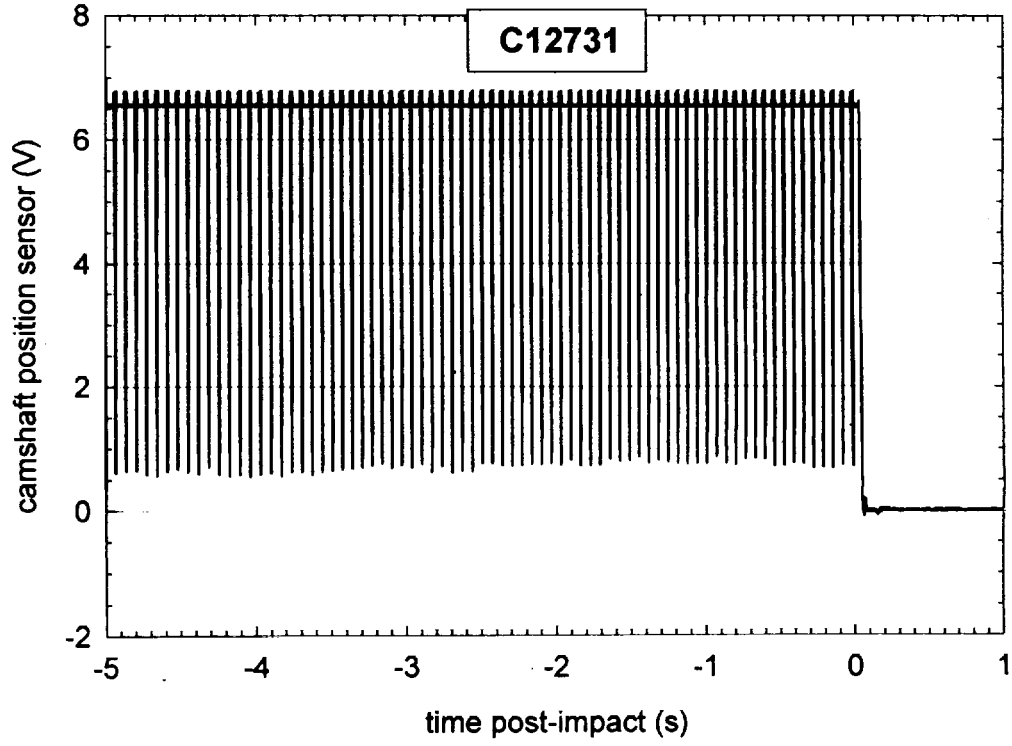


Plot E4. Crash Test C12731. Plot of camshaft position sensor output.

**Appendix F**

**Crash Tests C12730 and C12731**

**Sensing and Diagnostic Module Event Data Recorder Data**

The Sensing and Diagnostic Modules (SDM) of the Supplemental Inflatable Restraint (SIR) systems were removed from the test vehicles. The data stored in these SDM's was downloaded and interpreted using a Vetronix Crash Data Retrieval system tool version 1.3241 (Vetronix, Santa Barbara, CA).

Crash Test C12730

Vetronix

CDR CRASH DATA RETRIEVAL SYSTEM

| | |
|---|---|
| Vehicle Identification Number | 2G1FP22K8X2134711 |
| Investigator | DDF |
| Case Number | c12730 |
| Investigation Date | 1-9-02 |
| Crash Date | |
| Filename | 2G1FP22K8X2134711C.CDR |
| Saved on | 1/9/02 9:22:45 AM |
| Data check information | BDD80F21 |
| CDR version | Crash Data Retrieval Tool 1.3241 |
| Program verification number | EC73C0FB |
| Interface information | Block number: 00<br>Interface version: 28<br>Date: 10-29-01<br>Checksum: 3700 |
| Event(s) recovered | Deployment<br>Near deployment |

## SDM DATA LIMITATIONS

SDM Recorded Crash Events:
There are two types of SDM recorded crash events. The first is the Near Deployment Event. A Near Deployment Event is an event severe enough to "wake up" the sensing algorithm but not severe enough to deploy the air bag(s). It contains Pre-Crash and Crash data. The SDM can store up to one Near Deployment Event. This event can be overwritten by another Near Deployment event. This event will be cleared by the SDM after the ignition has been cycled 250 times.
The second type of SDM recorded crash event is the Deployment Event. It also contains Pre-Crash and Crash data. The SDM can store up to two different Deployment Events, if they occur within five seconds of one another. The first deployment event will be stored in the Deployment file (this would have been the event that deployed the air bag) and the second Deployment Event will be stored in the Near Deployment file. Deployment events can not be overwritten or cleared from the SDM. Once the SDM has deployed the air bag, the SDM must be replaced.
The data in the near deployment file will be locked after a deployment, if the near deployment occurred within 5 seconds before the deployment or a deployment level event occurs within 5 seconds after the deployment.

SDM Data Limitations:
-SDM Adjusted Algorithm Forward Velocity Change:
Once the crash data is downloaded, the CDR tool mathematically adjusts the recorded algorithm forward velocity data to generate an adjusted algorithm forward velocity change (AA/Delta V) that may more closely approximate the forward velocity change the sensing system experienced during the recorded portion of the event. The adjustment takes place within the downloading tool and does not affect the crash data, which remains stored in the SDM. The AA/Delta V may not closely approximate what the sensing system experienced in all types of events. For example, if a crash is preceded by other common events, such as rough road, struck objects, or off-road travel, the AA/Delta V may be less than, and some times significantly less than the actual forward velocity change the sensing system experienced. This data should be examined in conjunction with other available physical evidence from the vehicle and scene when assessing occupant or vehicle forward velocity change. The SDM will record 100 milliseconds of data after deployment criteria is met and up to 50 milliseconds before deployment criteria is met. The maximum value that can be recorded for SDM Adjusted Algorithm Forward Velocity Change is about 112 MPH.
-SDM Recorded Vehicle Speed accuracy can be affected if the vehicle has had the tire size or the final drive axle ratio changed from the factory build specifications.
-Brake Switch Circuit Status indicates the status of the brake switch circuit.
-Some of the Pre-Crash data, from the Deployment file, may be recorded after algorithm enable, if the Deployment event has a long crash pulse.
-Pre-Crash Electronic Data Validity Check Status indicates "Data Invalid" if the SDM does not receive a valid message for any of the four Pre-Crash data parameters (Vehicle Speed, Engine Speed, Percent Throttle, and Brake Switch Circuit Status).
-Driver's Belt Switch Circuit Status indicates the status of the driver's seat belt switch circuit. If the vehicle's electrical system is compromised during a crash, the state of the Driver's Belt Switch Circuit may be reported as unbuckled, although the driver's seat belt was buckled.
-Passenger Front Air Bag Suppression Switch Circuit Status indicates the status of the suppression switch circuit.
-The Time Between Events is displayed in seconds. If the time between the two events is greater than five seconds, "N/A" is displayed in place of the time.
-If power to the SDM is lost during a crash event, all or part of the crash record may not be recorded.

SDM Data Source:
All SDM recorded data is measured, calculated, and stored internally, except for the following:
-Vehicle Speed, Engine Speed, and Percent Throttle data are transmitted once a second by the Powertrain Control Module (PCM), via the Class 2 data link, to the SDM.
-Brake Switch Circuit Status data is transmitted once a second by either the ABS module or the PCM, via the Class 2 data link, to the SDM. Depending on vehicle option content, the Brake Switch Circuit Status data may not be available.
-In most vehicles, the Driver's Belt Switch Circuit is wired directly to the SDM. In some vehicles, the Driver's Belt Switch Circuit status data is transmitted from the Body Control Module (BCM), via the Class 2 data link, to the SDM.
-The Passenger Front Air Bag Suppression Switch Circuit is wired directly to the SDM.

## System Status At Deployment

| | |
|---|---|
| SIR Warning Lamp Status | OFF |
| Driver's Belt Switch Circuit Status | UNBUCKLED |
| Passenger Front Air Bag Suppression Switch Circuit Status | Air Bag Not Suppressed |
| Ignition Cycles At Deployment | 143 |
| Time Between Events (sec) | N/A |

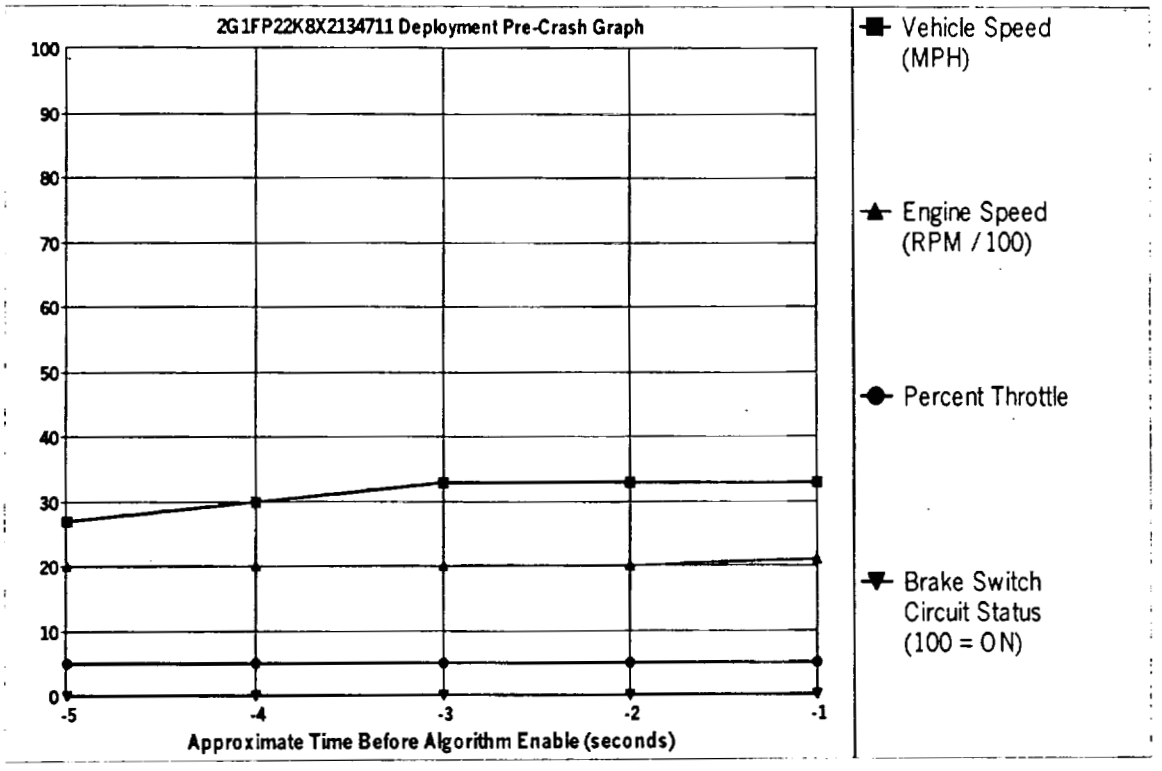


| Seconds Before AE | Vehicle Speed (MPH) | Engine Speed (RPM) | Percent Throttle | Brake Switch Circuit Status |
|---|---|---|---|---|
| -5 | 27 | 1984 | 5 | OFF |
| -4 | 30 | 2048 | 5 | OFF |
| -3 | 33 | 2048 | 5 | OFF |
| -2 | 33 | 2048 | 5 | OFF |
| -1 | 33 | 2112 | 5 | OFF |

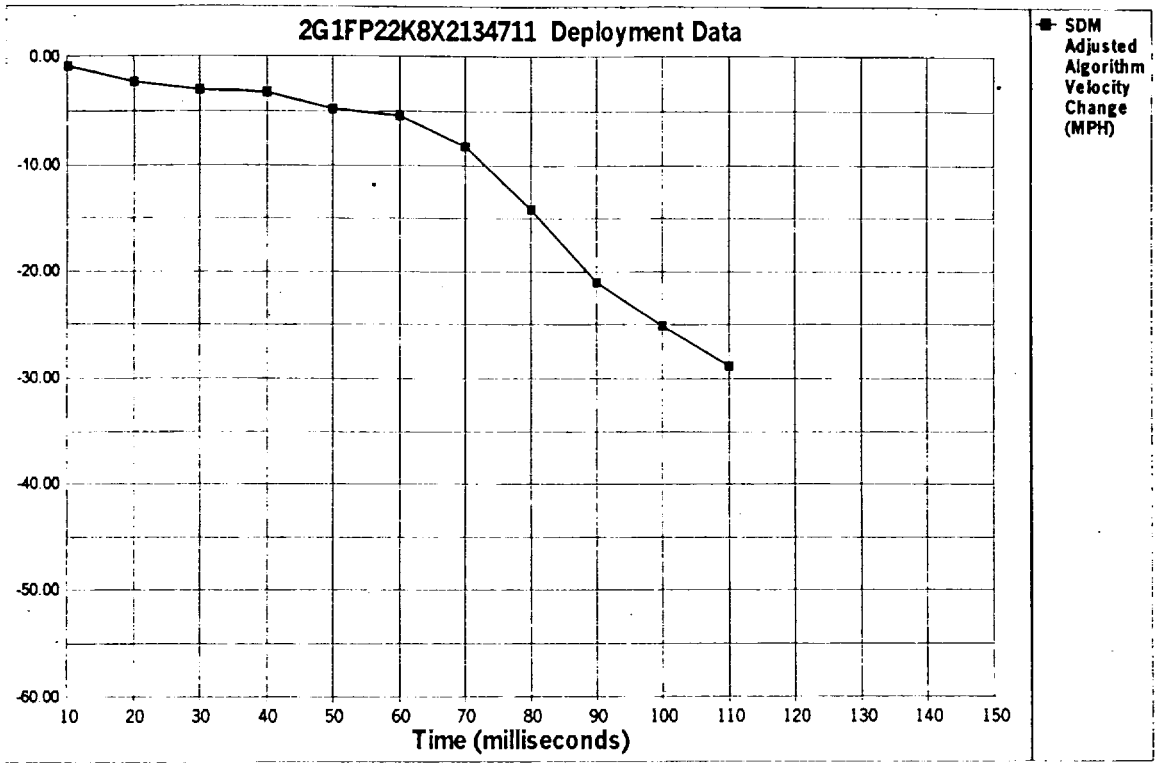


| Time (milliseconds) | 10 | 20 | 30 | 40 | 50 | 60 | 70 | 80 | 90 | 100 | 110 | 120 | 130 | 140 | 150 |
|---|---|---|---|---|---|---|---|---|---|---|---|---|---|---|---|
| Adjusted Algorithm Velocity Change | -0.75 | -2.28 | -2.94 | -3.16 | -4.70 | -5.36 | -8.21 | -14.13 | -20.94 | -25.11 | -28.84 | N/A | N/A | N/A | N/A |

Vetronix

CDR CRASH DATA RETRIEVAL SYSTEM

## System Status At Near Deployment

| | |
|---|---|
| SIR Warning Lamp Status | OFF |
| Driver's Belt Switch Circuit Status | BUCKLED |
| Passenger Front Air Bag Suppression Switch Circuit Status | Air Bag Not Suppressed |
| Ignition Cycles At Near Deployment | 30 |

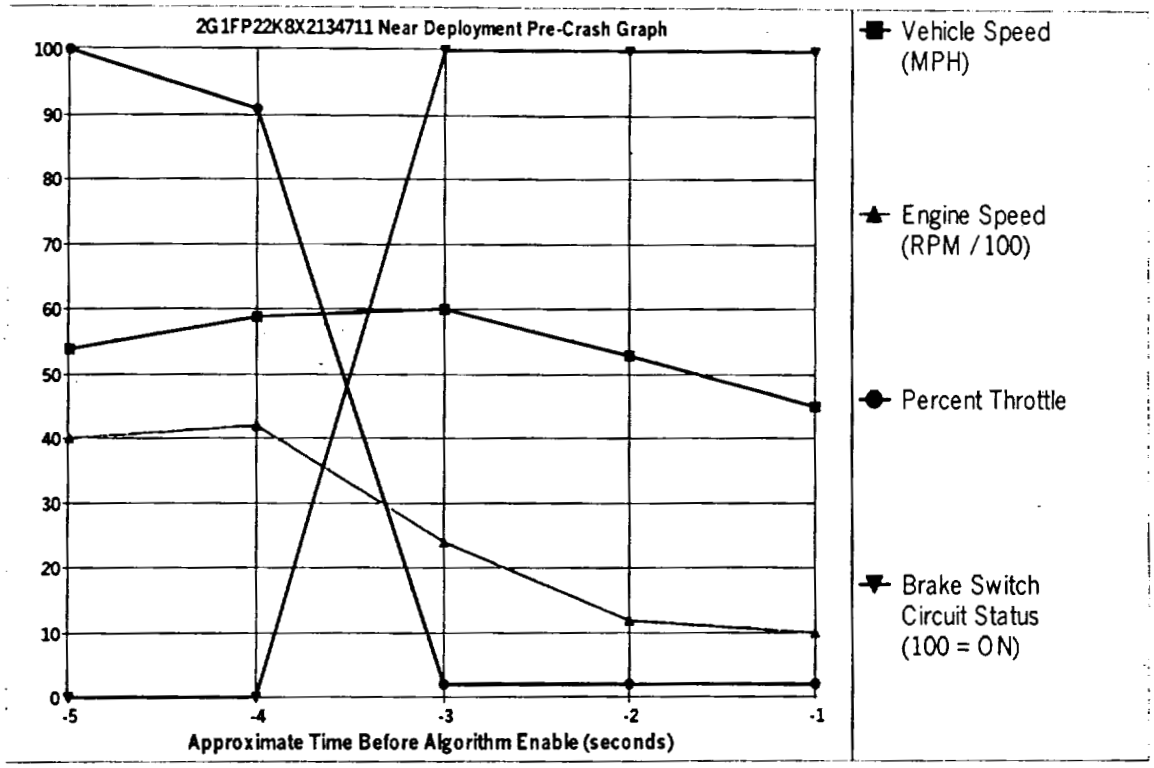


| Seconds Before AE | Vehicle Speed (MPH) | Engine Speed (RPM) | Percent Throttle | Brake Switch Circuit Status |
|---|---|---|---|---|
| -5 | 54 | 4032 | 100 | OFF |
| -4 | 59 | 4224 | 91 | OFF |
| -3 | 60 | 2368 | 2 | ON |
| -2 | 53 | 1152 | 2 | ON |
| -1 | 45 | 960 | 2 | ON |

## Hexadecimal Data

**This page displays all the data retrieved from the air bag module. It contains data that is not converted by this program.**

```
$01   7C 05 00 00
$02   8A 11
$03   41 53 39 31 30 39
$04   4B 33 4A 4A 58 31
$05   00
$06   16 24 31 31
$11   A0 A3 A2 FF AA 01
$14   03 04 B4 00
$18   7F 7E 80 CD FF 00
$1C   31 32 46 50 50 50
$1D   50 32 32 46 53 56
$1E   56 56
$1F   FF 02 00 00
$20   80 00 00 FF 03 F8
$21   FF FF FF FF FF FF
$22   FF FF 01 00 02 03
$23   00 00 00 00 00 00
$24   00 00 00 00 00 00
$25   00 00 FF 0E 48 56
$26   61 5F 57 00 E0 00
$27   06 06 06 E7 FF 00
$28   0F 12 25 42 3F 00
$29   FF FC C0 FF FF FF
$2A   FF FF FF FF E4 00
$2B   00 00 00 00 00
$30   80 00 00 FF 00 C0
$31   FF FF FE FF FF FF
$32   FF FF 0E 03 02 01
$33   04 05 05 08 09 0F
$34   1C 2B 34 3C FF FF
$35   FF FF 0B 53 07 97
$36   35 35 35 31 2B 00
$37   00 00 0D 0D 0D 0D
$38   0D 00 21 20 20 20
$39   1F 00 FF EE 80 00
$3A   F9 00 20 00
$40   FF FF FF FF FF FF
$41   FF FF FF FF FF FF
$42   FF FF
```

## Comments

DOT fire test

Crash Test C12731

| | |
|---|---|
| Vehicle Identification Number | 2G1FP22K9X2134474 |
| Investigator | DDF |
| Case Number | c12731 |
| Investigation Date | 1-9-02 |
| Crash Date | |
| Program verification number | EC73C0FB |
| Interface information | Block number: 00<br>Interface version: 28<br>Date: 10-29-01<br>Checksum: 3700 |
| Event(s) recovered | Deployment |

## SDM DATA LIMITATIONS

SDM Recorded Crash Events:
There are two types of SDM recorded crash events. The first is the Near Deployment Event. A Near Deployment Event is an event severe enough to "wake up" the sensing algorithm but not severe enough to deploy the air bag(s). It contains Pre-Crash and Crash data. The SDM can store up to one Near Deployment Event. This event can be overwritten by another Near Deployment event. This event will be cleared by the SDM after the ignition has been cycled 250 times.
The second type of SDM recorded crash event is the Deployment Event. It also contains Pre-Crash and Crash data. The SDM can store up to two different Deployment Events, if they occur within five seconds of one another. The first deployment event will be stored in the Deployment file (this would have been the event that deployed the air bag) and the second Deployment Event will be stored in the Near Deployment file. Deployment events can not be overwritten or cleared from the SDM. Once the SDM has deployed the air bag, the SDM must be replaced.
The data in the near deployment file will be locked after a deployment, if the near deployment occurred within 5 seconds before the deployment or a deployment level event occurs within 5 seconds after the deployment.

SDM Data Limitations:
-SDM Adjusted Algorithm Forward Velocity Change:
Once the crash data is downloaded, the CDR tool mathematically adjusts the recorded algorithm forward velocity data to generate an adjusted algorithm forward velocity change (AA/Delta V) that may more closely approximate the forward velocity change the sensing system experienced during the recorded portion of the event. The adjustment takes place within the downloading tool and does not affect the crash data, which remains stored in the SDM. The AA/Delta V may not closely approximate what the sensing system experienced in all types of events. For example, if a crash is preceded by other common events, such as rough road, struck objects, or off-road travel, the AA/Delta V may be less than, and some times significantly less than the actual forward velocity change the sensing system experienced. This data should be examined in conjunction with other available physical evidence from the vehicle and scene when assessing occupant or vehicle forward velocity change. The SDM will record 100 milliseconds of data after deployment criteria is met and up to 50 milliseconds before deployment criteria is met. The maximum value that can be recorded for SDM Adjusted Algorithm Forward Velocity Change is about 112 MPH.
-SDM Recorded Vehicle Speed accuracy can be affected if the vehicle has had the tire size or the final drive axle ratio changed from the factory build specifications.
-Brake Switch Circuit Status indicates the status of the brake switch circuit.
-Some of the Pre-Crash data, from the Deployment file, may be recorded after algorithm enable, if the Deployment event has a long crash pulse.
-Pre-Crash Electronic Data Validity Check Status indicates "Data Invalid" if the SDM does not receive a valid message for any of the four Pre-Crash data parameters (Vehicle Speed, Engine Speed, Percent Throttle, and Brake Switch Circuit Status).
-Driver's Belt Switch Circuit Status indicates the status of the driver's seat belt switch circuit. If the vehicle's electrical system is compromised during a crash, the state of the Driver's Belt Switch Circuit may be reported as unbuckled, although the driver's seat belt was buckled.
-Passenger Front Air Bag Suppression Switch Circuit Status indicates the status of the suppression switch circuit.
-The Time Between Events is displayed in seconds. If the time between the two events is greater than five seconds, "N/A" is displayed in place of the time.
-If power to the SDM is lost during a crash event, all or part of the crash record may not be recorded.

SDM Data Source:
All SDM recorded data is measured, calculated, and stored internally, except for the following:
-Vehicle Speed, Engine Speed, and Percent Throttle data are transmitted once a second by the Powertrain Control Module (PCM), via the Class 2 data link, to the SDM.
-Brake Switch Circuit Status data is transmitted once a second by either the ABS module or the PCM, via the Class 2 data link, to the SDM. Depending on vehicle option content, the Brake Switch Circuit Status data may not be available.
-In most vehicles, the Driver's Belt Switch Circuit is wired directly to the SDM. In some vehicles, the Driver's Belt Switch Circuit status data is transmitted from the Body Control Module (BCM), via the Class 2 data link, to the SDM.
-The Passenger Front Air Bag Suppression Switch Circuit is wired directly to the SDM.

## System Status At Deployment

| | |
|---|---|
| SIR Warning Lamp Status | OFF |
| Driver's Belt Switch Circuit Status | UNBUCKLED |
| Passenger Front Air Bag Suppression Switch Circuit Status | Air Bag Not Suppressed |
| Ignition Cycles At Deployment | 69 |
| Time Between Events (sec) | N/A |

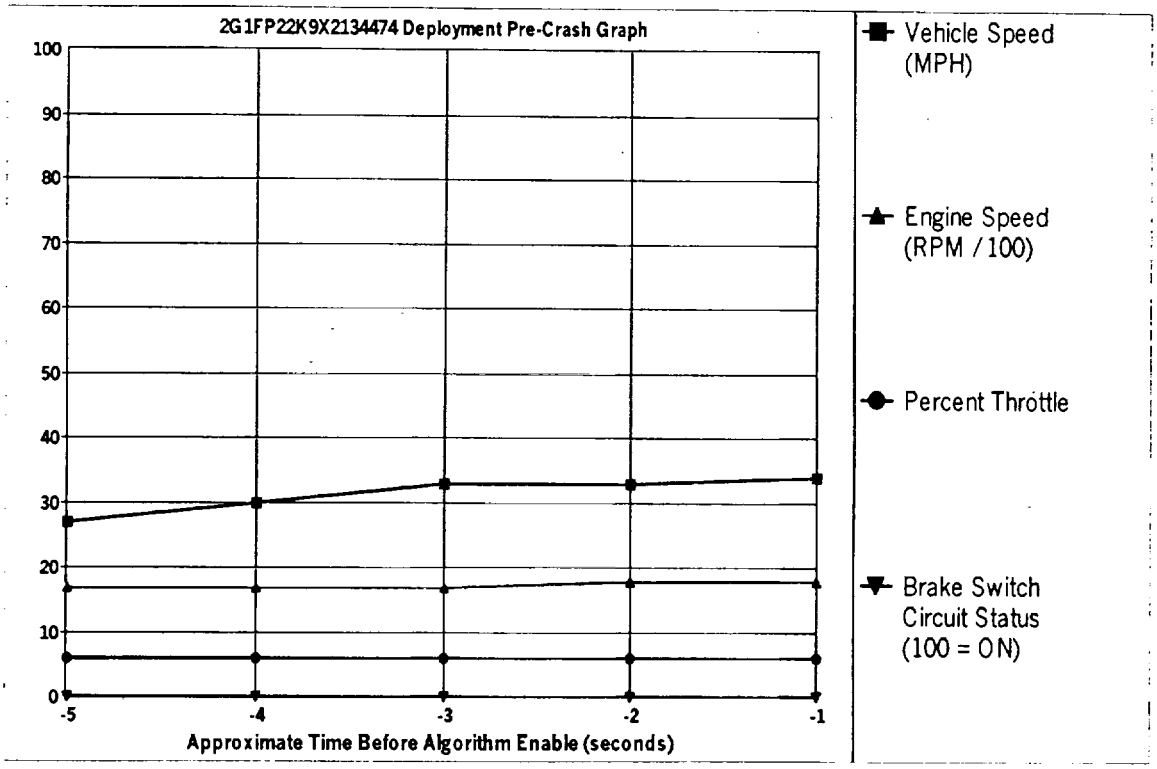


| Seconds Before AE | Vehicle Speed (MPH) | Engine Speed (RPM) | Percent Throttle | Brake Switch Circuit Status |
|---|---|---|---|---|
| -5 | 27 | 1728 | 6 | OFF |
| -4 | 30 | 1728 | 6 | OFF |
| -3 | 33 | 1728 | 6 | OFF |
| -2 | 33 | 1792 | 6 | OFF |
| -1 | 34 | 1792 | 6 | OFF |

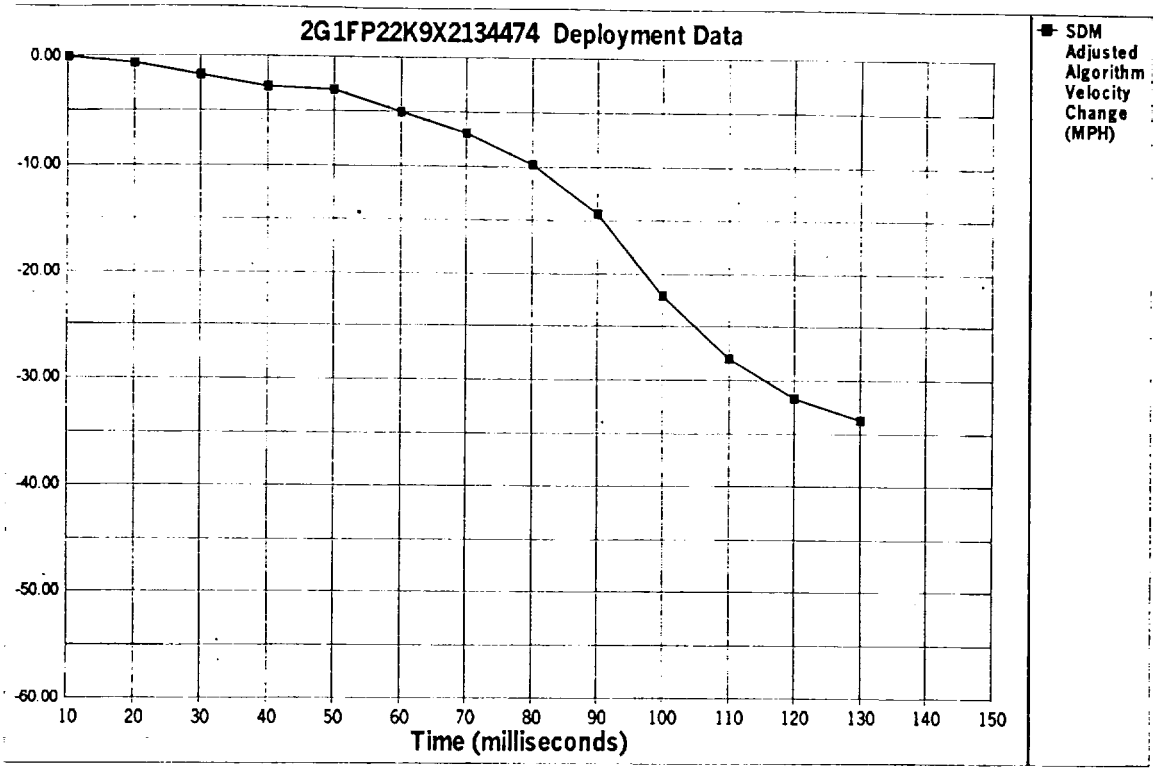


| Time (milliseconds) | 10 | 20 | 30 | 40 | 50 | 60 | 70 | 80 | 90 | 100 | 110 | 120 | 130 | 140 | 150 |
|---|---|---|---|---|---|---|---|---|---|---|---|---|---|---|---|
| Adjusted Algorithm Velocity Change | 0.00 | -0.55 | -1.65 | -2.74 | -2.96 | -4.94 | -6.91 | -9.77 | -14.38 | -22.05 | -27.98 | -31.71 | -33.68 | N/A | N/A |

## Hexadecimal Data

**This page displays all the data retrieved from the air bag module. It contains data that is not converted by this program.**

```
$01   7C 05 00 00
$02   8A 11
$03   41 53 39 31 30 38
$04   4B 33 4A 39 50 31
$05   00
$06   16 24 31 31
$11   A1 A4 A4 FF AC 01
$14   03 04 B4 00
$18   83 81 84 CE FF 00
$1C   31 32 46 50 50 50
$1D   50 32 32 46 53 56
$1E   56 56
$1F   FF 02 00 00
$20   FF FF FF FF FF FF
$21   FF FF FF FF FF FF
$22   FF FF FF FF FF FF
$23   FF FF FF FF FF FF
$24   FF FF FF FF FF FF
$25   FF FF FF FF FF FF
$26   FF FF FF FF FF FF
$27   FF FF FF FF FF FF
$28   FF FF FF FF FF FF
$29   FF FF FF FF FF FF
$2A   FF FF FF FF FF FF
$2B   FF FF FF FF FF
$30   80 00 00 FF 08 FC
$31   FF FF FE FF FF FF
$32   FF FF 0F 03 02 00
$33   01 03 05 05 09 0D
$34   13 1D 2E 3B 43 47
$35   FF FF 0D 5D 08 F6
$36   36 35 35 31 2B 00
$37   00 00 0F 0F 0F 0F
$38   0F 00 1C 1C 1B 1B
$39   1B 00 FF F7 E0 00
$3A   BD 00 20 00
$40   FF FF FF FF FF FF
$41   FF FF FF FF FF FF
$42   FF FF
```

## Comments

DOT fire test

## Appendix G

## Fire Tests F99B1401 and F99B1402
## Video Camera Set-up

Seven video cameras were used in Fire Test F99B1401 and eight video cameras were used in Fire Test F99B1402. Differences in the deformation of the test vehicles from the crash tests made it necessary to use an additional video camera in Fire Test F99B1402 to view the area in the engine compartment around the air cleaner housing. Figure G1 shows the approximate locations of the video cameras relative to the test vehicle during this test.

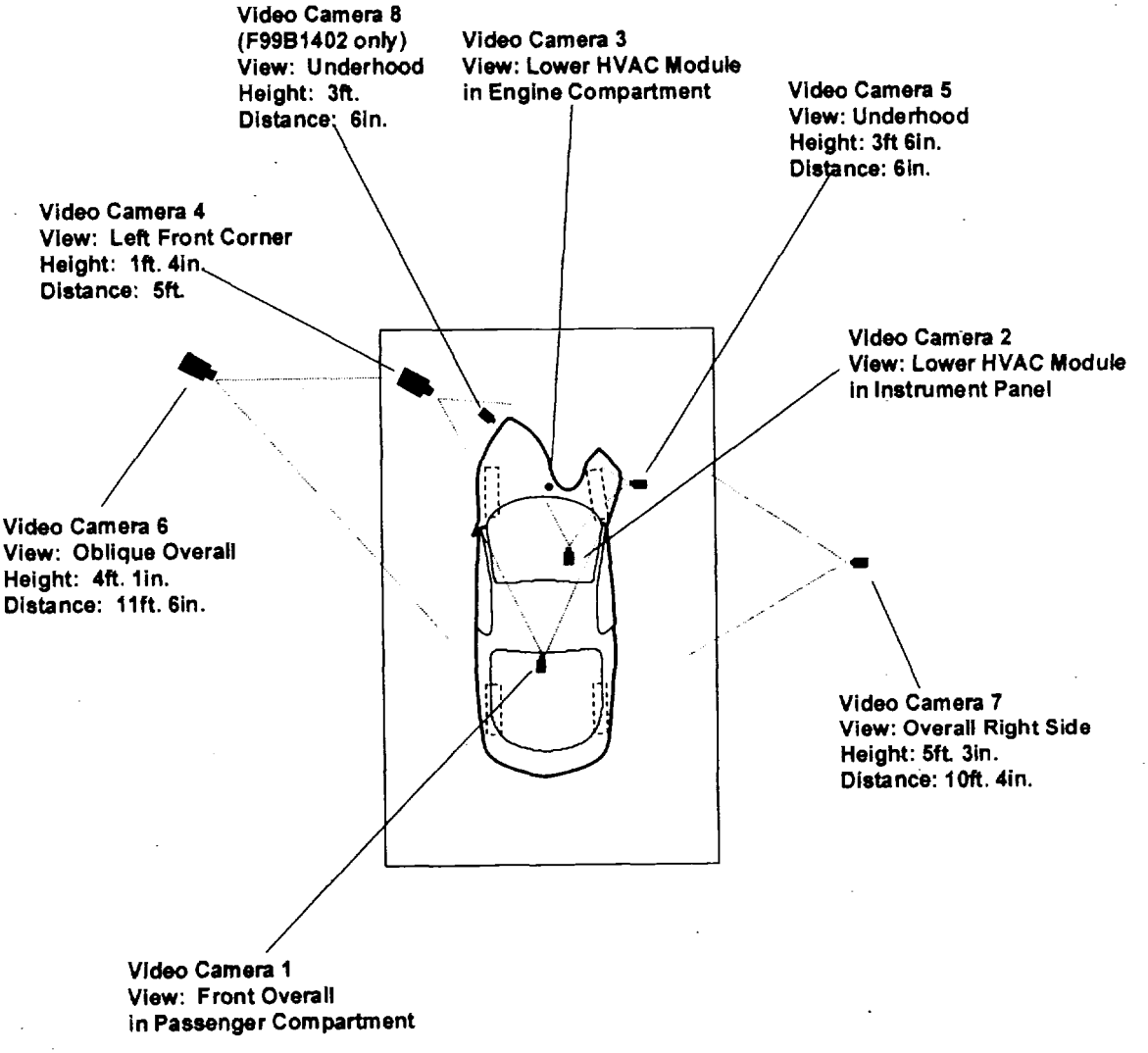


Figure G1. Video camera layouts in Fire Tests F99B1401 and F99B1402. Distances in this *figure are not to scale* in this diagram. All height are referenced to the surface of the fluid containment pan.

The Camera layouts were the same for both tests except for Camera 8. Camera 8 was used for test F99B1402 only. Camera 1 was a CCD camera mounted on top of the rear seat back, inside the passenger compartment. It had a field-of-view that included the windshield and instrument panel in the test vehicle. Camera 2 was a CCD camera mounted on the front passenger seat cushion. It had a field-of-view that included the center console to the passenger door and from bottom of the instrument panel to the floor in the test vehicle. Camera 3 was a CCD camera mounted on the exhaust crossover pipe. It had a field-of-view that included looking up at the underside of the HVAC unit in the engine compartment. Camera 4 was a Hi-8 camcorder mounted on a tripod approximately 1ft. 4in. above the test surface and approximately 5ft. from the test vehicle. Its field-of-view included the left front corner of the test vehicle, from left front tire to the center of front fascia and from the bottom of front fascia to just above the hood. Camera 5 was a CCD camera mounted on a stand approximately 3ft. 6in. above the test surface of the fluid containment pan, and 6in. from the test vehicle. Its field of view included the engine compartment area from the right side of the vehicle. Camera 6 was a Hi-8 camcorder mounted on a tripod approximately 4ft. 1in. above the test surface and approximately 11ft 6in. from the test vehicle. Its field-of-view included the left side from the front of the vehicle to the rear of the left front door and from just above roof to the test surface of the test vehicle. Camera 7 was a Hi-8 camcorder mounted on a tripod approximately 5ft. 3in. above the test surface and approximately 10ft 4in. from the test vehicle. Its field-of-view included the right side from the front of the vehicle to the rear of the right front door and from just above roof to the test surface of the test vehicle. Camera 8 (used in Fire Test F99B1402 only) was a CCD camera mounted on a stand approximately 3ft. above the test surface and 6in. from the test vehicle. Its field of view included the engine compartment area from the left side of the vehicle.

All video cameras were started before the test. A microphone on each camcorder (Cameras 4 and 6) recorded the air horn, which signaled when electrical power was supplied tot he igniter and the end of the test. The CCD cameras had no audio capabilities. To synchronize these cameras with the videos from the camcorders, the floodlights were switched off and then back on to provide a common visual timing reference on all videos.

Quartz-halogen floodlights were used to illuminate the exterior of the vehicle. One 12V halogen light with a magnetic base was mounted in the gap between the hood and fender to illuminate the underhood area on the right side of the test vehicle. One 12V halogen light was mounted on the frame to illuminate the lower section of the HVAC unit in the engine compartment of the test vehicle. One 12V halogen light was mounted on the floor between the seat and the door on the passenger side to illuminate the lower section of HVAC unit in the passenger compartment of the test vehicle.

## Appendix H

## Fire Tests F99B1401 and F99B1402

## Thermocouple Data

The thermocouples used in this test were type-N thermocouples fabricated by Medtherm Corporation (Huntsville, AL). Each thermocouple consisted of an ungrounded thermocouple junction (30 AWG thermocouple wire) enclosed in an Inconel 600 sheath insulated with magnesium oxide (o.d. = 0.040 in. (1 mm), length = 50 ft. (15.2 m)). A transition was made through a stress-relief bushing to a duplex thermocouple extension cable (24 AWG) with fiberglass insulation and a stainless steel over-braid (length = 1 ft. (0.28 m)). Each thermocouple wire terminated in a grounded, compensated Type-N thermocouple plug. The thermocouples were connected to the data acquisition system using Type-N thermocouple extension cables (length = 50 ft. (15.2 m)).

The data acquisition system consisted of a PC (75 MHz Pentium Processor, 16 MB RAM, an 814 MB hard disk, and a 16-bit, Model BG45-AP5CP, ACER Inc., Taiwan R. O. C.) with a 100 kHz I/O board with 16 analog input channels (DaqBoard 200A, IOTech, Inc., Cleveland, OH). Thermocouple multiplex expansion cards (DBK-19, IOTech, Inc., Cleveland, OH) were used for data acquisition from the thermocouples. The expansion cards were mounted in an electronics cabinet and hard-wired to a panel containing compensated Type-N thermocouple jacks.

To reduce electronic noise on the thermocouples, the ground leads from each thermocouple jack was connected to the electronic chassis ground of the thermocouple mutliplex extension cards. The vehicle chassis was connected to the electronic chassis ground by a large-gauge cable. The electronic chassis ground was connected to an isolated earth ground.

The data acquisition software (DASYLab, Daten System Technik GmbH, Mönchengladbach, Germany) was configured to sample each channel at a rate of 10 Hz and store the data in 10-point block averages.

Figures H1 through H6 show the approximate locations of thermocouples in the test vehicle. Plots H1 through H113 show plots of the temperature data recorded from these thermocouples during this test.

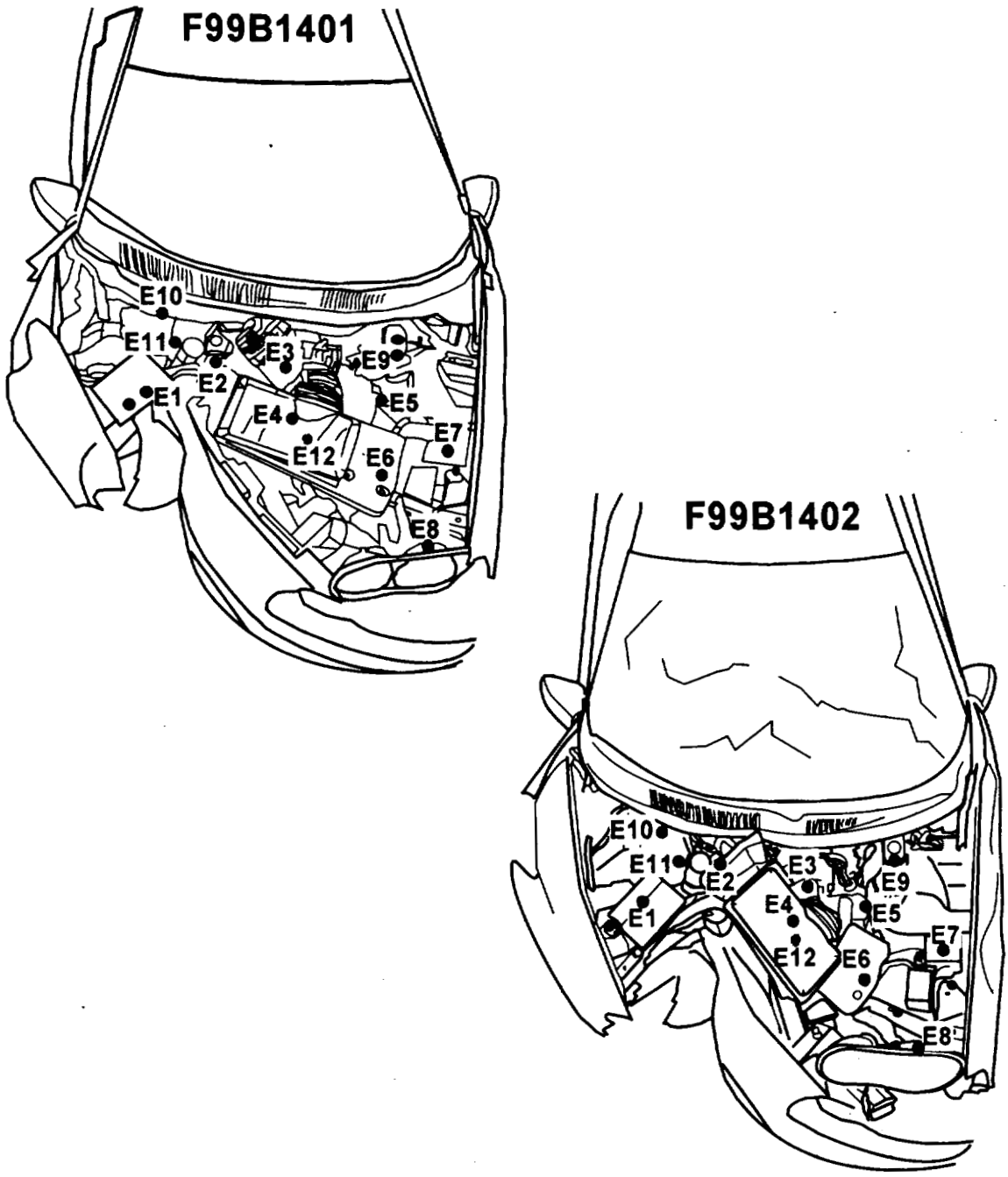


Figure H1. Fire Test F99B1401 and F99B1402. Diagram showing the approximate locations of thermocouples in the engine compartment in the front of test vehicle. Thermocouple E1 was located on the upper surface of the battery. Thermocouples E2, E3, E4, E5, and E6 were located in the air cleaner assembly. Thermocouple E7 was located on the upper surface of the power distribution center. Thermocouple E8 was located on the upper surface of the left front headlight. Thermocouple E9 was located on the upper surface of the brake fluid reservoir. Thermocouple E10 was located on the right side exterior surface of the HVAC. Thermocouple E11 was located on the left side exterior surface of the HVAC. Thermocouple E12 was located inside the air cleaner assembly above the igniter.

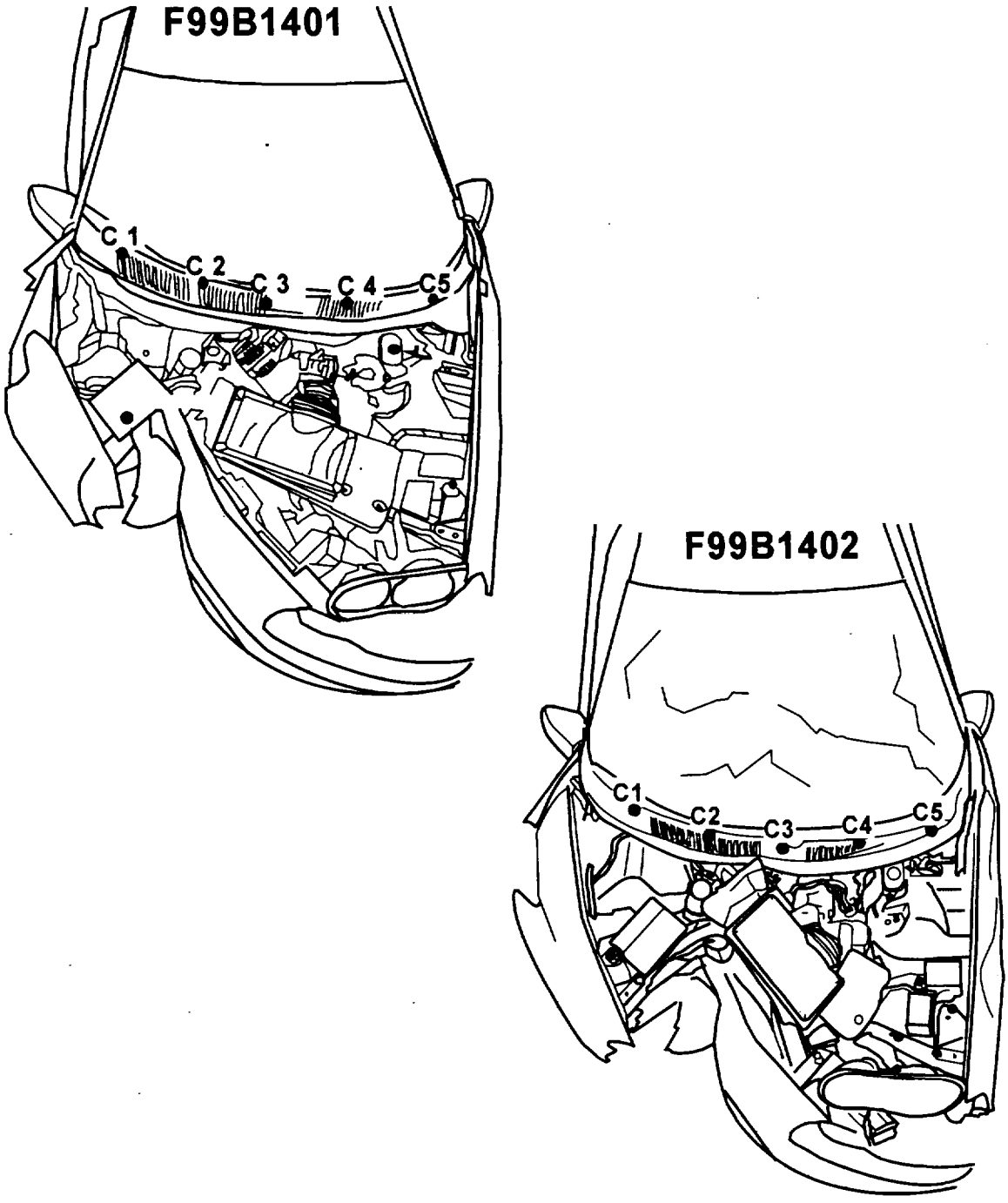


Figure H2. Fire Test F99B1401 and F99B1402. Diagram showing the approximate locations of thermocouples in the HVAC air intake cowl in the front of the test vehicle. Thermocouples C1, C2, C3, C4, and C5 were located through the upper surface of the HVAC air intake cowl cover extending into the HVAC air intake.

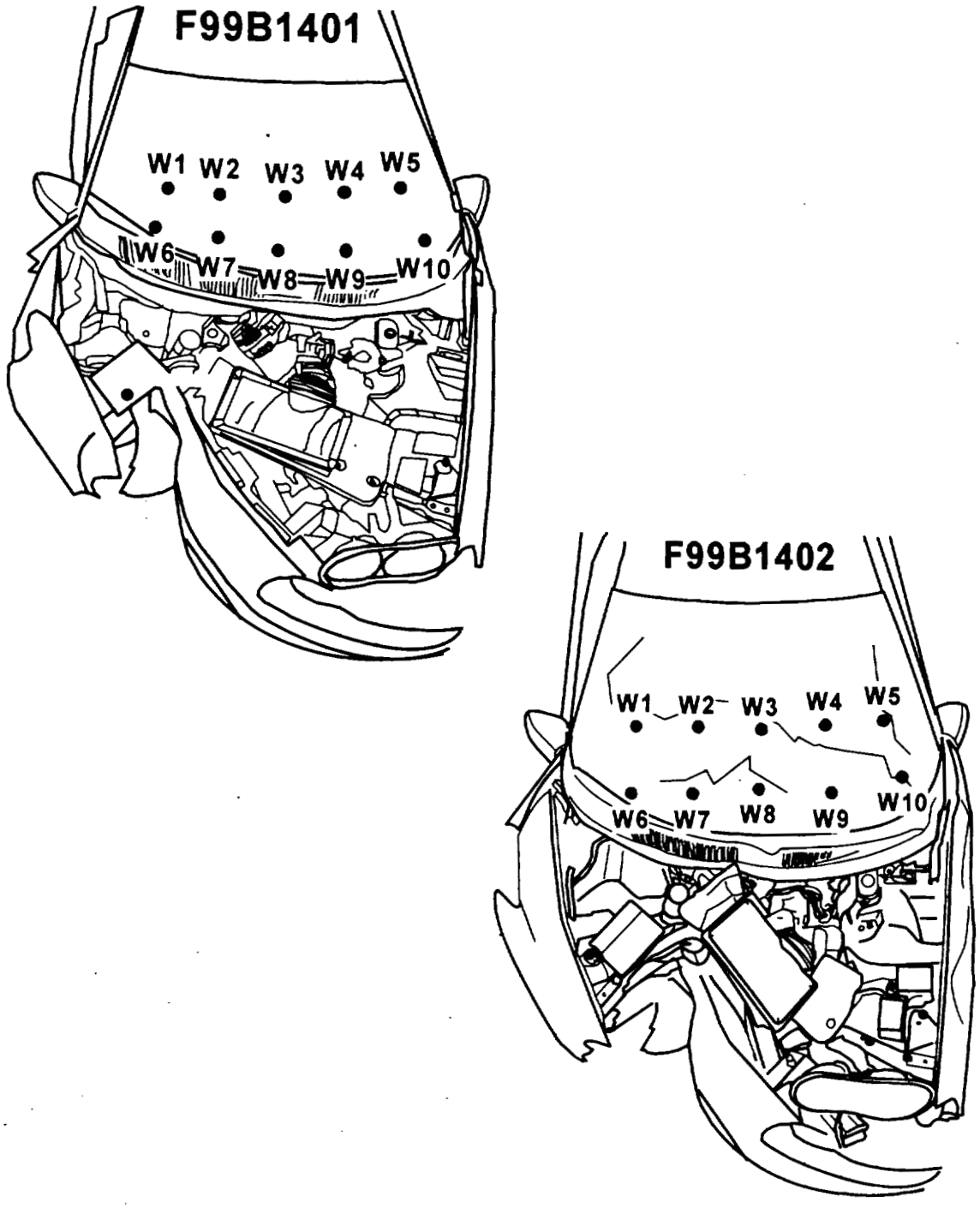


Figure H3. Fire Test F99B1401 and F99B1402. Diagram showing the approximate locations of thermocouples on the windshield of the test vehicle. Thermocouples W1 through W10 were located on the outer surface of the windshield in the front of the test vehicle.

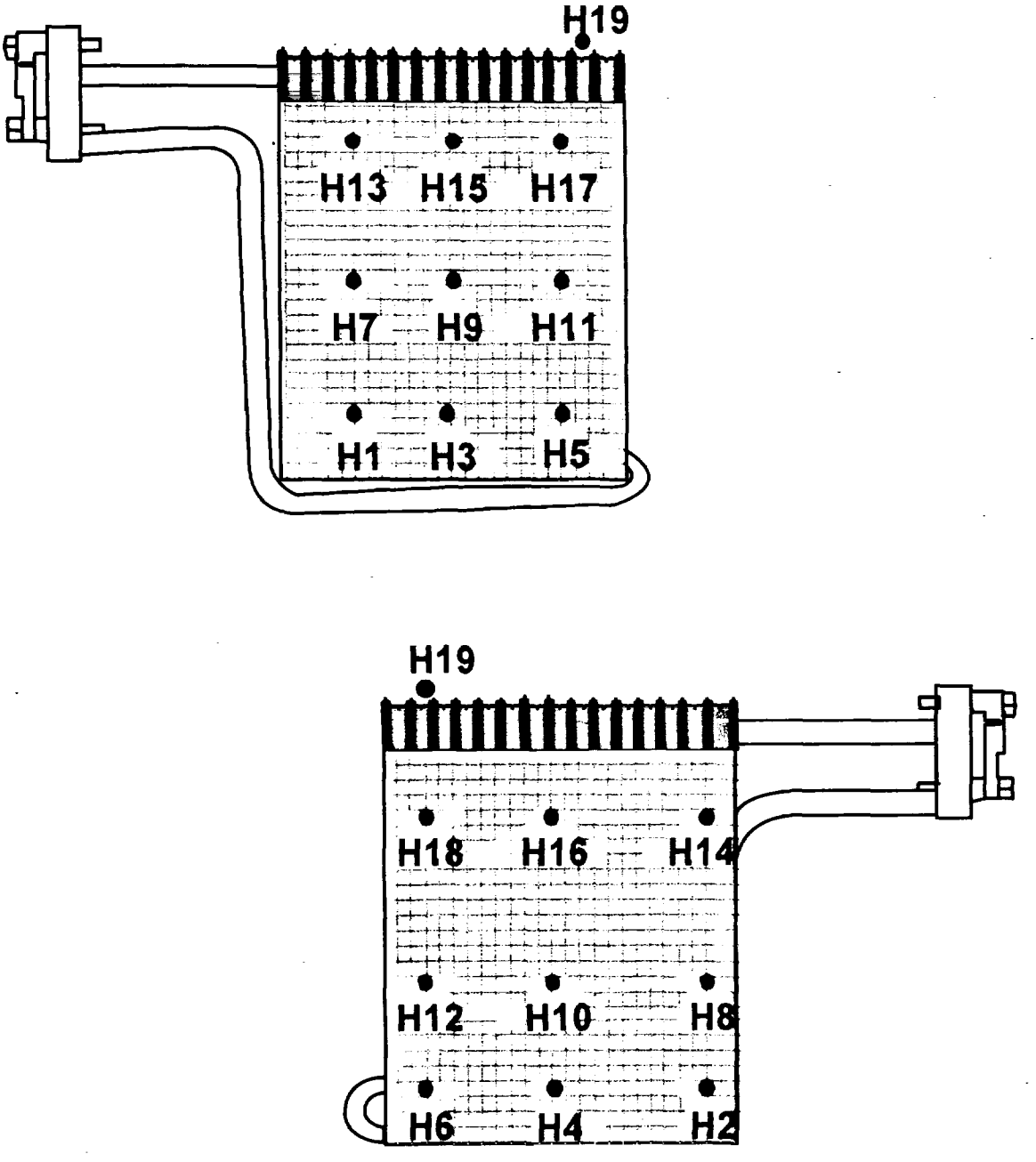


Figure H4. Fire Test F99B1401 and F99B1402. Diagram showing the approximate locations of thermocouples on the HVAC evaporator in the test vehicles. Thermocouples H1, H3, H5, H7, H9, H11, H13, H15, and H17 extended approximately 2.5-cm outward from the left side surface of the evaporator. Thermocouples H2, H4, H6, H8, H10, H12, H14, H16, and H18 extended approximately 2.5-cm outward from the right side surface of the evaporator.

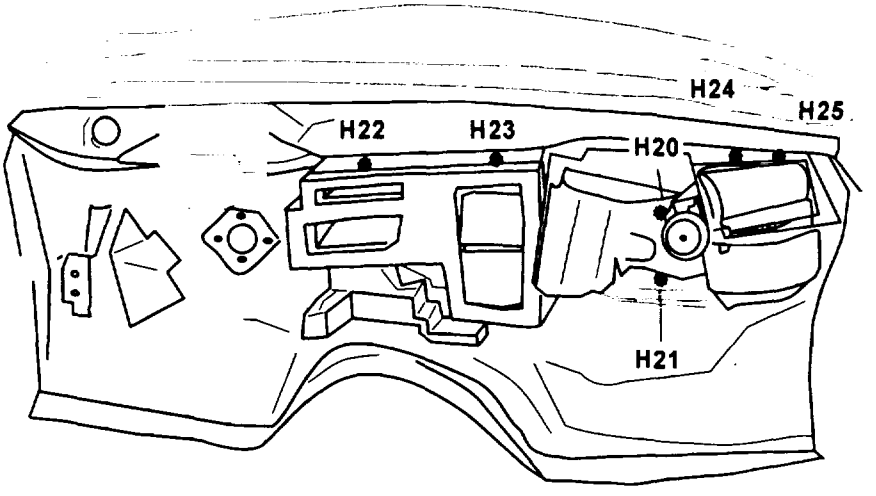


Figure H5. Fire Test F99B1401 and F99B1402. Diagram showing the approximate locations of thermocouples in the HVAC module in the test vehicle. Thermocouples H20, H21, were located approximately 2.5-cm forward of the front surface of the heater core. Thermocouple H22 was located approximately 1-cm below the top surface of the HVAC module distribution ducts. Thermocouple H23 was located approximately 1-cm below the top surface of the HVAC module mixing doors. H24 was located in the HVAC air intake opening approximately 5-cm into the opening from the right side and centered for and aft. H25 was located in the HVAC air intake opening approximately 5-cm into the opening from the left side and centered for and aft.

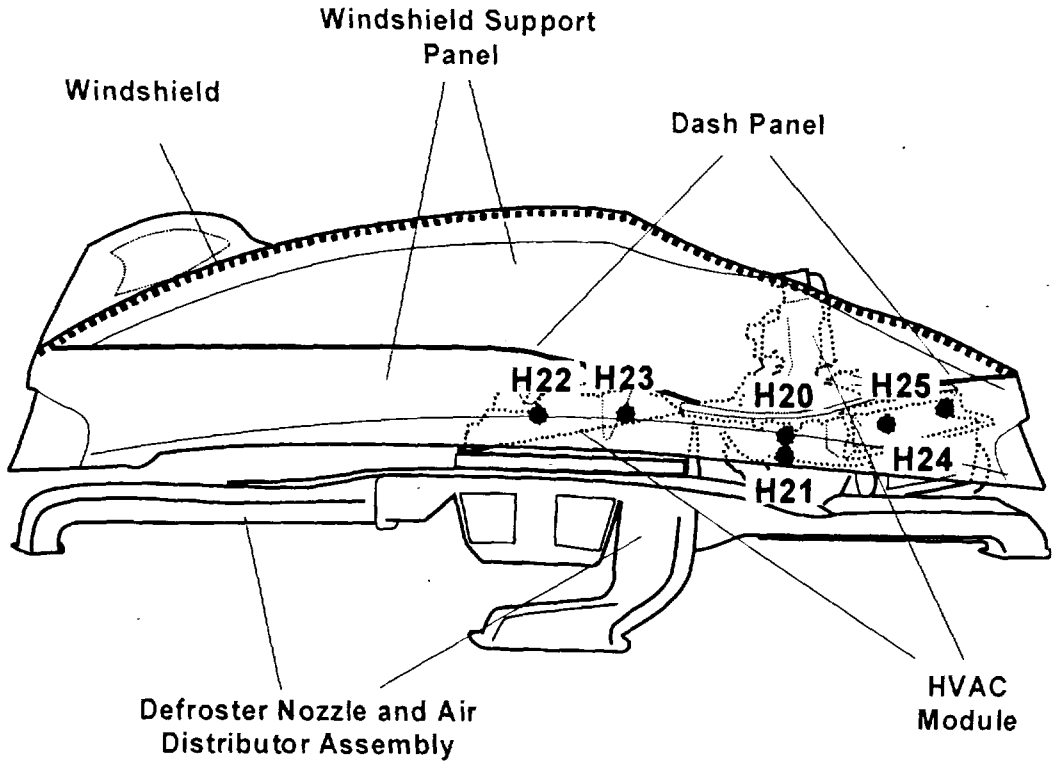


Figure H6. Fire Test F99B1401 and F99B1402. Diagram showing the approximate locations of thermocouples in the HVAC module in the test vehicle. Thermocouples H20, H21, were located approximately 2.5-cm forward of the front surface of the heater core. Thermocouple H22 was located approximately 1-cm below the top surface of the HVAC module distribution ducts. Thermocouple H23 was located approximately 1-cm below the top surface of the HVAC module mixing doors. H24 was located in the HVAC air intake opening approximately 5-cm into the opening from the right side and centered for and aft. H25 was located in the HVAC air intake opening approximately 5-cm into the opening from the left side and centered for and aft.

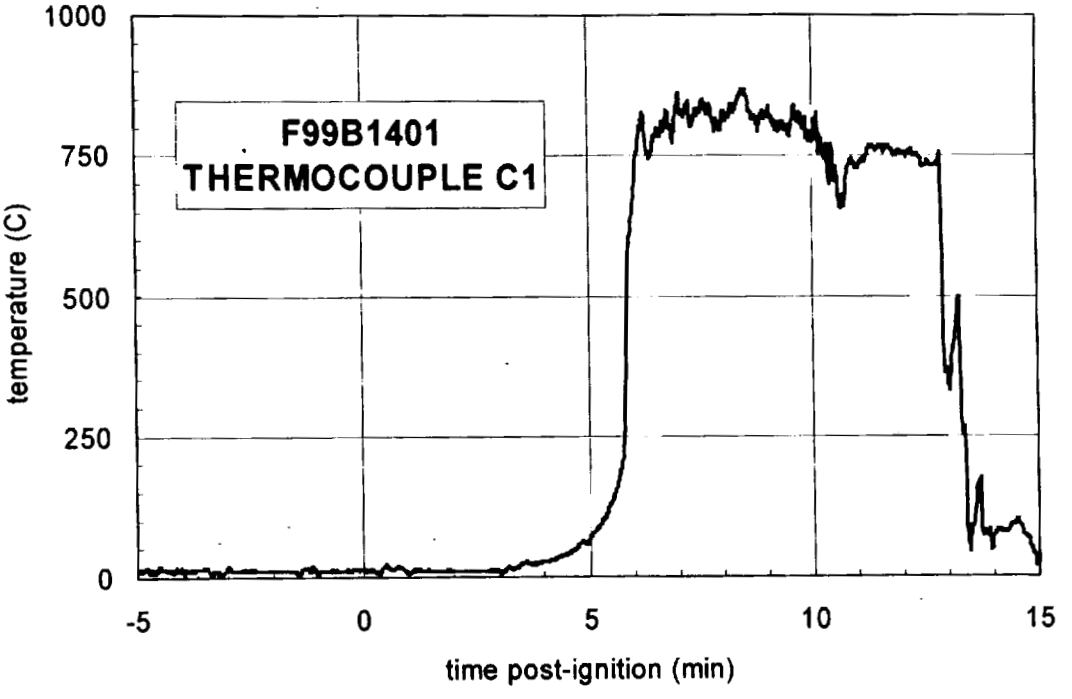


Plot H1. Fire Test F99B1401. Data plot from thermocouple C1.

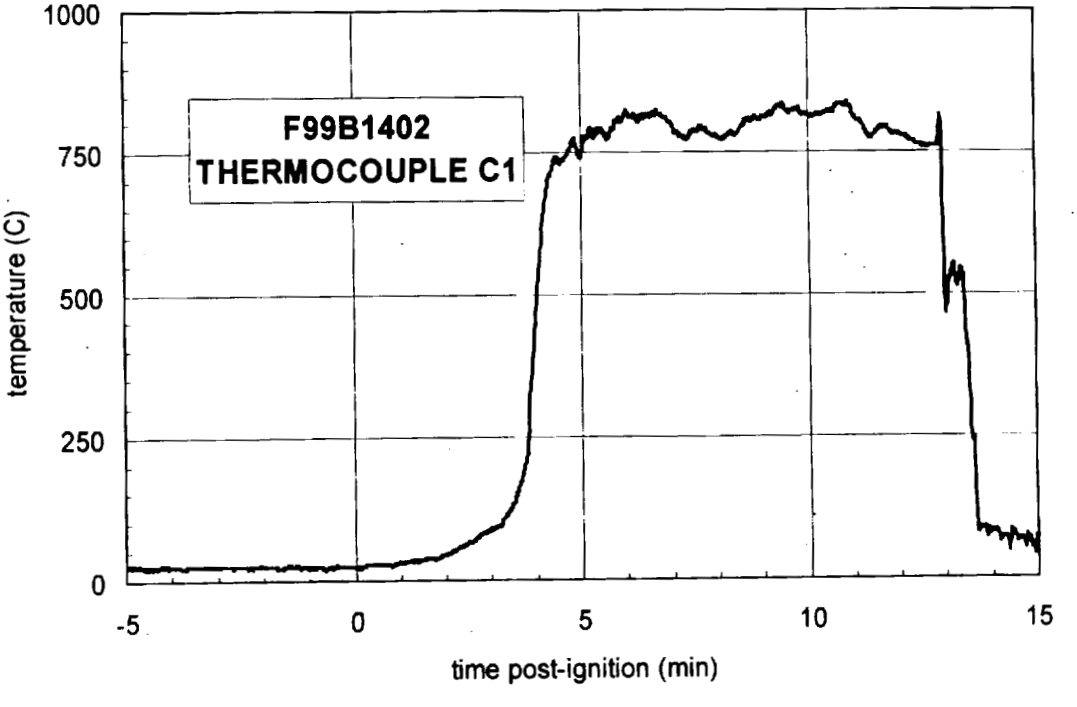


Plot H2. Fire Test F99B1402. Data plot from thermocouple C1.

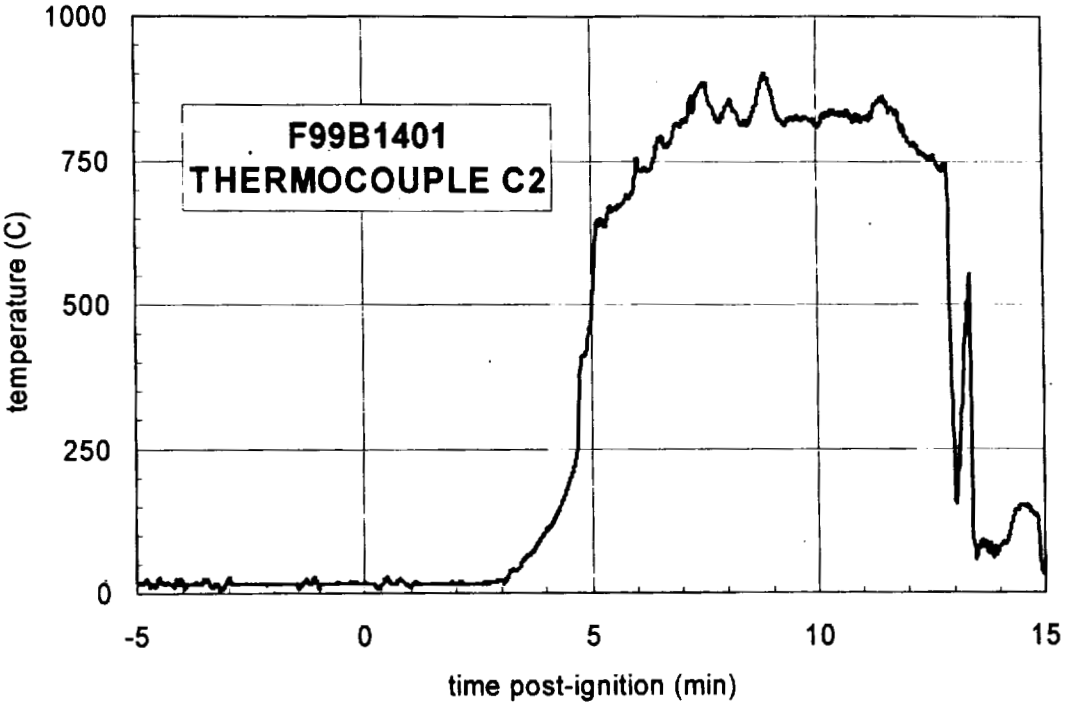


Plot H3. Fire Test F99B1401. Data plot from thermocouple C2.

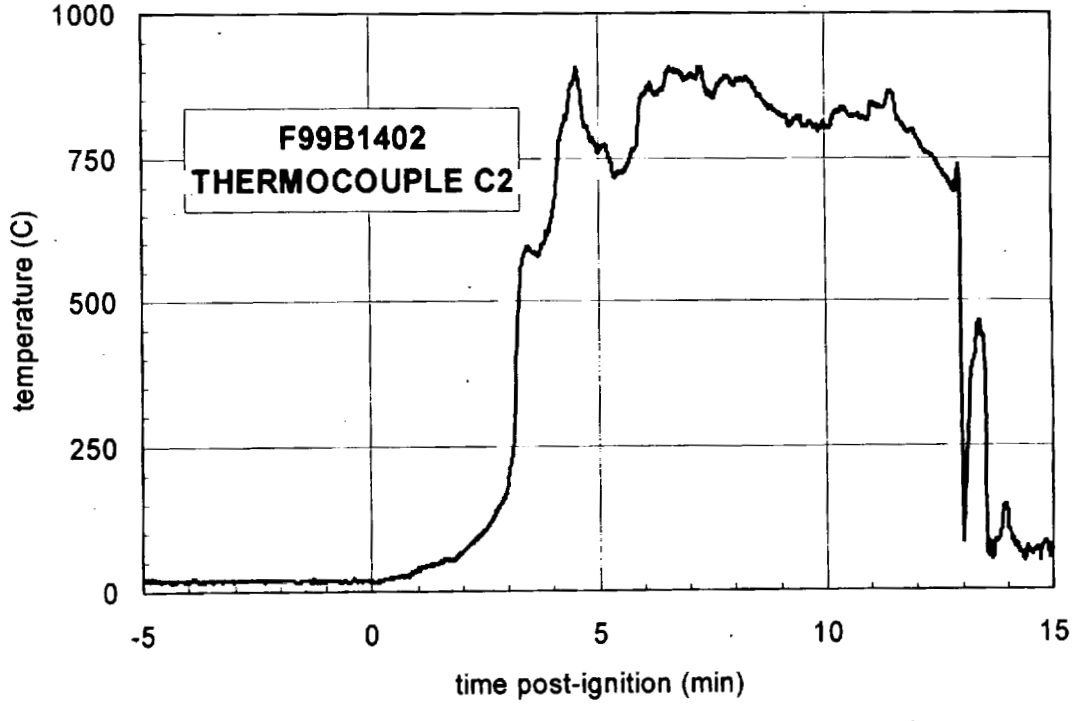


Plot H4. Fire Test F99B1402. Data plot from thermocouple C2.

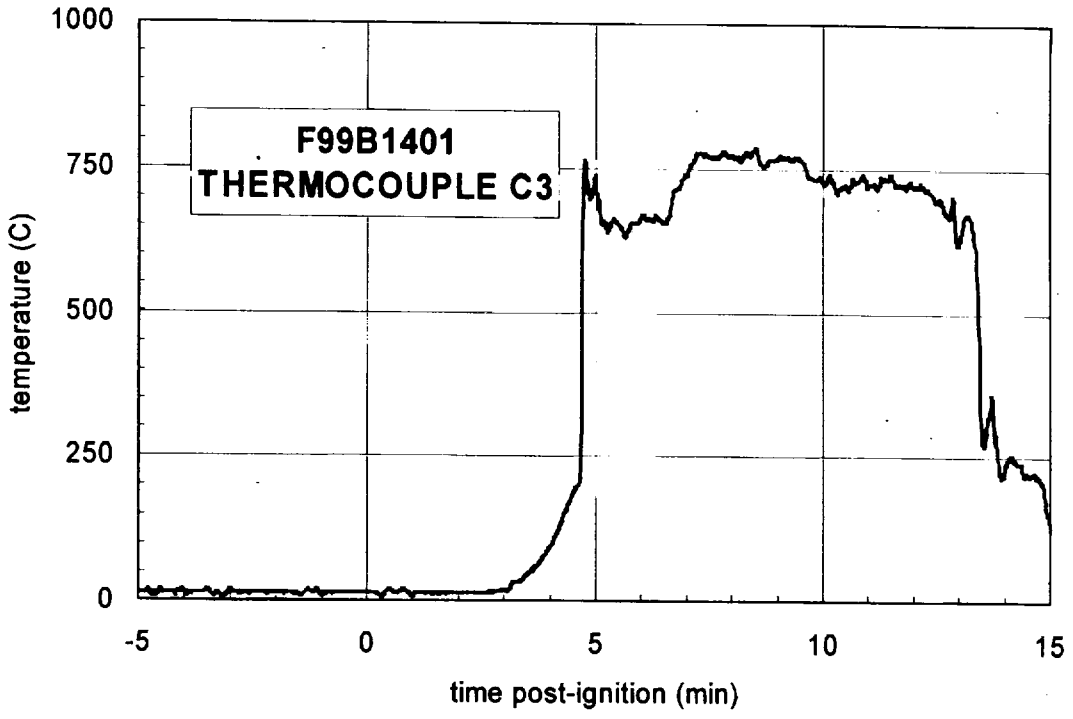


Plot H5. Fire Test F99B1401. Data plot from thermocouple C3.

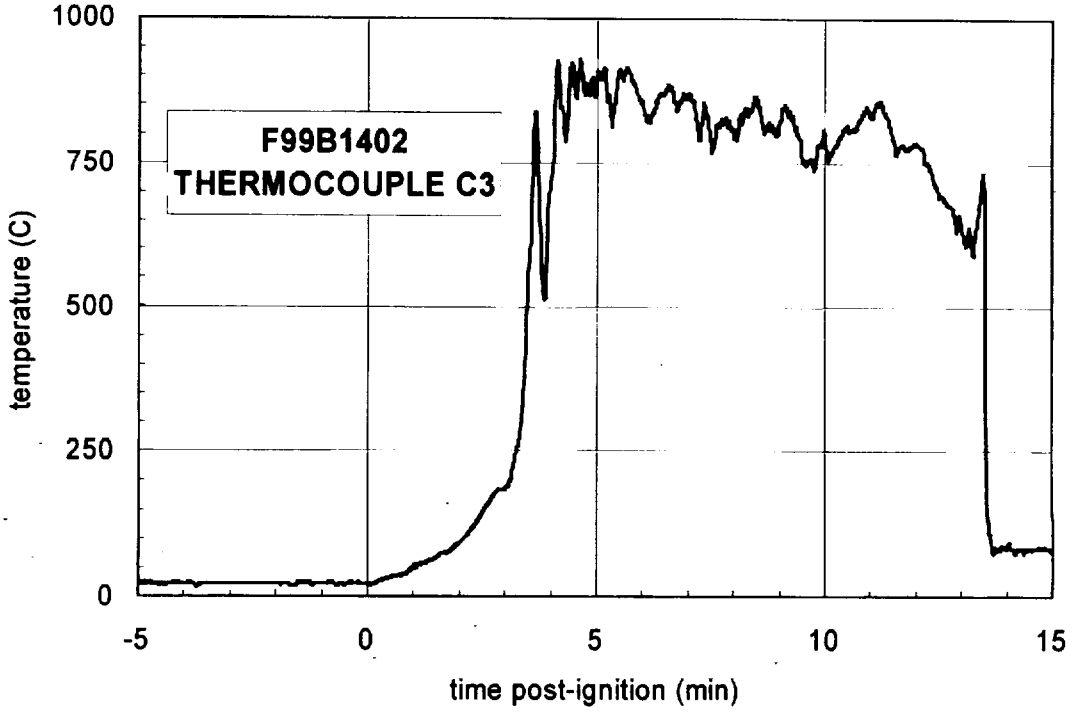


Plot H6. Fire Test F99B1402. Data plot from thermocouple C3.

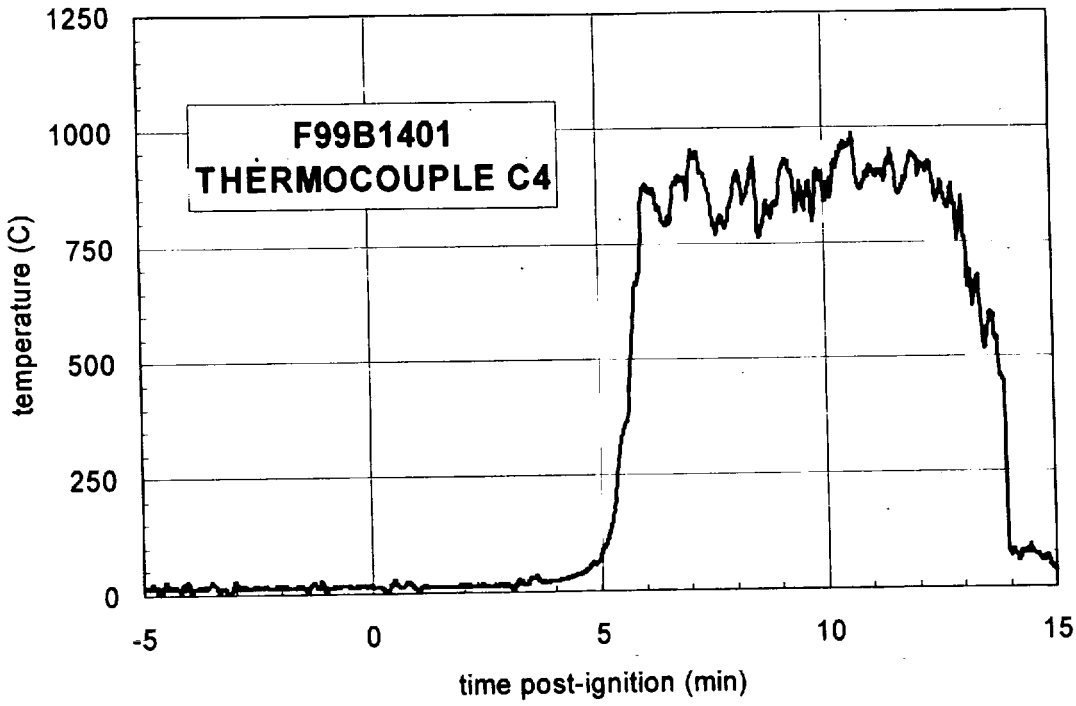


Plot H7. Fire Test F99B1401. Data plot from thermocouple C4.

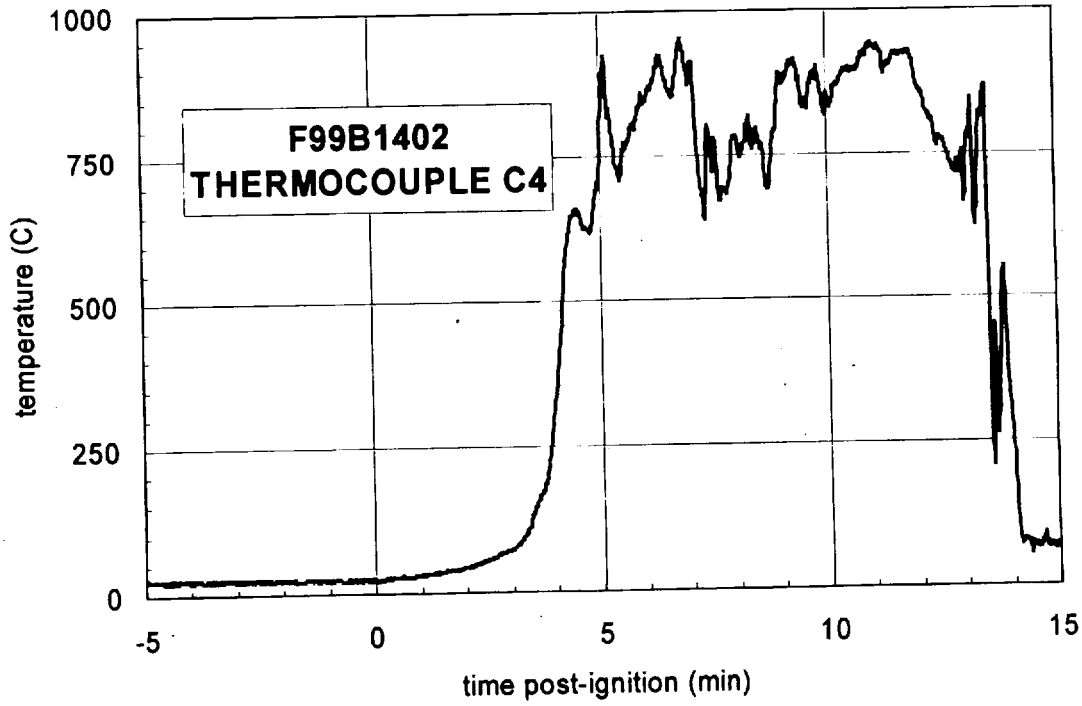


Plot H8. Fire Test F99B1402. Data plot from thermocouple C4.

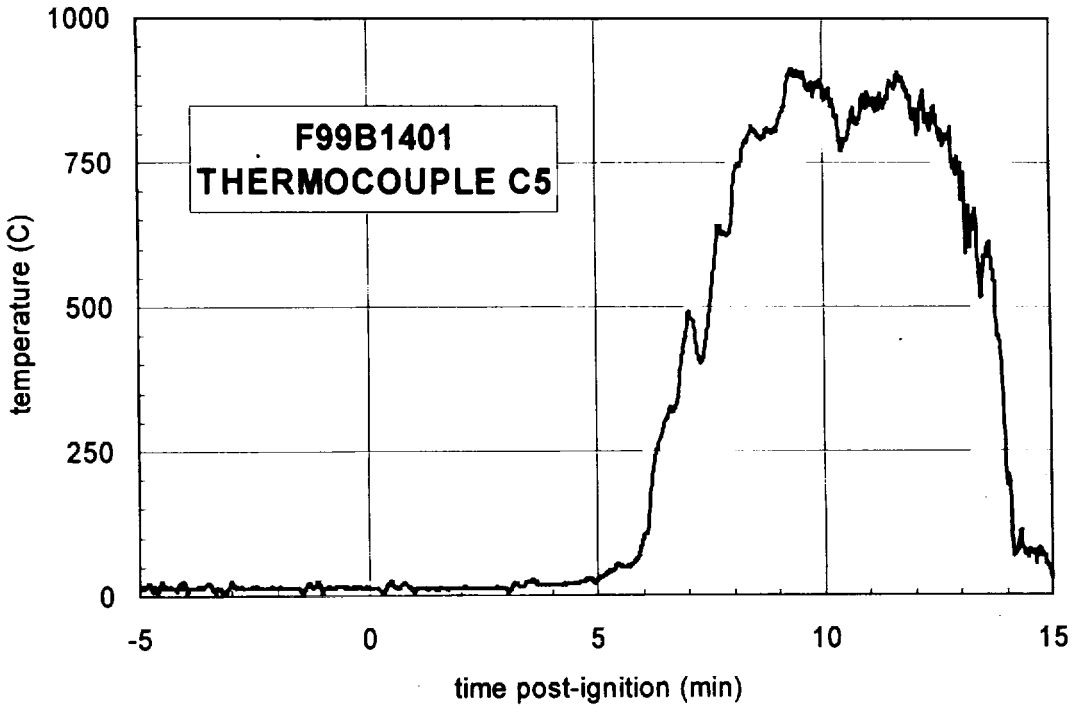


Plot H9. Fire Test F99B1401. Data plot from thermocouple C5.

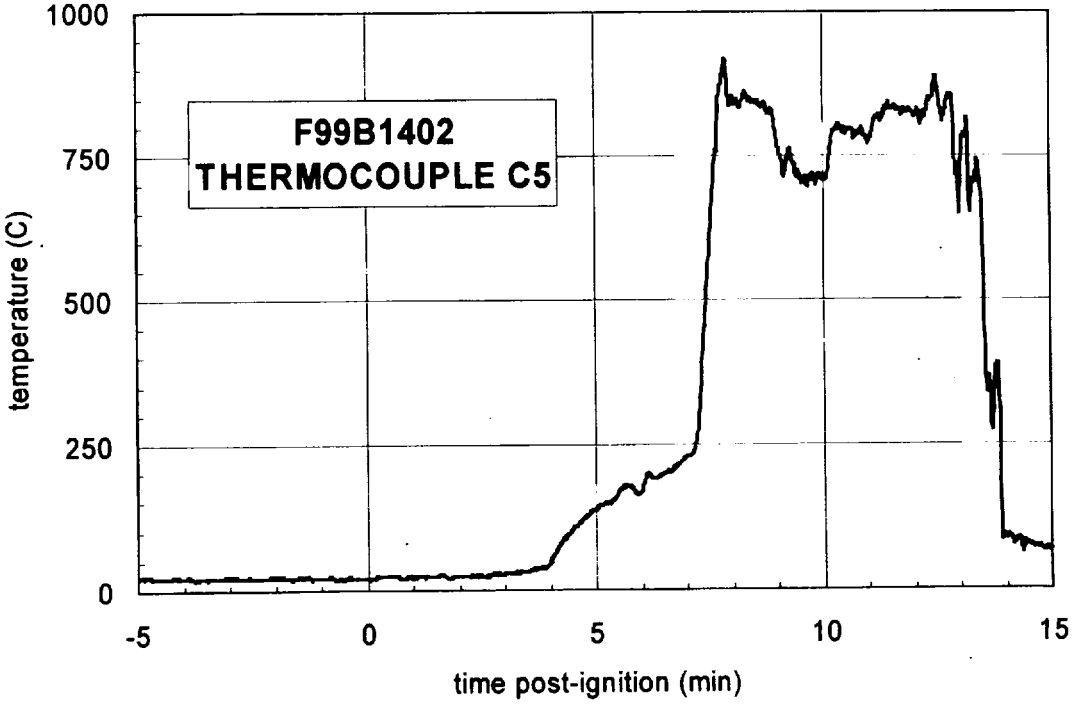


Plot H10. Fire Test F99B1402. Data plot from thermocouple C5.

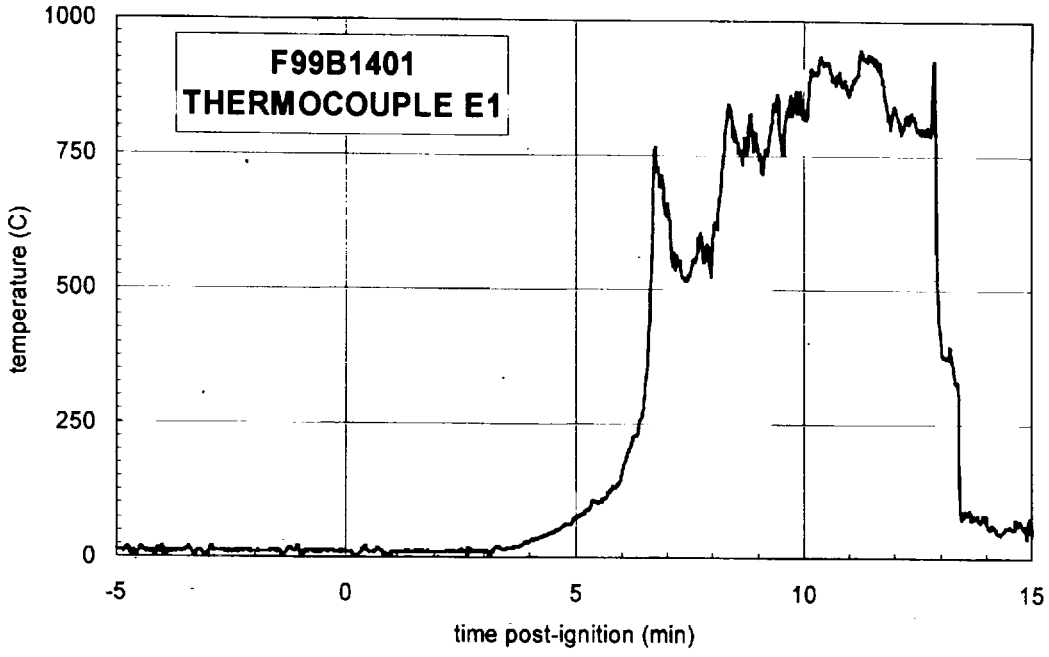


Plot H11. Fire Test F99B1401. Data plot from thermocouple E1.

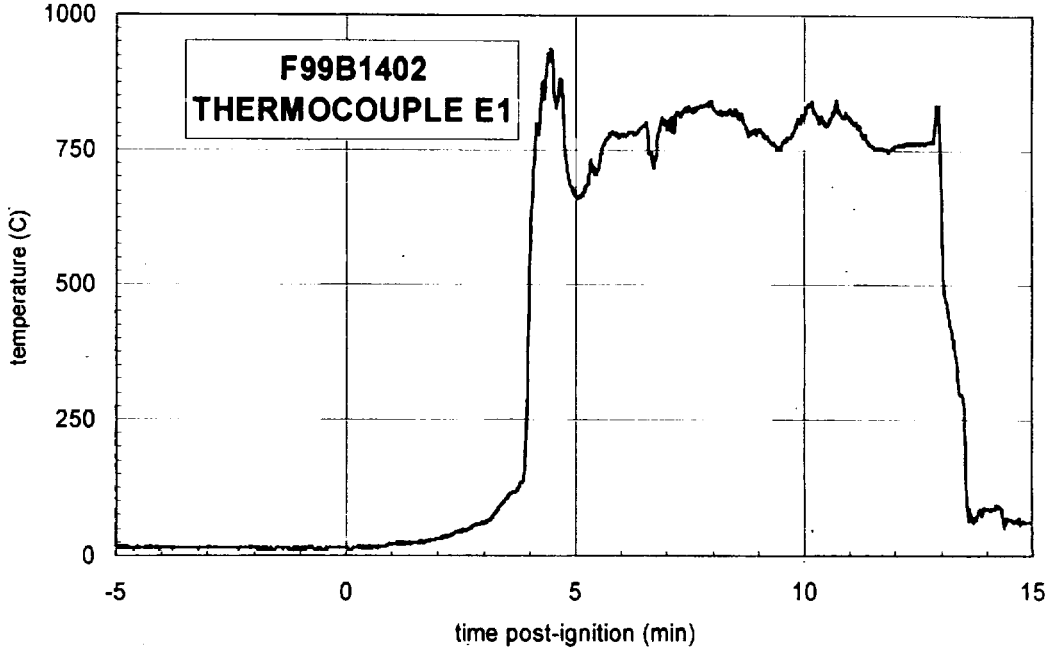


Plot **H12**. Fire Test F99B1402. Data plot from thermocouple E1

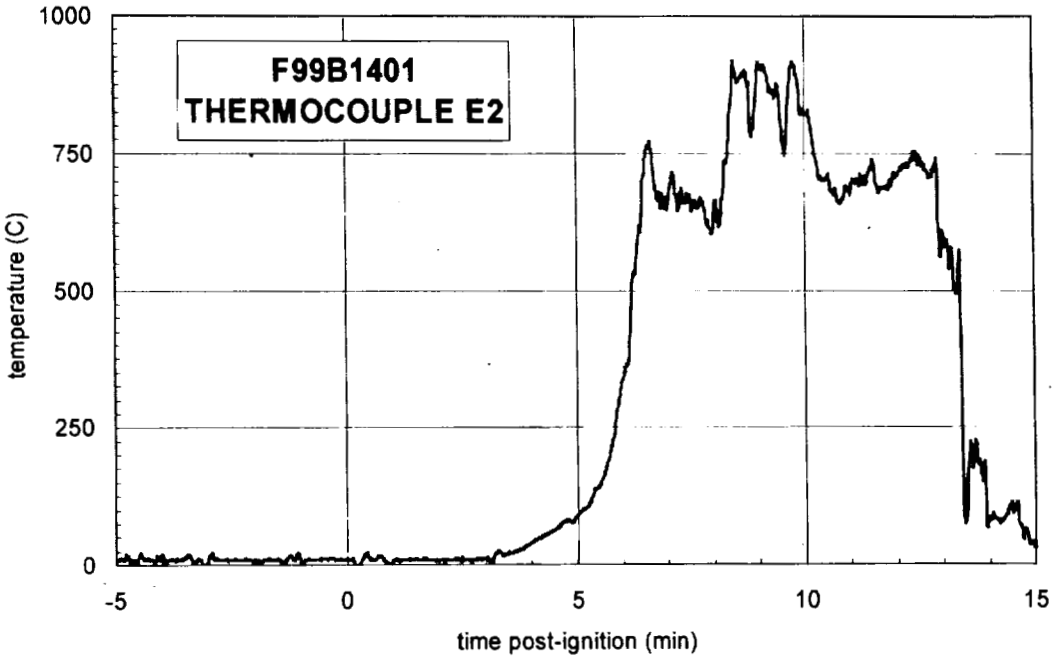


Plot H13. Fire Test F99B1401. Data plot from thermocouple E2.

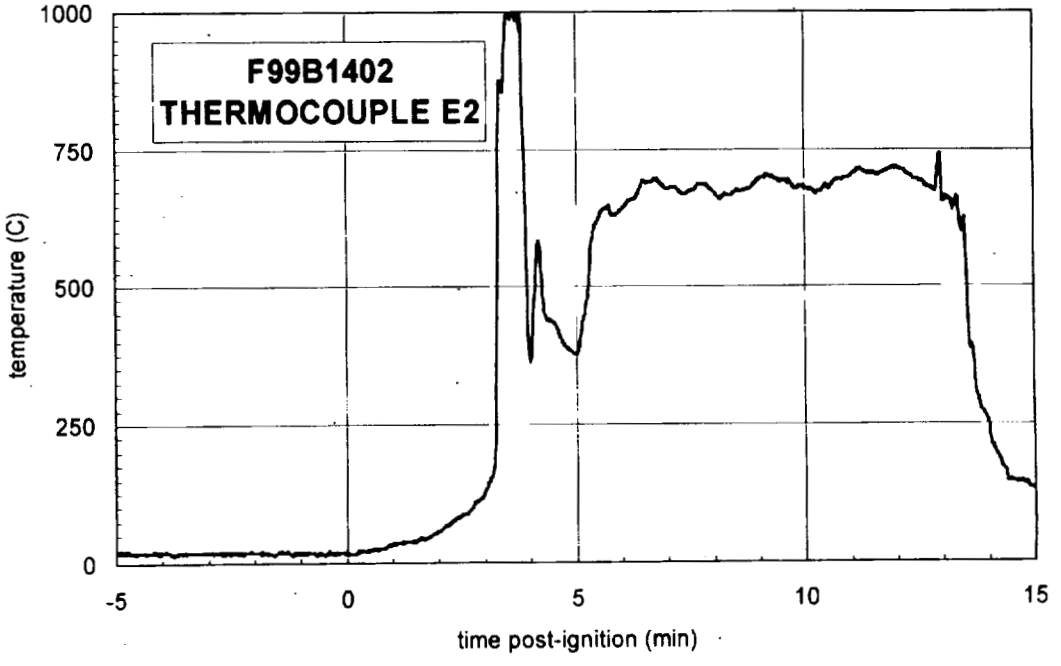


Plot H14 Fire Test F99B1402 Data Plot From Thermocouple E2

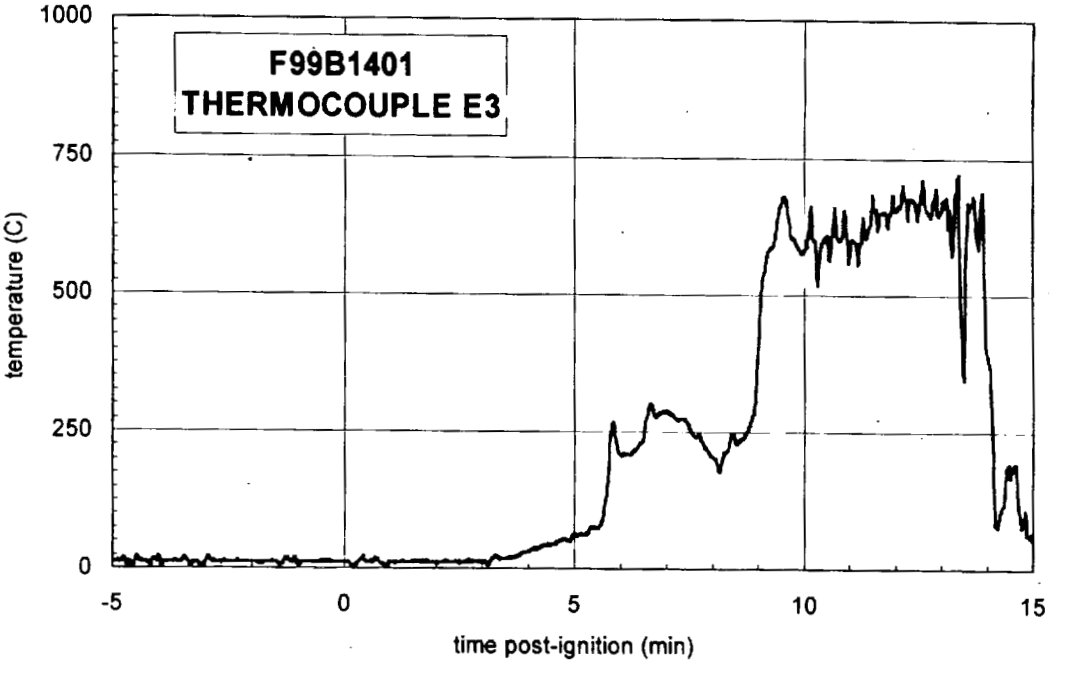


Plot H15. Fire Test F99B1401. Data plot from thermocouple E3.

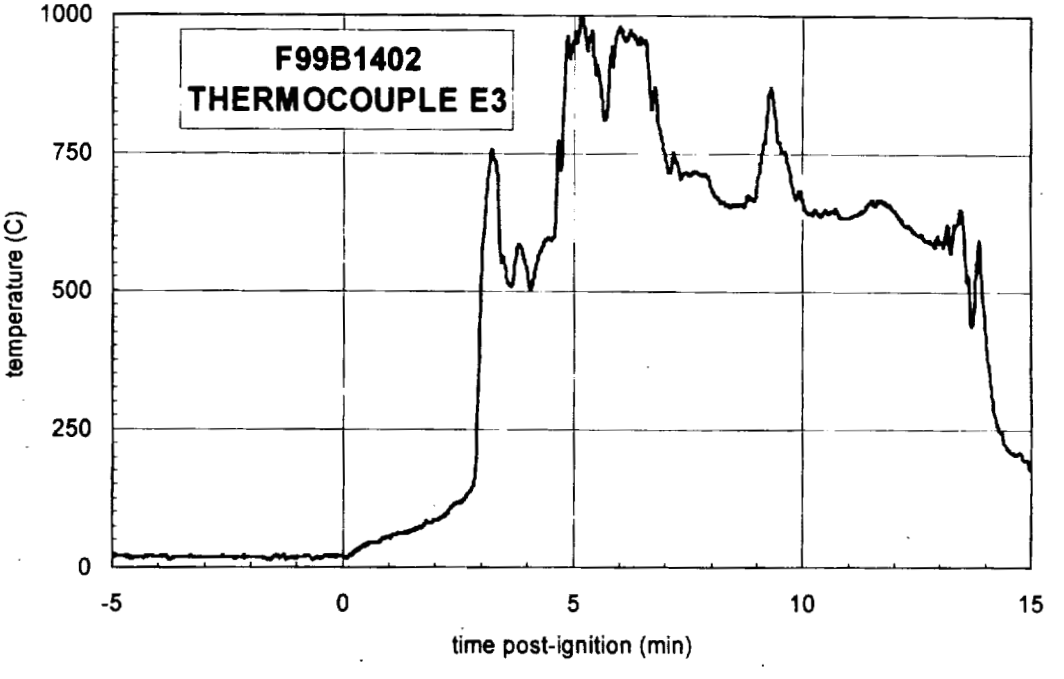


Plot H16. Fire Test F99B1402. Data plot from thermocouple E3.

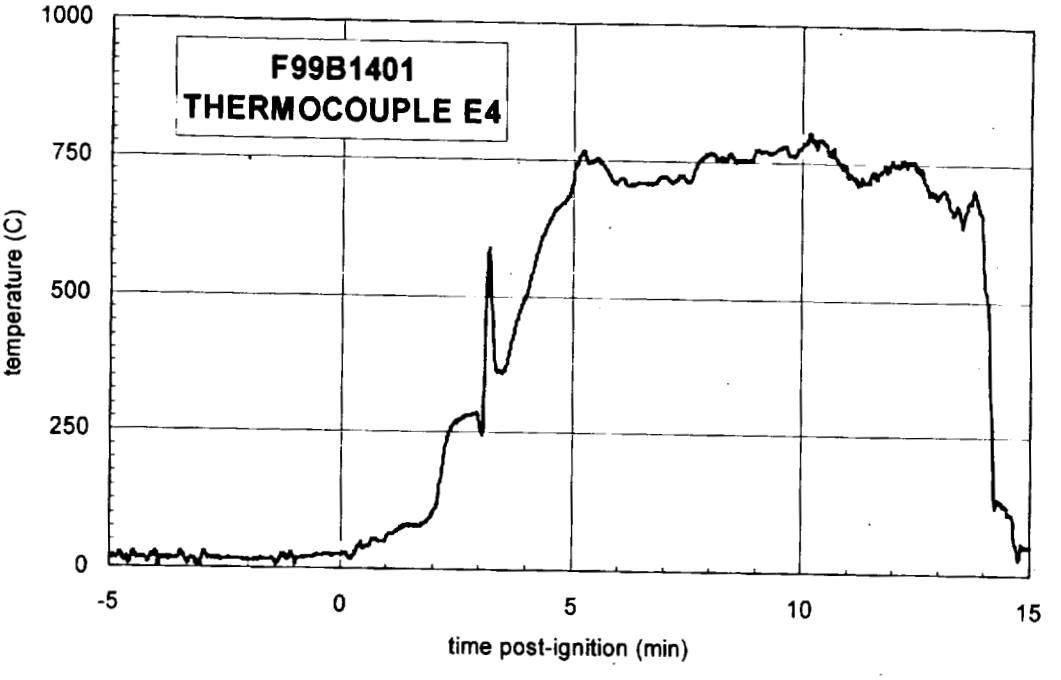


Plot H17. Fire Test F99B1401. Data plot from thermocouple E4.

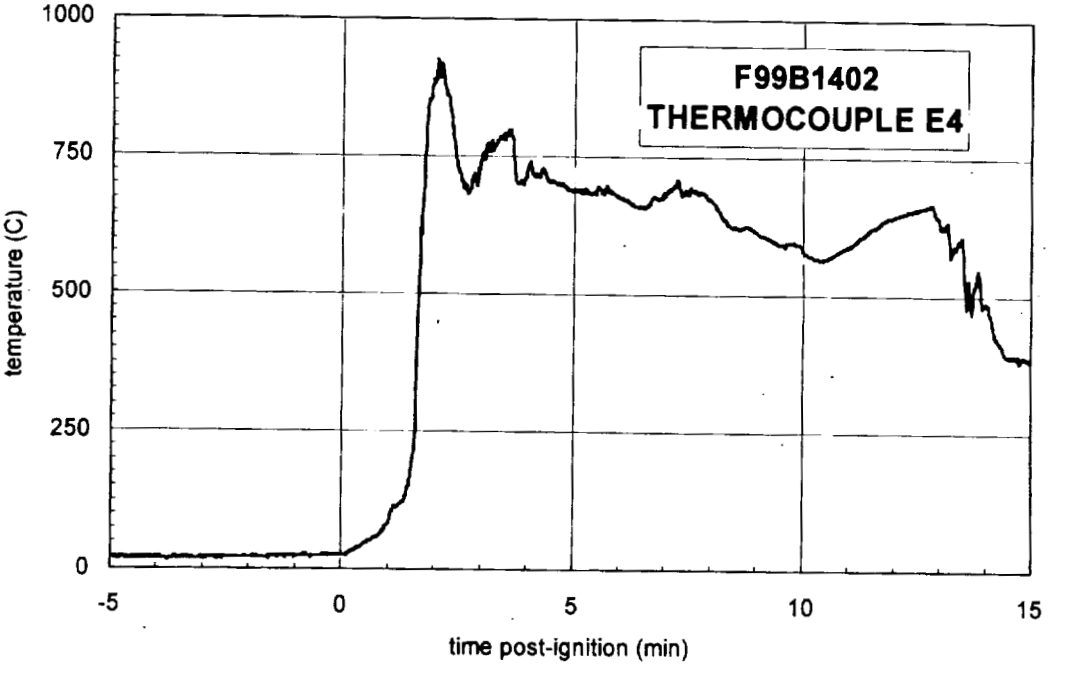


Plot H18. Fire Test F99B1402. Data plot from thermocouple E4.

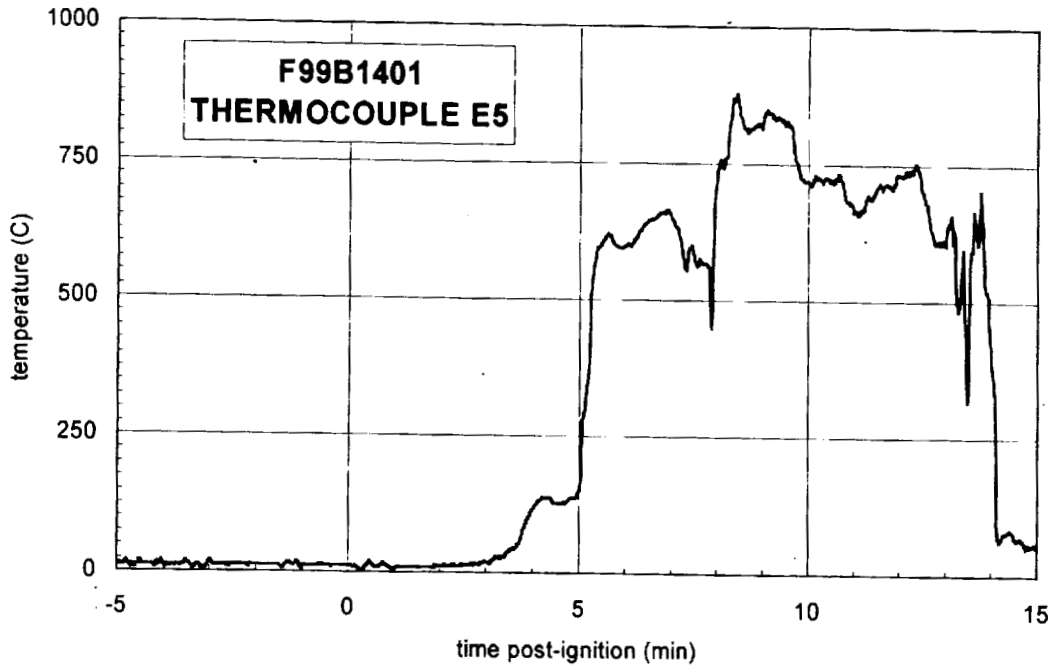


Plot H19. Fire Test F99B1401. Data plot from thermocouple E5.

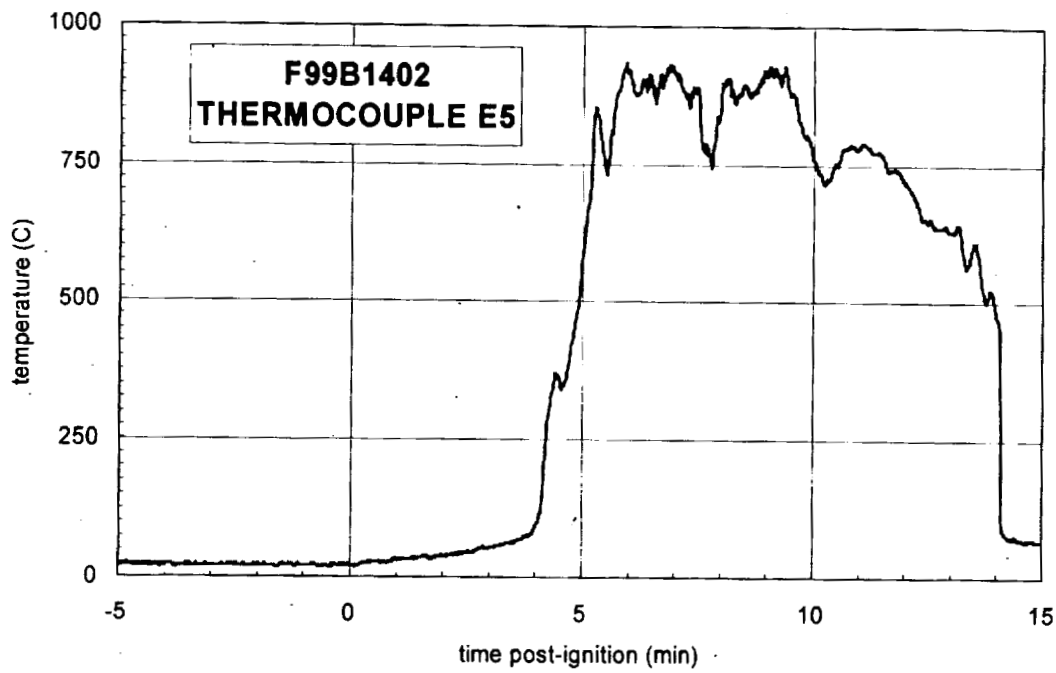


Plot H20. Fire Test F99B1402. Data plot from thermocouple E5.

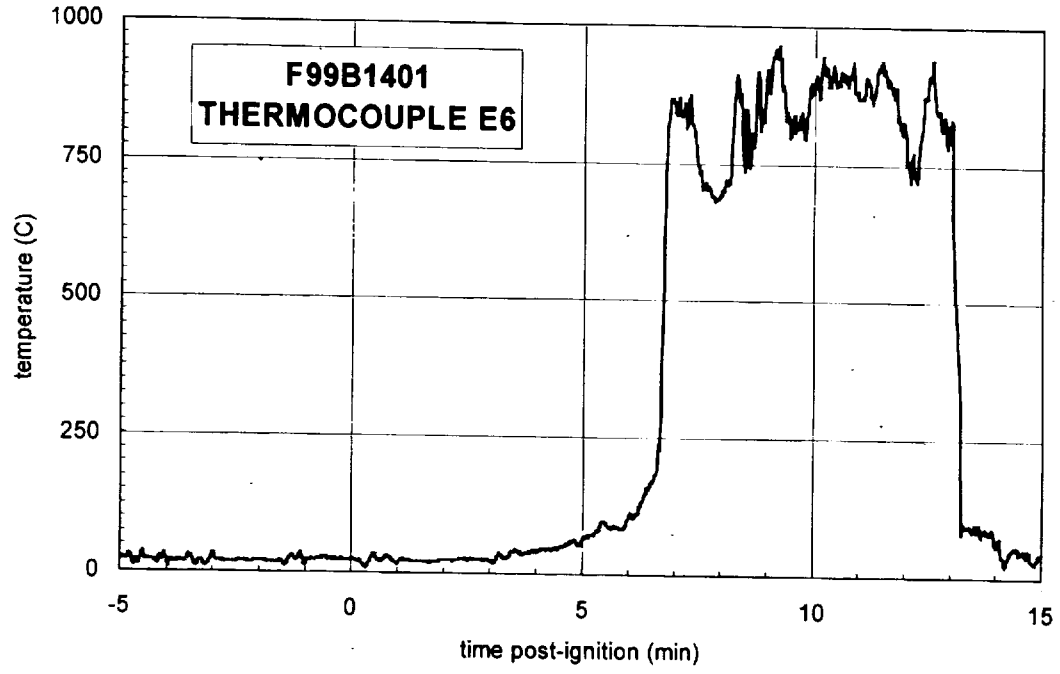


Plot H21. Fire Test F99B1401. Data plot from thermocouple E6.

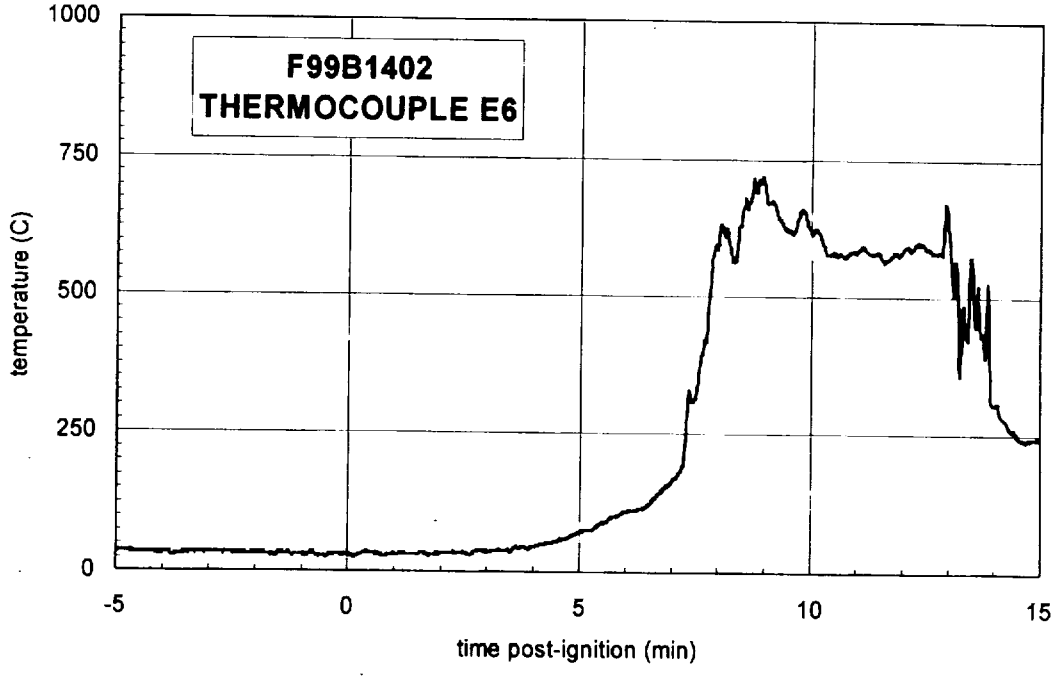


Plot H22. Fire Test F99B1402. Data plot from thermocouple E6.

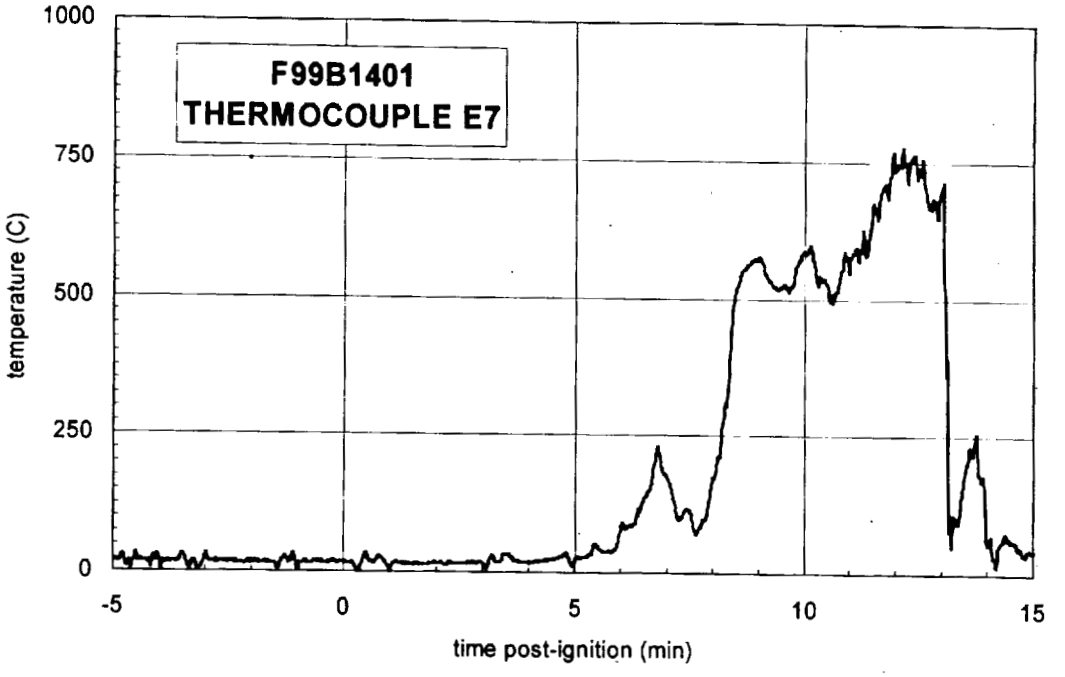


Plot H23. Fire Test F99B1401. Data plot from thermocouple E7.

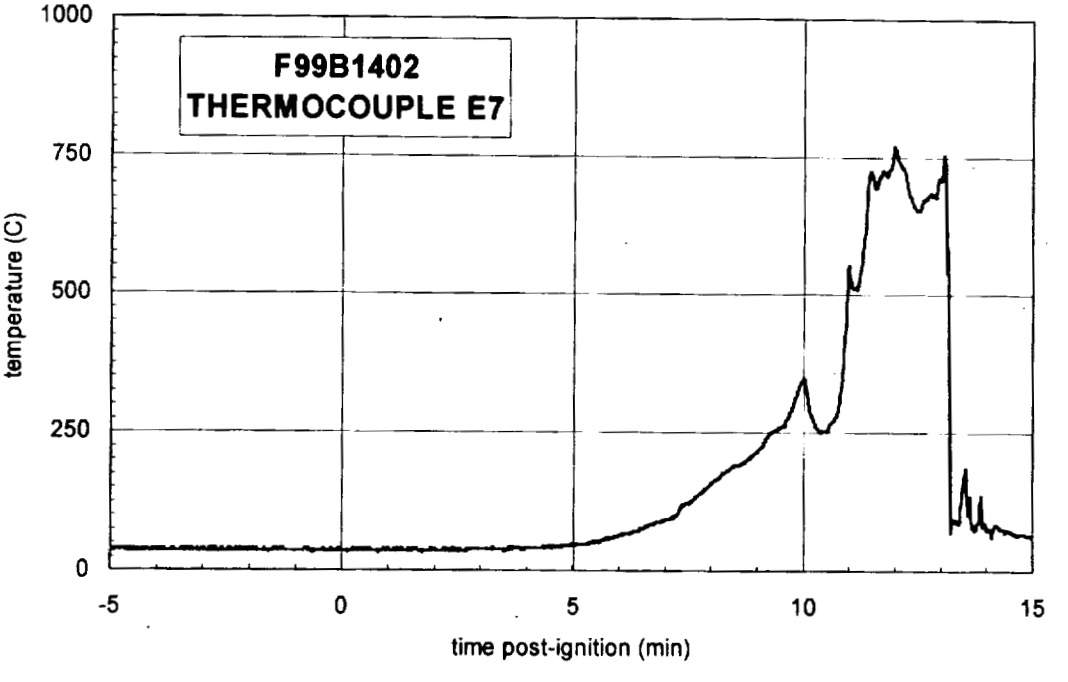


Plot H24. Fire Test F99B1402. Data plot from thermocouple E7.

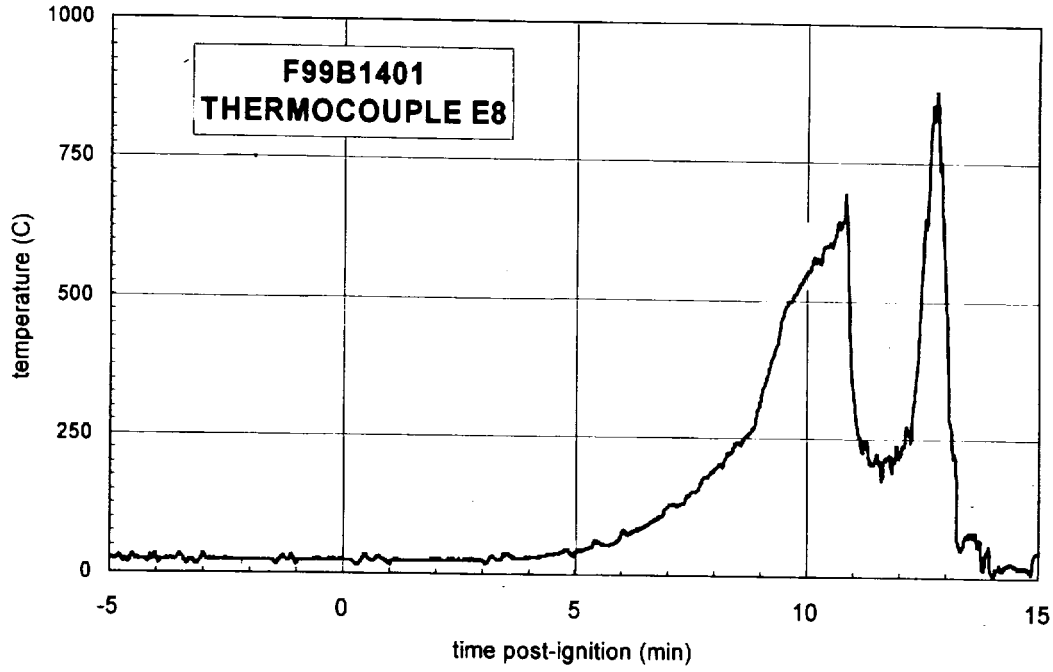


Plot H25. Fire Test F99B1401. Data plot from thermocouple E8.

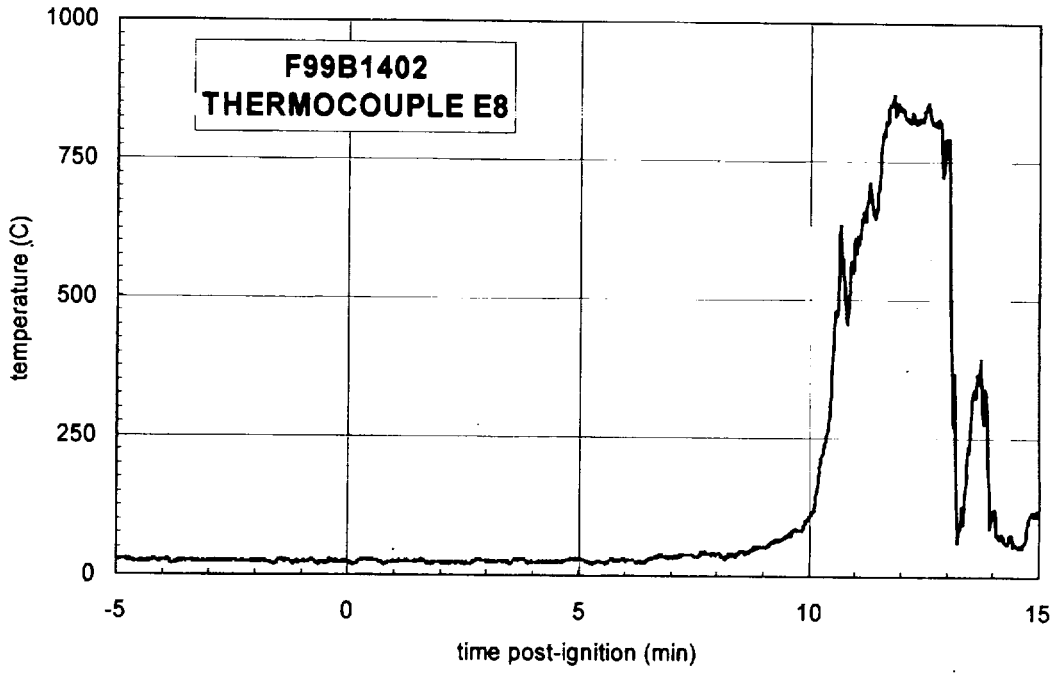


Plot H26. Fire Test F99B1402. Data plot from thermocouple E8.

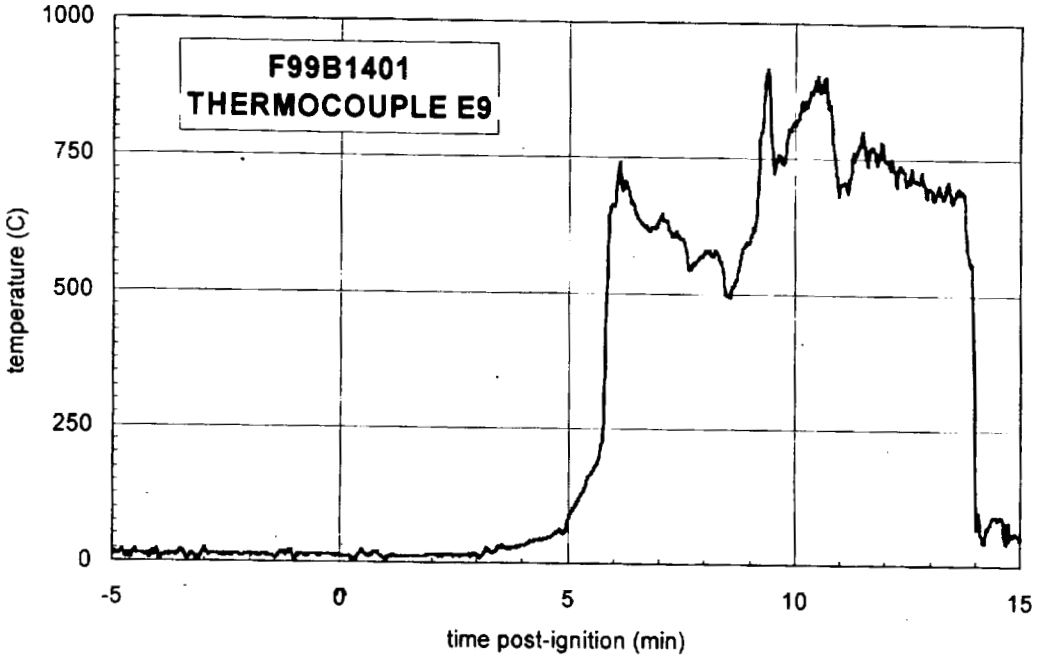


Plot H27. Fire Test F99B1401. Data plot from thermocouple E9.

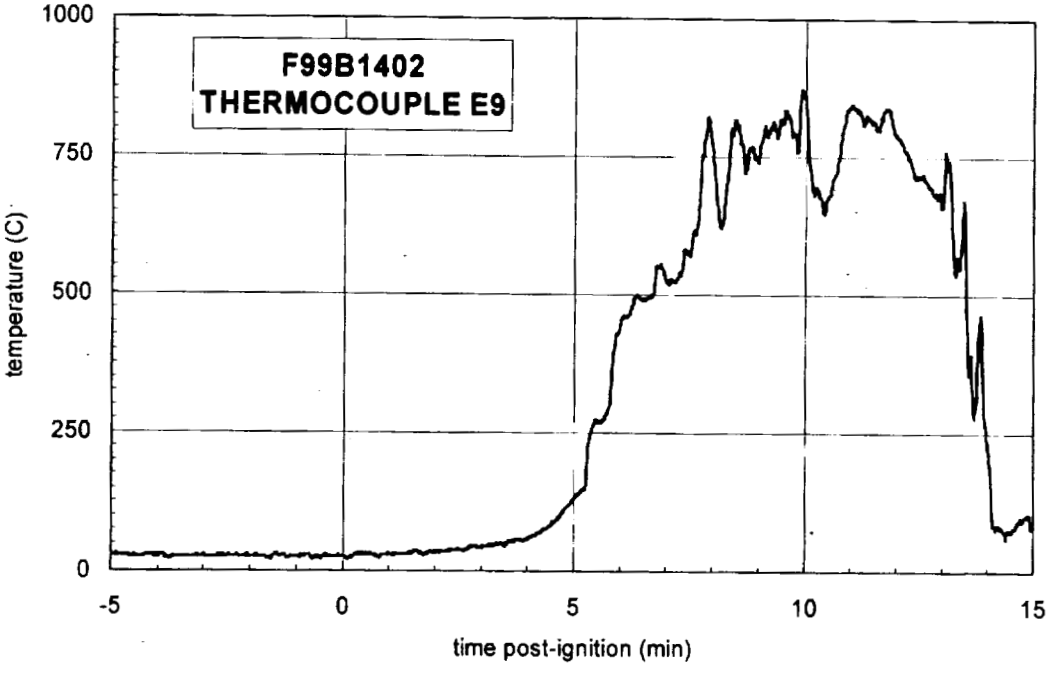


Plot H28. Fire Test F99B1402. Data plot from thermocouple E9.

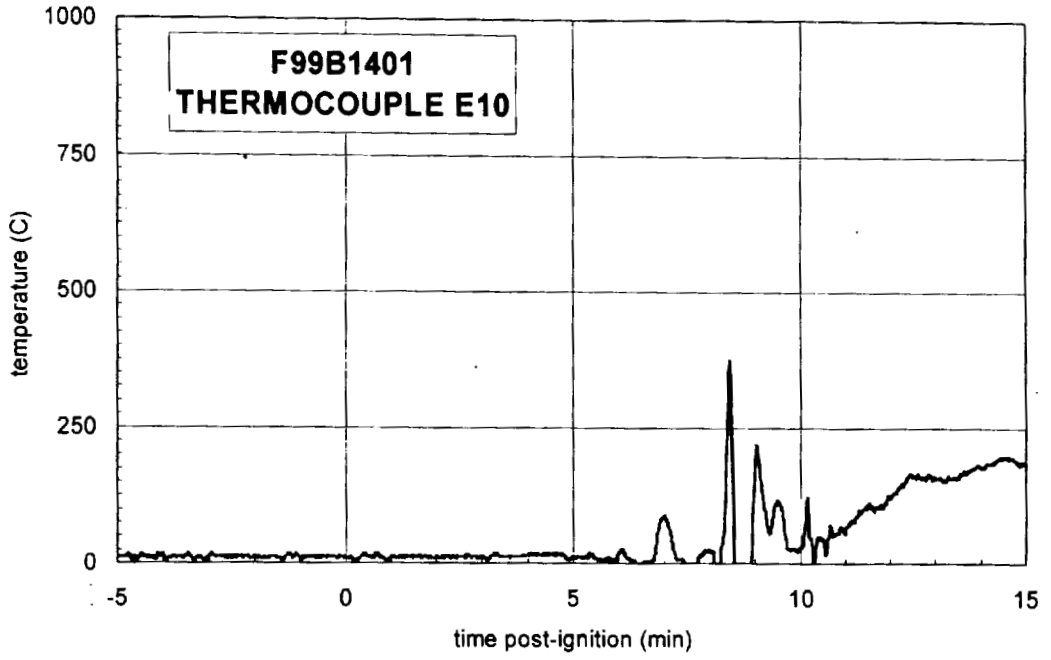


Plot H29. Fire Test F99B1401. Data plot from thermocouple E10.

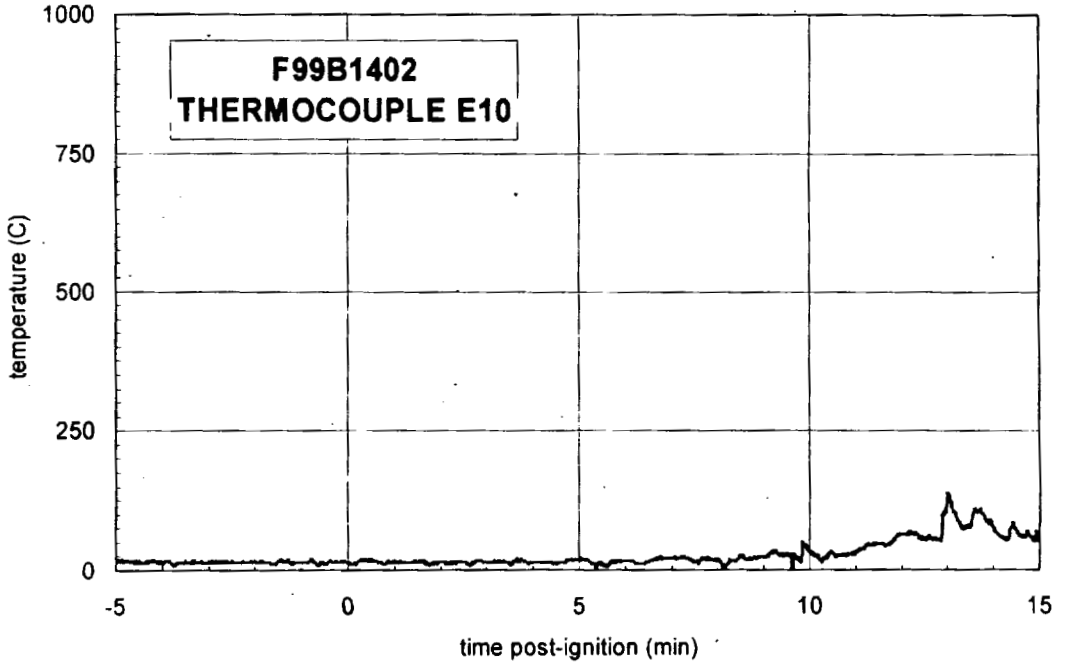


Plot H30. Fire Test F99B1402. Data plot from thermocouple E10.

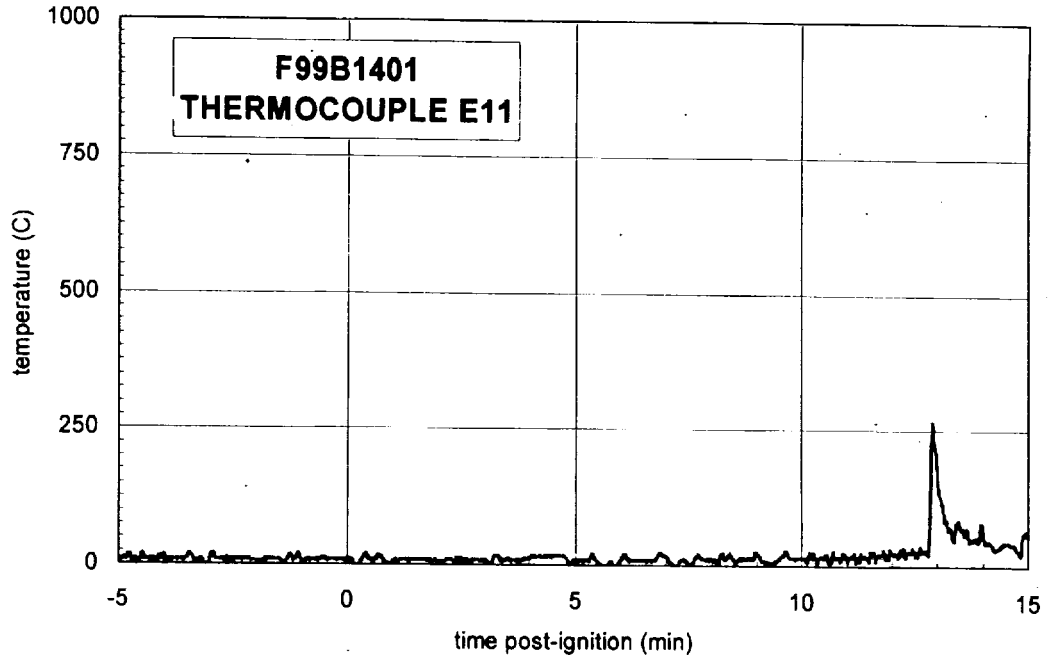


Plot H31. Fire Test F99B1401. Data plot from thermocouple E11.

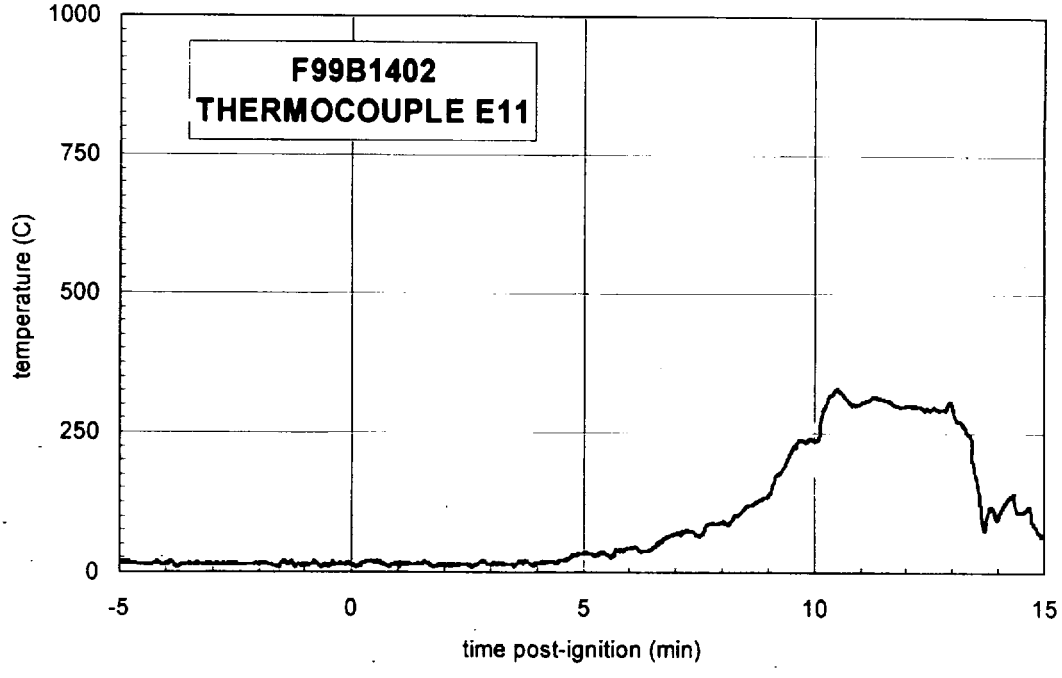


Plot H32. Fire Test F99B1402. Data plot from thermocouple E11.

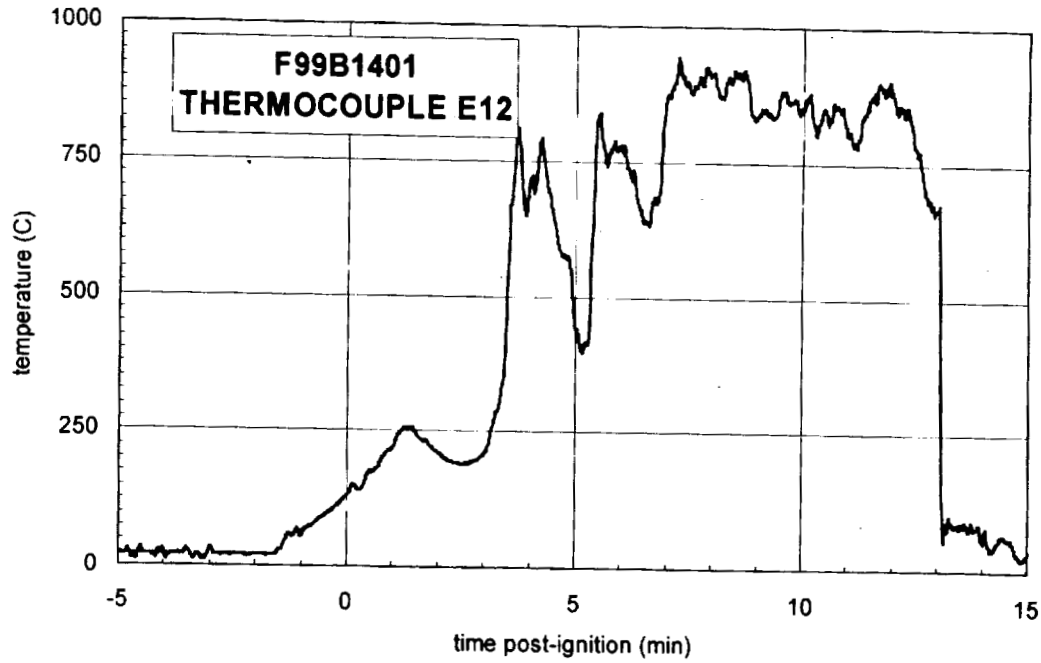


Plot H33. Fire Test F99B1401. Data plot from thermocouple E12.

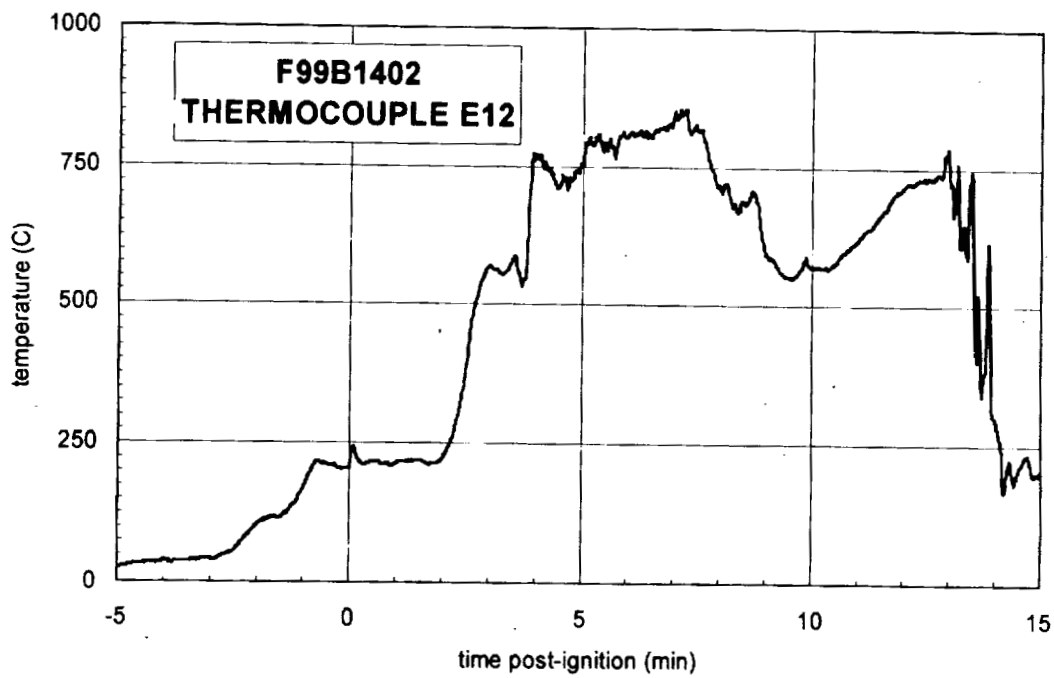


Plot H34. Fire Test F99B1402. Data plot from thermocouple E12.

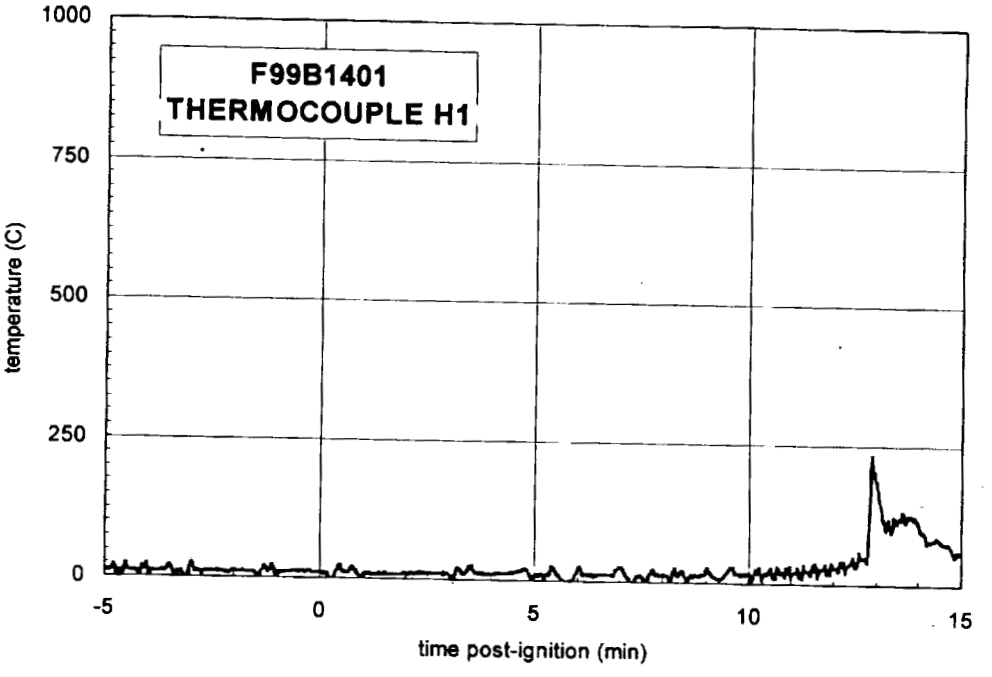


Plot H35. Fire Test F99B1401. Data plot from thermocouple H1.

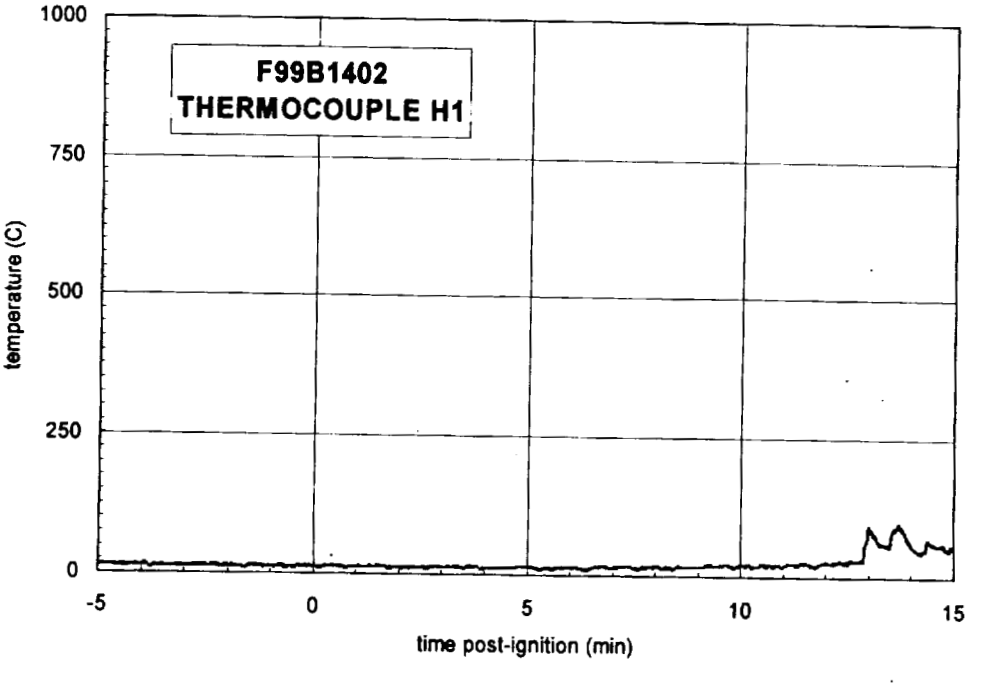


Plot H36. Fire Test F99B1402. Data plot from thermocouple H1.

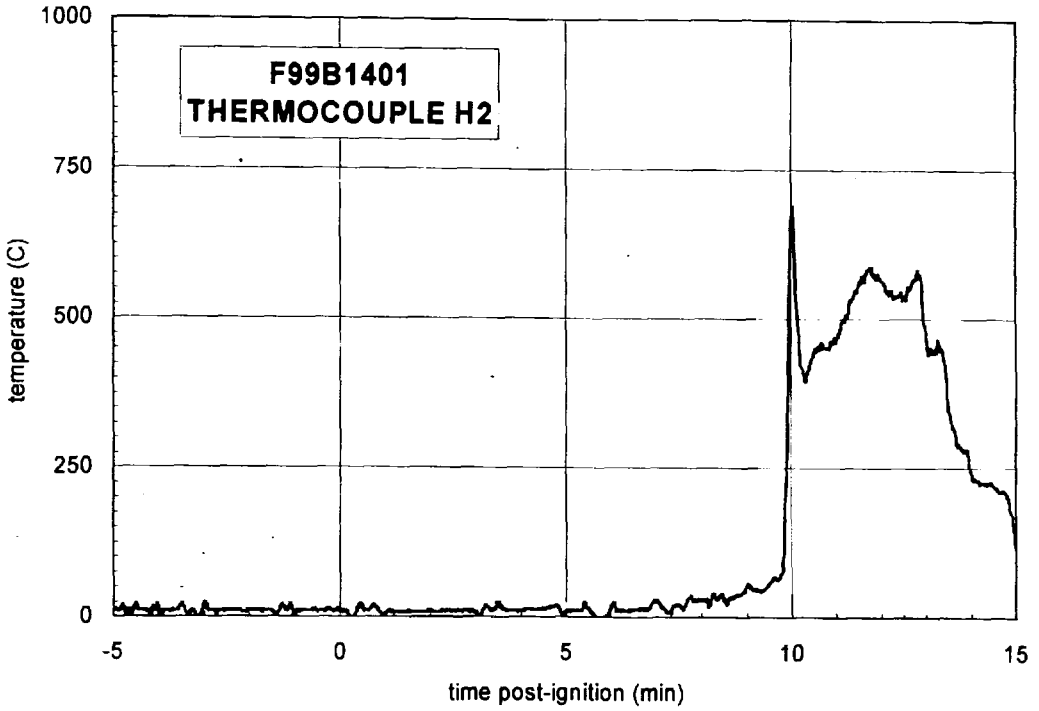


Plot H37. Fire Test F99B1401. Data plot from thermocouple H2.

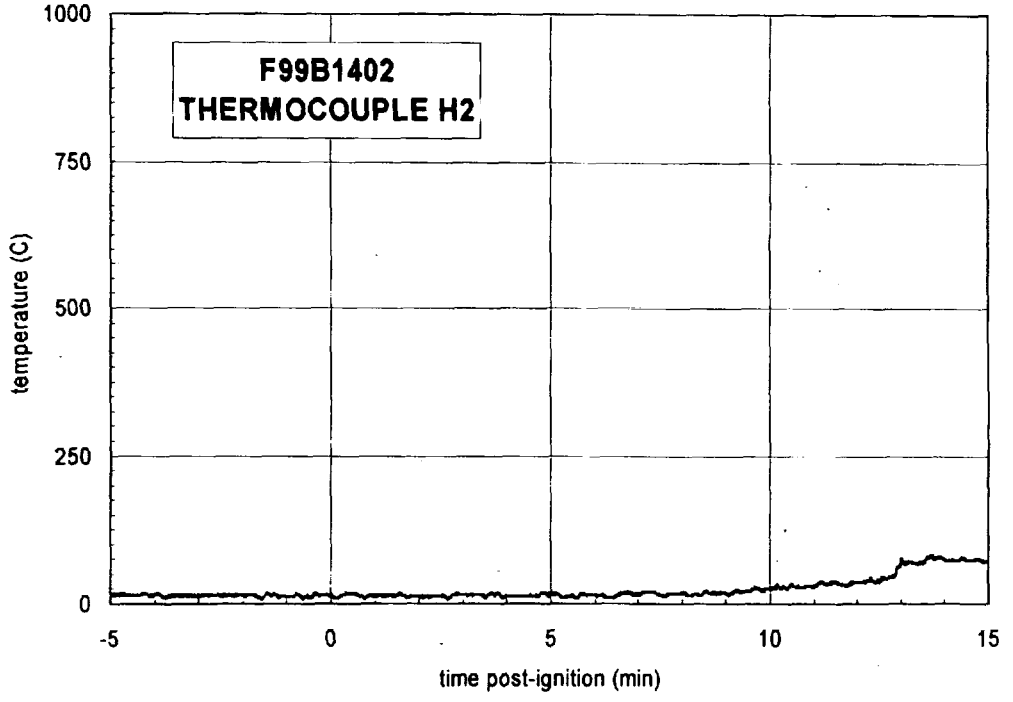


Plot H38. Fire Test F99B1402. Data plot from thermocouple H2.

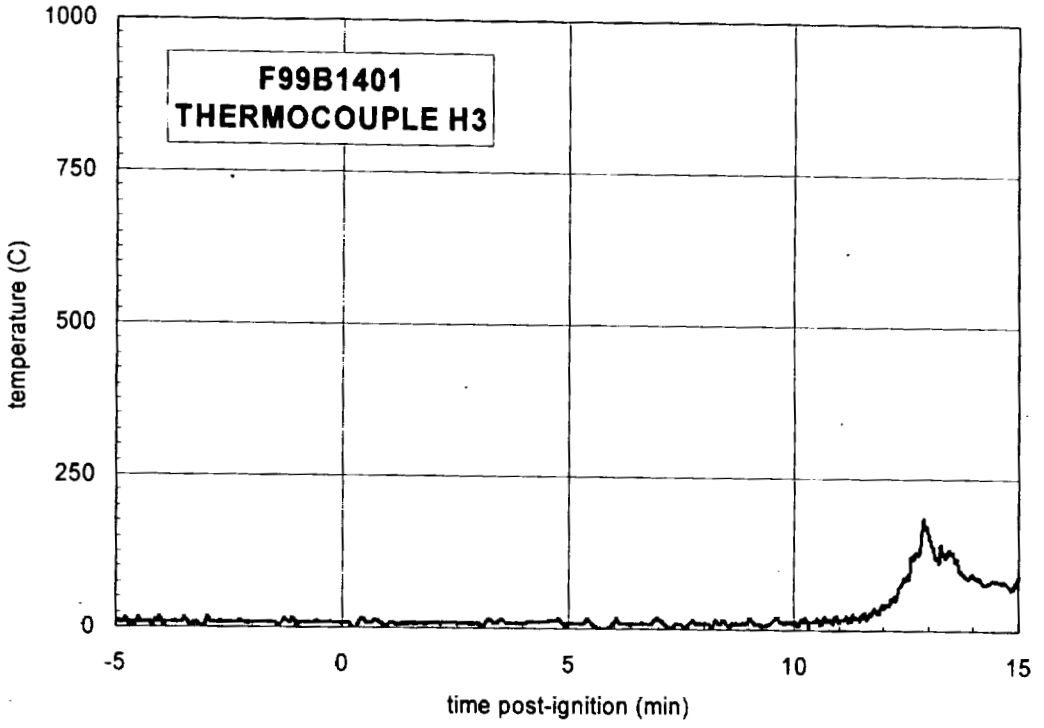


Plot H39. Fire Test F99B1401. Data plot from thermocouple H3.

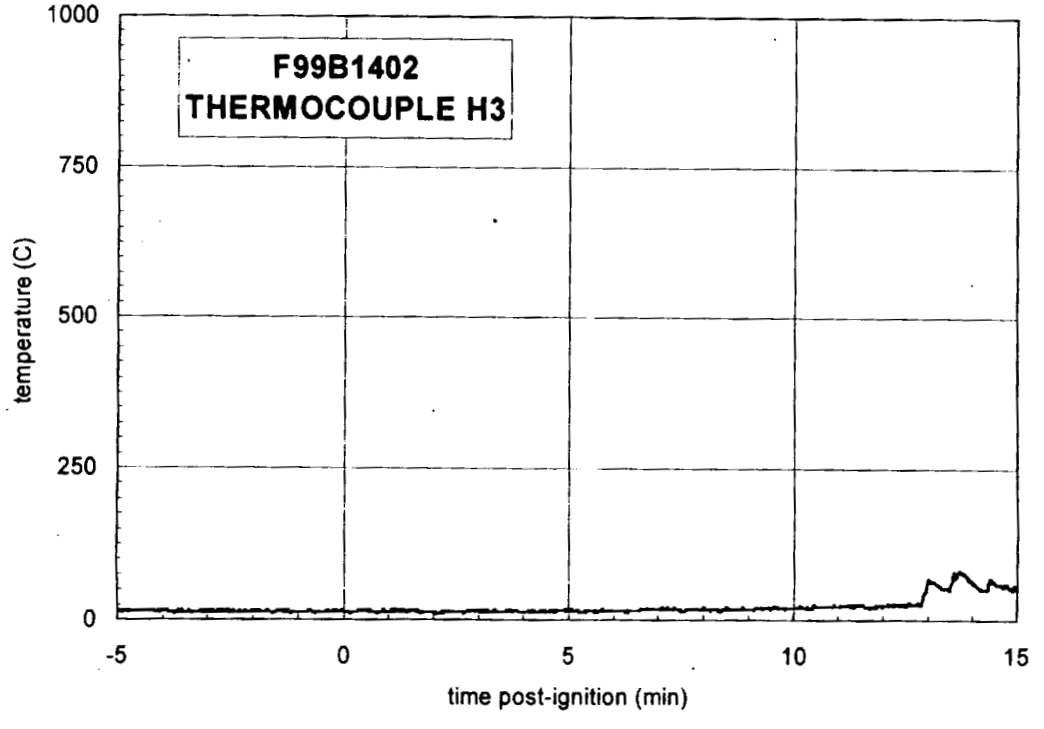


Plot H40. Fire Test F99B1402. Data plot from thermocouple H3.

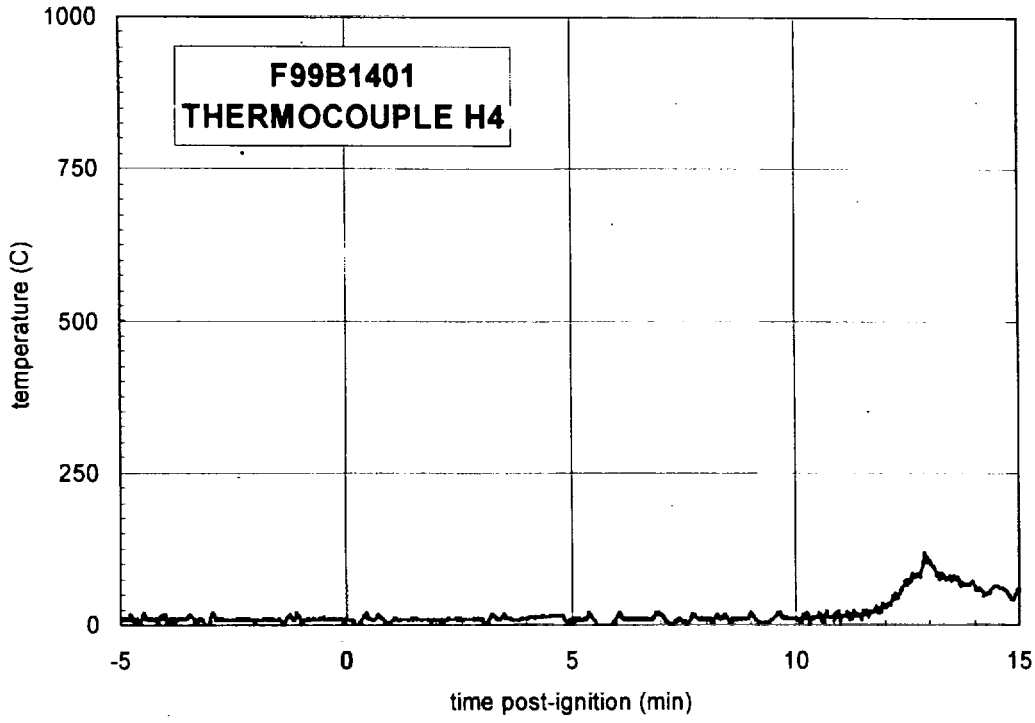


Plot H41. Fire Test F99B1401. Data plot from thermocouple H4.

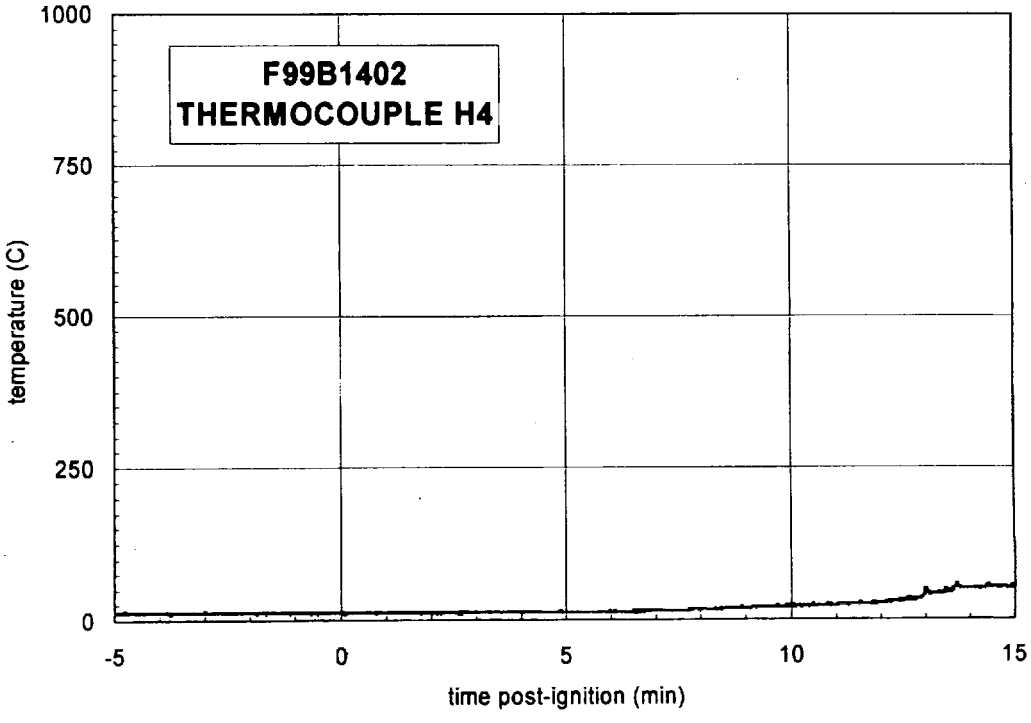


Plot H42. Fire Test F99B1402. Data plot from thermocouple H4.

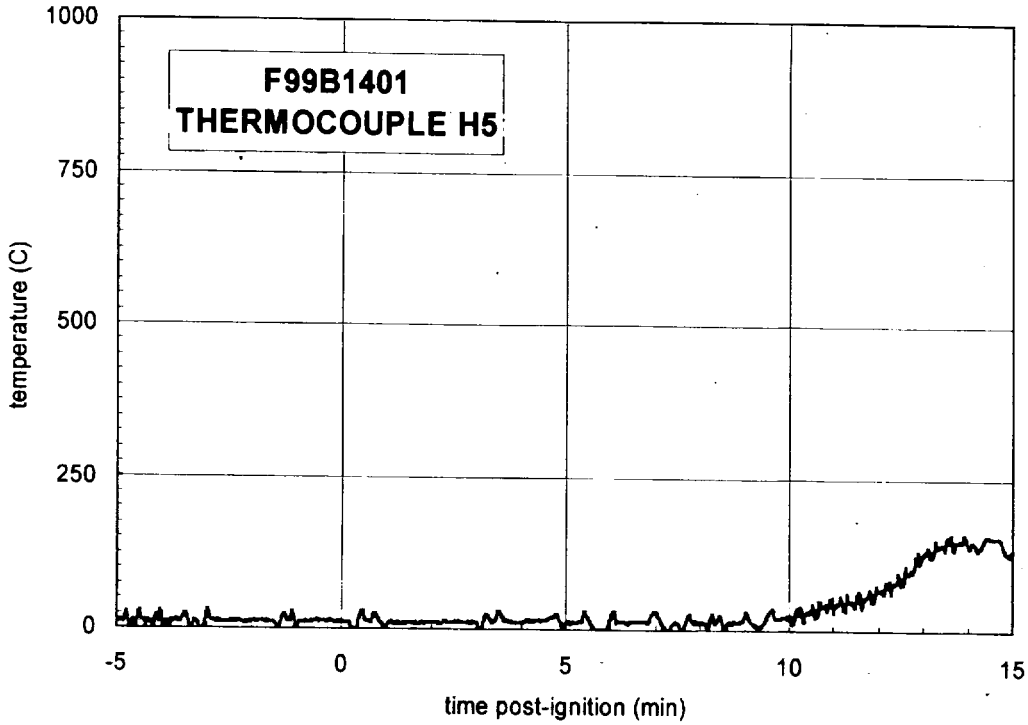


Plot H43. Fire Test F99B1401. Data plot from thermocouple H5

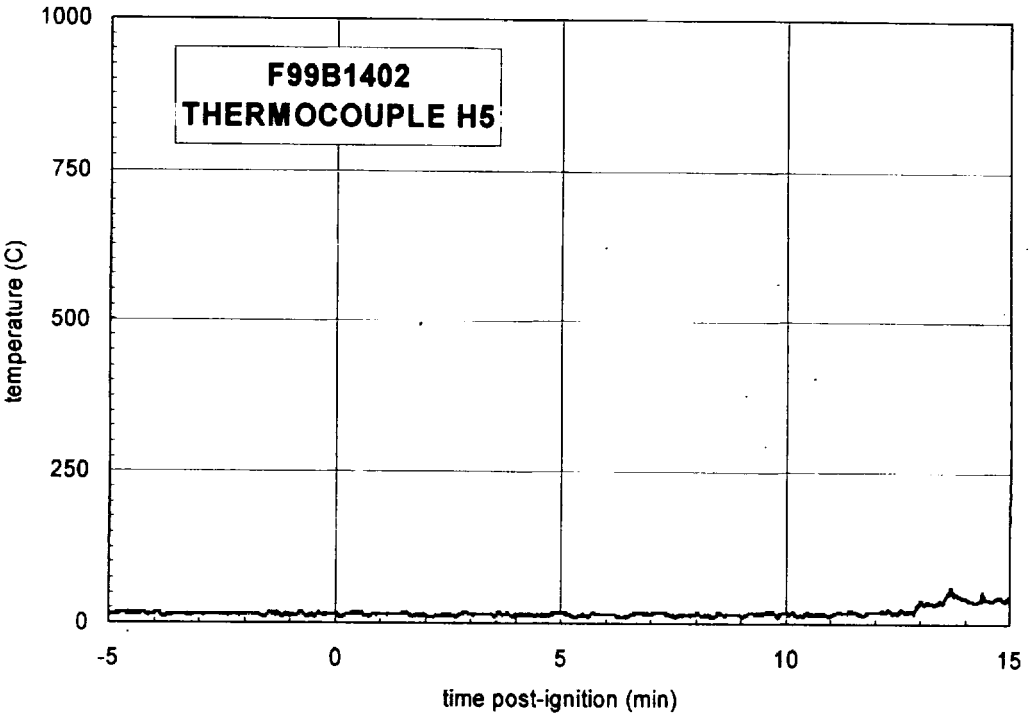


Plot H44. Fire Test F99B1402. Data plot from thermocouple H5.

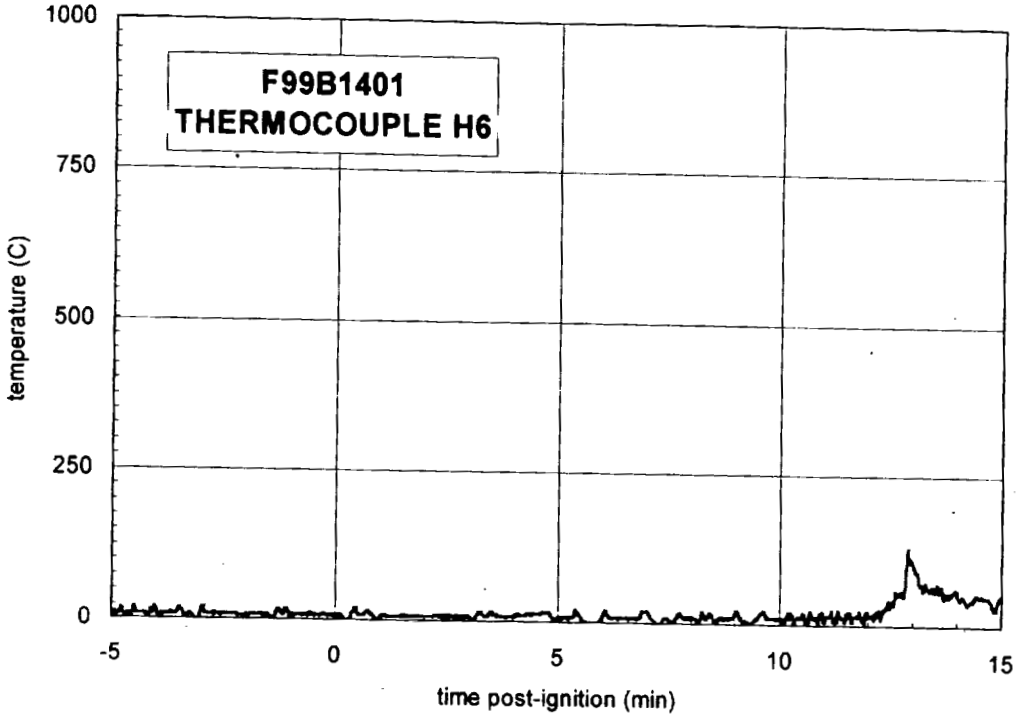


Plot H45. Fire Test F99B1401. Data plot from thermocouple H6.

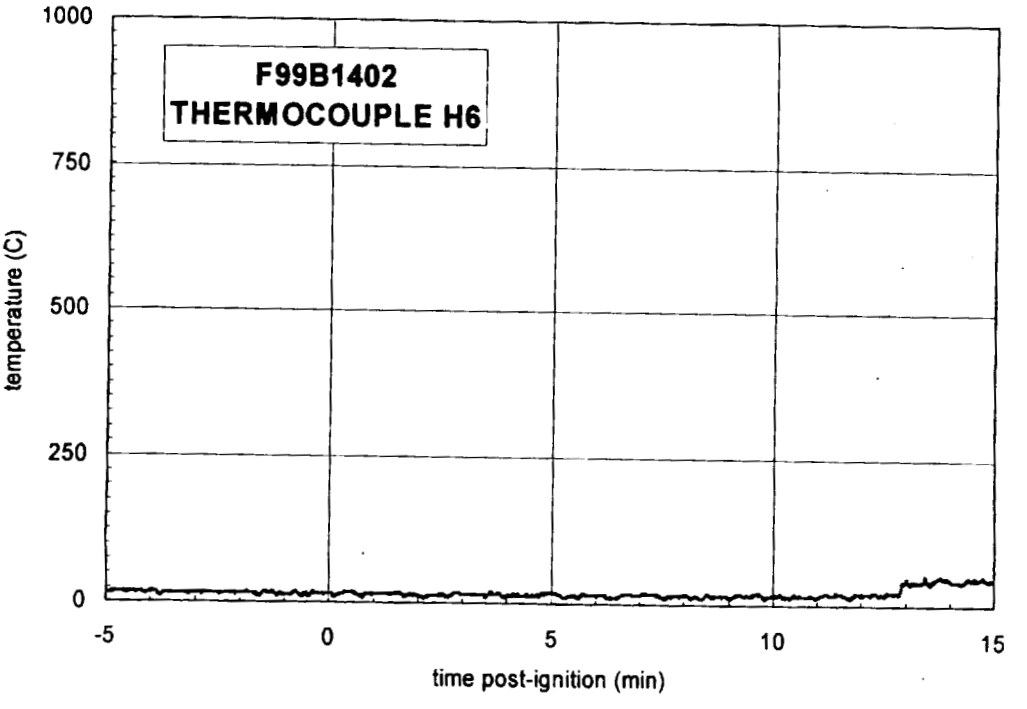


Plot H46. Fire Test F99B1402. Data plot from thermocouple H6.

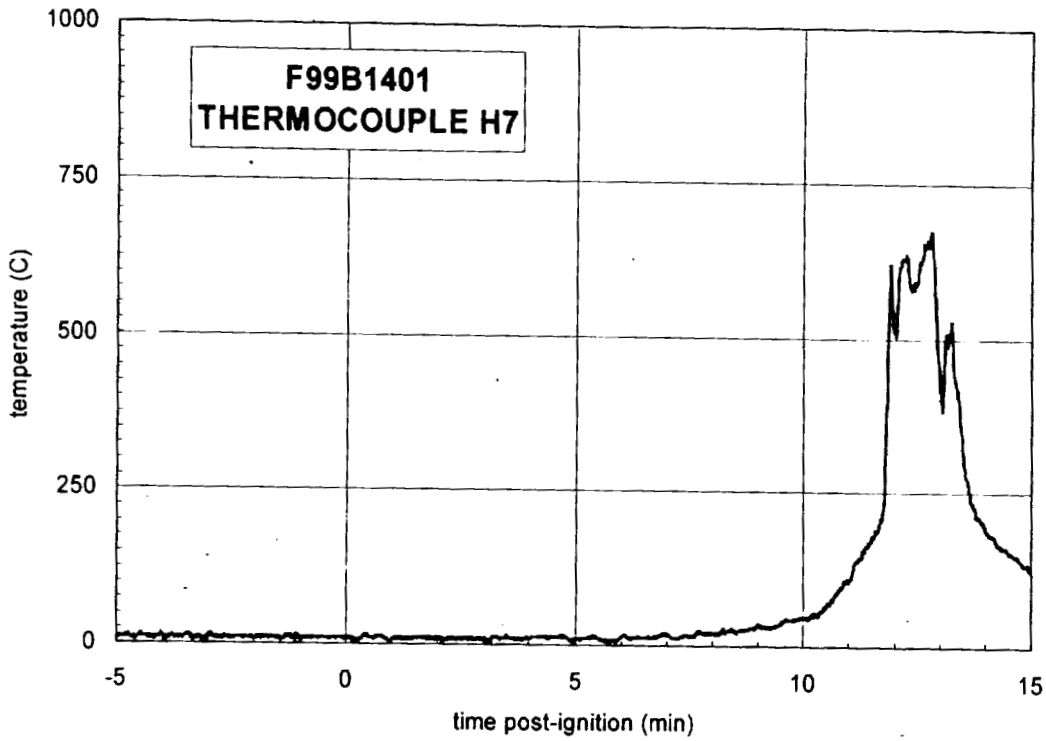


Plot H47. Fire Test F99B1401. Data plot from thermocouple H7.

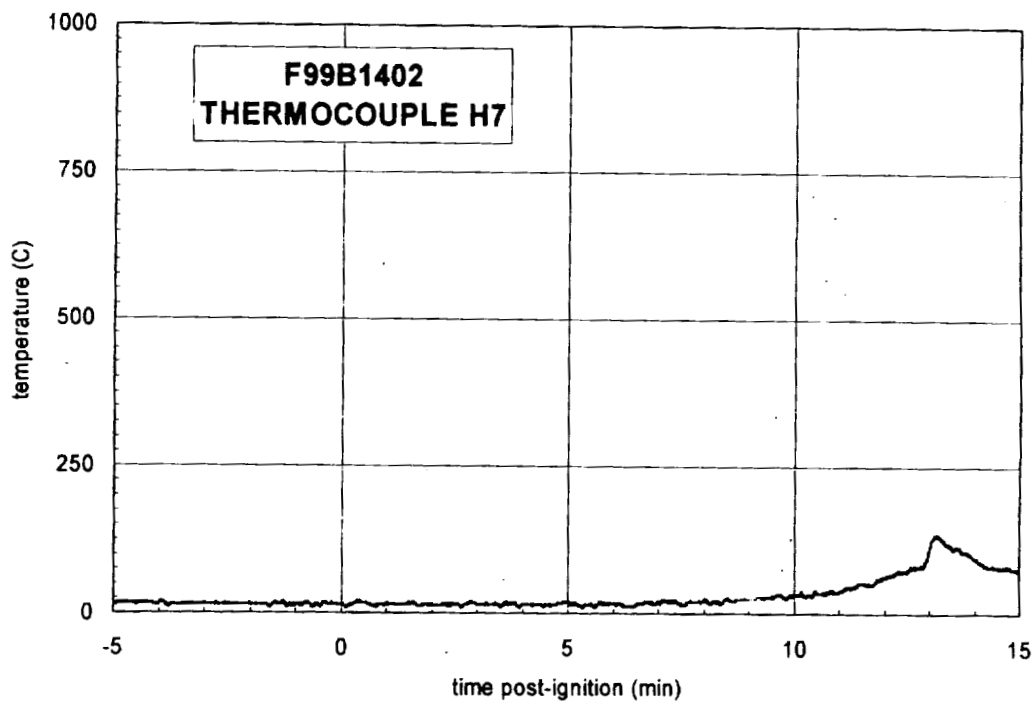


Plot H48. Fire Test F99B1402. Data plot from thermocouple H7.

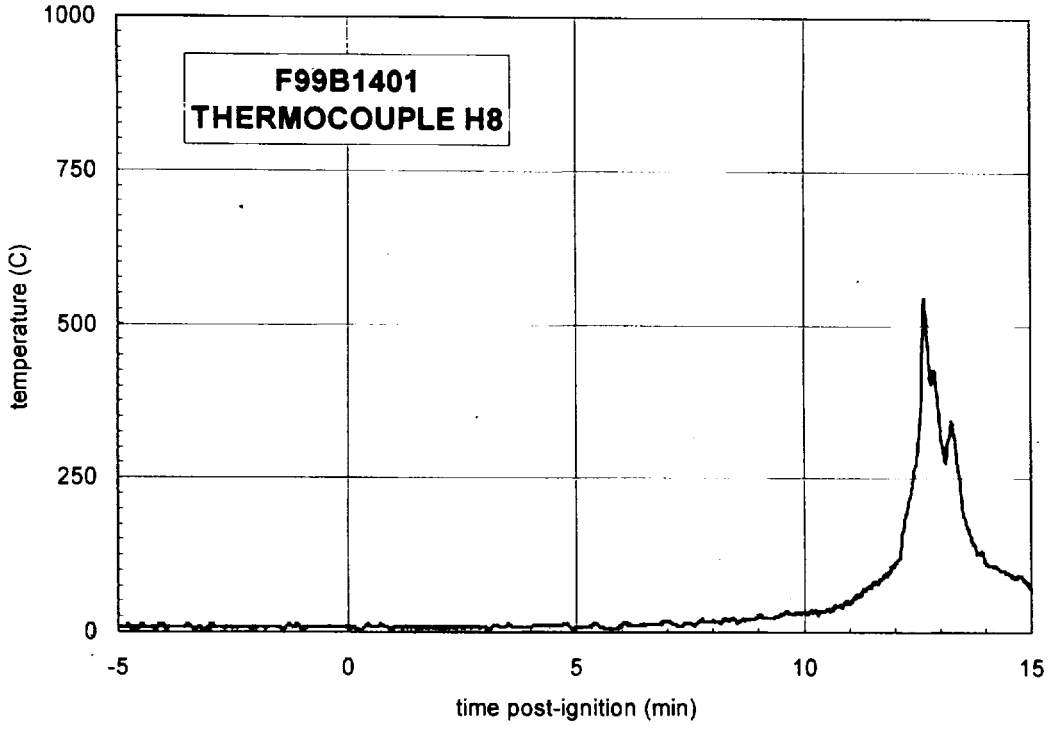


Plot H49. Fire Test F99B1401. Data plot from thermocouple H8.

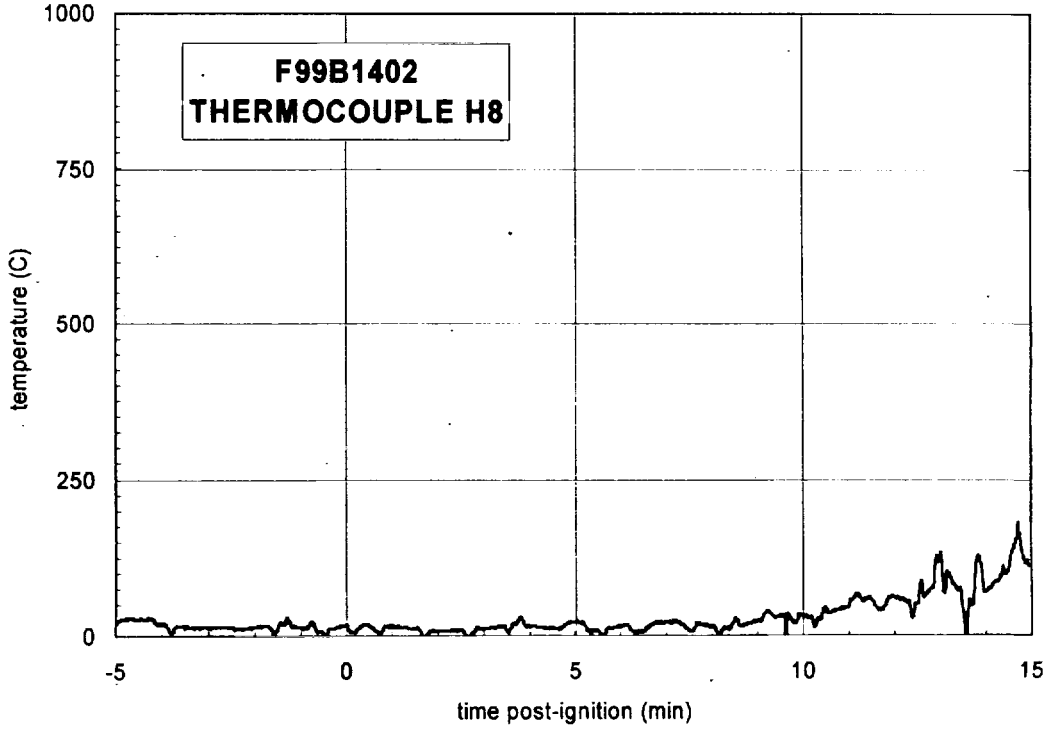


Plot H50. Fire Test F99B1402. Data plot from thermocouple H8.

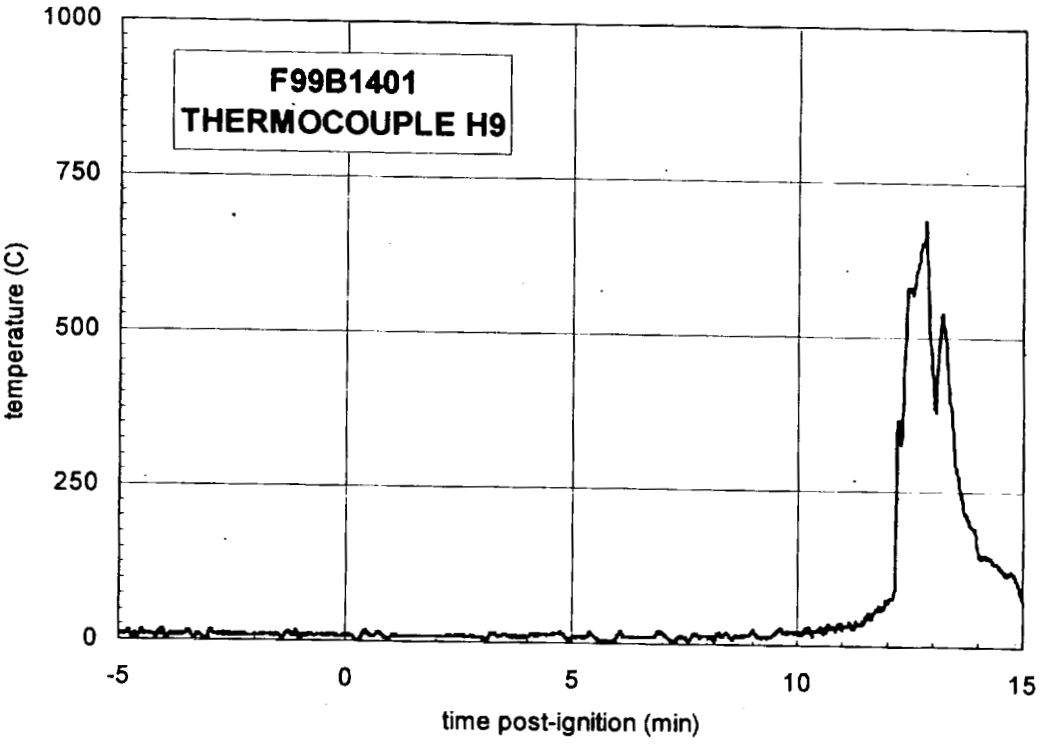


Plot H51. Fire Test F99B1401. Data plot from thermocouple H9.

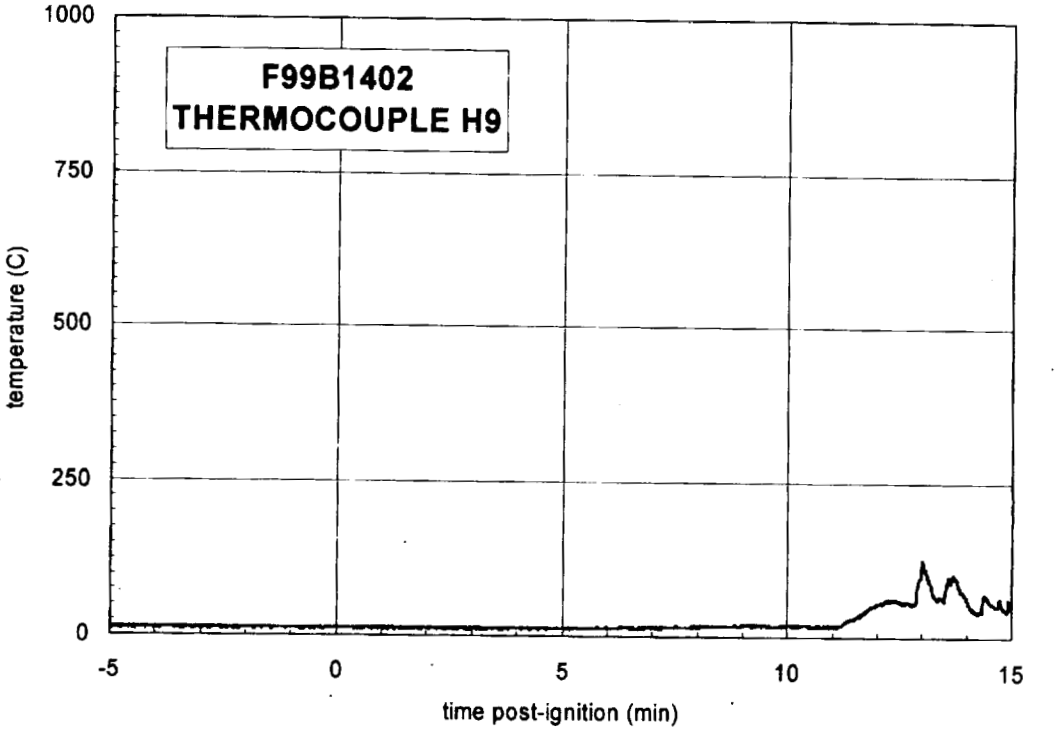


Plot H52. Fire Test F99B1402. Data plot from thermocouple H9.

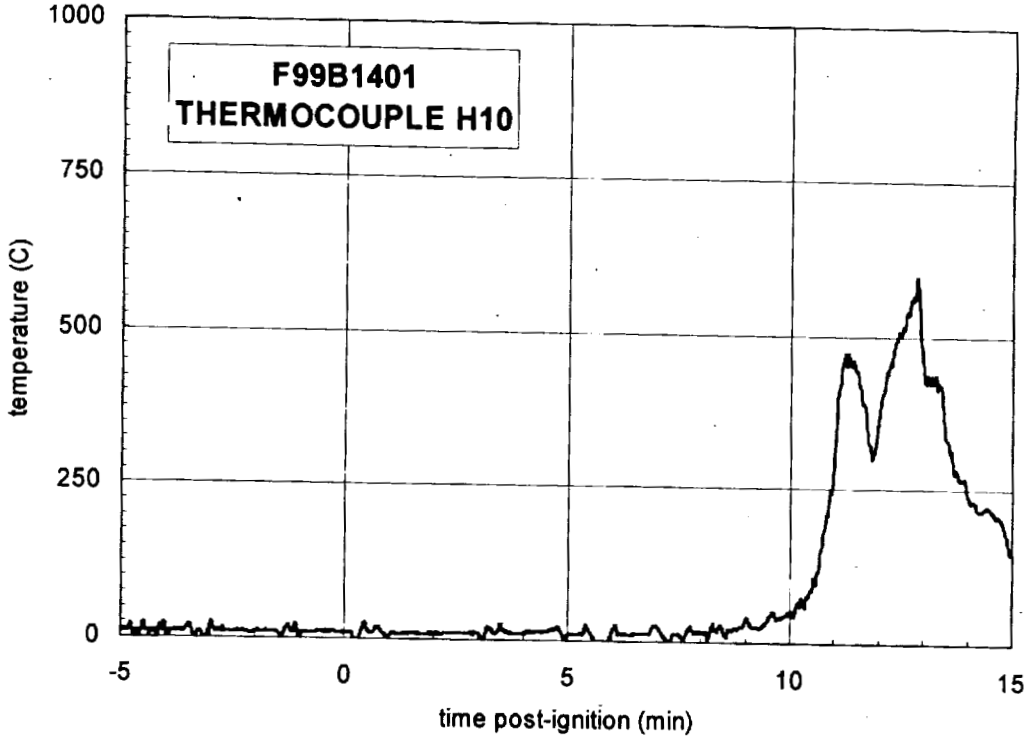


Plot H53. Fire Test F99B1401. Data plot from thermocouple H10.

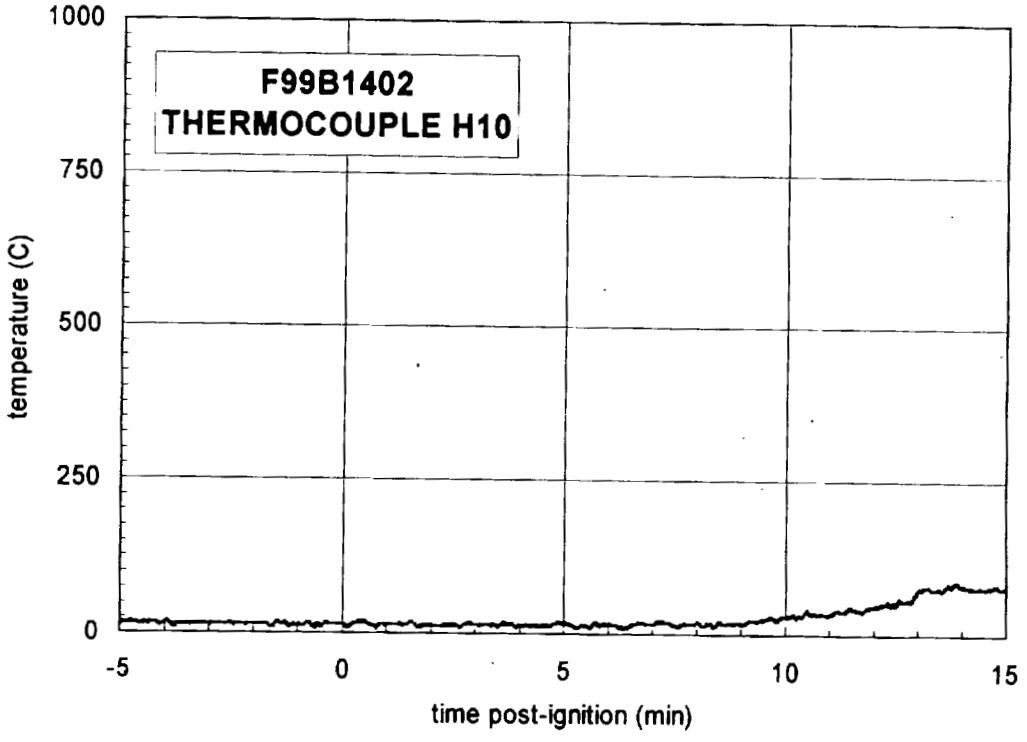


Plot H54. Fire Test F99B1402. Data plot from thermocouple H10.

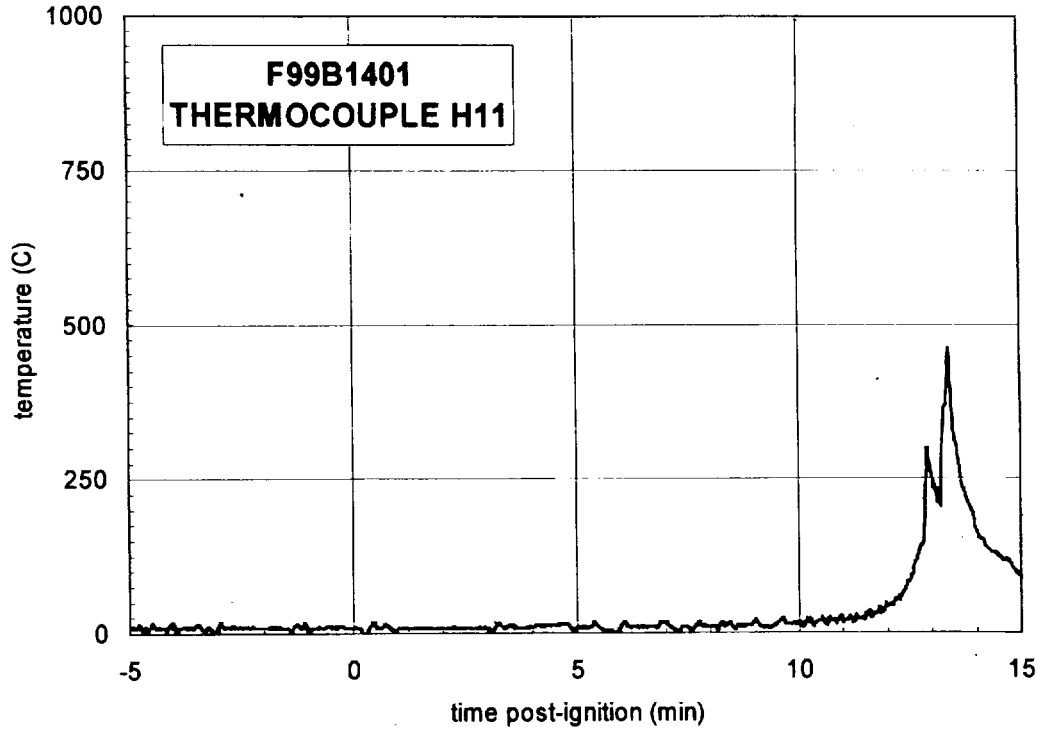


Plot H55. Fire Test F99B1401. Data plot from thermocouple H11.

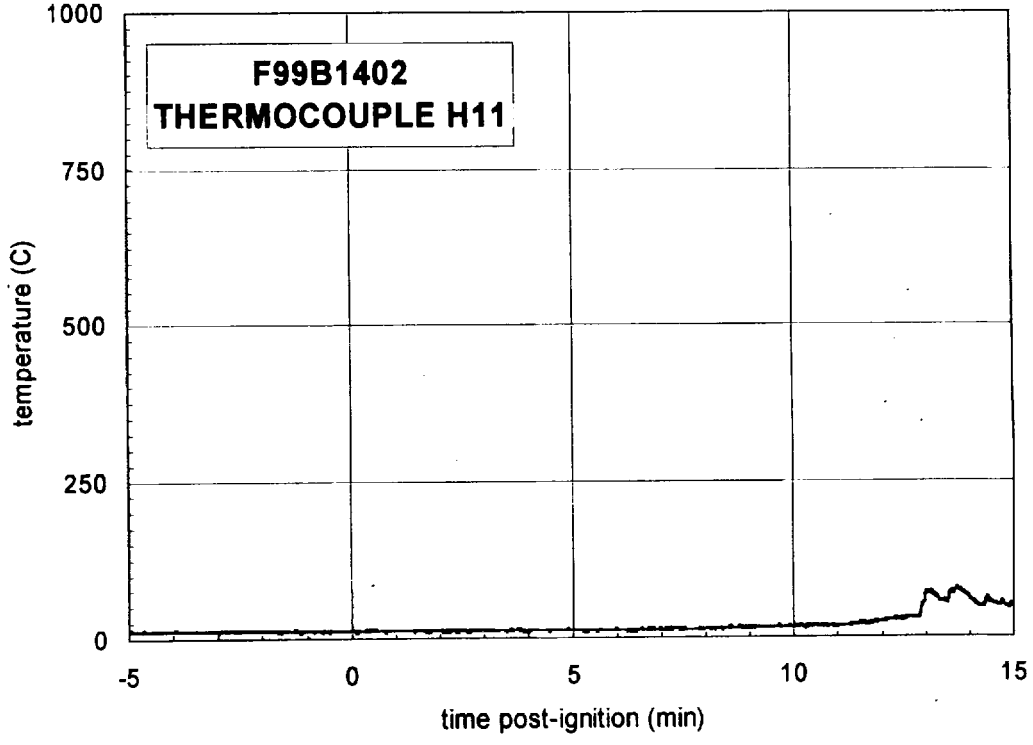


Plot H56. Fire Test F99B1402. Data plot from thermocouple H11.

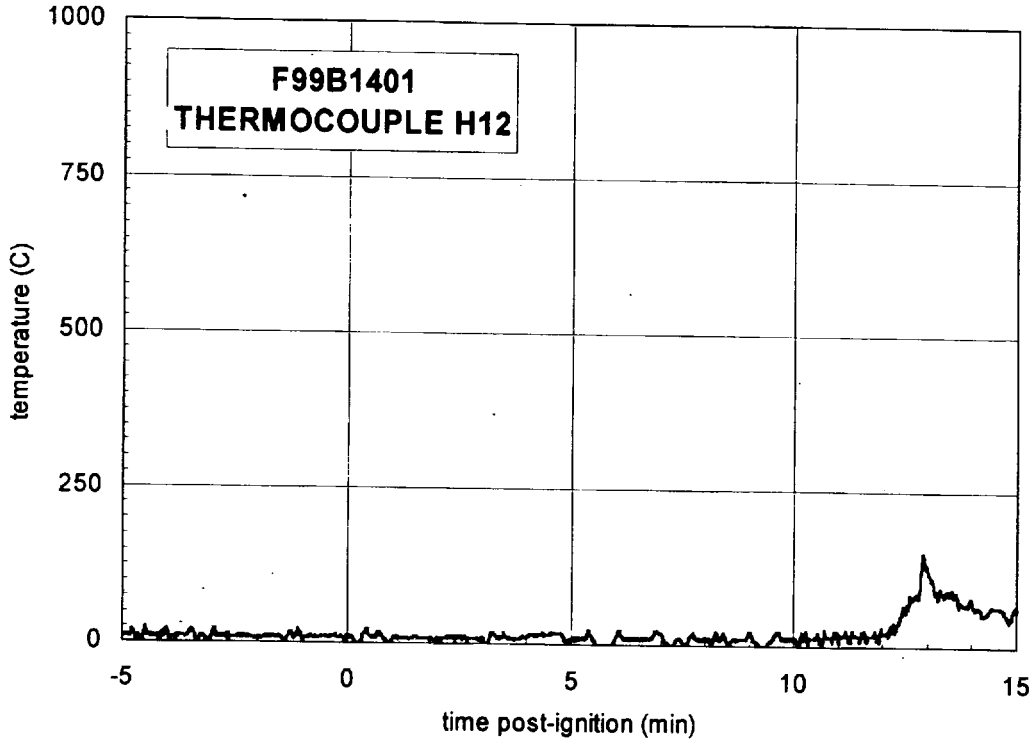


Plot H57. Fire Test F99B1401. Data plot from thermocouple H12.

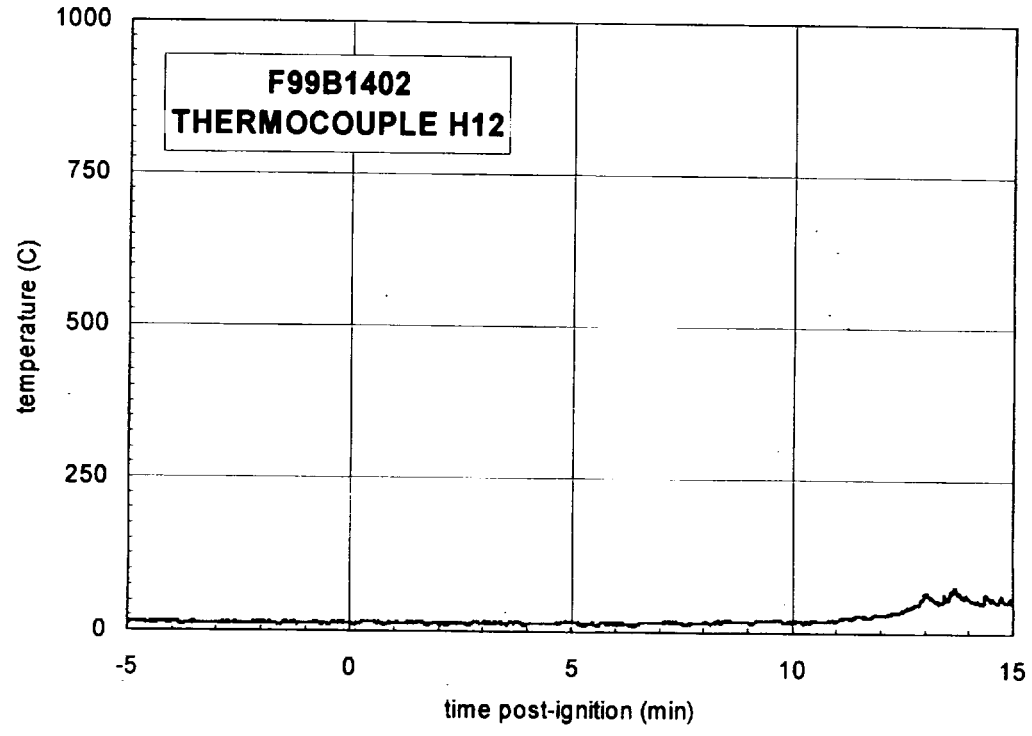


Plot H58. Fire Test F99B1402. Data plot from thermocouple H12.

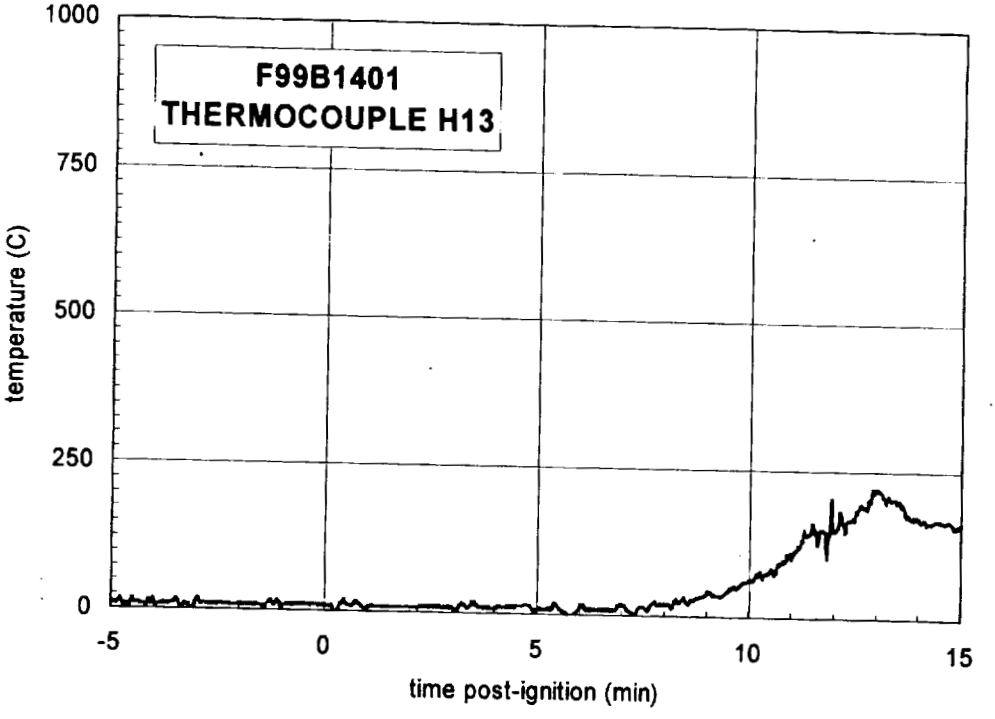


Plot H59. Fire Test F99B1401. Data plot from thermocouple H13.

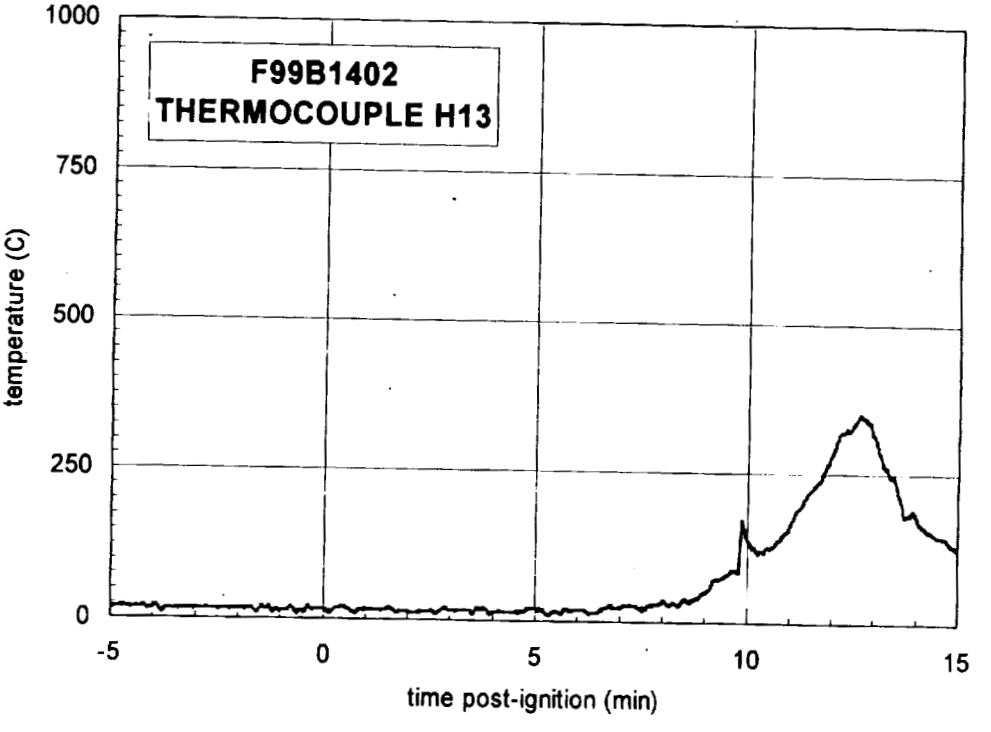


Plot H60. Fire Test F99B1402. Data plot from thermocouple H13.

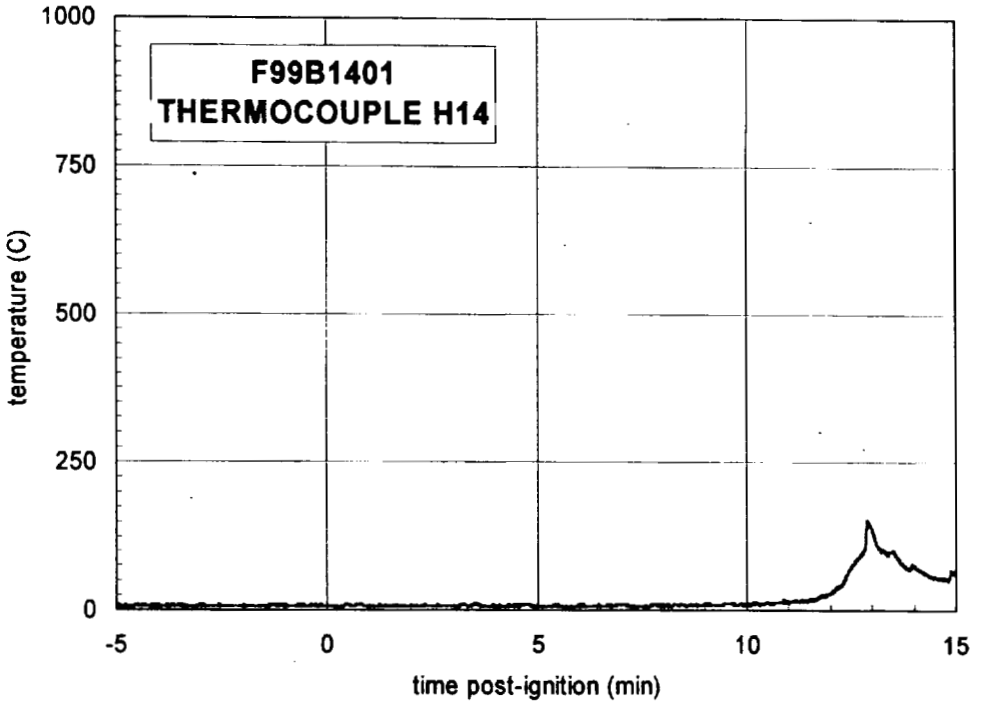


Plot H61. Fire Test F99B1401. Data plot from thermocouple H14.

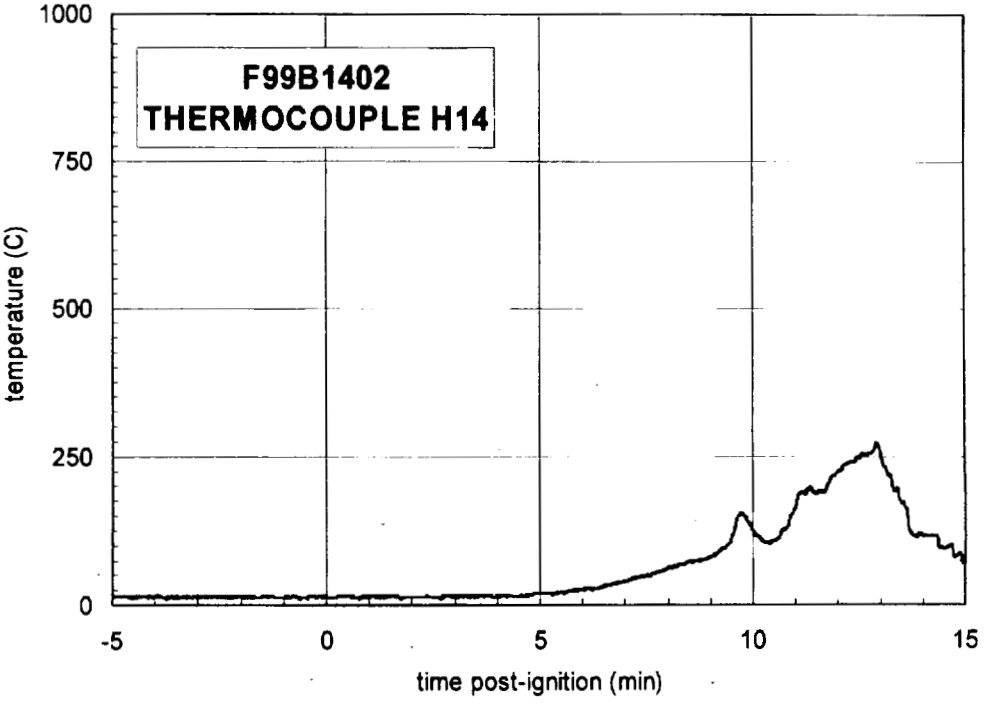


Plot H62. Fire Test F99B1402. Data plot from thermocouple H14.

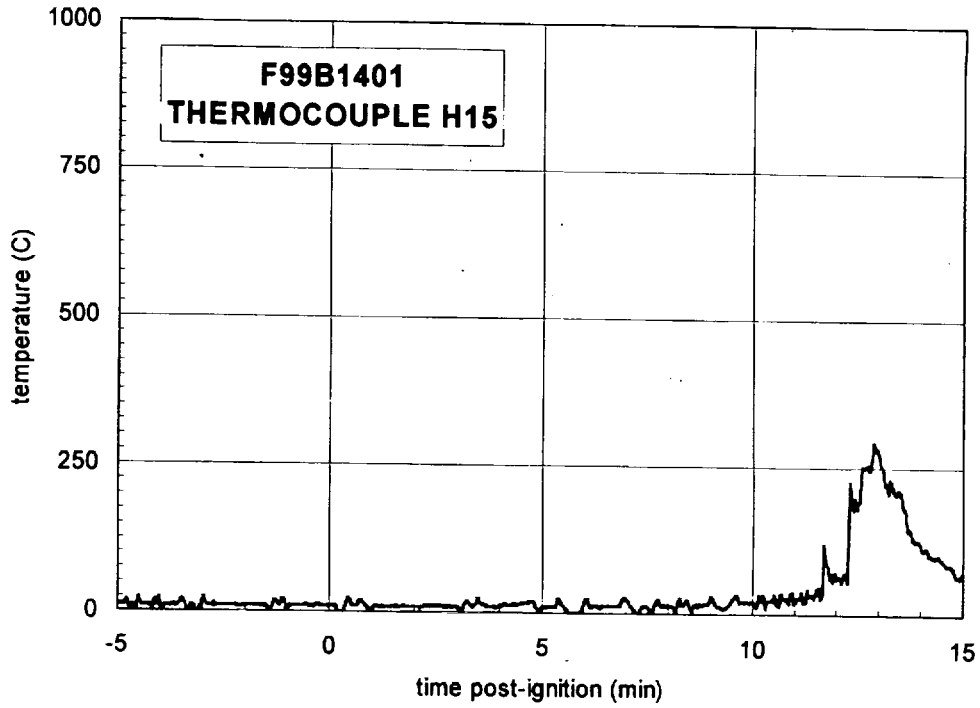


Plot H63. Fire Test F99B1401. Data plot from thermocouple H15.

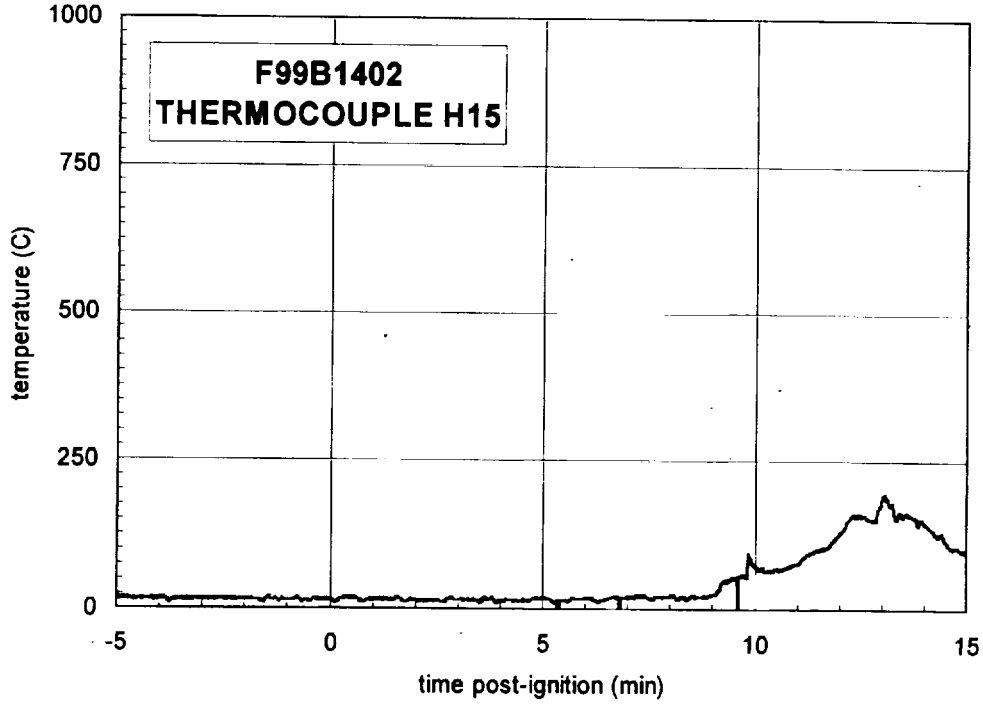


Plot H64. Fire Test F99B1402. Data plot from thermocouple H15.

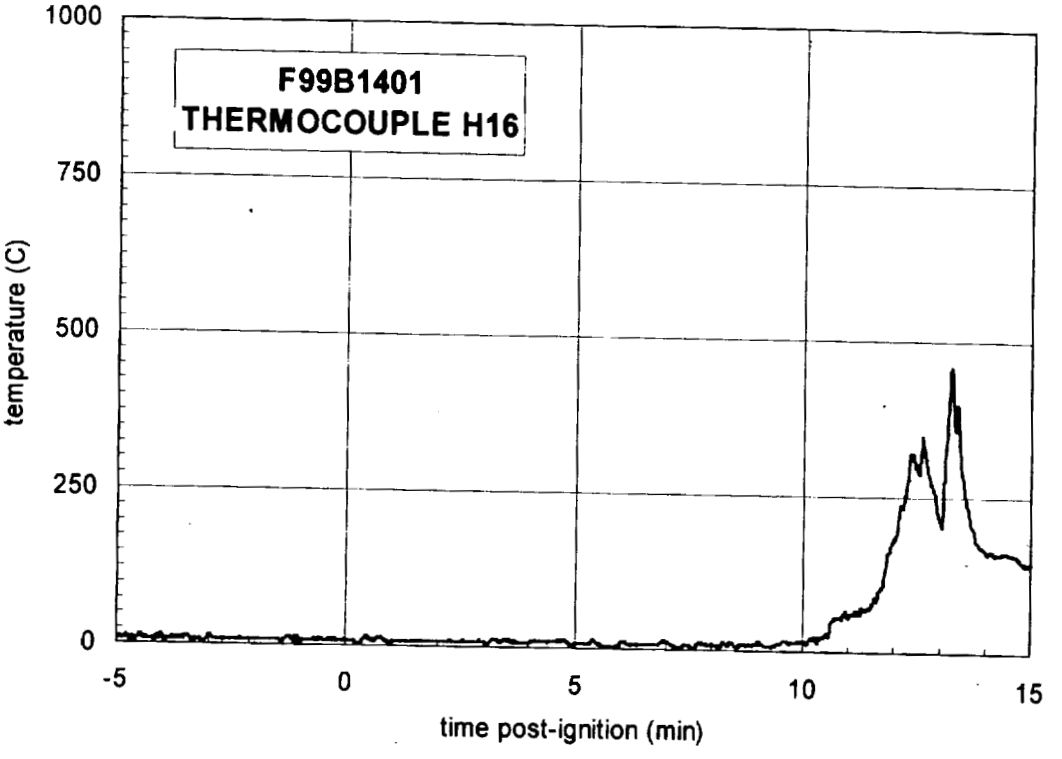


Plot H65. Fire Test F99B1401. Data plot from thermocouple H16.

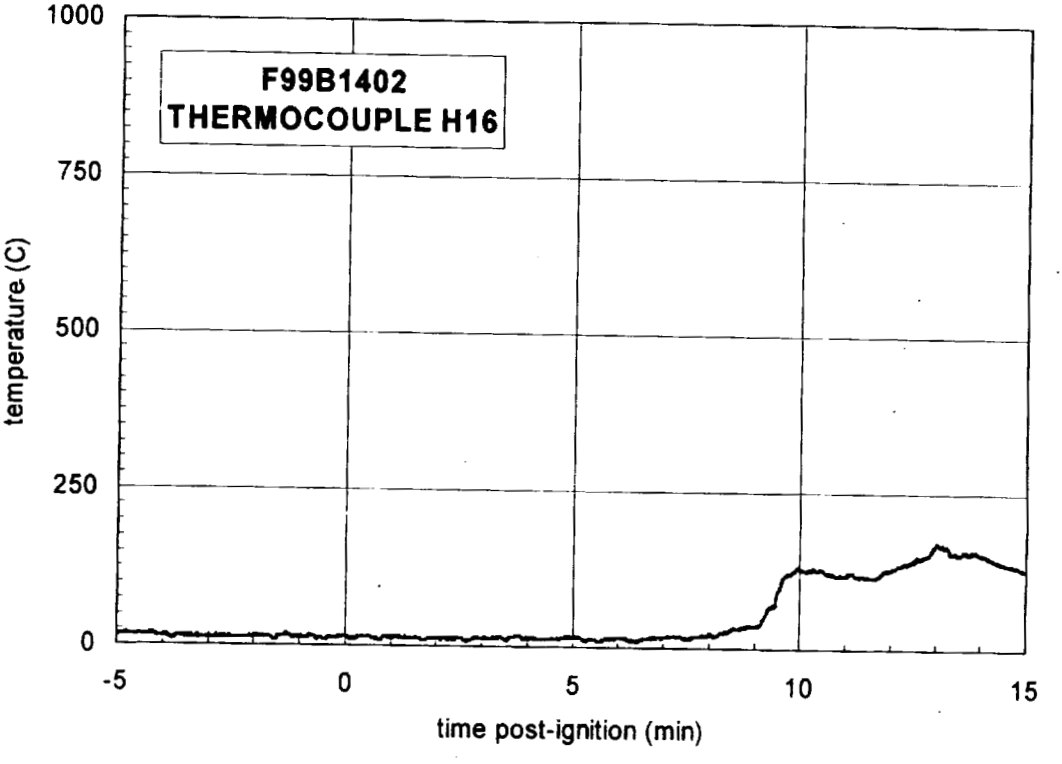


Plot H66. Fire Test F99B1402. Data plot from thermocouple H16.

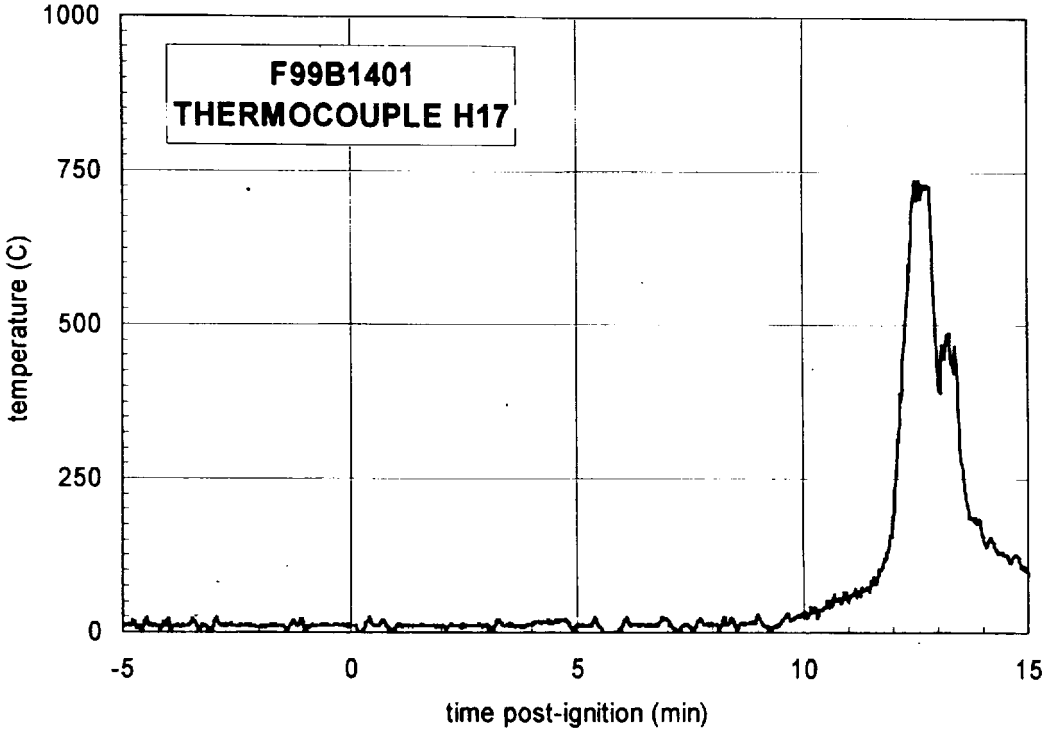


Plot H67. Fire Test F99B1401. Data plot from thermocouple H17.

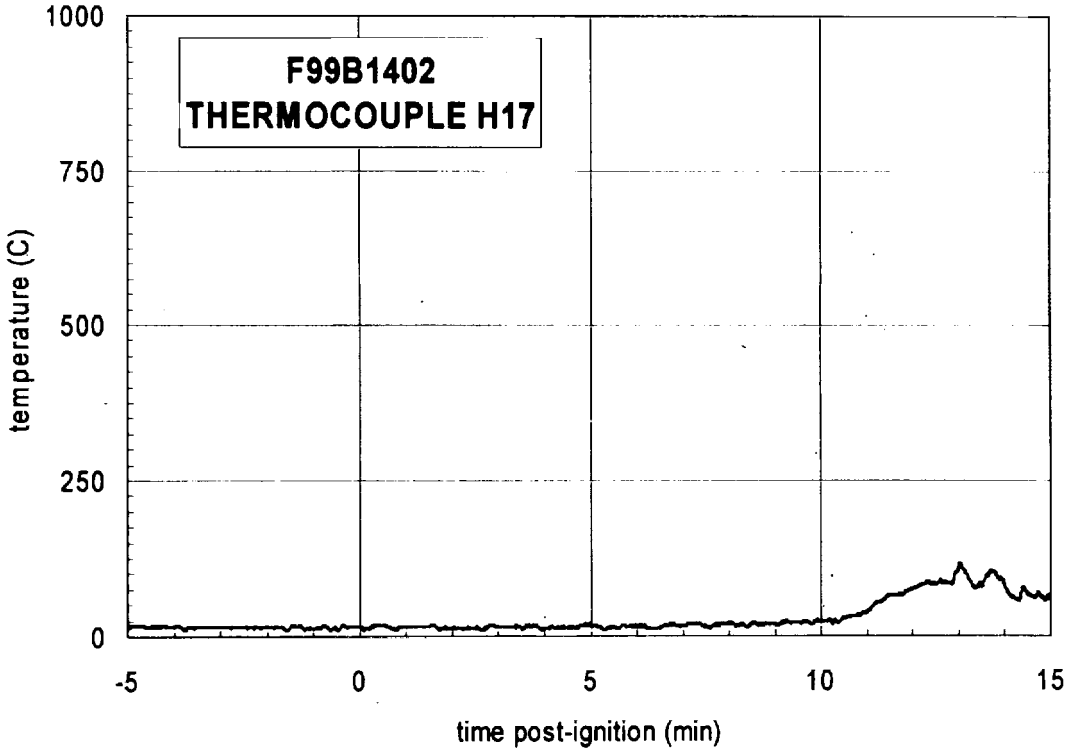


Plot H68. Fire Test F99B1402. Data plot from thermocouple H17.

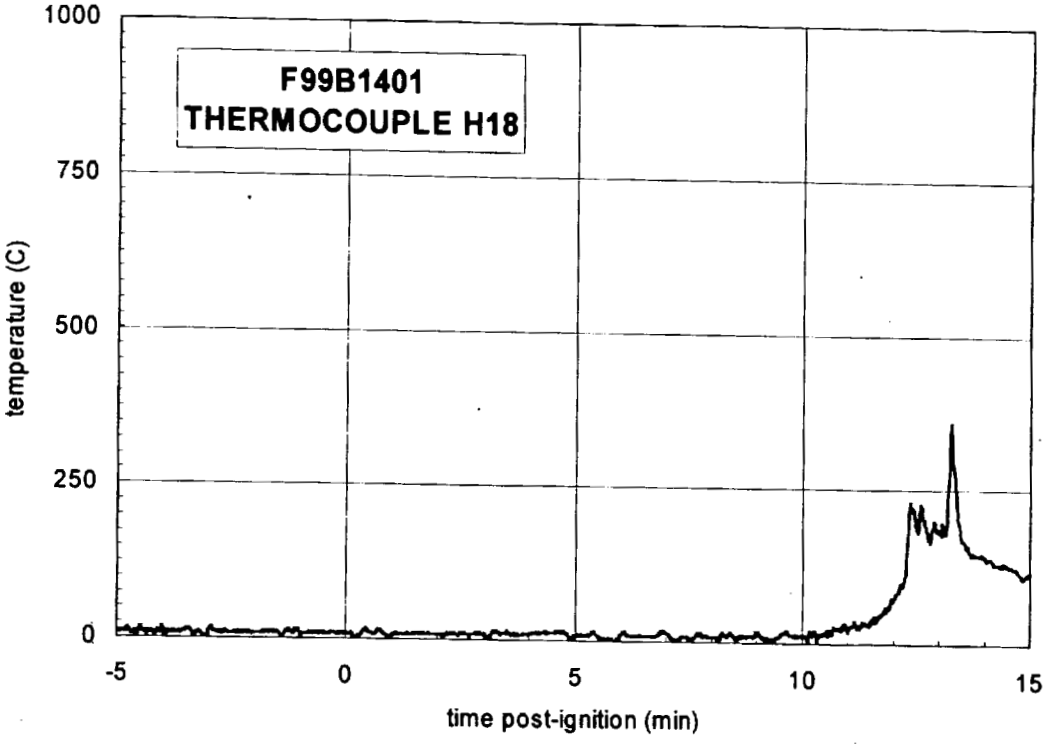


Plot H69. Fire Test F99B1401. Data plot from thermocouple H18.

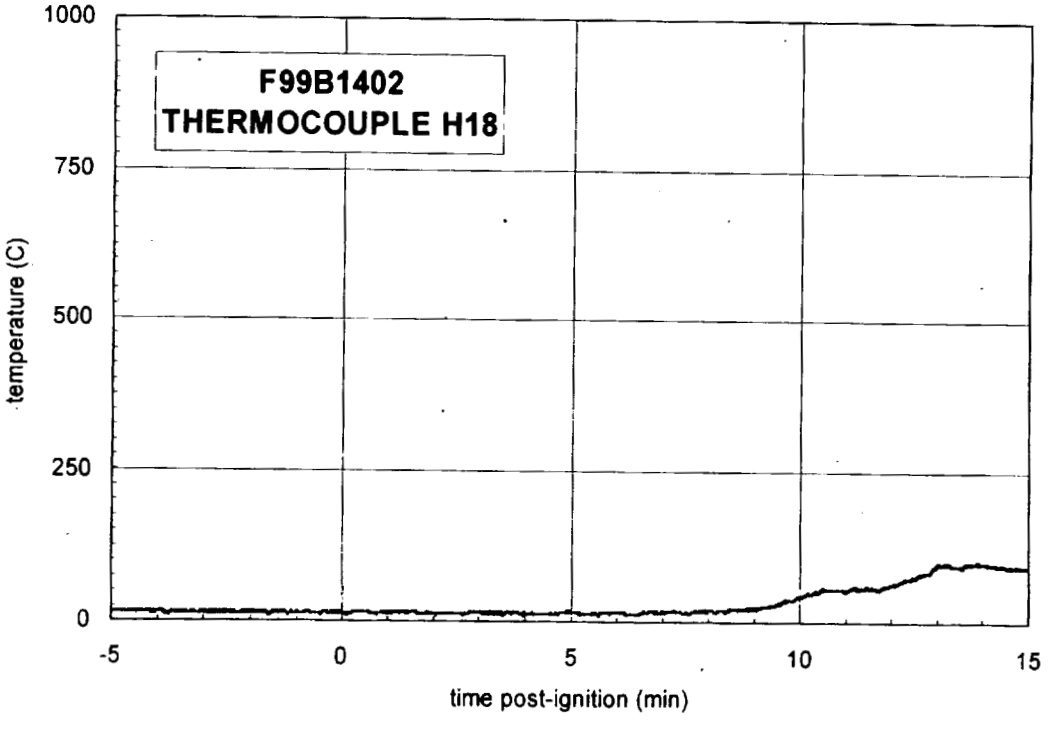


Plot H70. Fire Test F99B1402. Data plot from thermocouple H18.

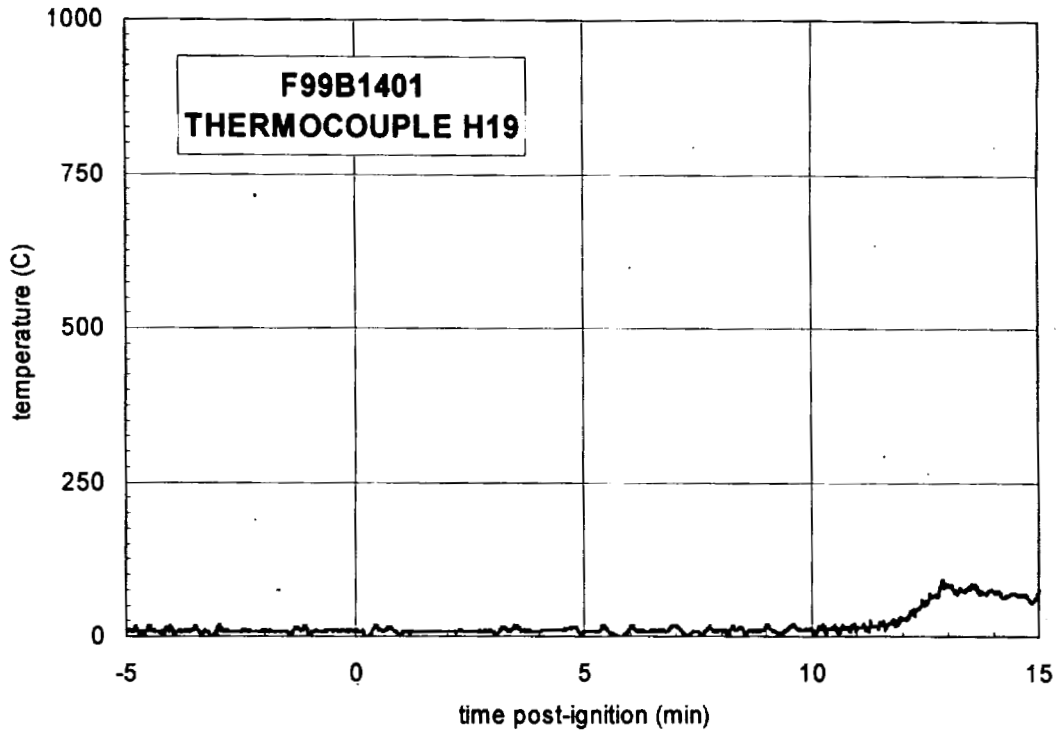


Plot H71. Fire Test F99B1401. Data plot from thermocouple H19.

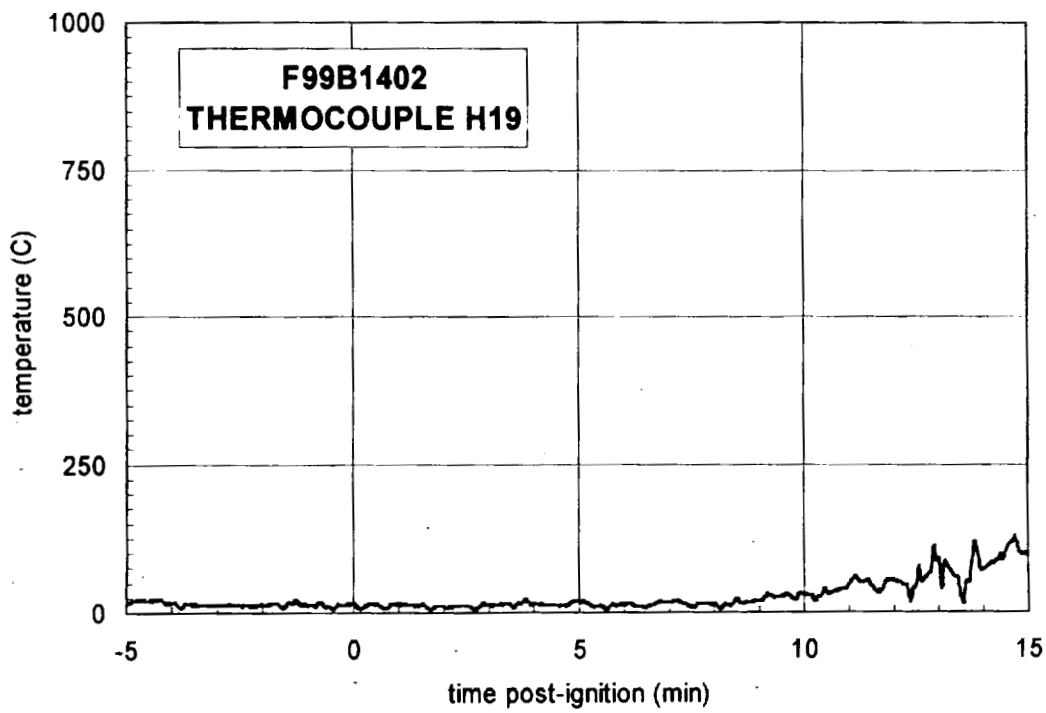


Plot H72. Fire Test F99B1402. Data plot from thermocouple H19.

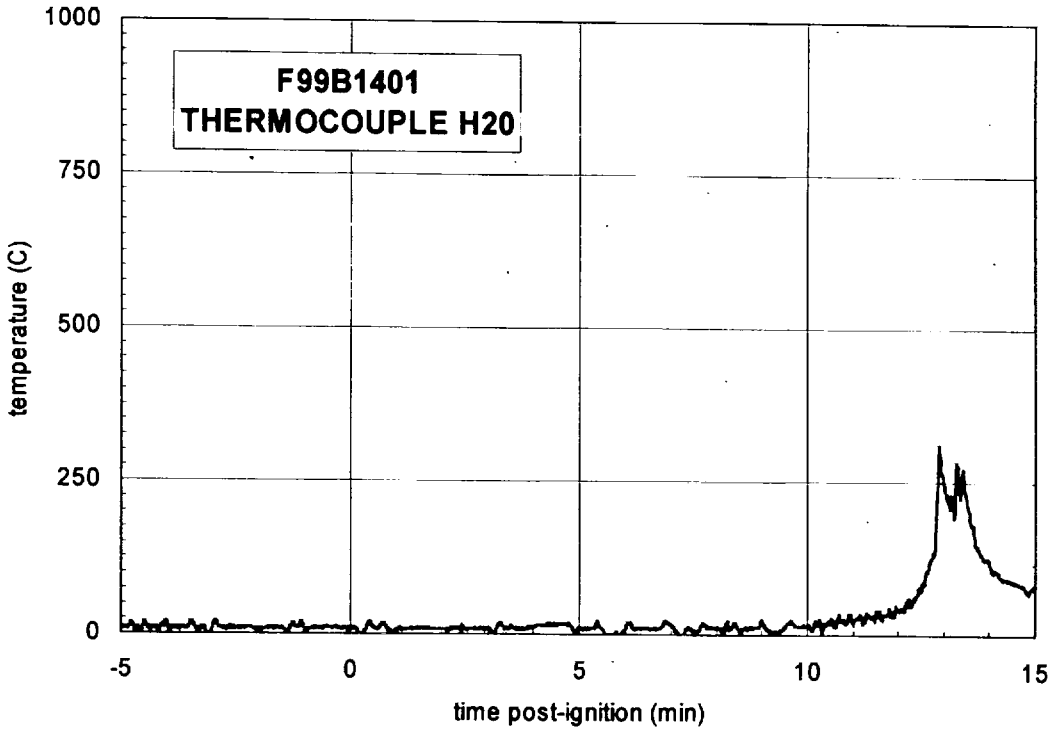


Plot H73. Fire Test F99B1401. Data plot from thermocouple H20.

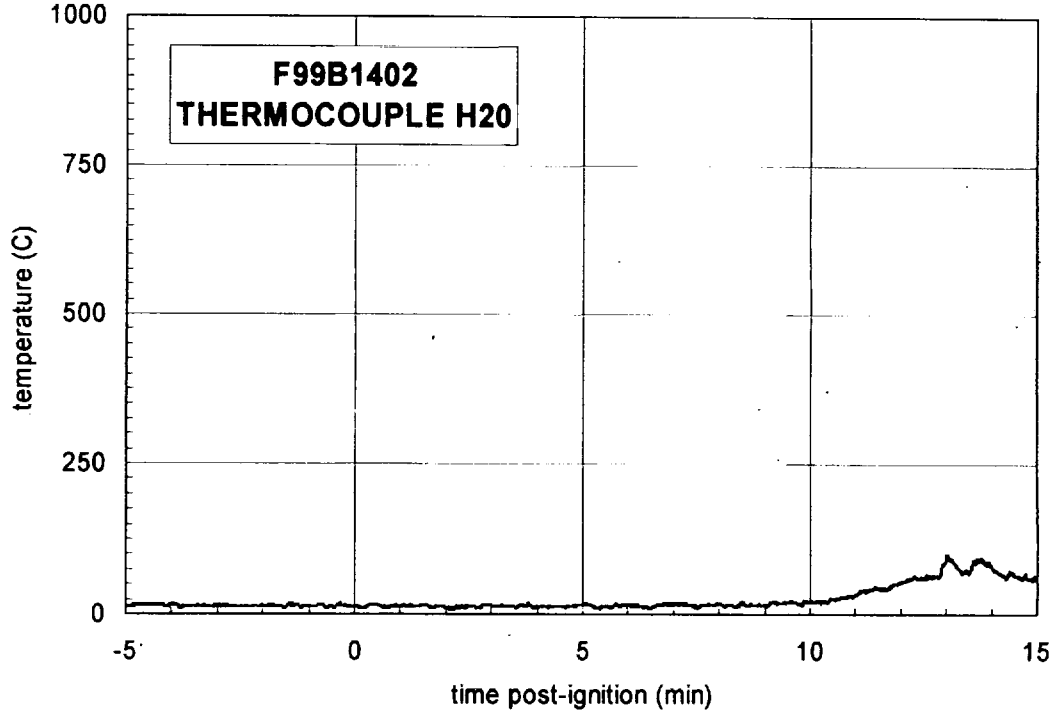


Plot H74. Fire Test F99B1402. Data plot from thermocouple H20.

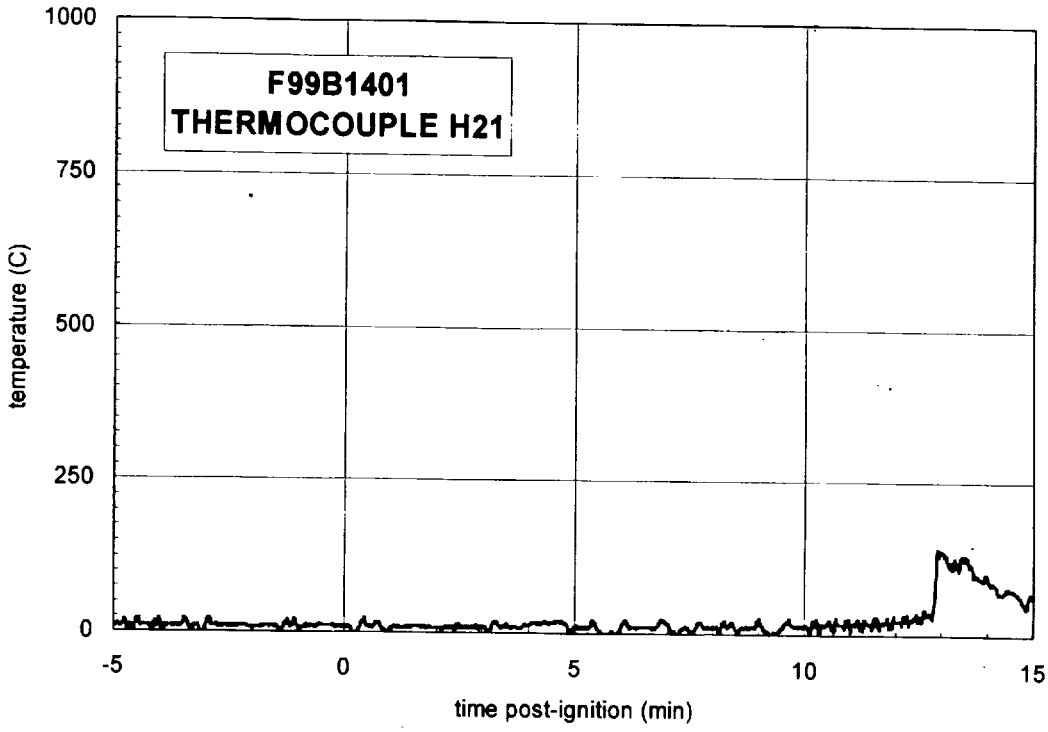


Plot H75. Fire Test F99B1401. Data plot from thermocouple H21.

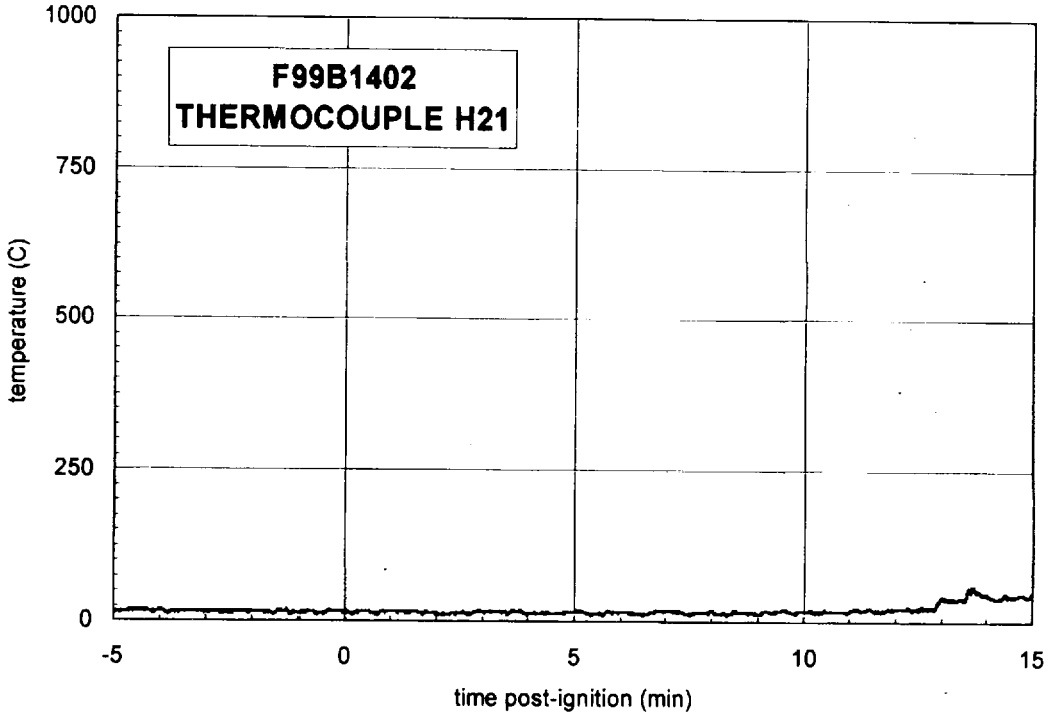


Plot H76. Fire Test F99B1402. Data plot from thermocouple H21.

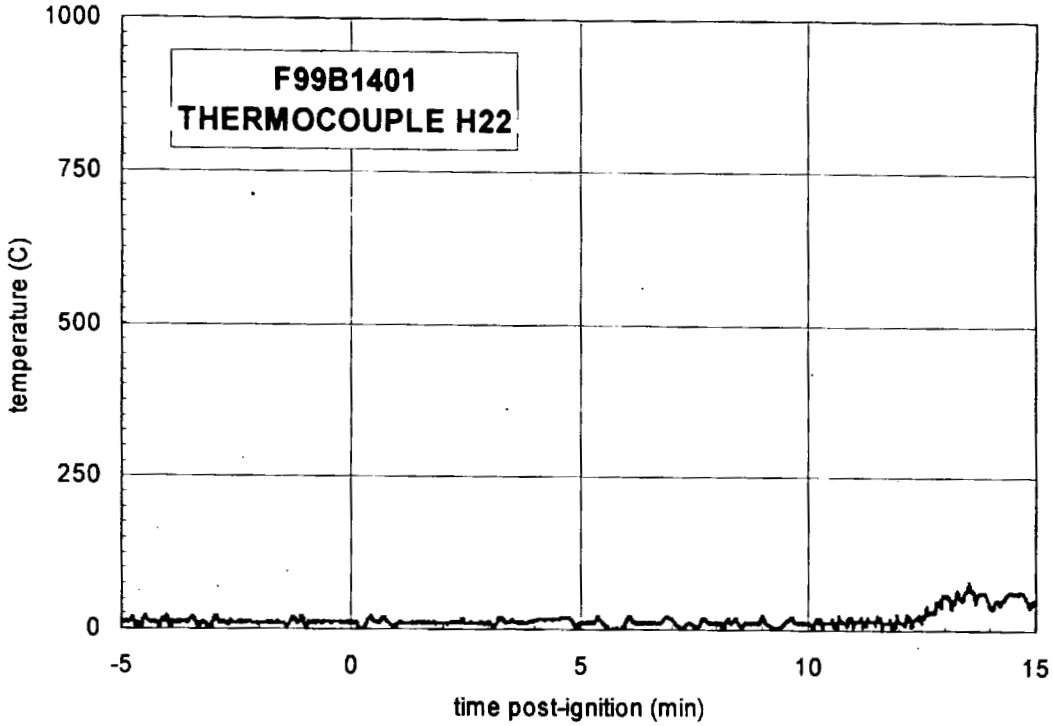


Plot H77. Fire Test F99B1401. Data plot from thermocouple H22.

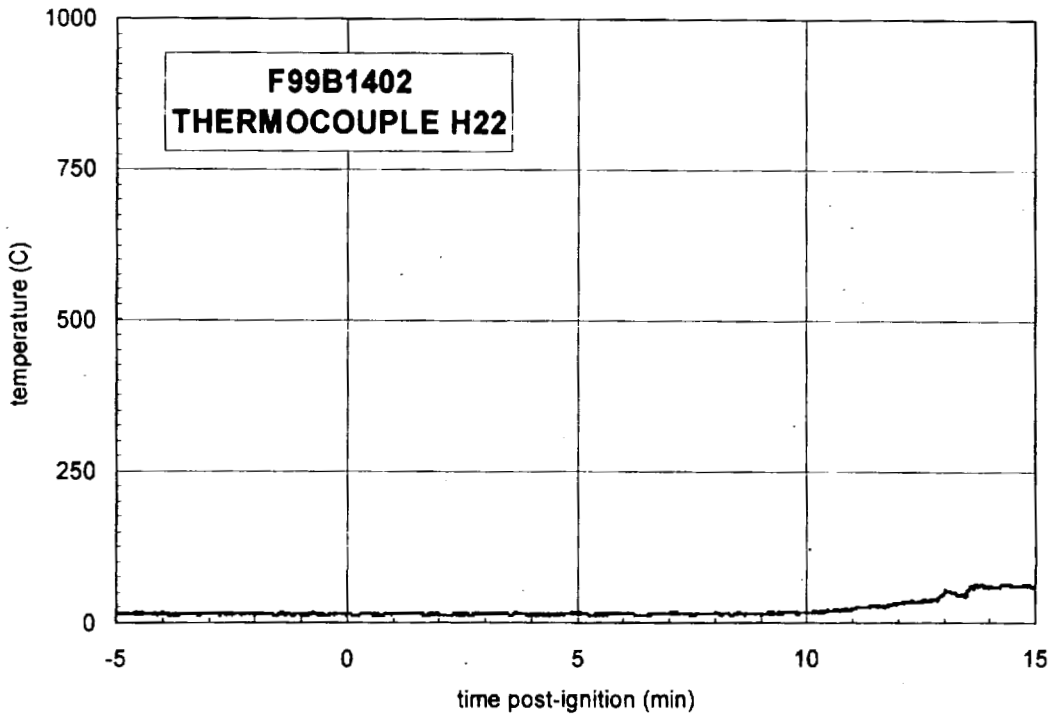


Plot H78. Fire Test F99B1402. Data plot from thermocouple H22.

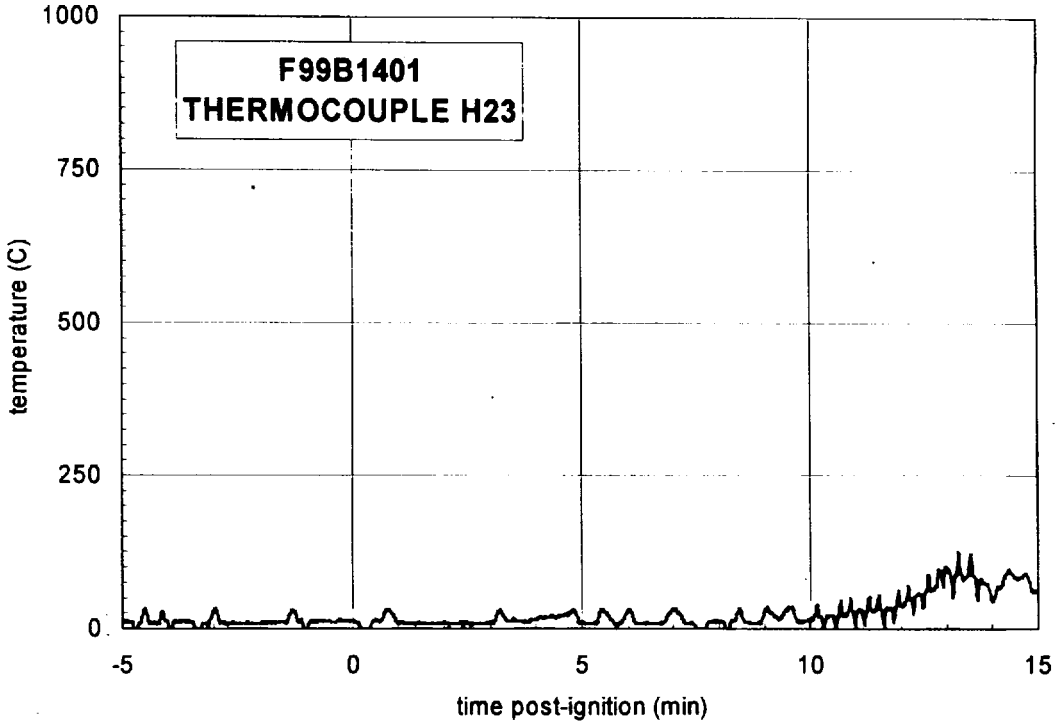


Plot H79. Fire Test F99B1401. Data plot from thermocouple H23.

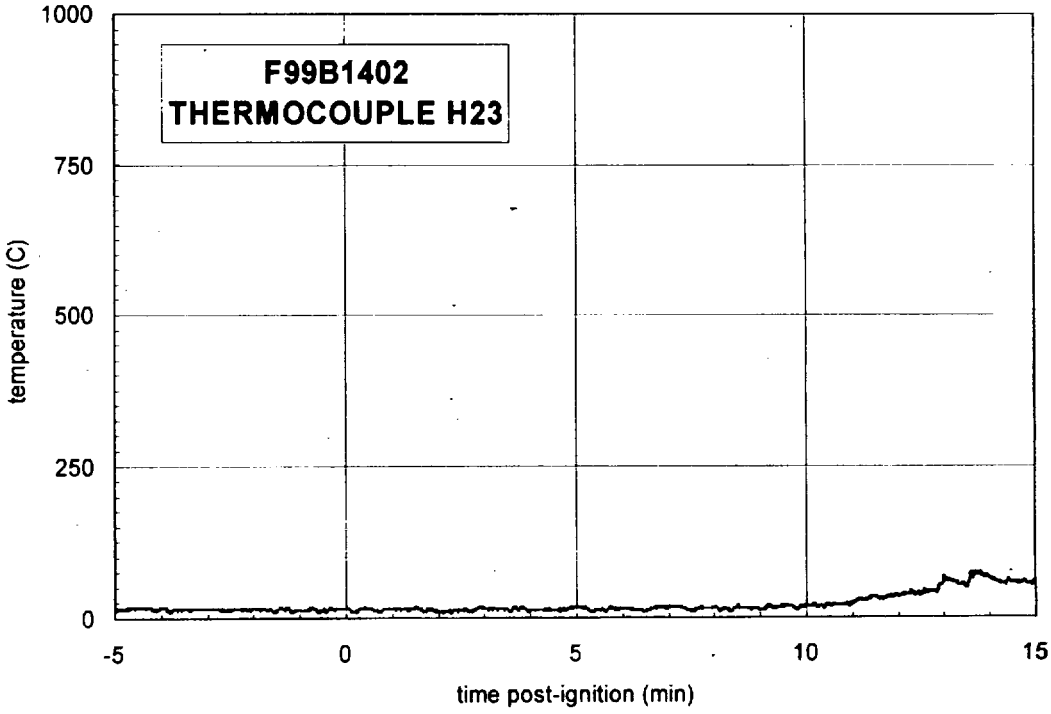


Plot H80. Fire Test F99B1402. Data plot from thermocouple H23.

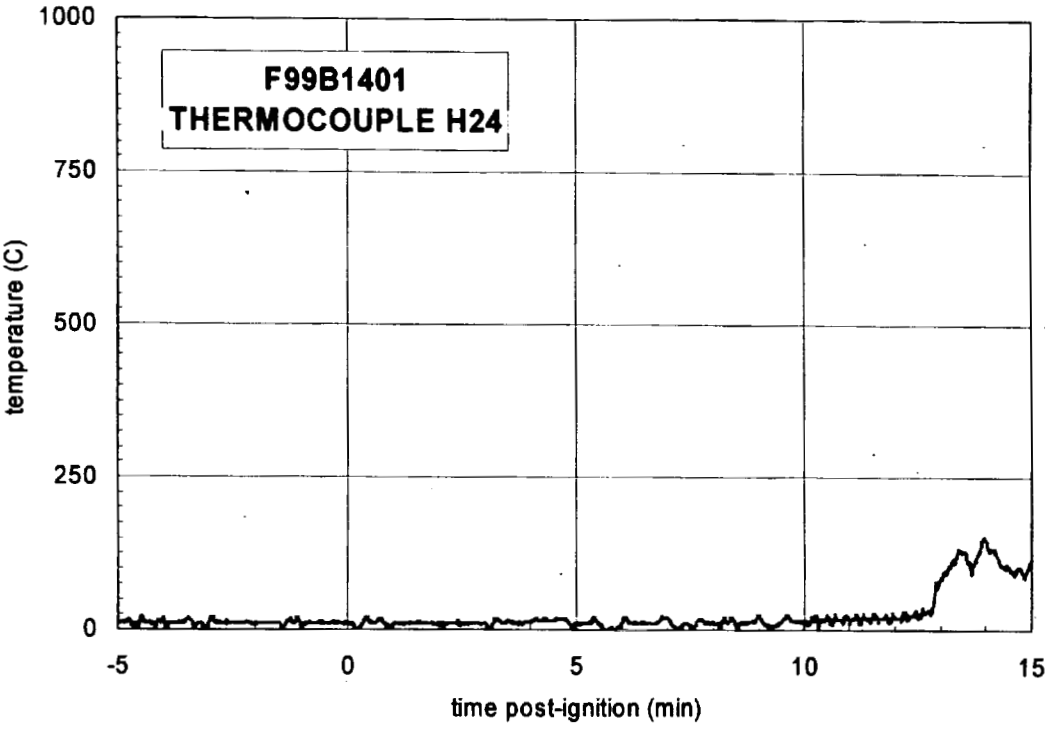


Plot H81. Fire Test F99B1401. Data plot from thermocouple H24.

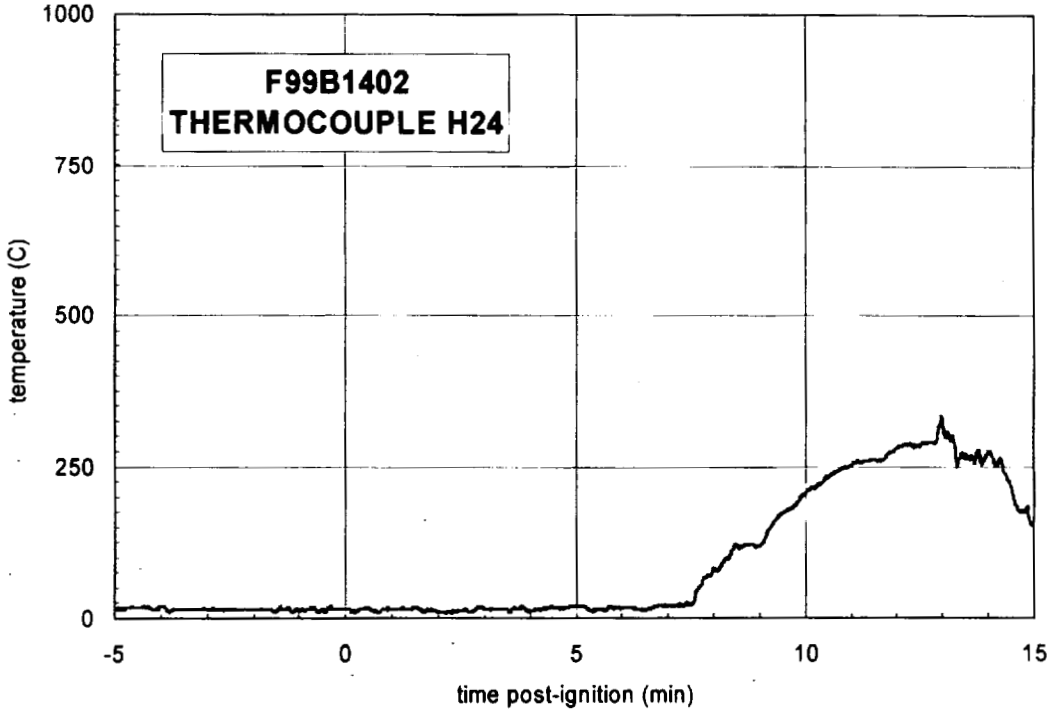


Plot H82. Fire Test F99B1402. Data plot from thermocouple H24.

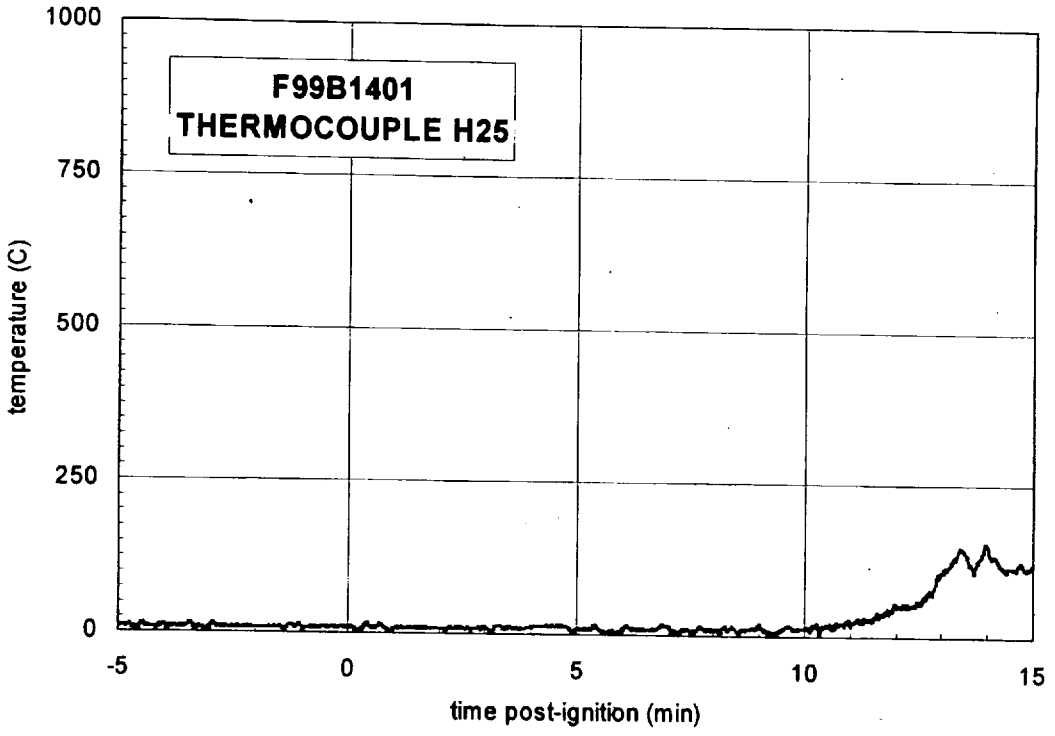


Plot H83. Fire Test F99B1401. Data plot from thermocouple H25.

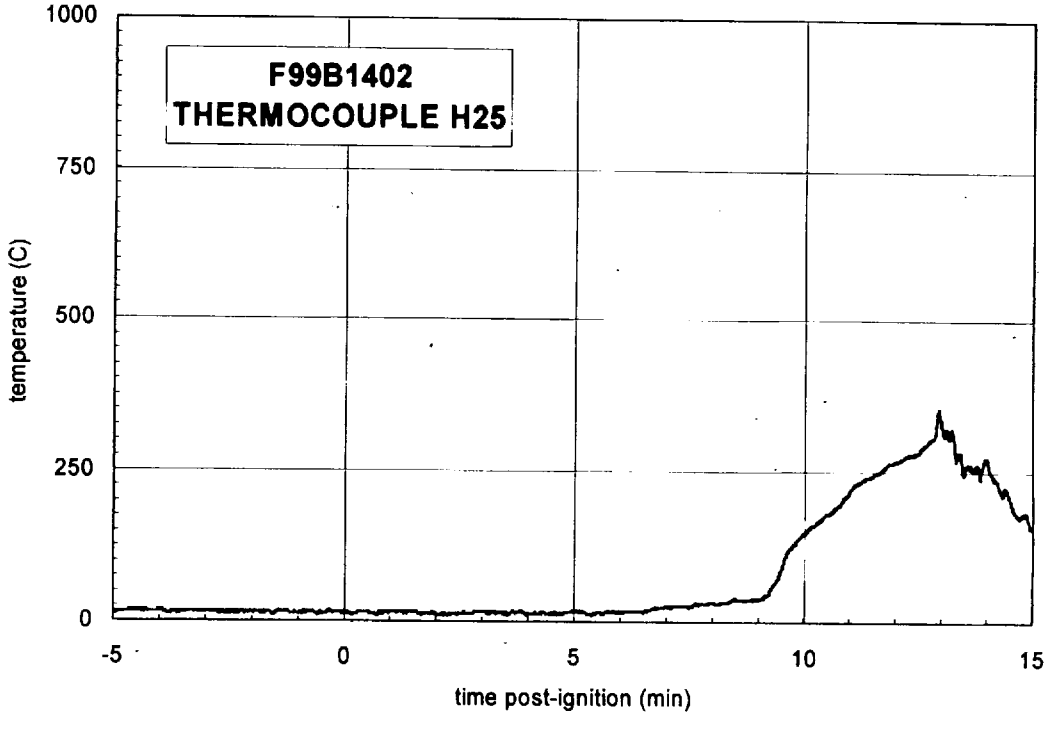


Plot H84. Fire Test F99B1402. Data plot from thermocouple H25.

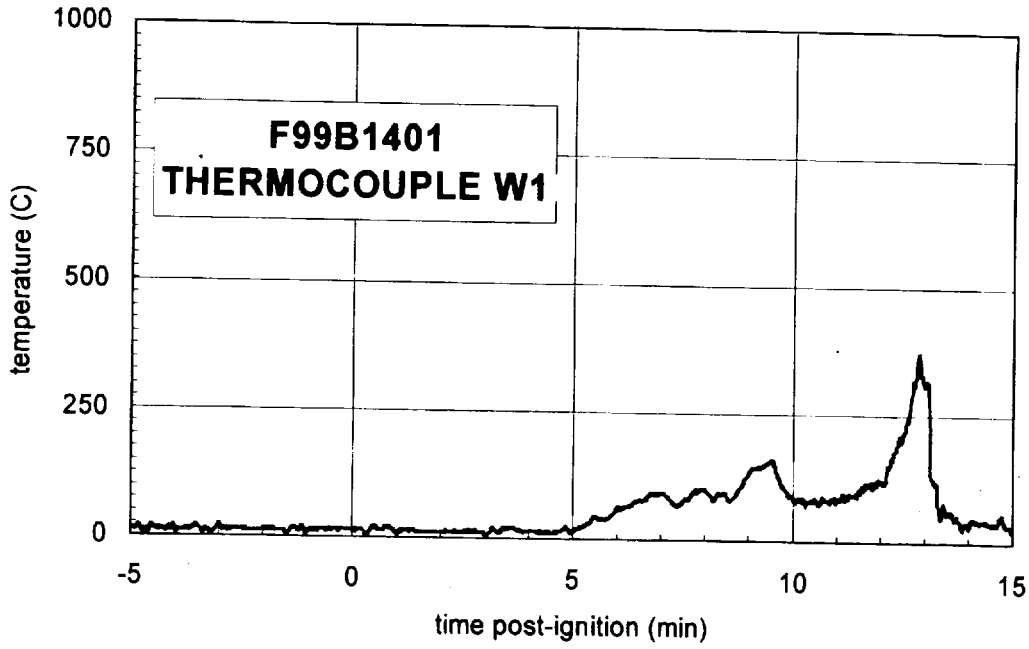


Plot H85. Fire Test F99B1401. Data plot from thermocouple W1.

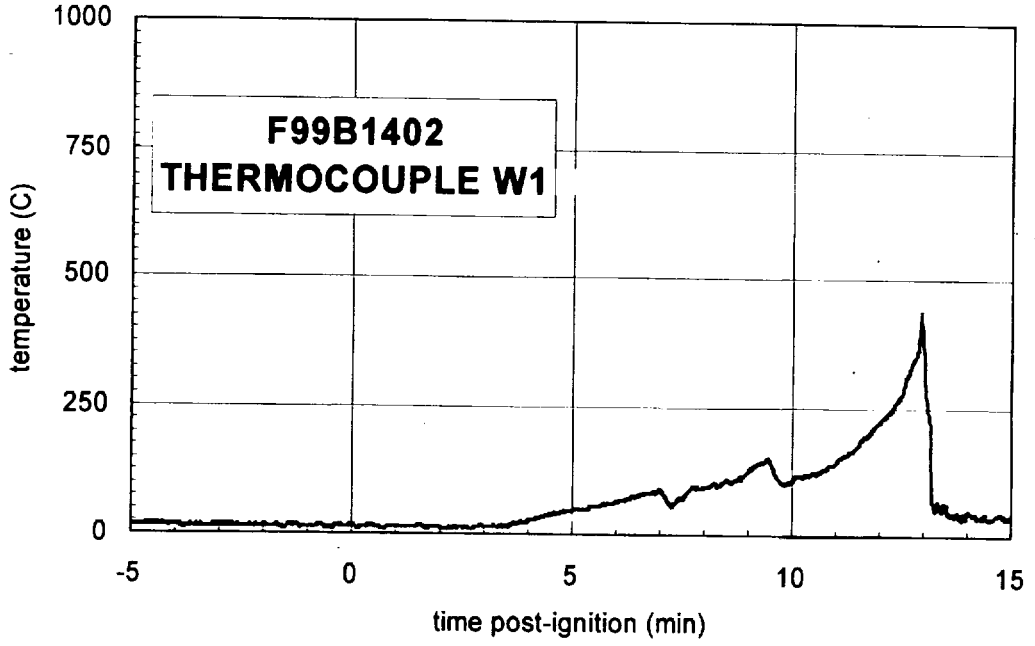


Plot H86. Fire Test F99B1402. Data plot from thermocouple W1.

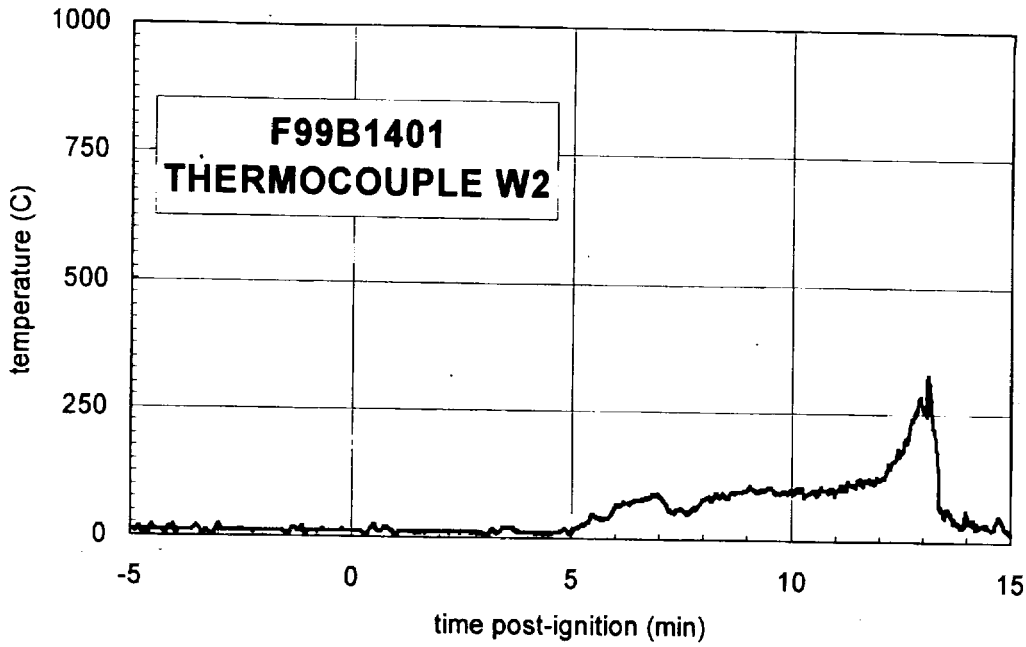


Plot H87. Fire Test F99B1401. Data plot from thermocouple W2.

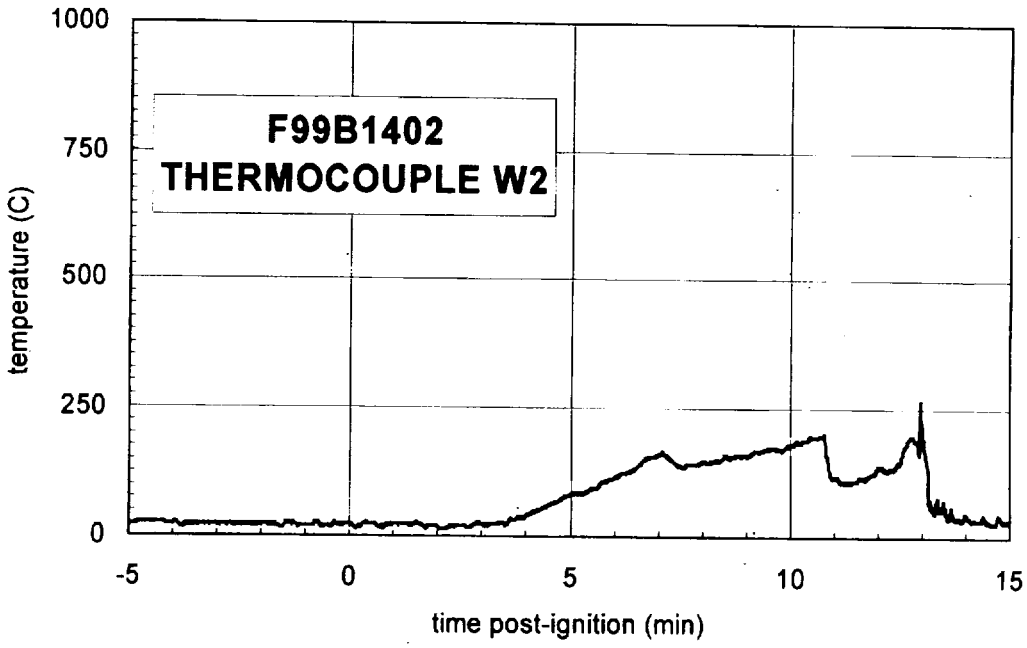


Plot H88. Fire Test F99B1402. Data plot from thermocouple W2.

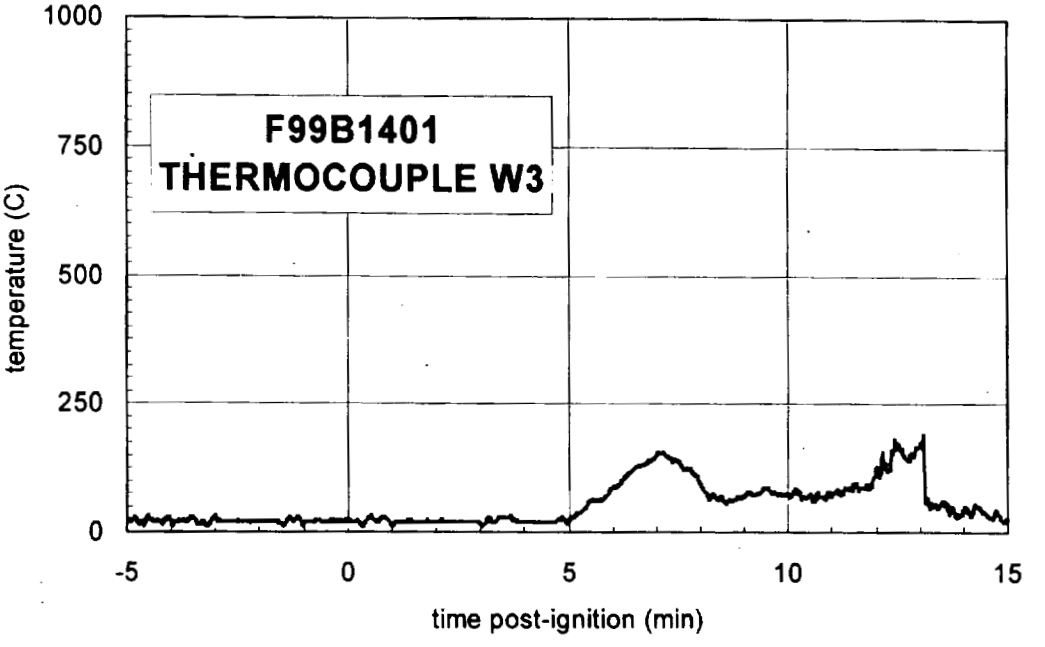


Plot H89. Fire Test F99B1401. Data plot from thermocouple W3.

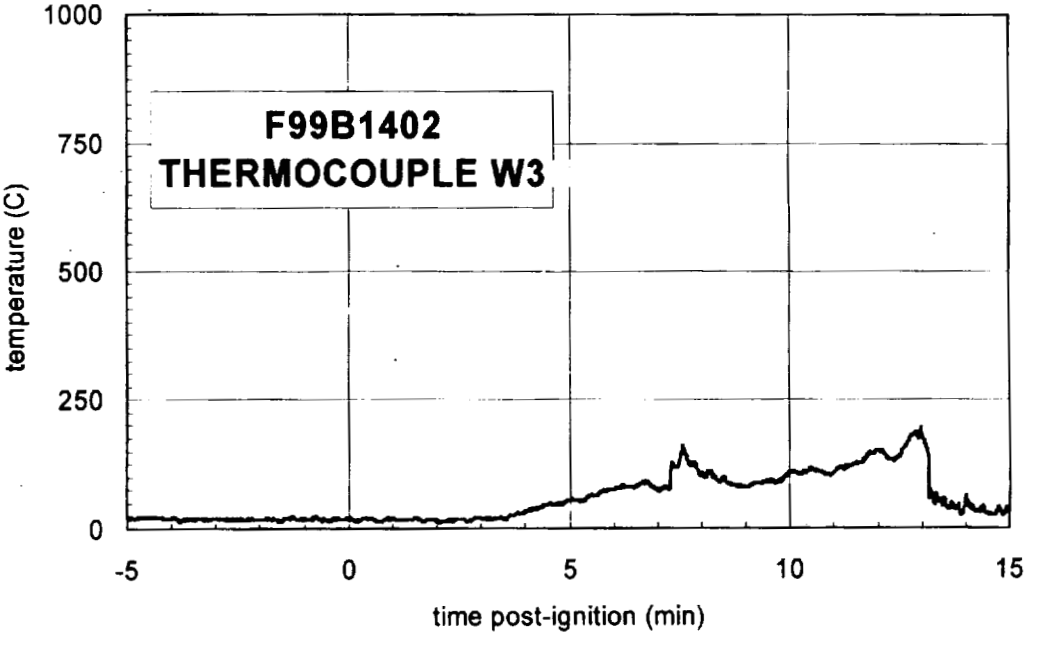


Plot H90. Fire Test F99B1402. Data plot from thermocouple W3.

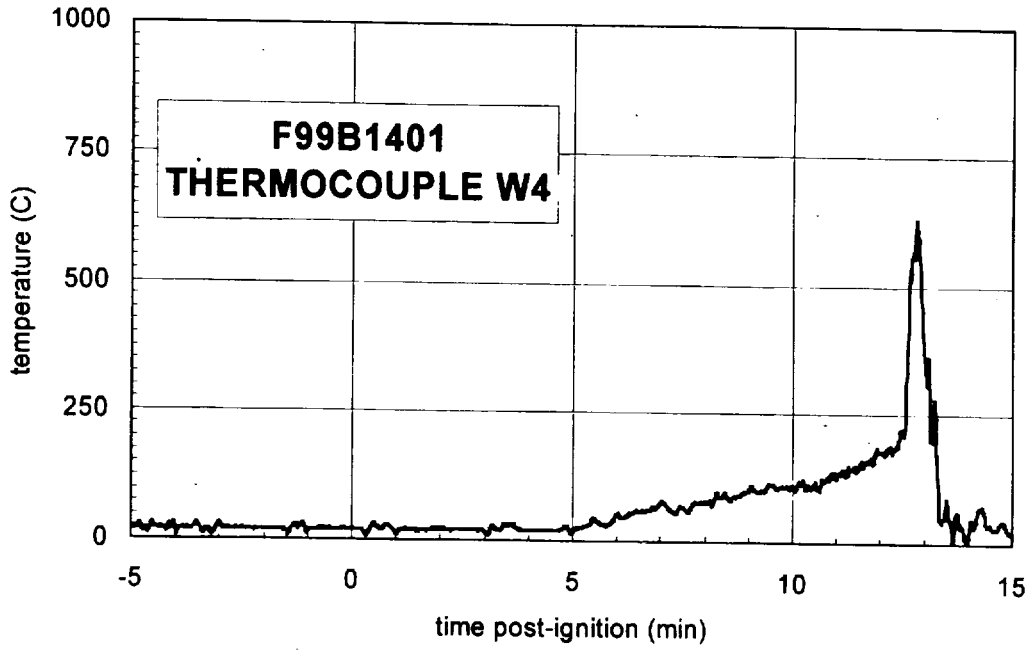


Plot H91. Fire Test F99B1401. Data plot from thermocouple W4.

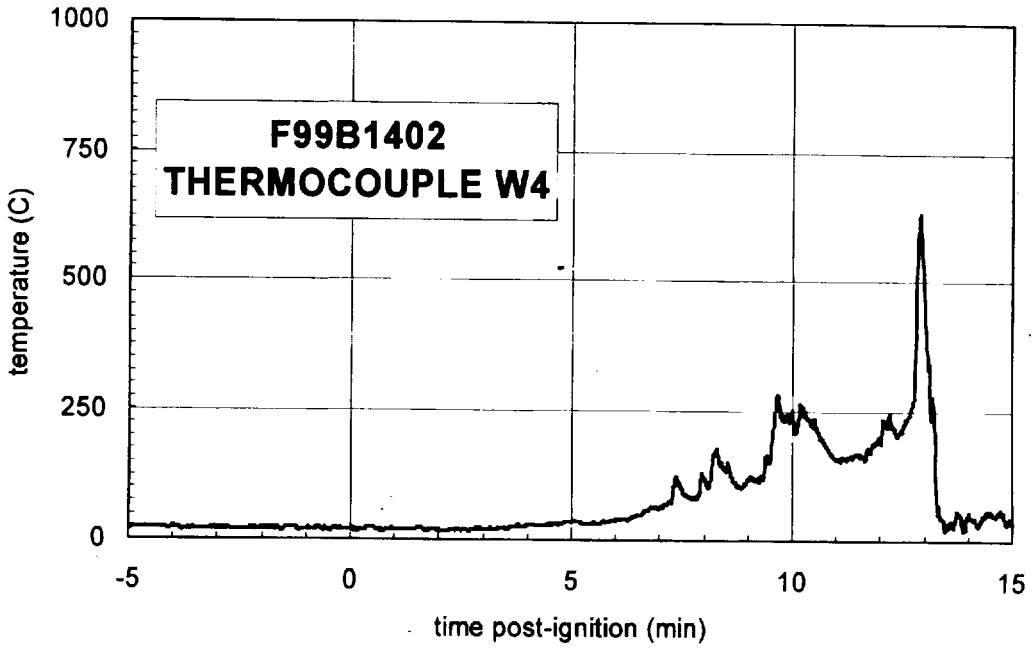


Plot 92. Fire Test F99B1402. Data plot from thermocouple W4.

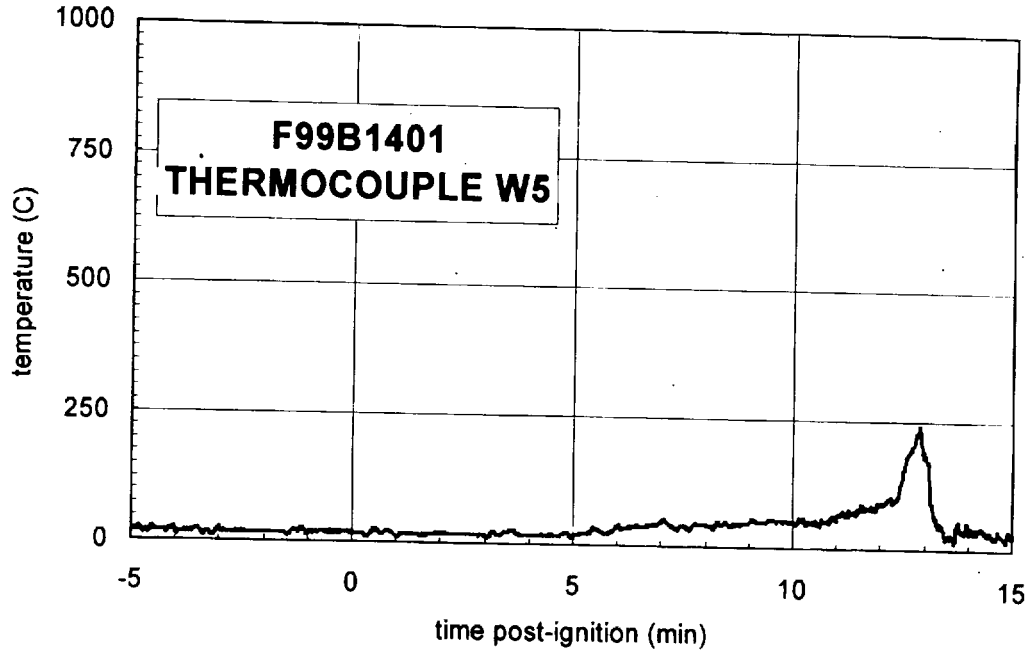


Plot H93. Fire Test F99B1401. Data plot from thermocouple W5.

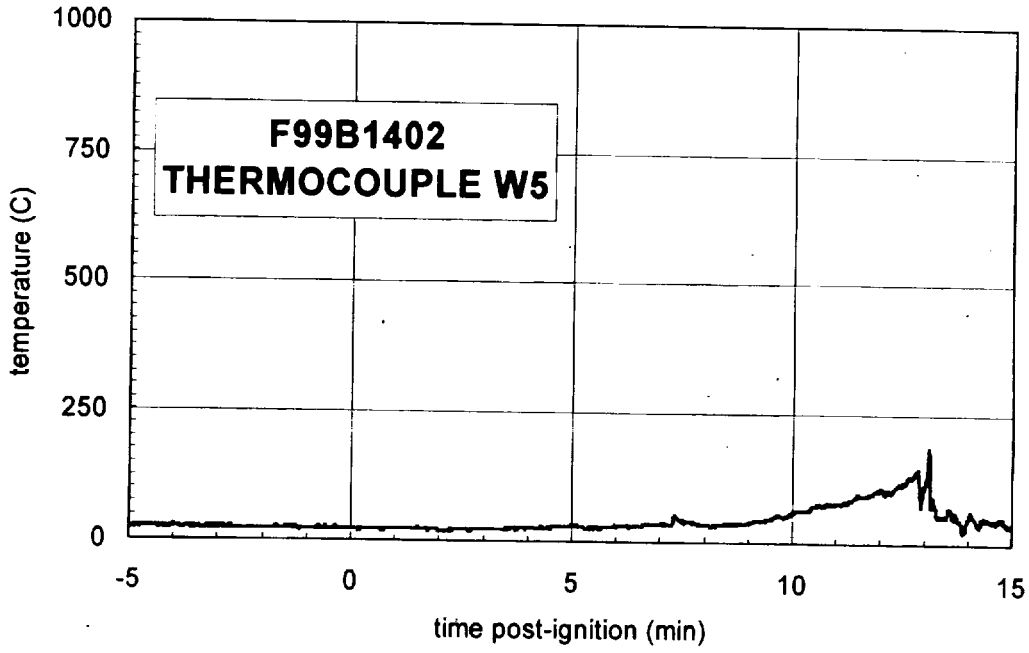


Plot H94. Fire Test F99B1402. Data plot from thermocouple W5.

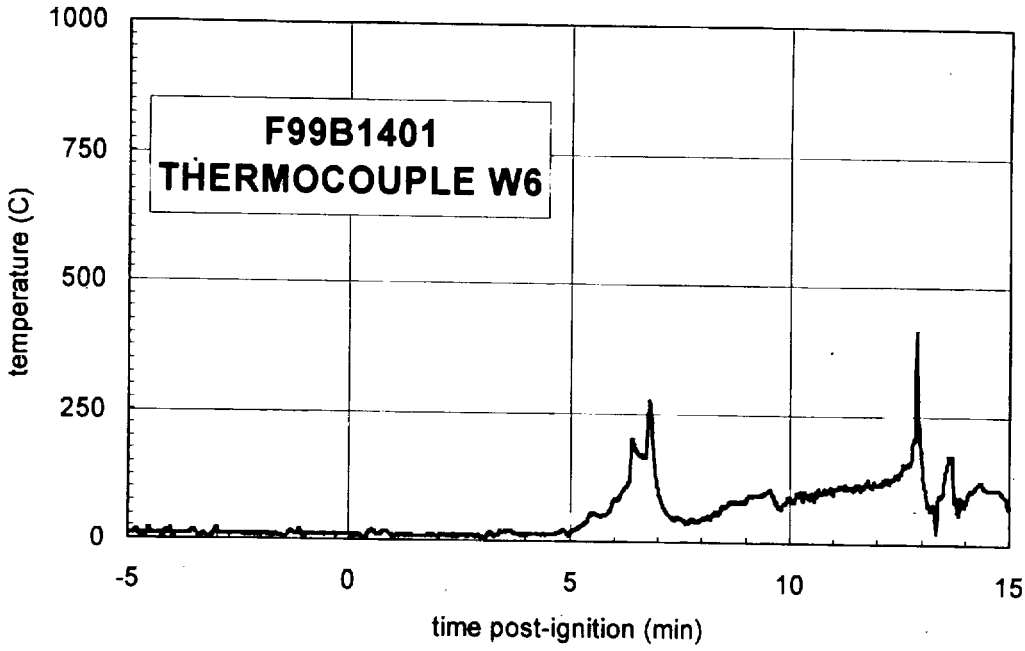


Plot H95. Fire Test F99B1401. Data plot from thermocouple W6.

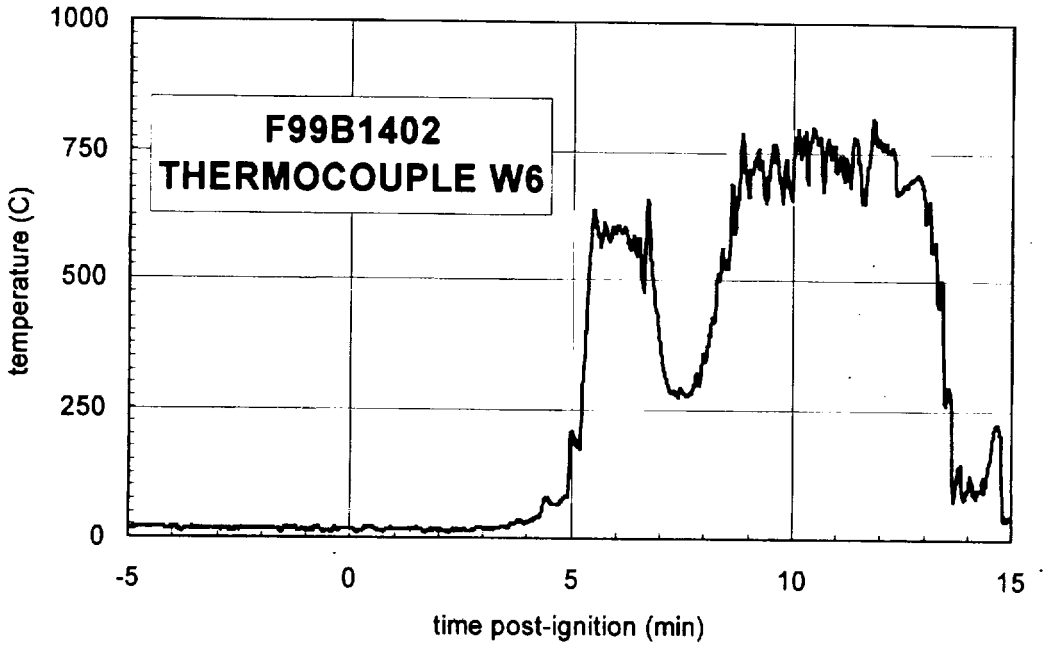


Plot H96. Fire Test F99B1402. Data plot from thermocouple W6.

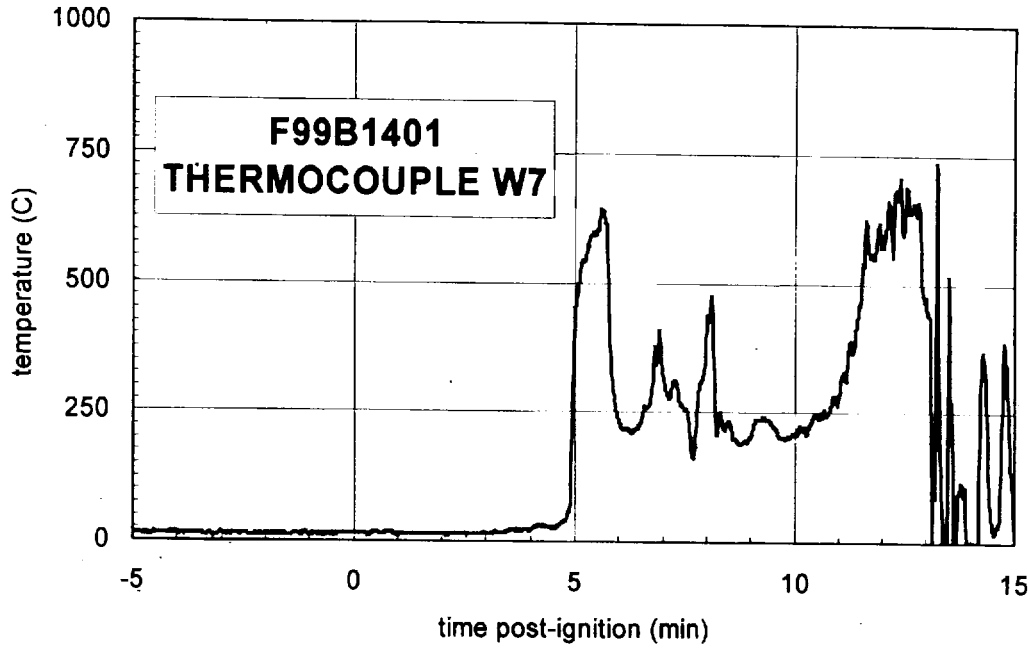


Plot H97. Fire Test F99B1401. Data plot from thermocouple W7.

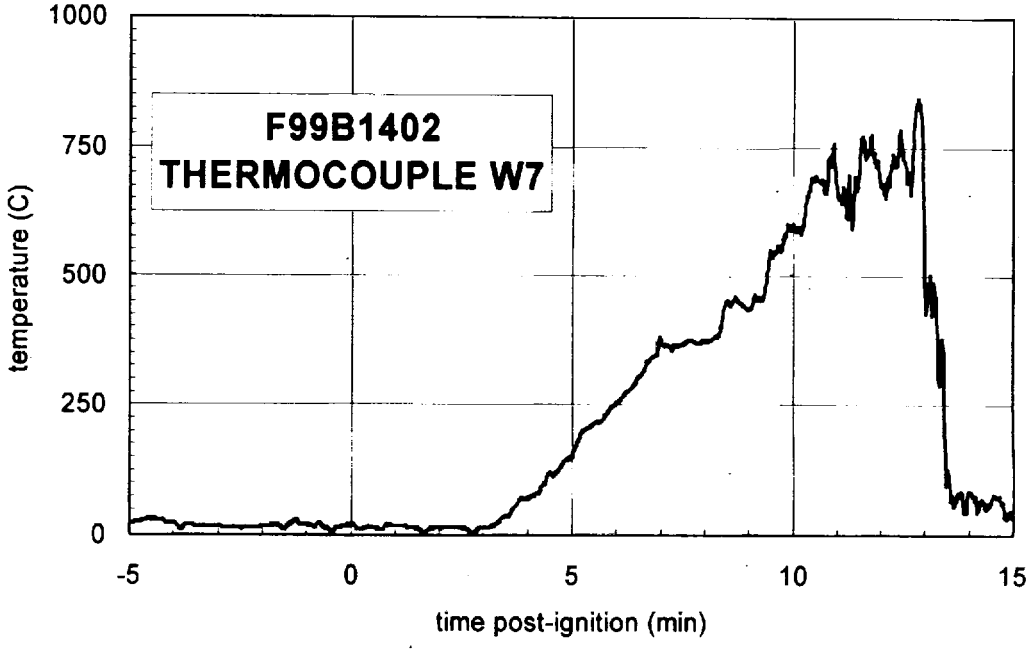


Plot H98. Fire Test F99B1402. Data plot from thermocouple W7.

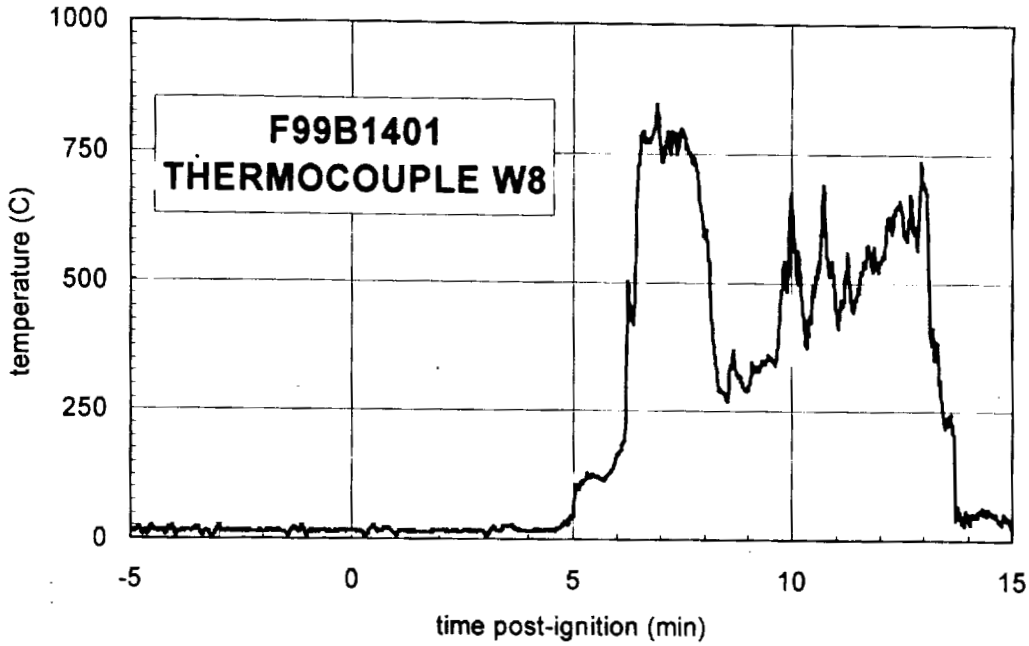


Plot H99. Fire Test F99B1401. Data plot from thermocouple W8.

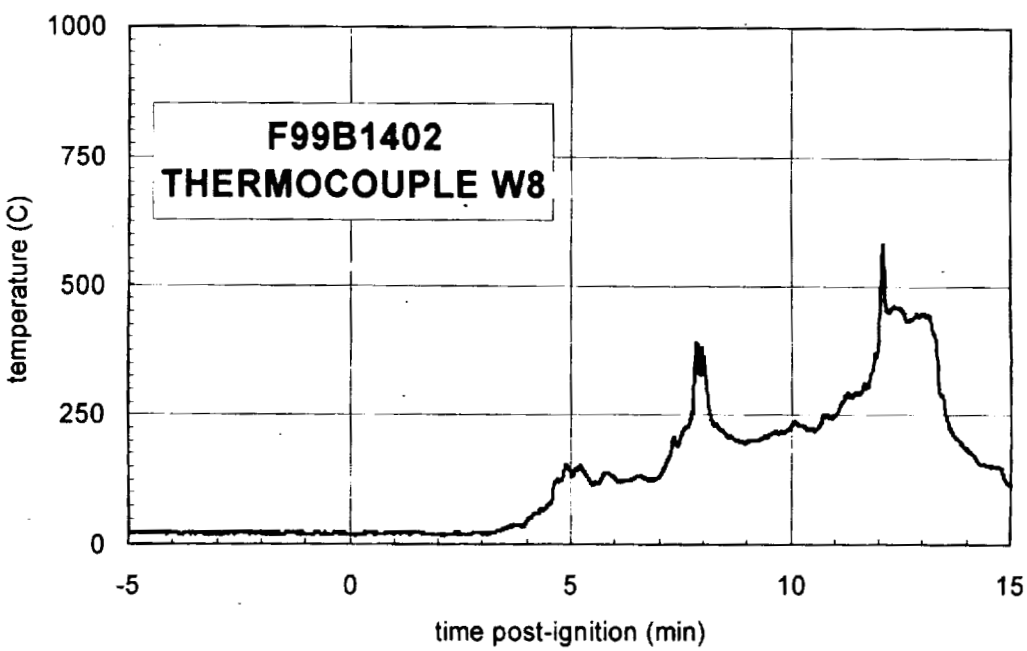


Plot H100. Fire Test F99B1402. Data plot from thermocouple W8.

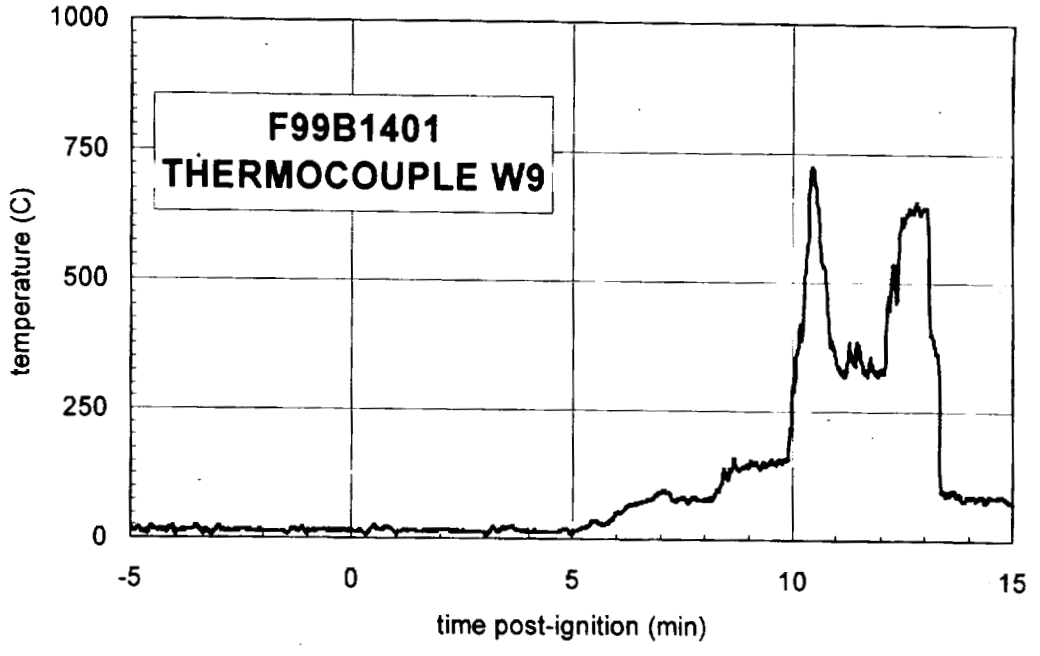


Plot H101. Fire Test F99B1401. Data plot from thermocouple W9.

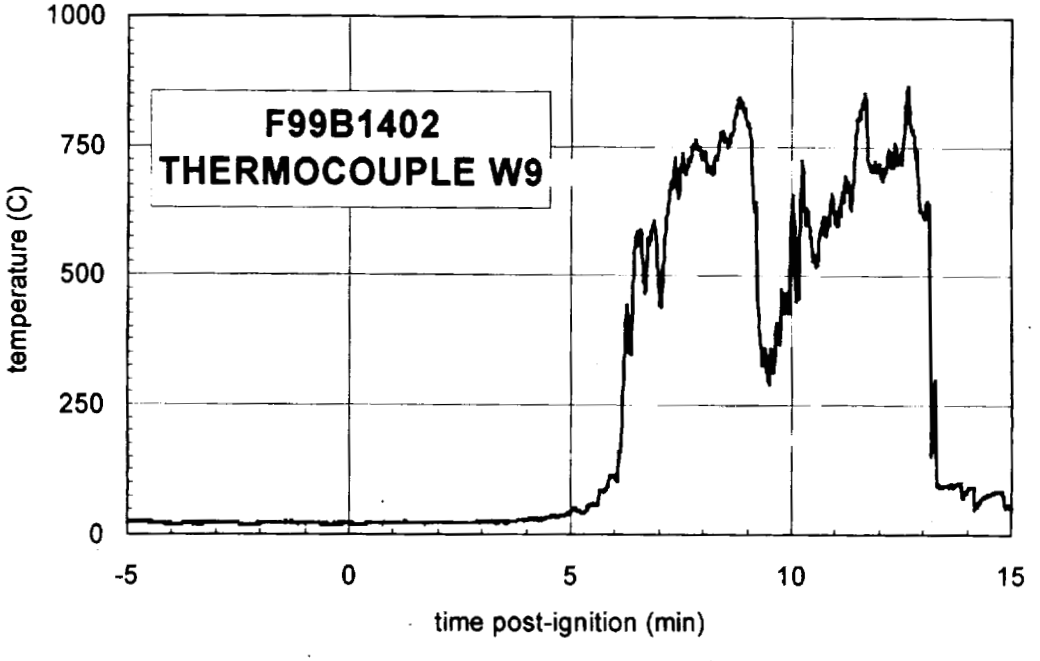


Plot H102. Fire Test F99B1402. Data plot from thermocouple W9.

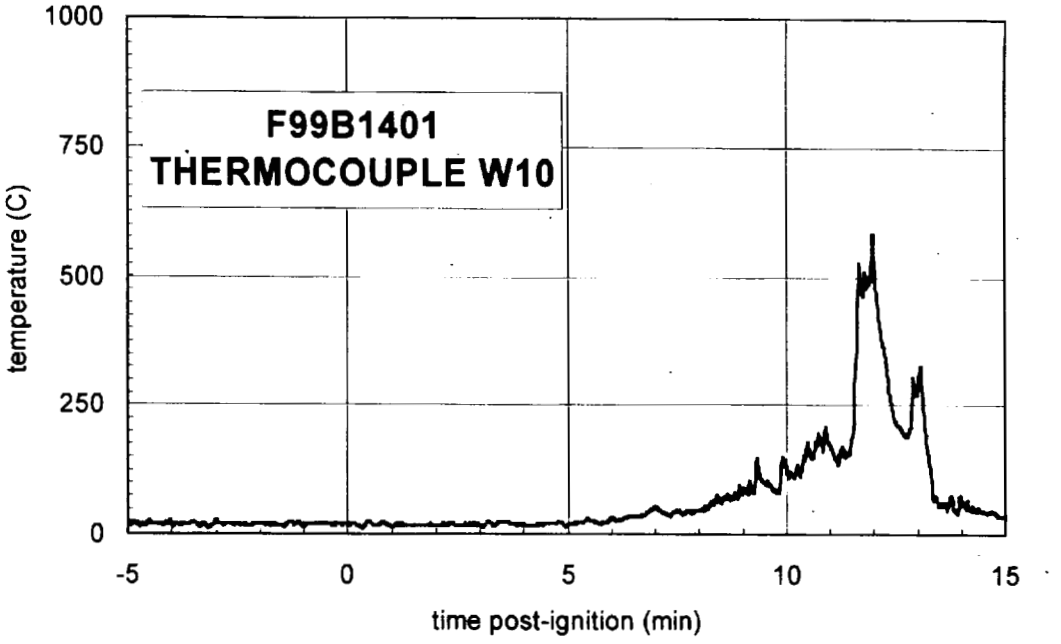


Plot H103. Fire Test F99B1401. Data plot from thermocouple W10.

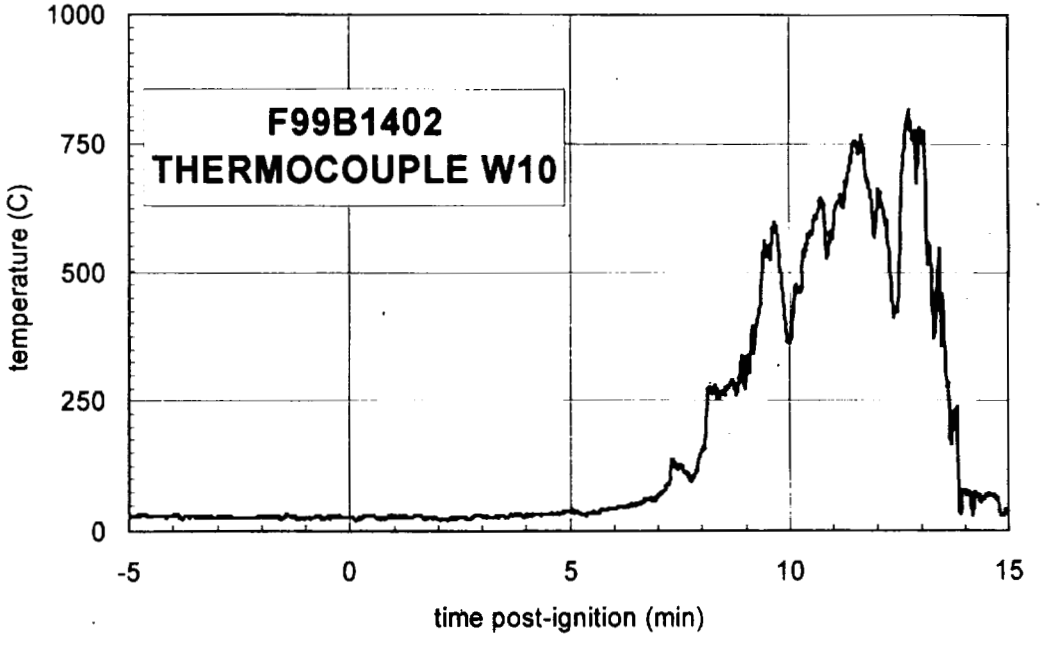


Plot H104. Fire Test F99B1402. Data plot from thermocouple W10.

# Appendix I

## Fire Tests F99B1401 and F99B1402
## Aspirated Thermocouple Data

One aspirated thermocouple assembly (Medtherm Corporation) was installed in each of the test vehicles (Fig. I1). The aspirated thermocouple assembly was fabricated from Inconel 600 tubing. Each assembly consisted of a vertical manifold (o.d. = 0.375 in. (9.5 mm), i.d. = 0.25 in. (6.4 mm), length = 16 in. (406 mm)) with six horizontal radiation shields (o.d. = 0.25 in. (6.4 mm), i.d. = 0.19 in. (4.8 mm), length = 1.00 in. (25.4 mm)). The vertical spacing between the radiation shields along the manifold was 3 in. (75 mm). Three radial holes were drilled near the tip of each radiation shield. The holes were sized to approximately balance the airflow-rates over each thermocouple. A Type-N thermocouple inserted into each radiation shield so that the thermocouple junction was positioned approximately 0.2 in. (5.1 mm) down-stream from the inlet holes.

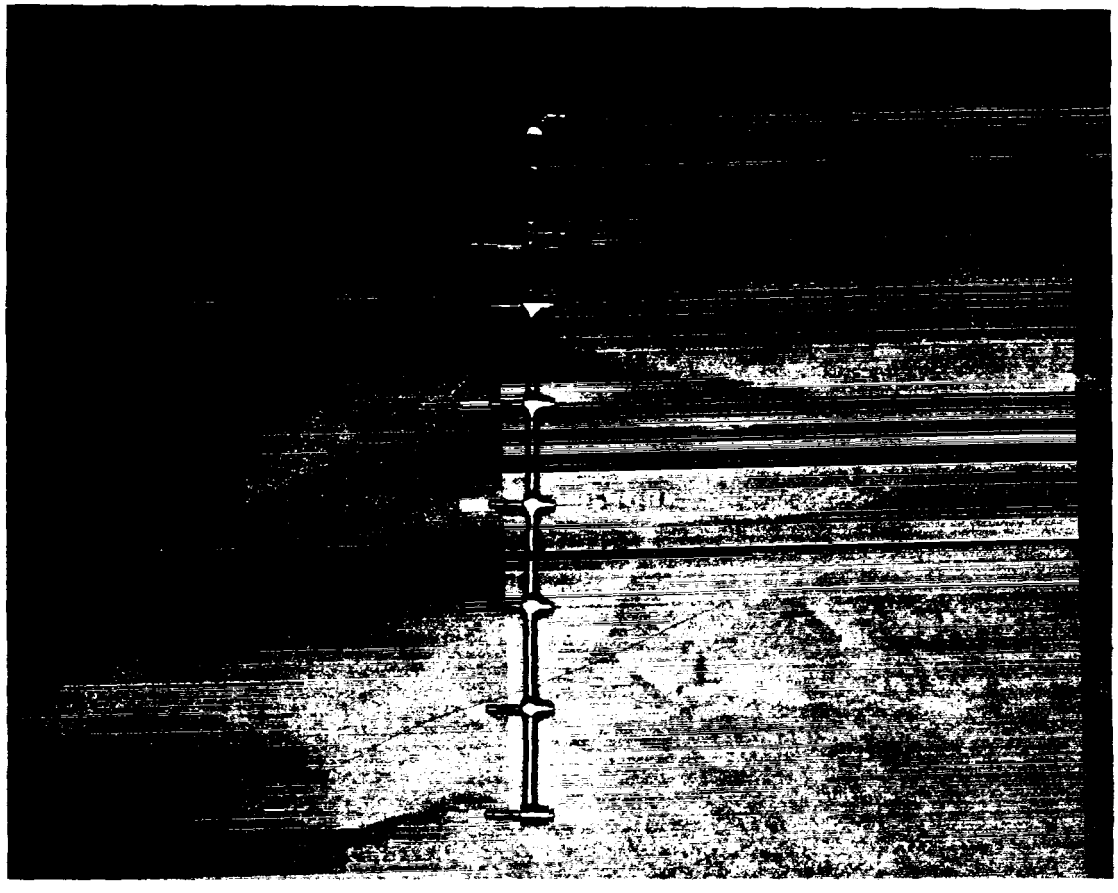

Figure I1. Fire Tests F99B1401 and F99B1402. Photograph of the aspirated thermocouple assembly used in the passenger compartment of the test vehicle.

The mounting flange of the aspirated thermocouple probe assembly was attached to the roof of the vehicle. The probe extended into the passenger compartment through a hole in the roof so that all 6 thermocouples were located below the headliner. The probe was vertical and located

along the longitudinal mid-line of the vehicle approximately equidistant from the A and B pillars. The upper-most aspirated thermocouple was approximately 0.5 in. (12 mm) below the lower surface of the headliner. The manifold was connected to a rotary-vane pump with flexible copper tubing (o.d. = 0.5 in. (12 mm), length = 15 ft. (4.6 m)). The capacity of the pump was 50 L/min at atmospheric pressure.

Figures I2 and I3 show the approximate location of the aspirated thermocouple probe assembly in the test vehicle for this test.

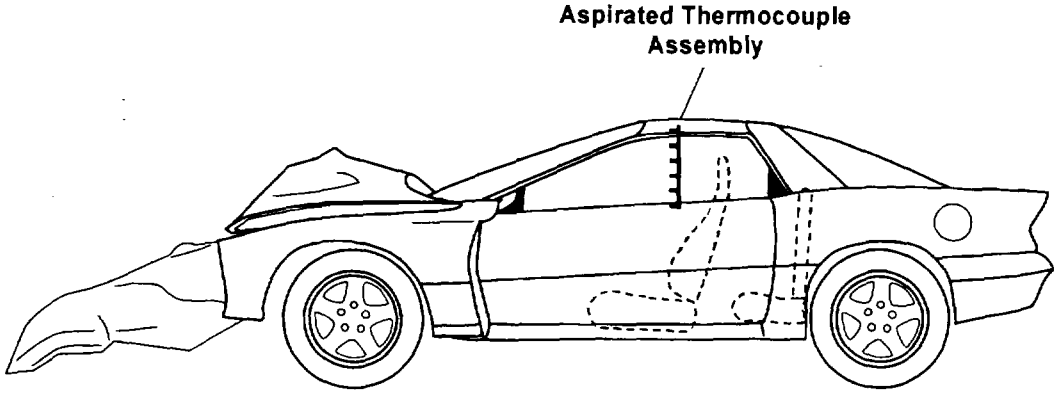


Figure I2. Fire Tests F99B1401 and F99B1402. Side view of the test vehicles showing the approximate location of the aspirated thermocouple probe assembly in the passenger compartment.

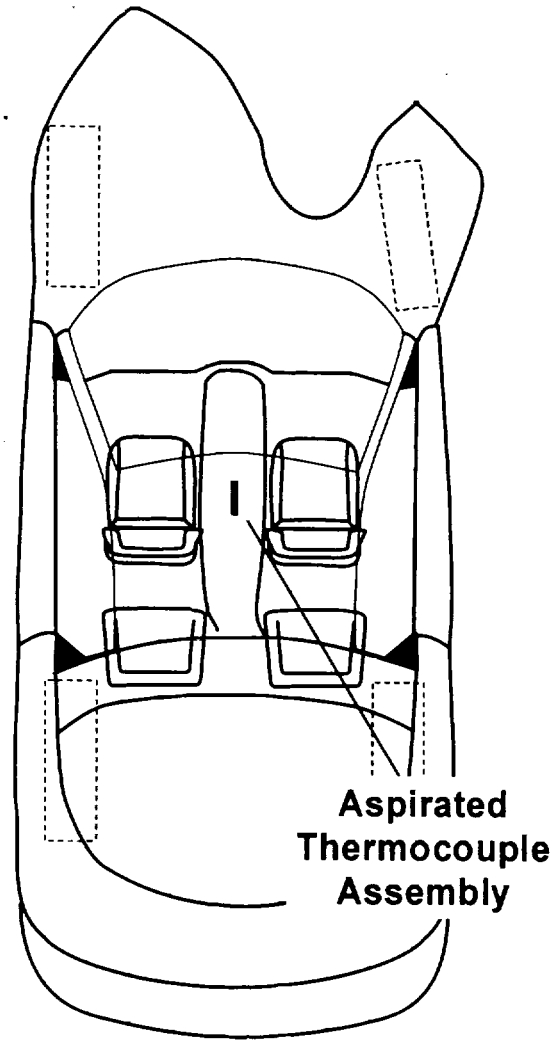


Figure I3. Fire Test F99B1401 and F99B1402. Top view of the test vehicles showing the approximate location of the aspirated thermocouple probe assembly in the passenger compartment.

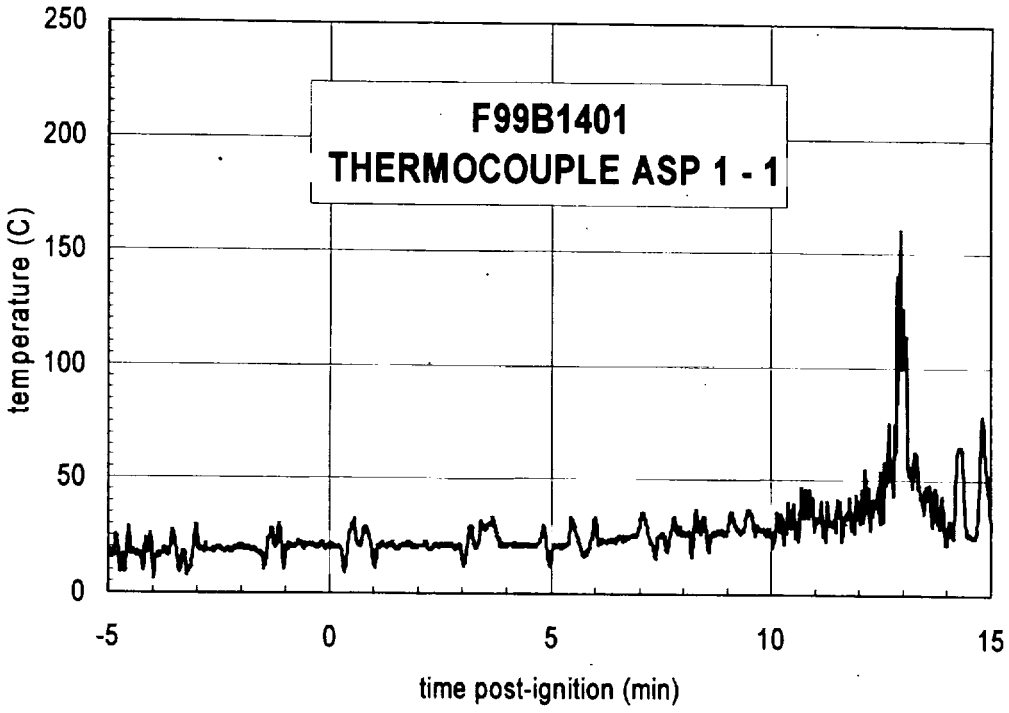


Plot I1. Fire Test F99B1401. Data plot from thermocouple ASP1-1.

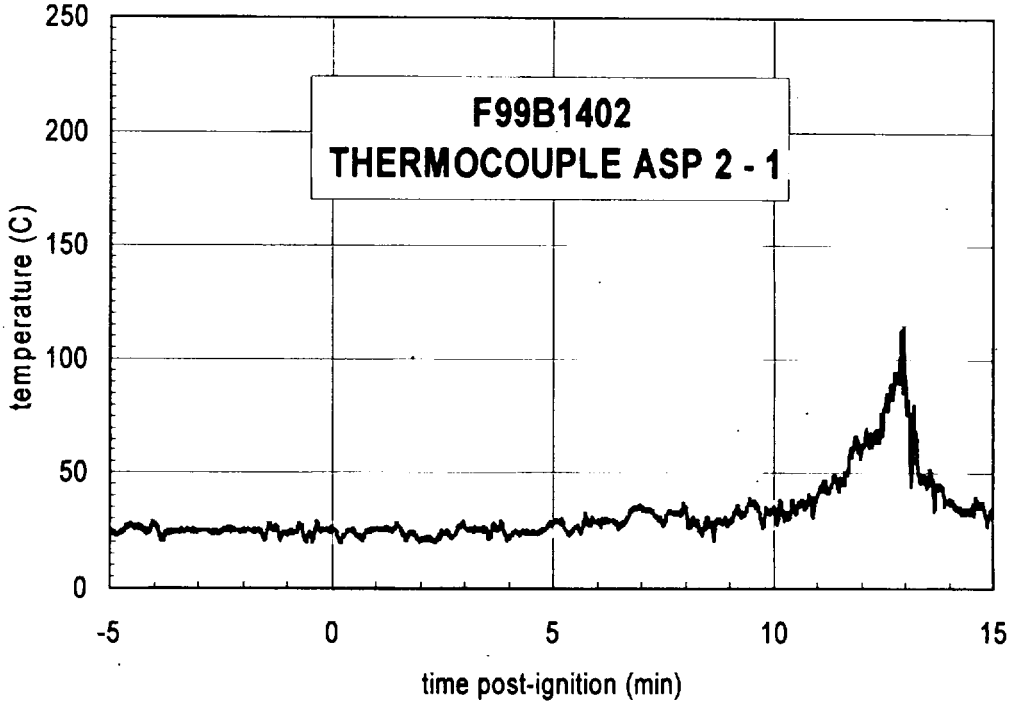


Plot I2. Fire Test F99B1402. Data plot from thermocouple ASP2 - 1.

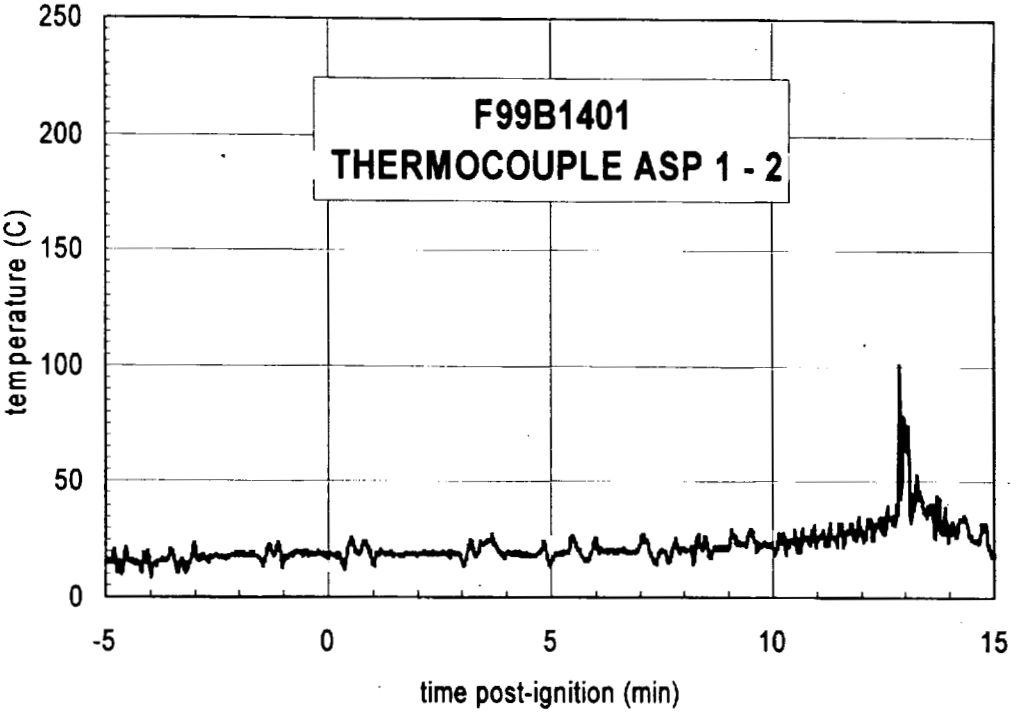


Plot I3. Fire Test F99B1401. Data plot from thermocouple ASP1 - 2.

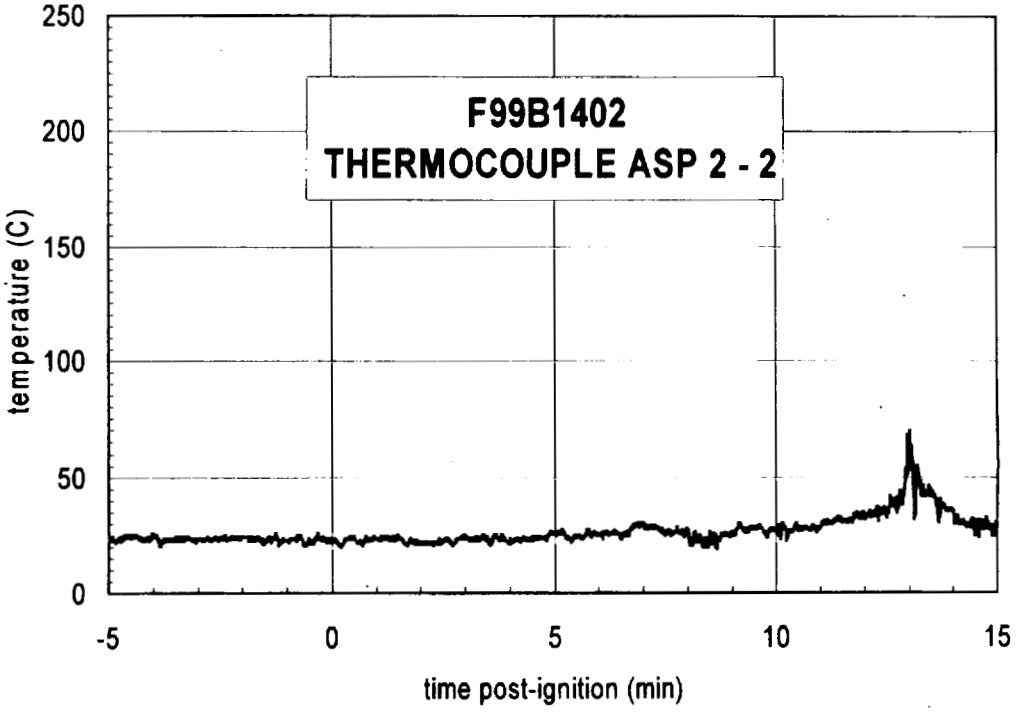


Plot I4. Fire Test F90B1402. Data plot from thermocouple ASP2 - 2.

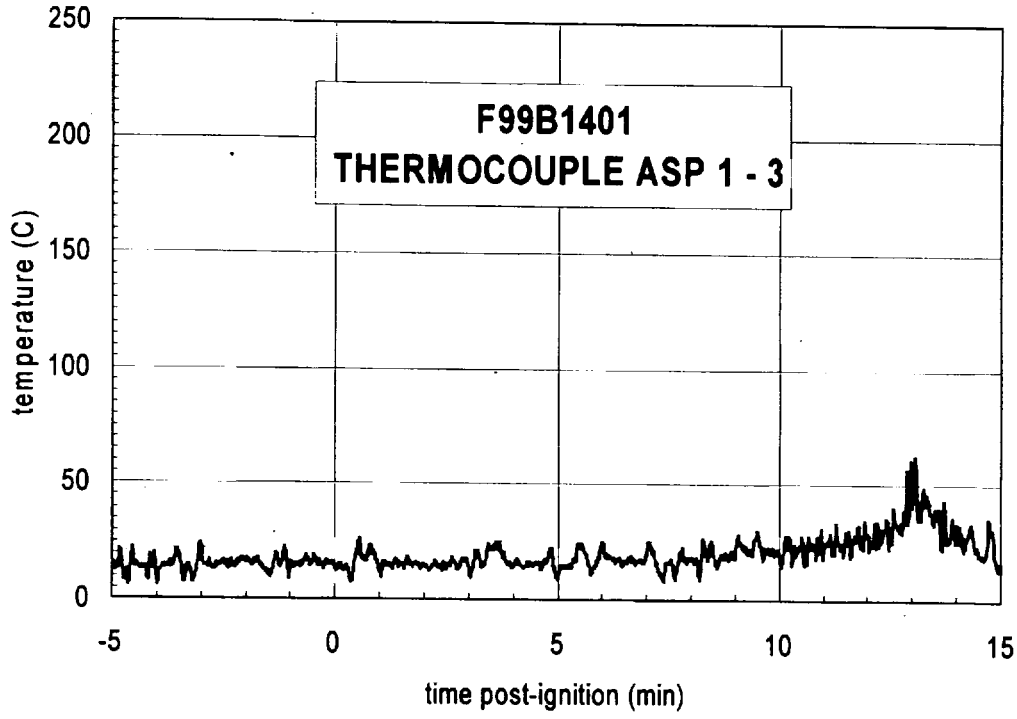


Plot I5. Fire Test F99B1401. Data plot from thermocouple ASP1 - 3.

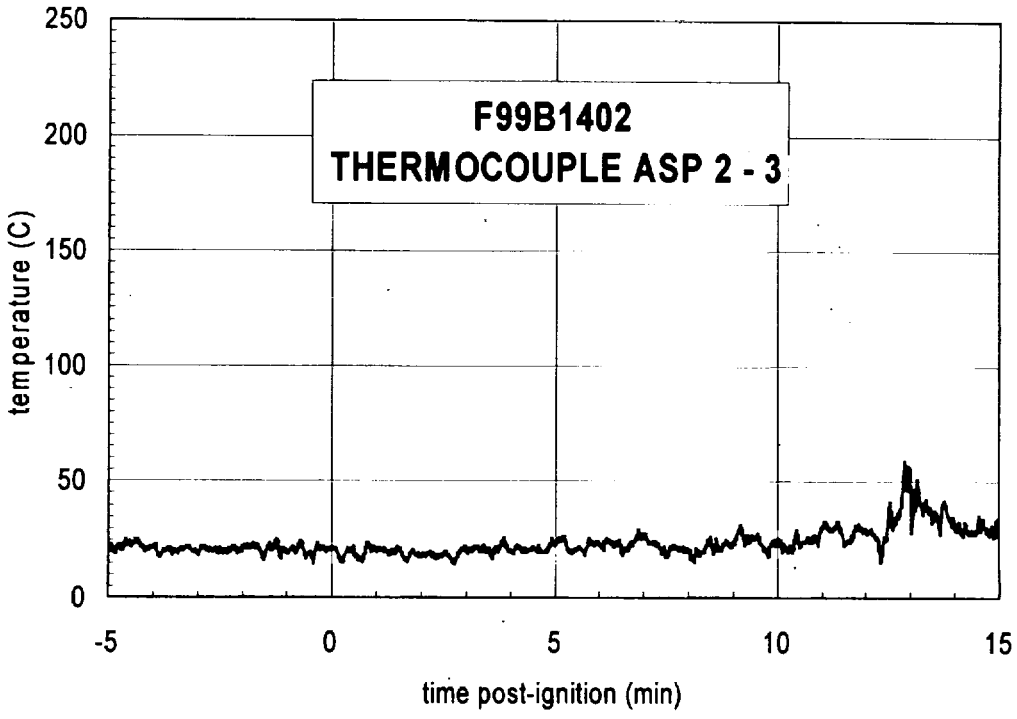


Plot I6. Fire Test F99B1402. Data plot from thermocouple ASP 2 - 3.

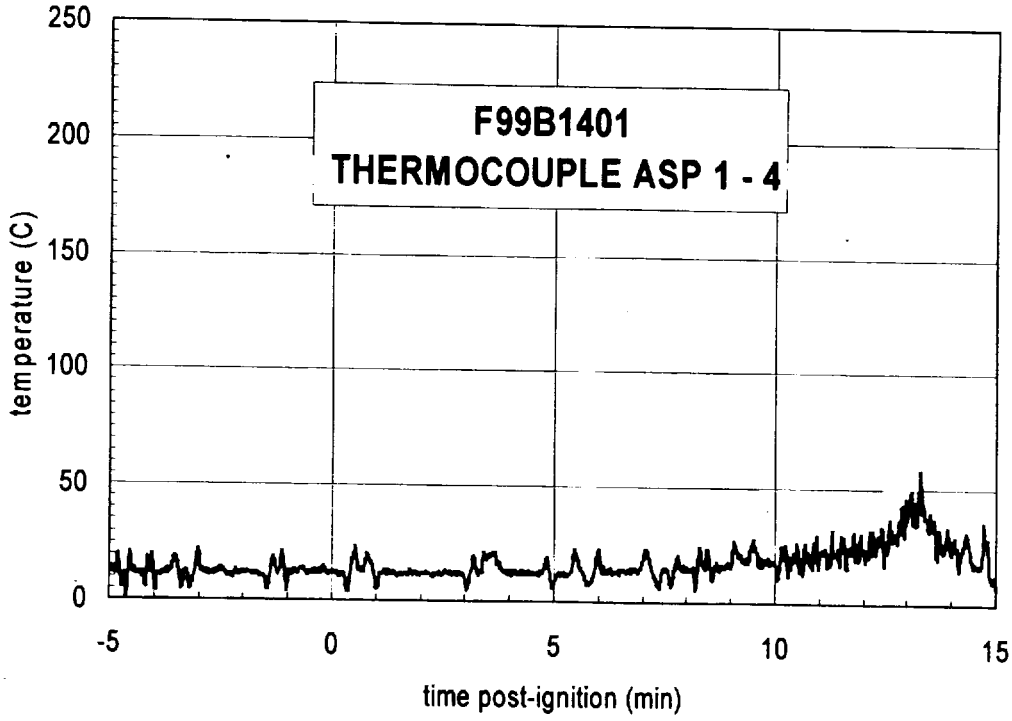


Plot I7. Fire Test F99B1401. Data plot from thermocouple ASP1 - 4.

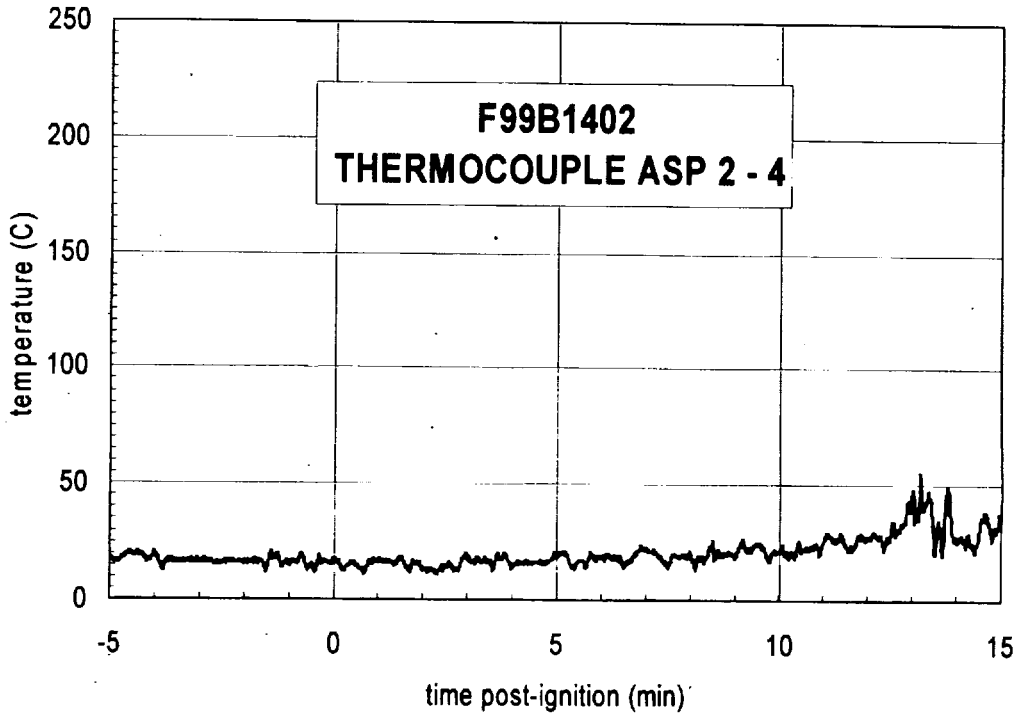


Plot I8. Fire Test F99B1402. Data plot from thermocouple ASP2 - 4.

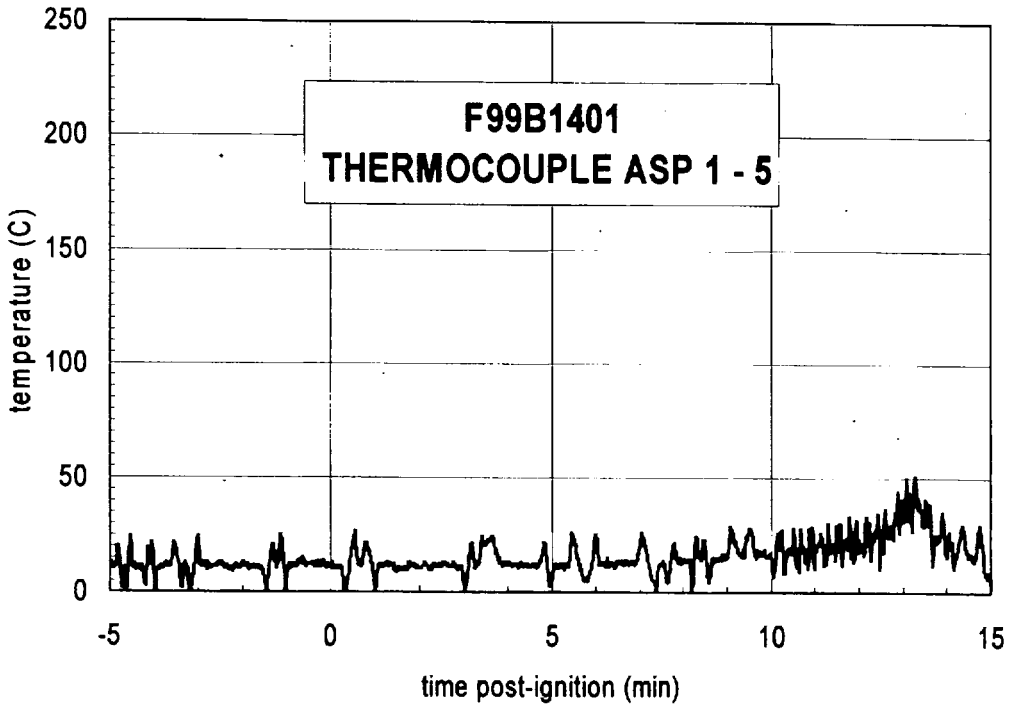


Plot I9. Fire Test F99B1401. Data plot from thermocouple ASP1 - 5.

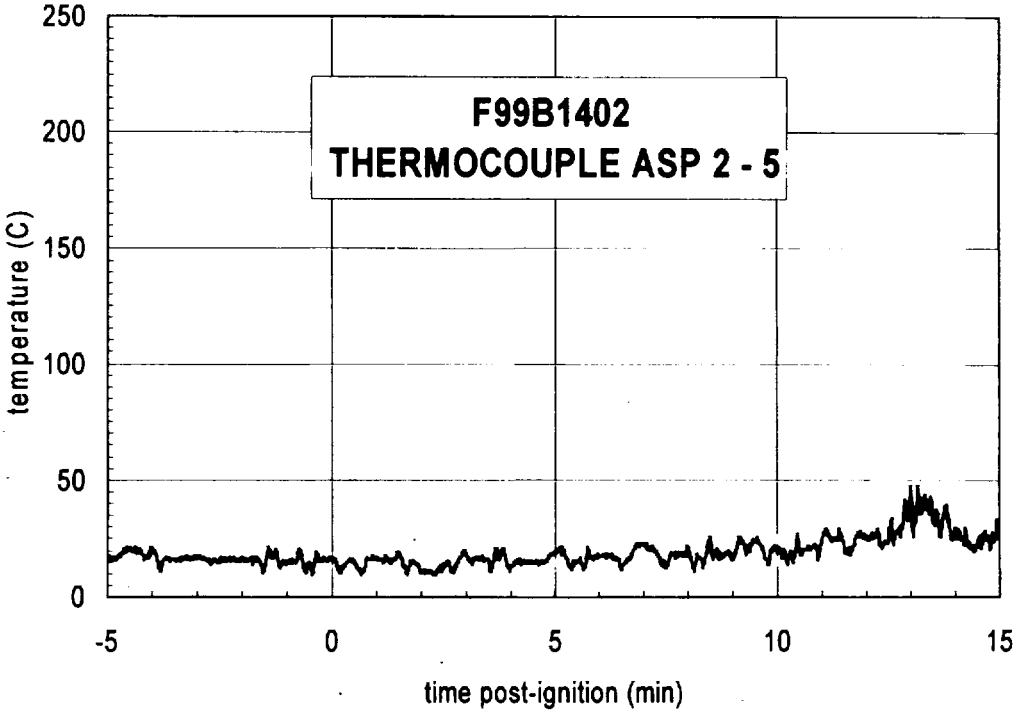


Plot I10. Fire Test F99b1402. Data plot from thermocouple ASP2 - 5.

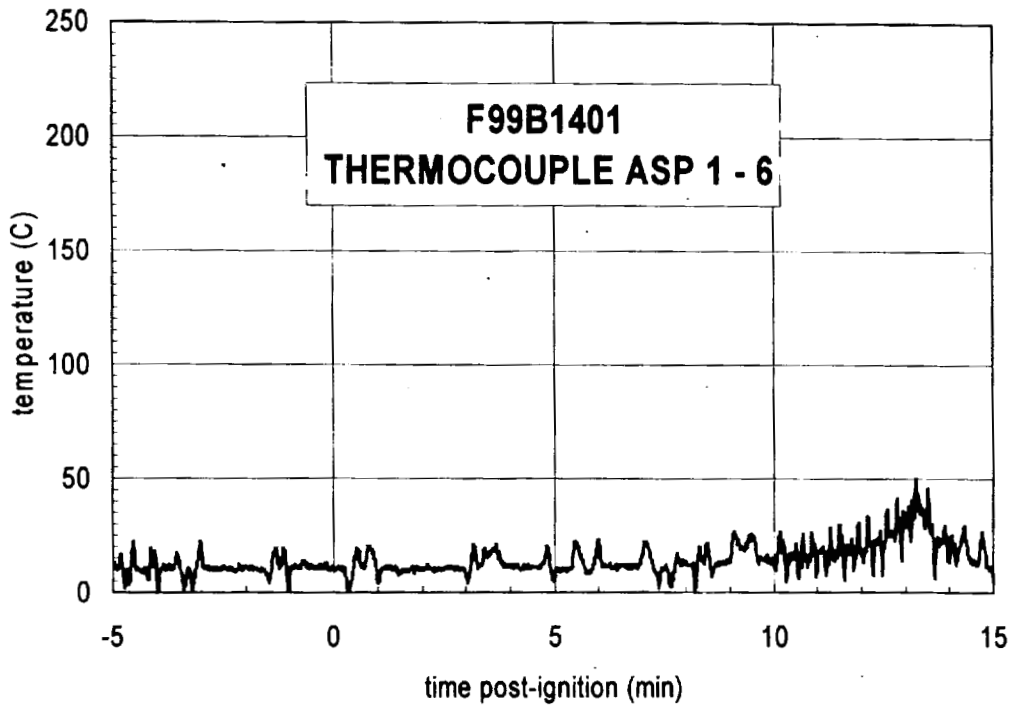


Plot I11. Fire Test F99B1401. Data plot from thermocouple ASP1 - 6.

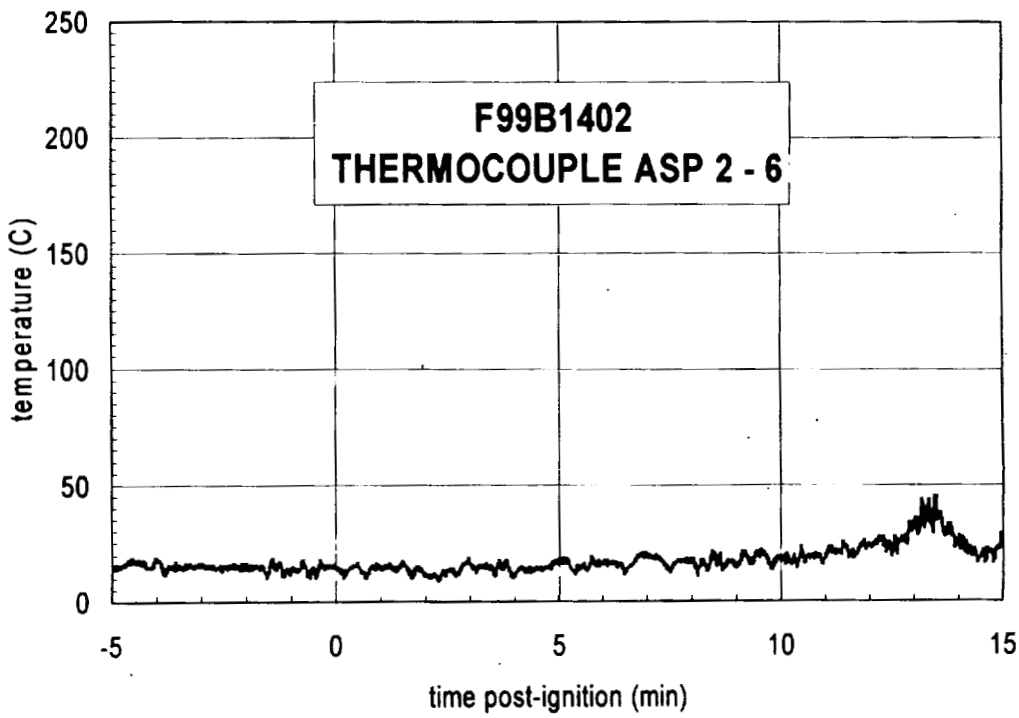


Plot I12. Fire Test F99B1402. Data plot from thermocouple ASP2 - 6.

# Appendix J

## Fire Tests F99B1401 and F99B1402
## Heat Flux Transducer/Radiometer Data

Heat-flux transducer/radiometer assemblies (64 Series, Medtherm Corporation) were used to measure convective and radiative heat transfer to selected objects in the vehicle. Each assembly contained two Schmidt-Boelter thermopiles in a water-cooled copper body (diameter = 1 in. (25.4 mm), length = 1 in. (25.4 mm)). The faces of the heat flux transducers were coated with high-temperature optical black paint. The radiometers had permanent sapphire windows (view-angle = 150°; optical transmittance range 0.4 to 4.2 μm). Both transducers were calibrated to 100 $kW/m^2$ at a reference temperature of 25°C.

The PC-based data system used to acquire data from the thermocouples (**APPENDIX H**) also was used to acquire data from the heat flux transducers and radiometers. The electrical signal wires from these transducers terminated in a 5-pin circular connector (165 Series, Amphenol). Each connector was plugged into a panel-mounted jack, which was hard wired to an analog-input multiplex expansion card (DBK-12, IOTech, Inc., Cleveland, OH). As with the thermocouples, the electrical shields on the signal cables were connected to the electronic chassis grounds on the analog-input expansion cards. The data acquisition software (DASYLab) was configured to sample each channel at a rate of 10 Hz and store the data in 10-point block averages.

Figures J1 and J2 show the approximate locations of heat flux transducer/radiometer assemblies in the test vehicle.

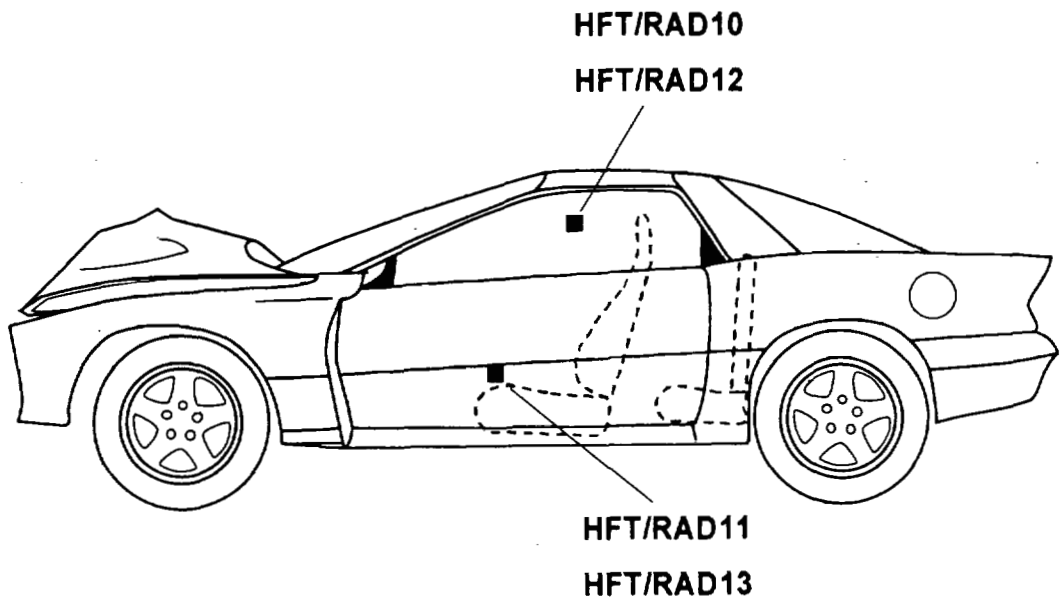


Figure J1. Fire Tests F99B1401 and F99B1401. Side view of the test vehicles showing the approximate locations of heat flux transducer/radiometer (HFT/RAD) assemblies in the test vehicles.

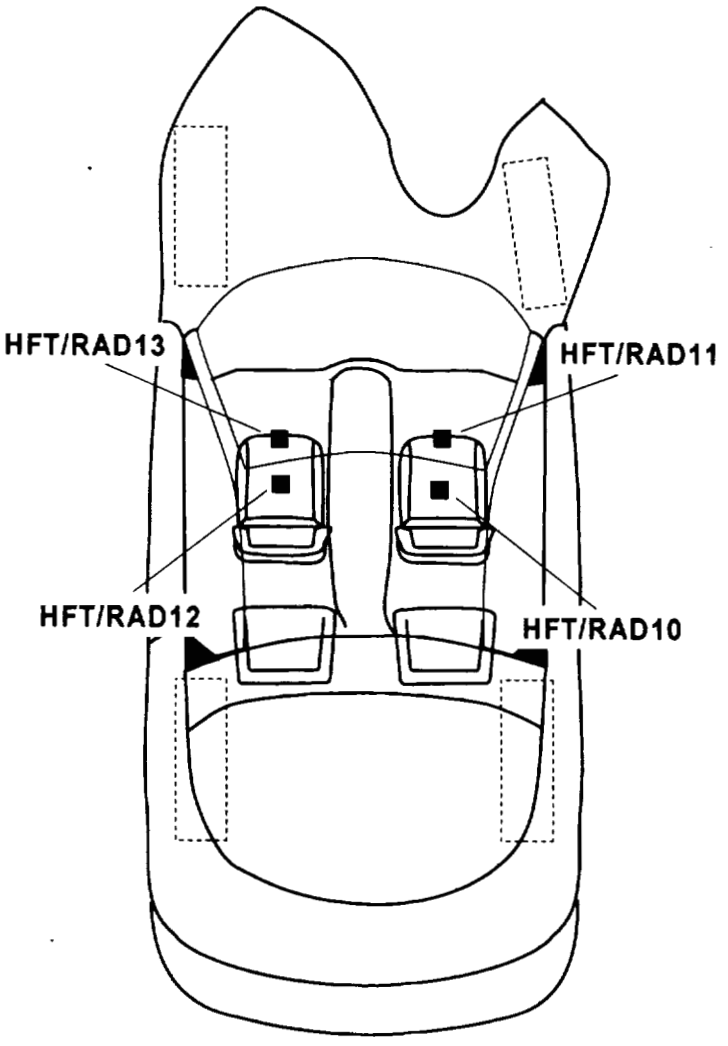


Figure J2. Fire Test F99B1401 and F99B1402. Top view of the test vehicles showing the approximate locations of heat flux transducer/radiometer (HFT/RAD) assemblies mounted in the test vehicles.

HTF/RAD10 and HFT/RAD12 were mounted to threaded rods (diameter = ½ in.) inserted through holes drilled in the roof. The lower end of each rod was secured to a seat cushion to stabilize the transducers during the test. The transducer was approximately 30 in. above the upper surface of the seat cushion with the transducer faces facing forward. HFT/RAD11 and HFT/RAD13 were attached to the forward edges of the front seat cushions, with the transducer faces facing forward. Copper tubing (o.d. = 0.25 in. (6.4 mm)) was used for the cooling water supply and waste lines. The temperature of the water supplied to the HFT/RAD assemblies was approximately 80°C, and the flow rate of water through each body was approximately 100 mL/min.

Thermocouples O10, O11, O12 and O13 were located in the bodies of each heat flux transducer or heat flux transducer/radiometer assemblies HFT/RAD10, HFT/RAD11, HFT/RAD12 and HFT/RAD13, respectively.

Data recorded from these transducers is shown in Plots J1 through J8.

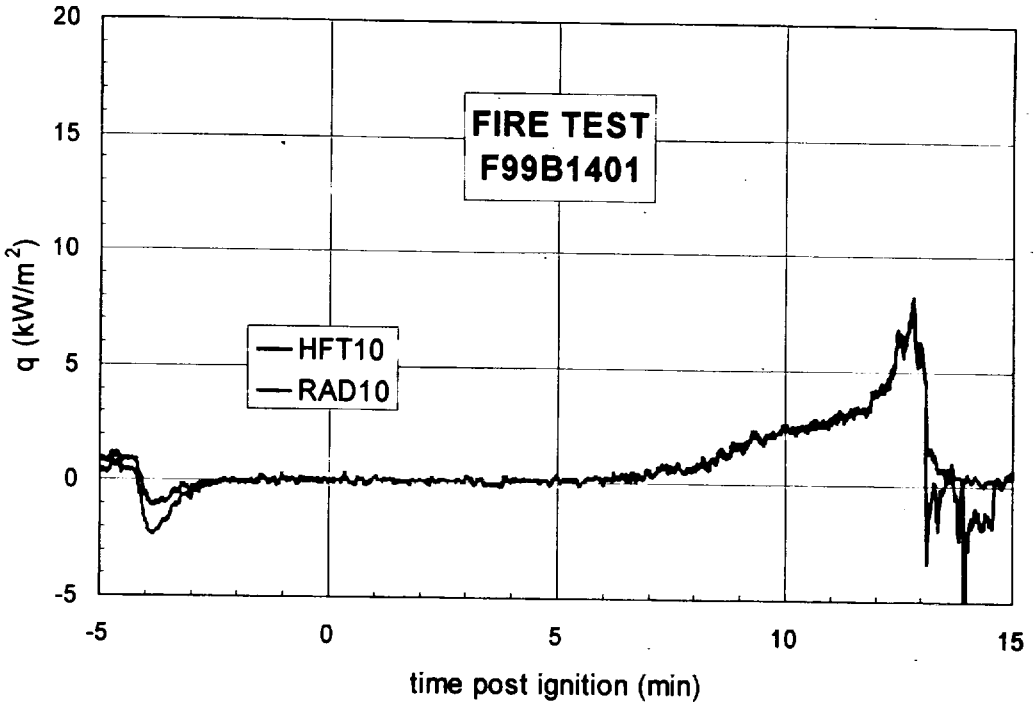


Plot J1. Fire Test F999B1401. Data plot from Heat Flux Transducer 10 and Radiometer 10.

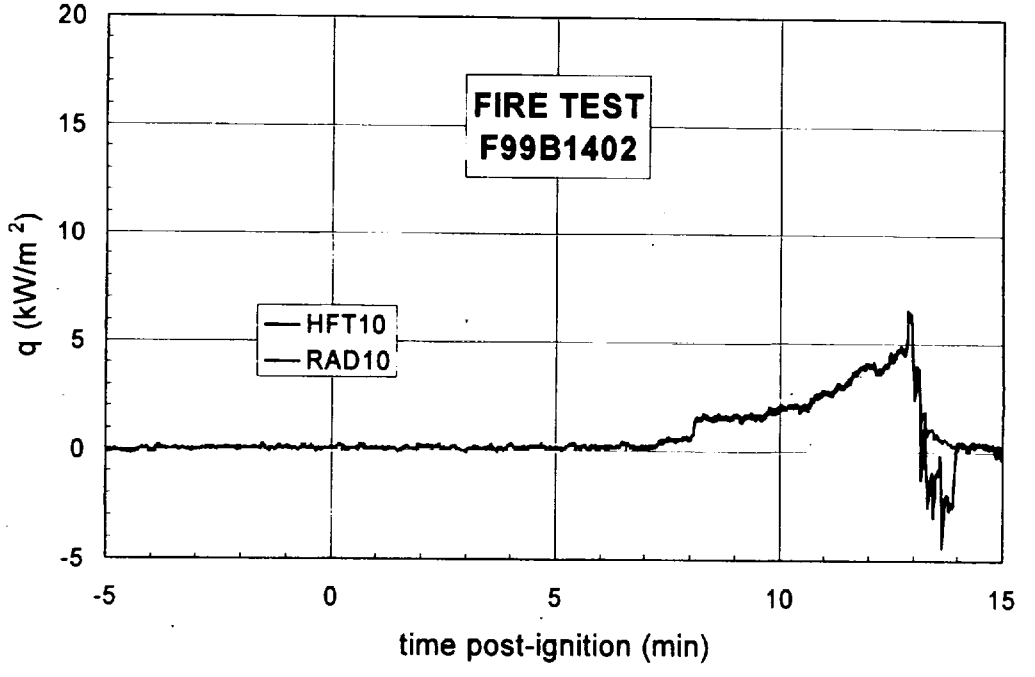


Plot J2. Fire Test F99B1402. Data plot from Heat Flux Transducer 10 and Radiometer 10.

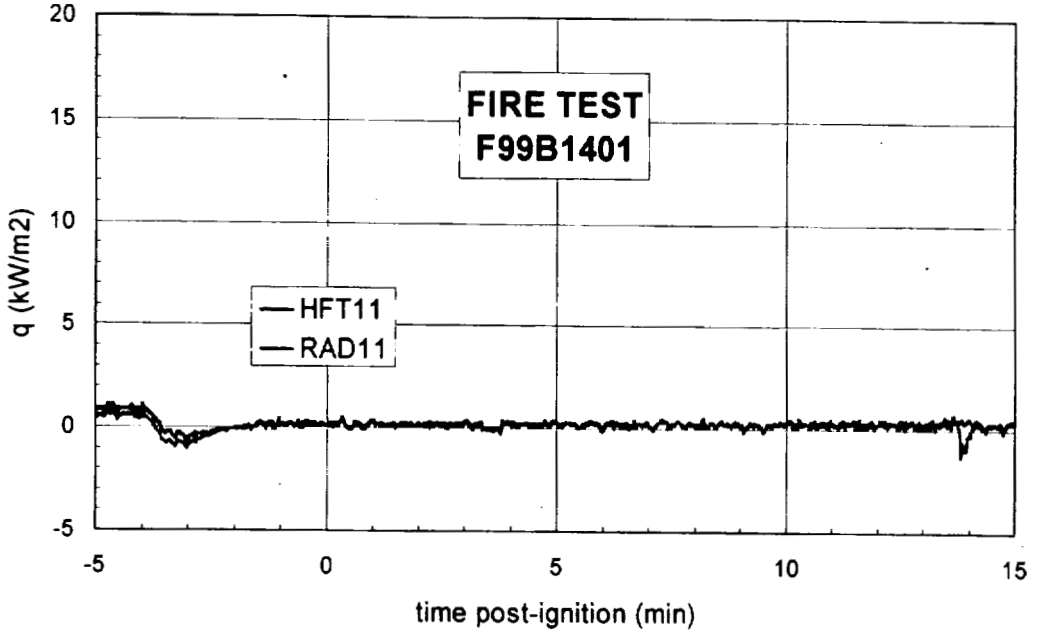


Plot J3. Fire Test F99B1401. Data plot from Heat Flux Transducer 11 and Radiometer 11.

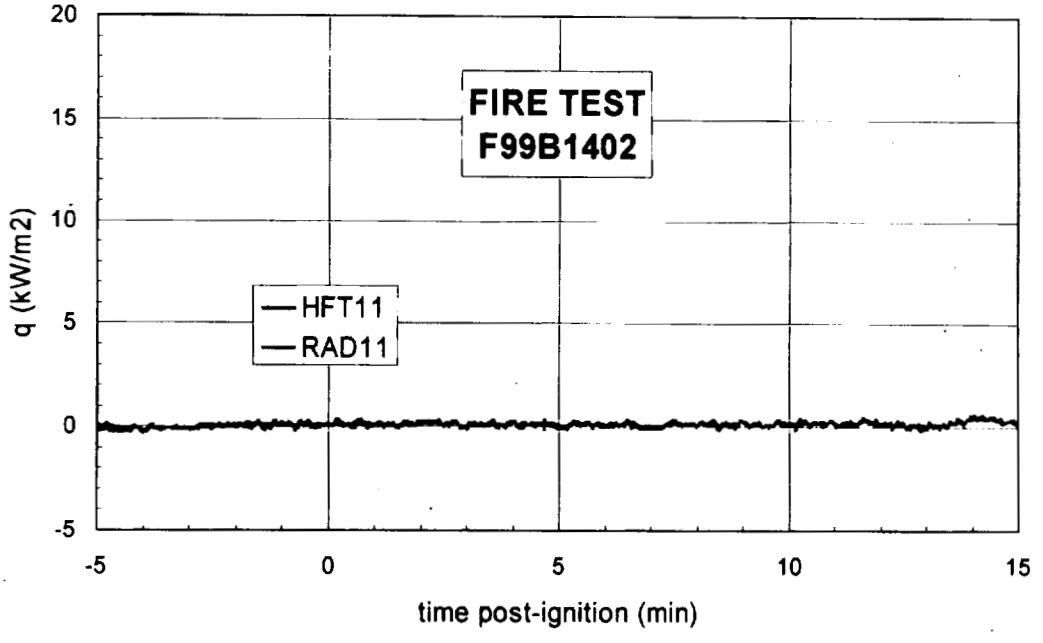


Plot J4. Fire Test F99B1402. Data plot from Heat Flux Transducer 11 and Radiometer 11.

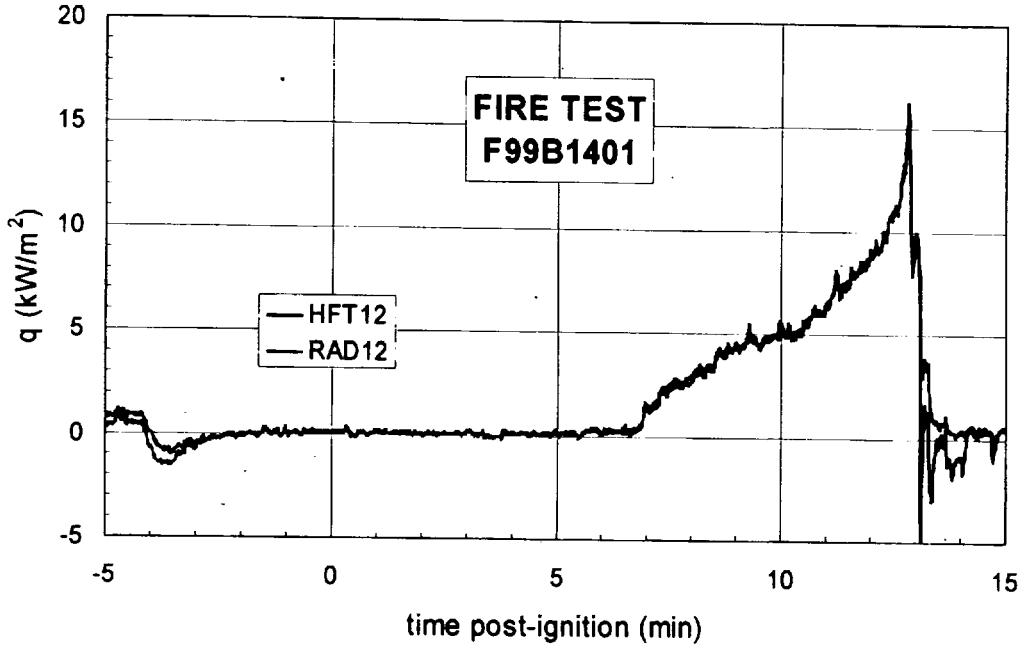


Plot J5. Fire Test F99B1401. Data plot from Heat Flux Transducer 12 and Radiometer 12.

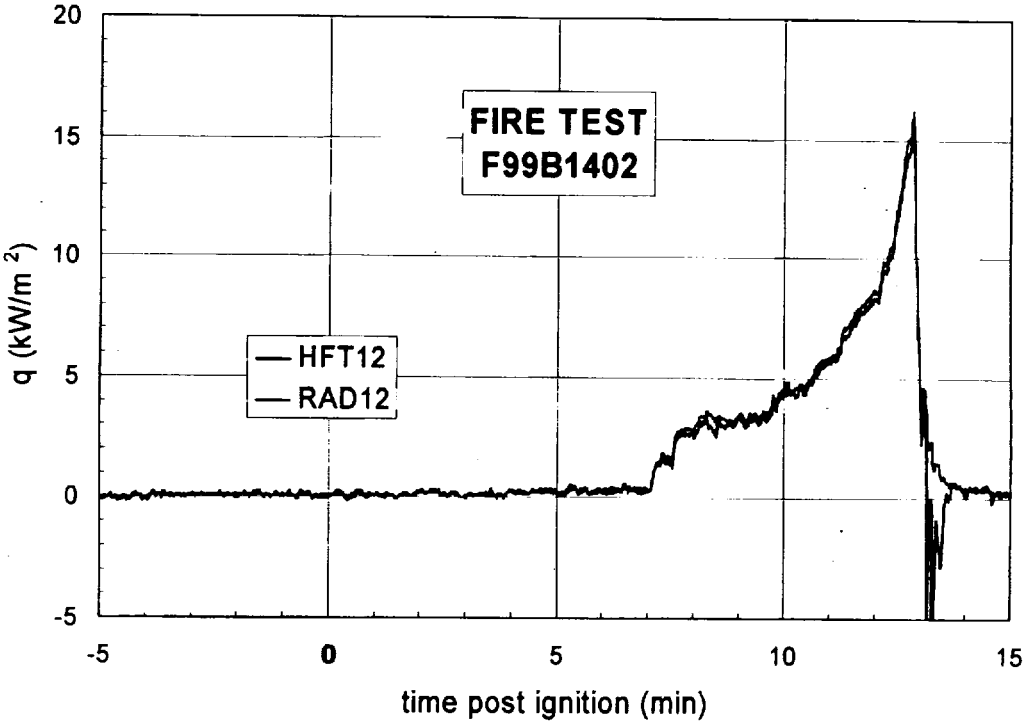


Plot J6. Fire Test F99B1402. Data plot from Heat Flux Transducer 12 and Radiometer 12.

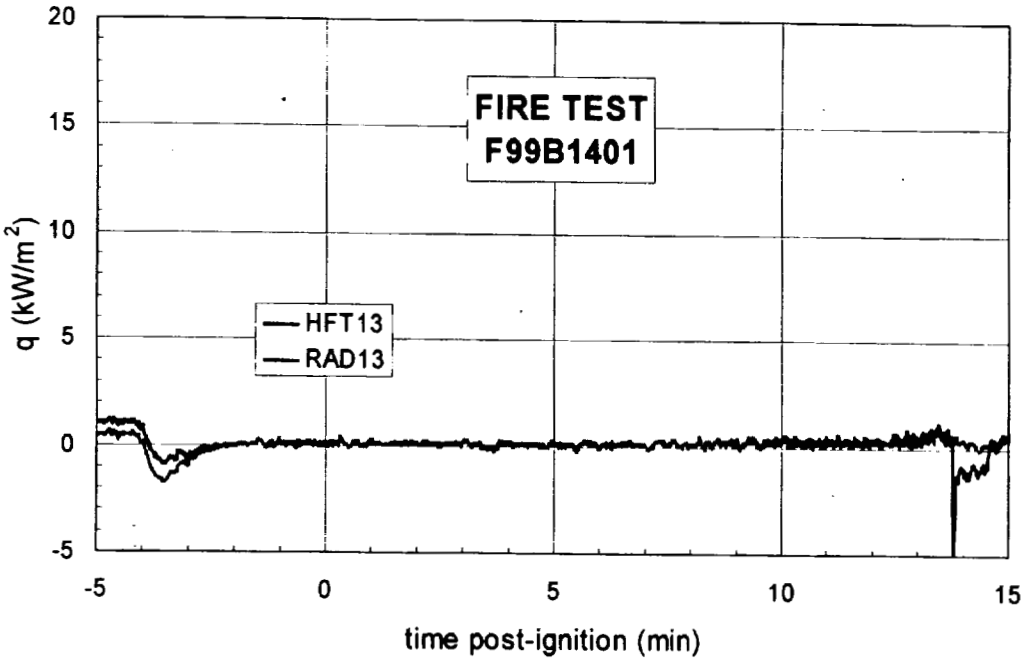


Plot J7. Fire Test F99B1401. Data plot from Heat Flux Transducer 13 and Radiometer 13.

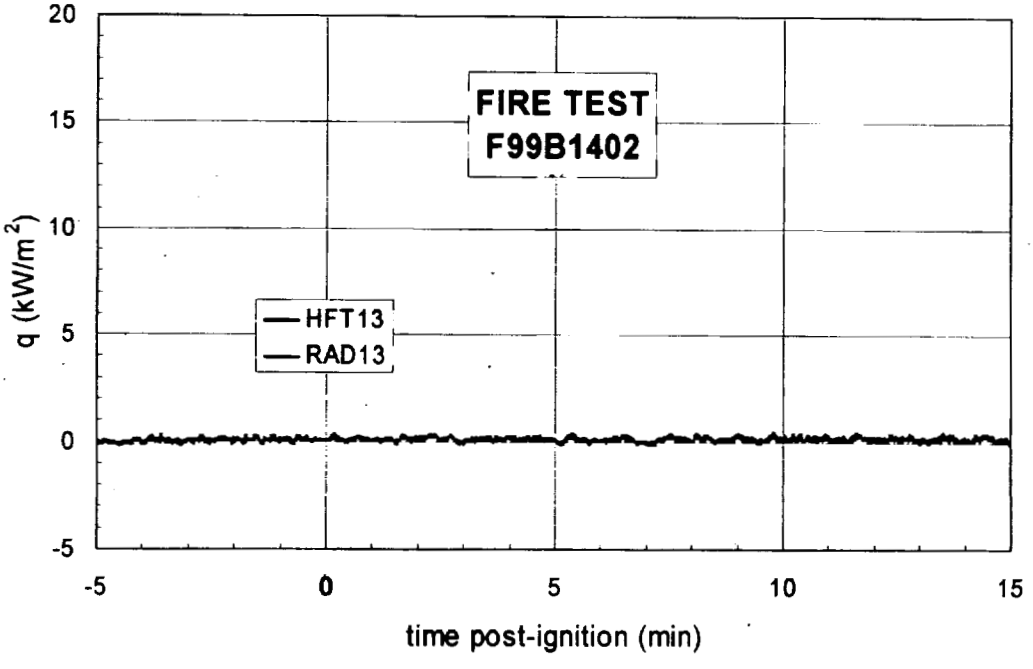


Plot J8. Fire Test F99b1402. Data plot from Heat Flux Transducer 13 and Radiometer 13.

# Appendix K

## Fire Tests F99B1401 and F99B1402
## Pressure Data

Figures K1 and K2 show the approximate locations of the pressure taps and bi-directional flow probe in the test vehicle.

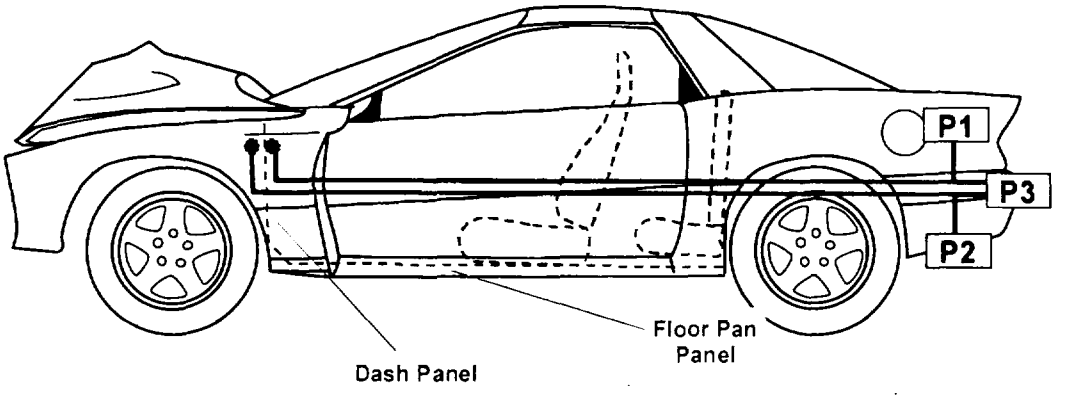


Figure K1. Fire Tests F99B1401 and F99B1402. Side view showing the approximate locations of the pressure taps in the test vehicles.

Two pressure taps were installed in the test vehicle for this test in the following locations: exterior surface of the dash panel (engine compartment side) inboard of the HVAC module; and interior surface of the dash panel (passenger compartment side) inboard of the HVAC module.

Both pressure taps was constructed from stainless steel tubing (o.d. = 0.250 in.). A union-T fitting with compression-type couplings (Parker) was attached to the inlet of the stainless steel tubing, with two of the three positions in the union-T fitting were left open. The other end of stainless steel tubing was connected to a pressure gauge with solvent-resistant flexible tubing (Tygon Masterflex® 6049; i.d. = 0.250 in.; o.d. = 0.438 in.). The total length of the stainless steel and flexible tubing was approximately 10 m.

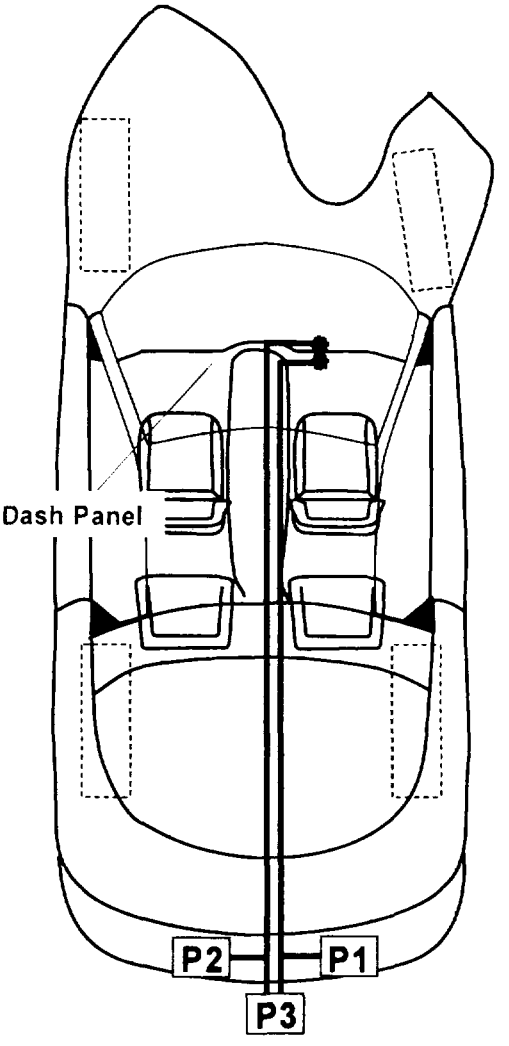


Figure K2. Fire Tests F99B1401 and F99B1402. Top view showing the approximate locations of the pressure taps in the test vehicles the approximate locations of pressure taps in the test vehicles.

Pressure gauges (Model C-264, Setra Systems, Acton, MA) with two pressure ranges were used for this test: - 0.5 to 0.5 (± 0.0013) in. W.C. (-124.5 to 124.5 Pascal) and -0.1 to 0.1 (± 0.0003) in. W.C. (-24.9 to 24.9 Pascal). Both gauges were accurate to 0.25% full scale. The gages were powered with a 24 volt non-regulated power supply (Setra Systems). The high-pressure inlet of Pressure Gauge P1 was connected to the pressure tap located at the interior surface of the dash panel, and its low-pressure inlet was left open to atmosphere. The high-pressure inlet of Pressure Gauge P2 was connected to the pressure tap located at the exterior surface of the dash panel, and its low-pressure inlet was left open to atmosphere. The high-pressure inlet of

Pressure Gauge P3 was connected to the pressure tap located at the exterior surface of the dash panel, and its low-pressure inlet was connected to the pressure tap located at the interior surface of the dash panel.

The PC-based data acquisition system described in **APPENDIX H** also was used to record the electronic signals from the pressure gauges during the test. The signal leads from the pressure gauges were plugged into panel-mounted connectors, which were hard-wired to a low-gain analog-input multiplex expansion card (DBK12, IOTech). The analog-input expansion card was interfaced to the main A/D card in the PC. The signal from each pressure gauge was sampled at a rate of 100 Hz. The analog data was stored to a data file in 100-point block-averages so that the effective sampling rate during the test was 1 Hz.

Plots of the pressure data recorded with from Gauges P1 through P3 during F99B1401 and F99B1401 are shown in Plots K1 through K6. Steam generated by the start of fire suppression caused the positive- and negative-going pressure deflections starting between 12 and 13 minutes post-ignition.

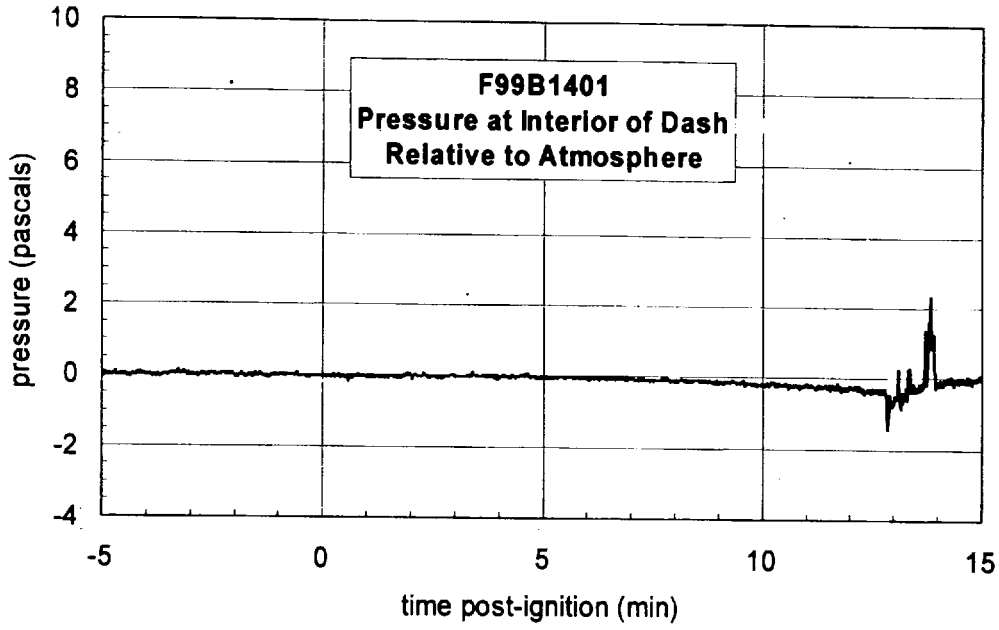


Plot K1. Fire Test F99B1401. Pressure at the interior surface of the dash panel relative to atmospheric pressure measured with pressure gauge P1.

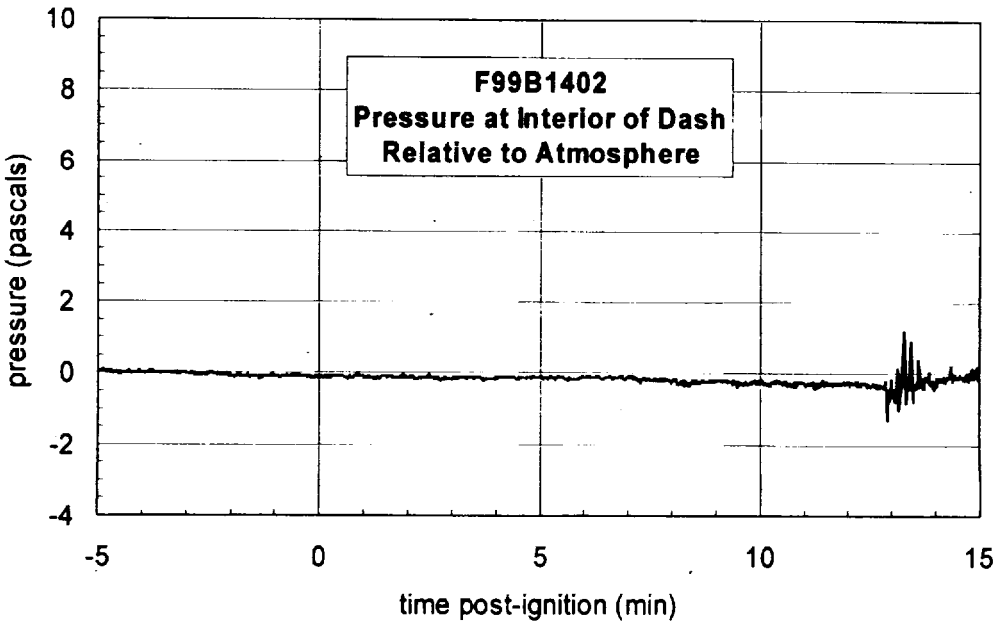


Plot K2. Fire Test F99B1402. Pressure the interior surface of the dash panel relative to atmospheric pressure measured with pressure gauge P1.

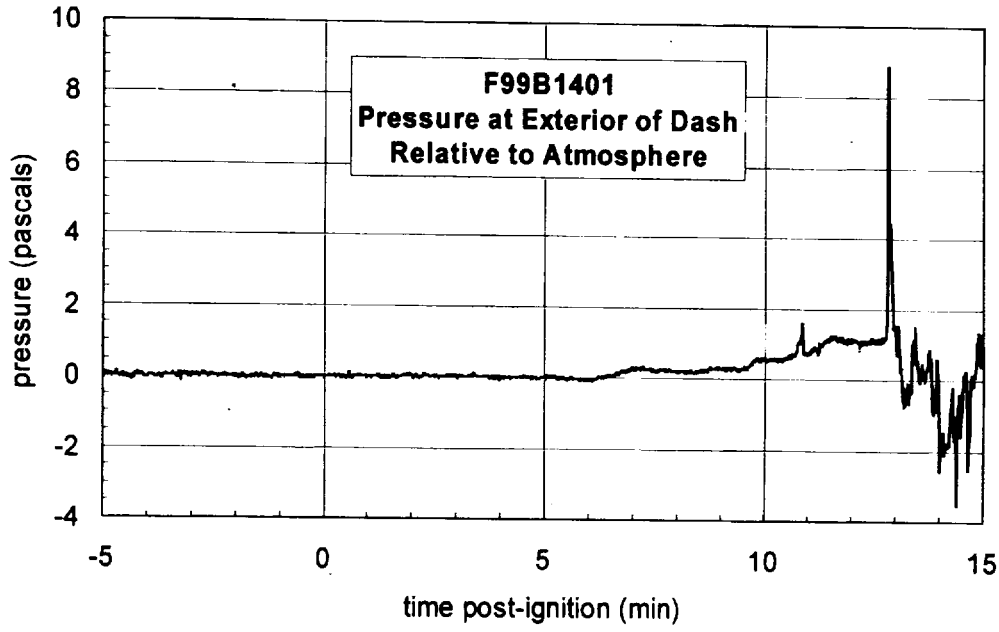


Plot K3. Fire Test F99B1401. Pressure at the exterior surface of the dash panel relative to atmospheric pressure measured with pressure gauge P2.

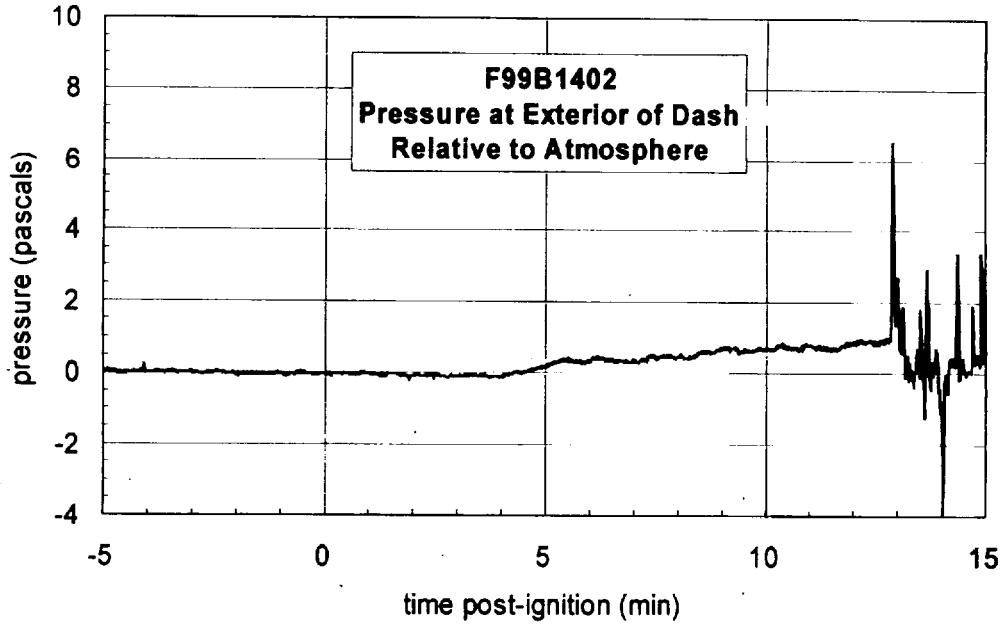


Plot K4. Fire Test F99B1402. Pressure the exterior surface of the dash panel relative to atmospheric pressure measured with pressure gauge P2.

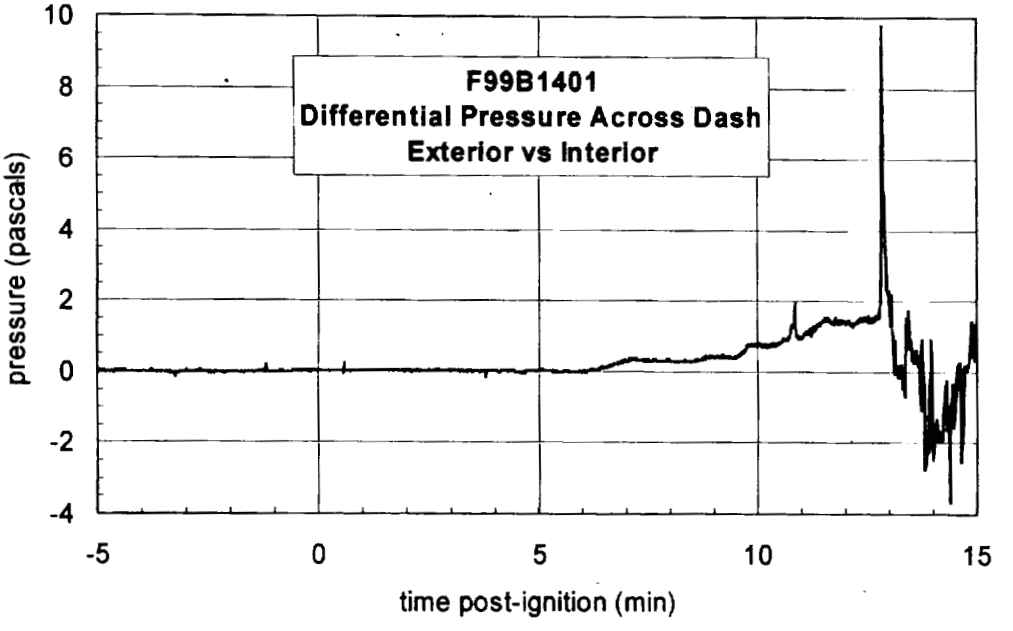


Plot K5. Fire Test F99B1401. Differential pressure across the dash panel measured with pressure gauge P3 (—) and the difference between pressures recorded from P2 and P1 (—).

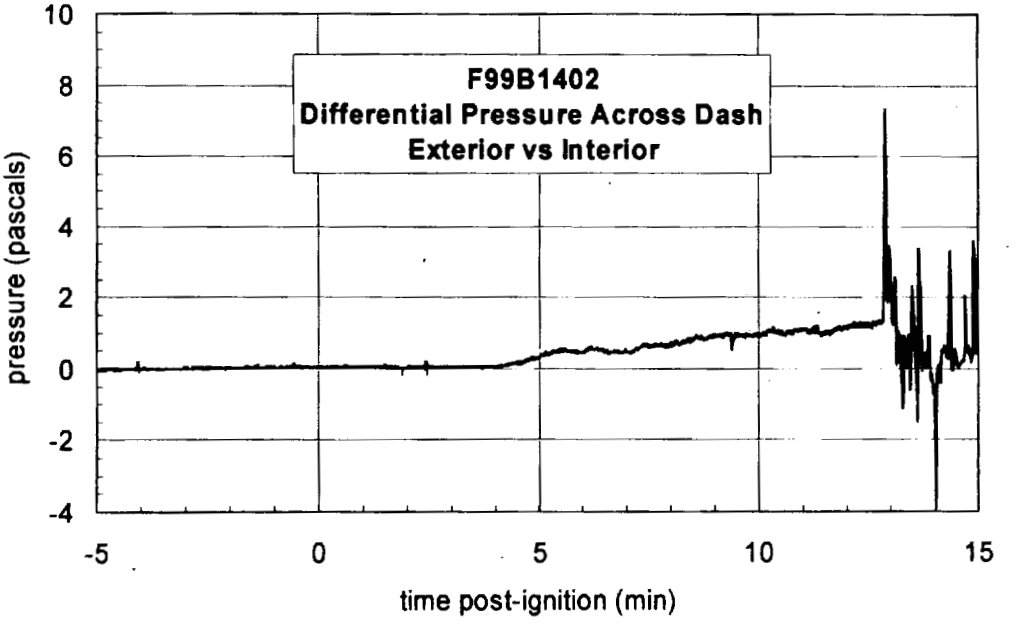


Plot K6. Fire Test F99B1402. Differential pressure across the dash panel measured with pressure gauge P3 (—) and the difference between pressures recorded from P2 and P1 (—).

## Appendix L

## Fire Tests F99B1401 and F99B1402

## Fourier Transform Infrared Spectroscopy
## Gas Analysis Data

The sampling-line for FTIR analysis consisted of a stainless-steel tube (o.d. = 0.250 in. (6.4 mm), i.d. = 0.125 in. (3.2 mm), l = 20 ft (6.1 m)) inserted through the roof between the front seats along the longitudinal midline of the test vehicle (Fig.'s L1 and L2). The inlet of the sample-tube extended approximately 10 in. below the headlining (Fig.'s L1 and L2). The tube was not heated. The outlet of the sample tube was connected to a heated Teflon® transfer-line (o.d. = 0.250 in. (6.4 mm), i.d. = 0.125 in. (3.2 mm), l = 75 ft. (23 m)), which was connected to the gas cell of the FTIR spectrometer. The transfer-line was heated to 105°C during the test to prevent condensation of water and water-soluble gases (*e.g.*, HCl, HCN, NO, and $NO_2$). An in-line stainless steel filter holder containing a quartz fiber filter (o.d. = 47 mm) was placed between the sample-tube and the transfer-line to prevent smoke particles from contaminating analytical instrumentation.

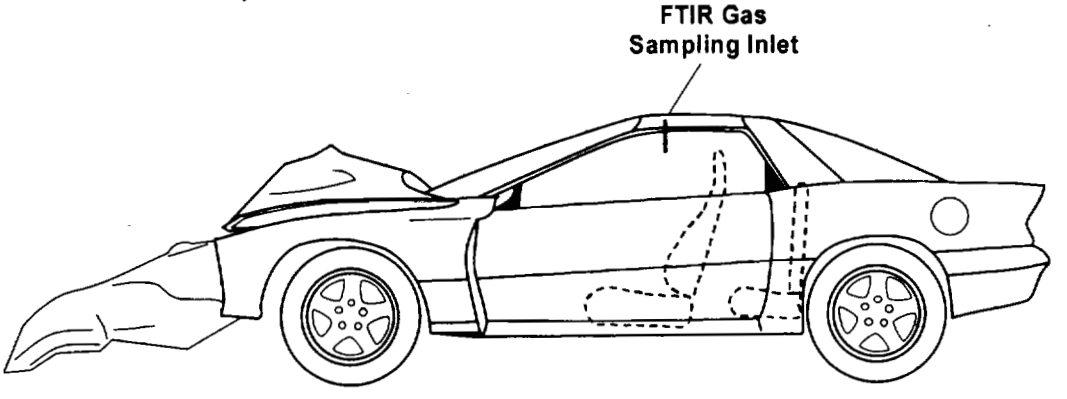


Figure L1. Fire Tests F99B1401 and F99B1402. Side-view of the test vehicle show the approximate location of the FTIR gas-sampling inlet in the passenger compartment.

The FTIR spectrometer was a Model I-1000 Series FTIR Spectrometer (MIDAC Corporation, Riverside, California), with a KBr beam-splitter; a liquid nitrogen-cooled Mercury-Cadmium-Telluride detector; and gold-surfaced aluminum optics. This instrument was fitted with a stainless steel, multiple-reflectance gas cell (path length = 10 m) with zinc selenide windows. The gas cell was heated to 105°C. The optical bench was filled with clean, dry argon and hermetically sealed. The usable spectral range of this instrument was approximately 7400-700 $cm^{-1}$. Pressure in the gas cell during the fire tests was measured with a Baratron pressure gauge (MKS Instruments, Burlington, MA). The spectrometer was operated at a spectral resolution of 0.5 $cm^{-1}$.

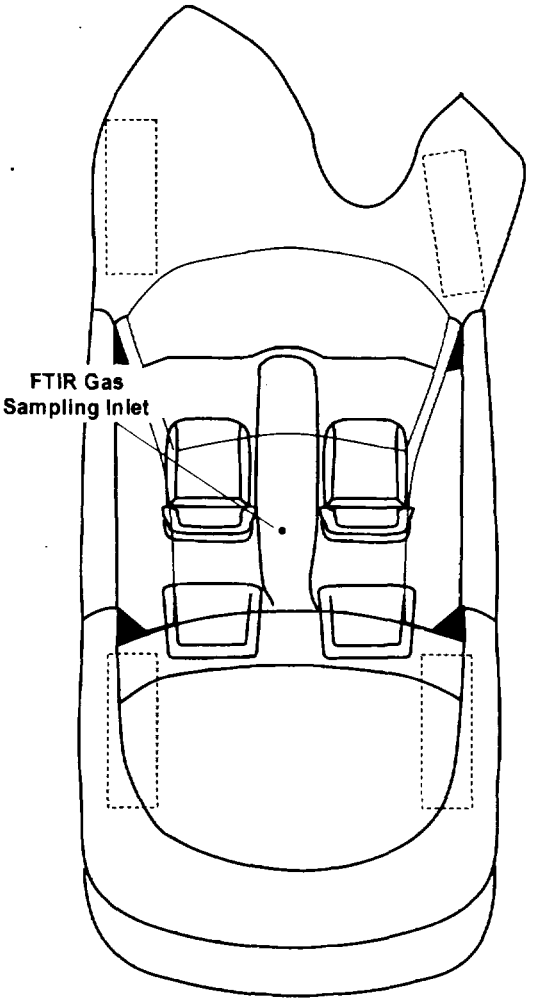


Figure L2. Fire Tests F99B1401 and F99B1402. Top view of the test vehicle showing the approximate location of the FTIR gas sampling inlet in the passenger compartment.

The sampling line and gas cell were equilibrated to a temperature of 105°C for at least 60 minutes before sample acquisition. A reference spectrum was acquired while the gas cell was evacuated. During the fire tests, the gas cell was purged continuously with air withdrawn from the passenger compartment at a flow rate of 7 L/min. Single-scan absorbance spectra were acquired and stored to disk at intervals of 10 s. After the test, the stored spectra were analyzed using the quantitative analysis software provided by the instrument manufacturer (AutoQuant, MIDAC). This software uses a Classical Least Squares algorithm to determine gas concentrations. The method developed for analysis of combustion gases was calibrated with gas standards (Scott Specialty Gases, Inc., Troy, MI). The standards were either NIST-traceable or produced by a gravimetric blending process.

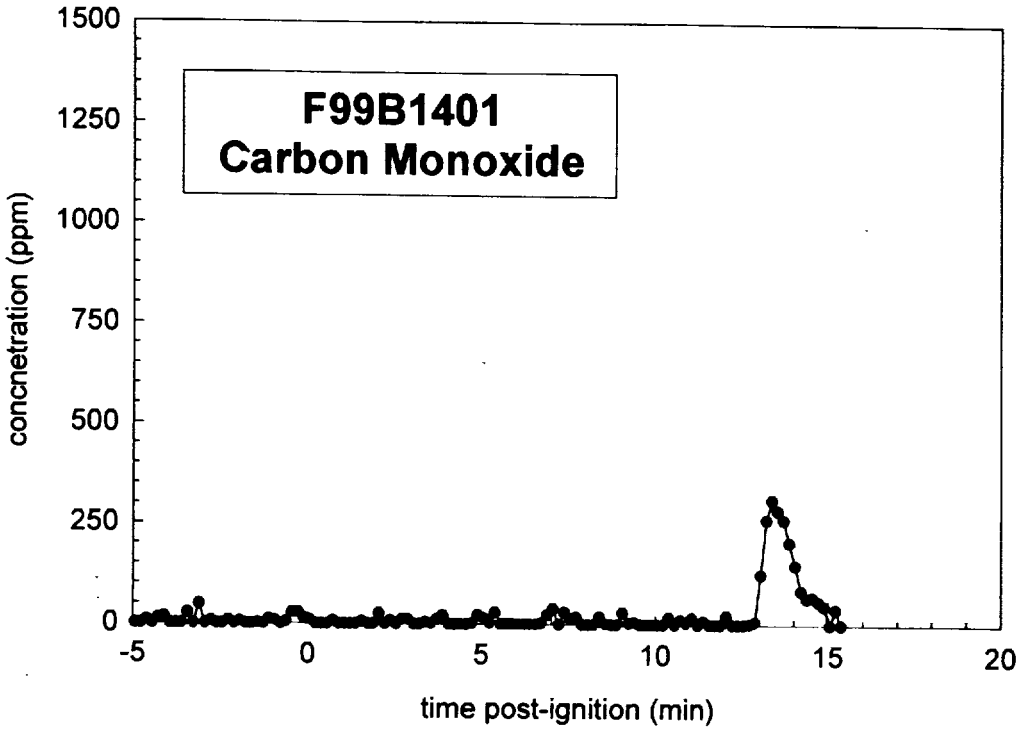


Plot L1. Fire Test F99B1401. Concentration of carbon monoxide (CO) in the passenger compartment determined by FTIR analysis.

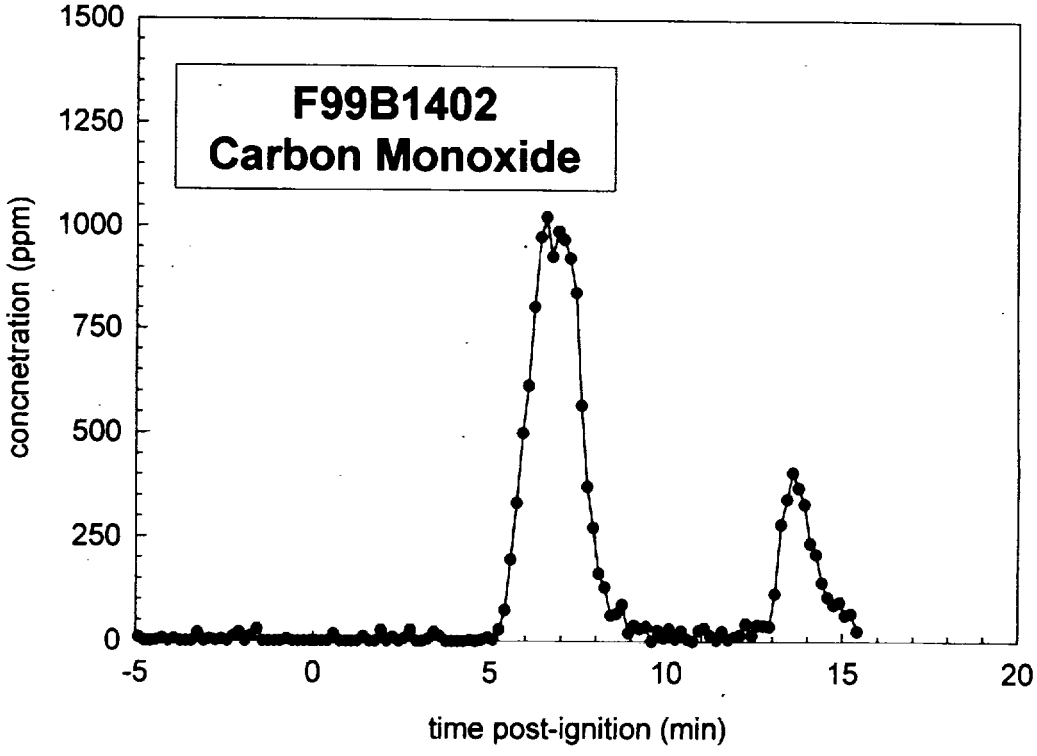


Plot L2. Fire Test F99B1402. Concentration of carbon monoxide (CO) in the passenger compartment determined by FTIR analysis.

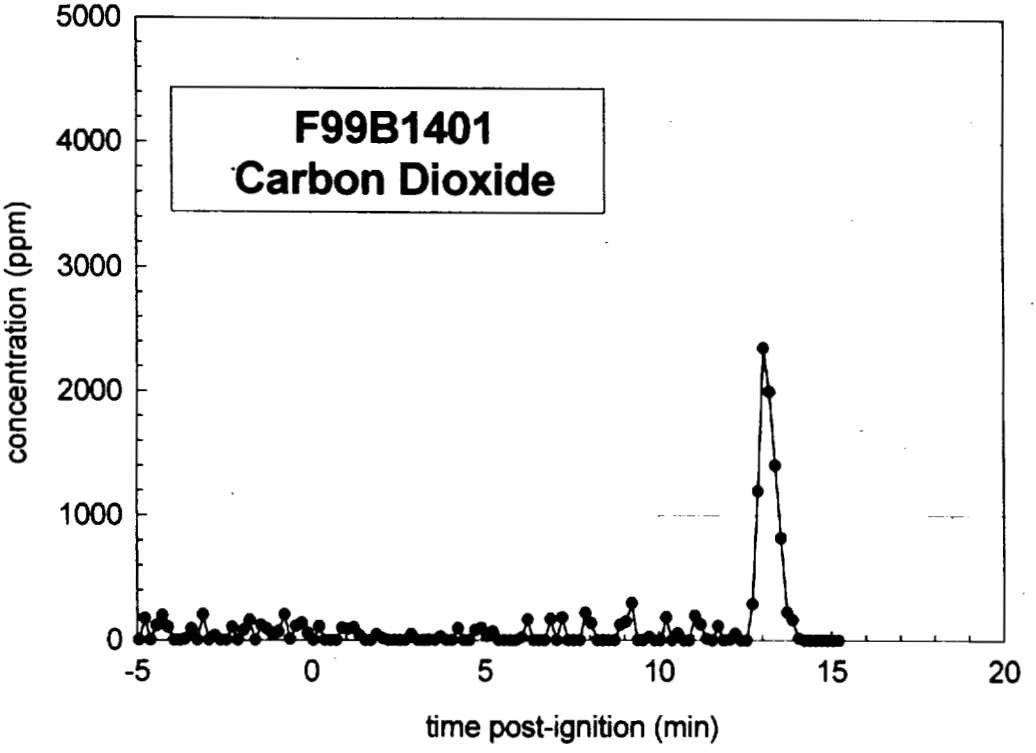


Plot L3. Fire Test F99B1401. Concentration of carbon dioxide ($CO_2$) in the passenger compartment determined by FTIR analysis.

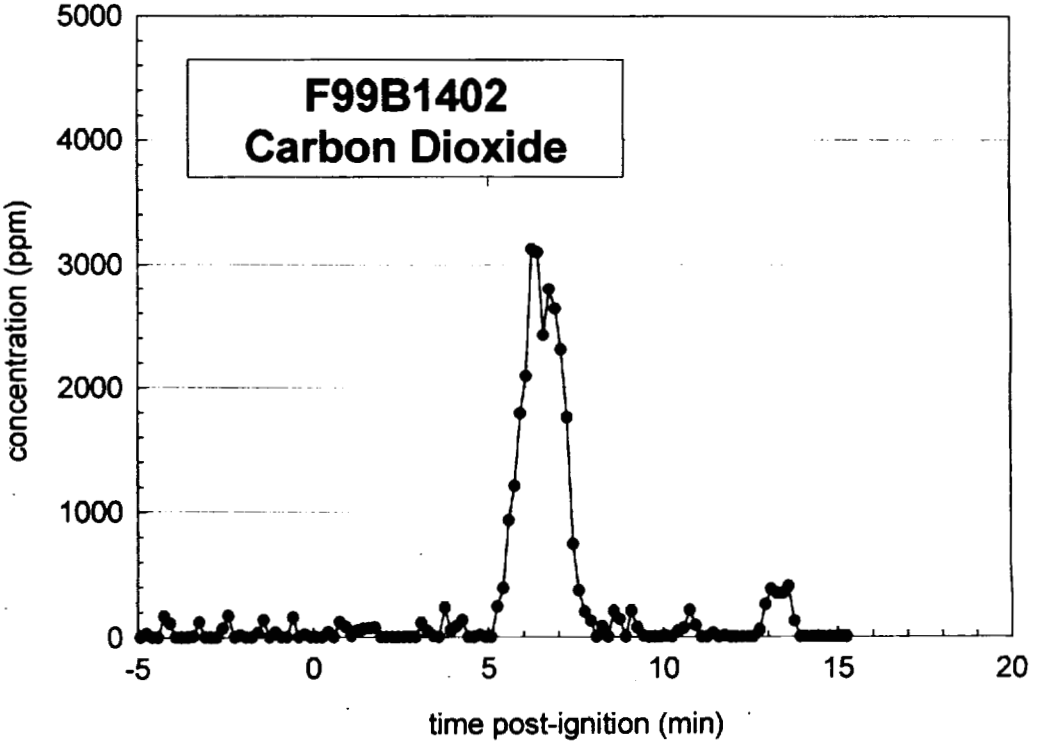


Plot L4. Fire Test F99B1402. Concentration of carbon dioxide ($CO_2$) in the passenger compartment determined by FTIR analysis.

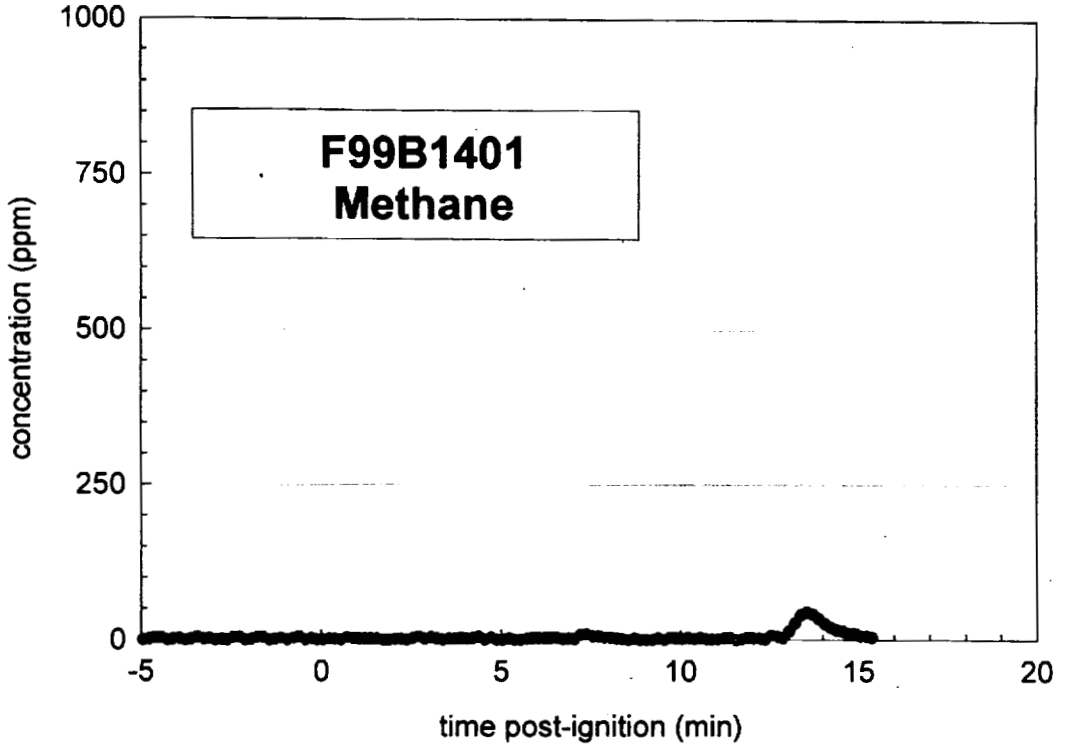


Plot L5. Fire Test F99B1401. Concentration of methane ($CH_4$) in the passenger compartment determined by FTIR analysis.

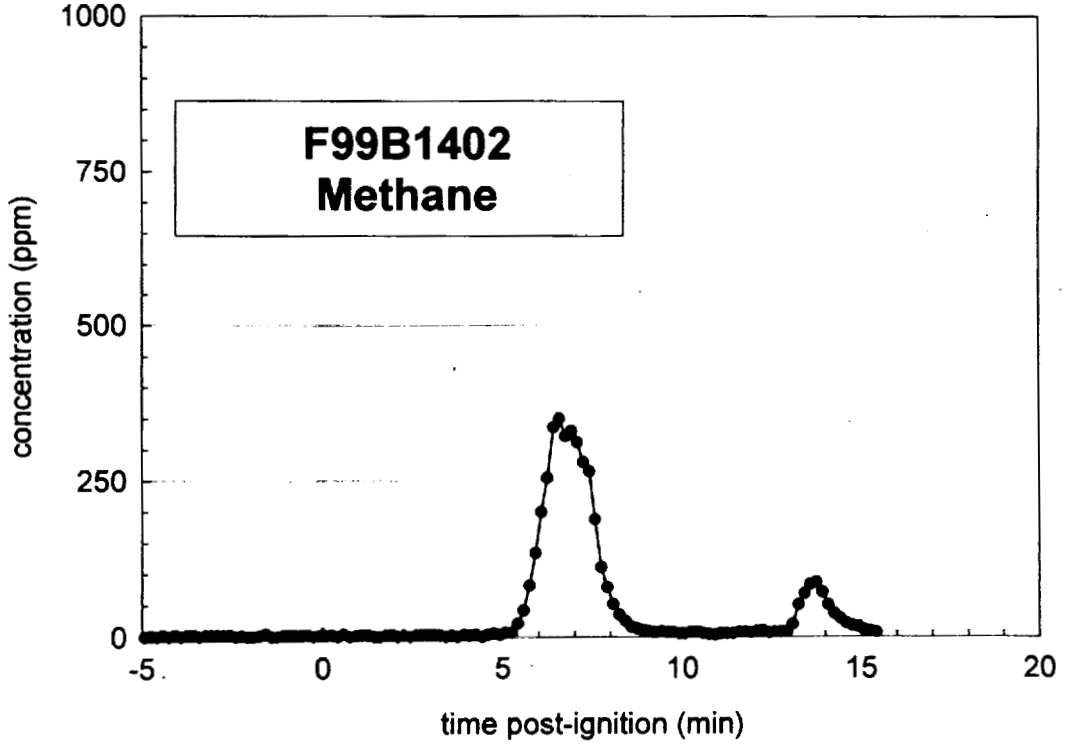


Plot L6. Fire Test F99B1402. Concentration of methane ($CH_4$) in the passenger compartment determined by FTIR analysis.

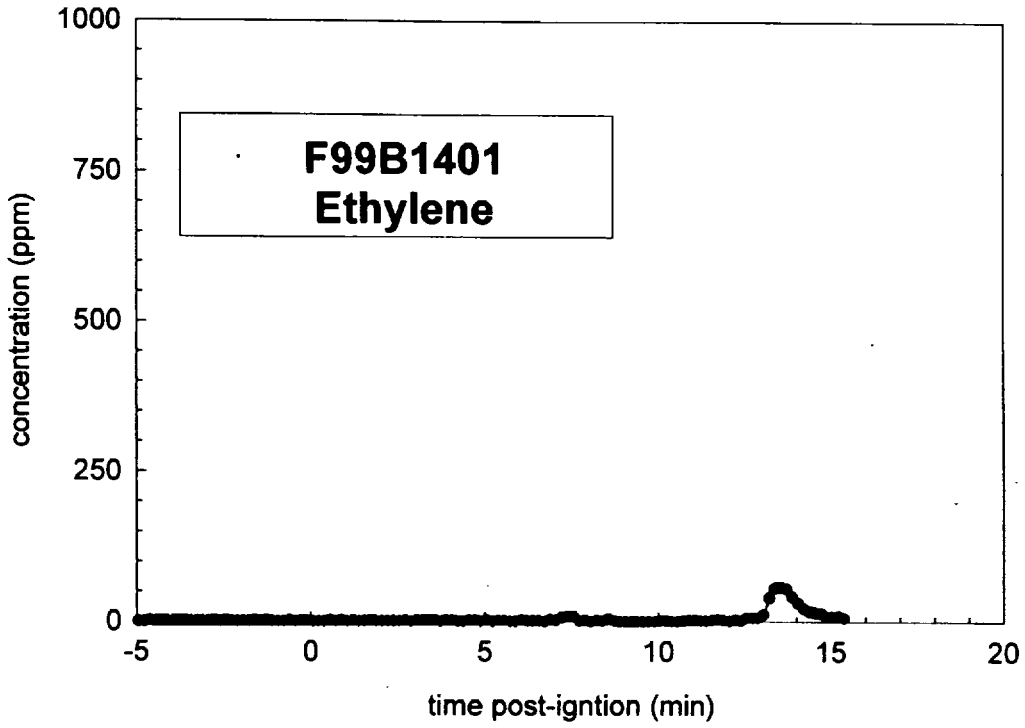


Plot L7. Fire Test F99B1401. Concentration of ethylene ($C_2H_4$) in the passenger compartment determined by FTIR analysis.

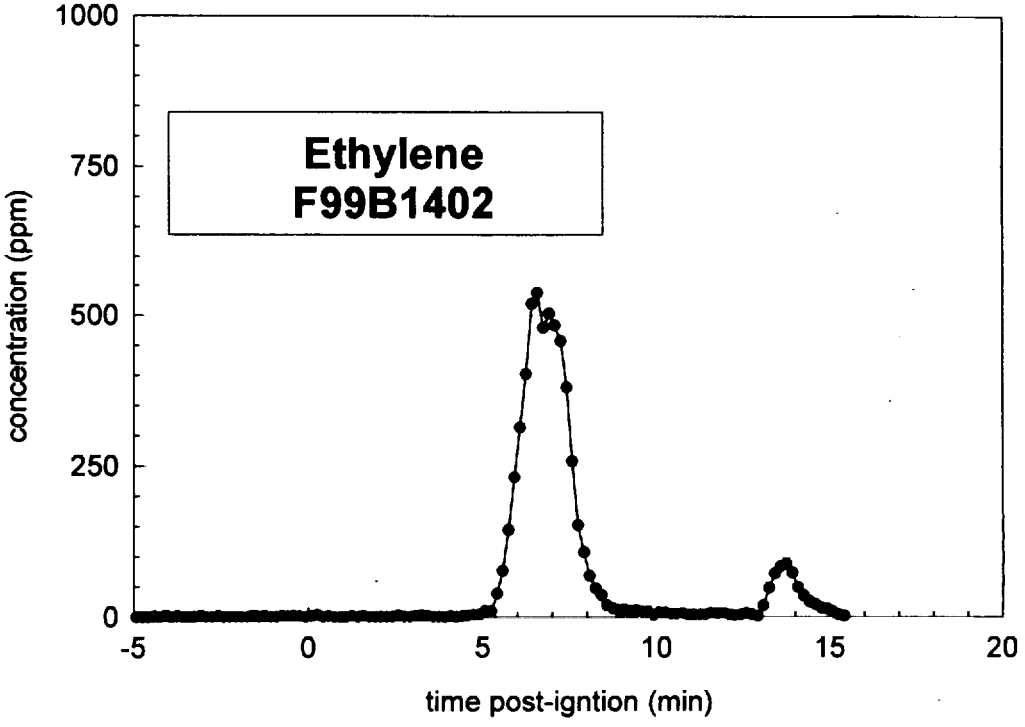


Plot L8. Fire Test F99B1401. Concentration of ethylene ($C_2H_4$) in the passenger compartment determined by FTIR analysis.

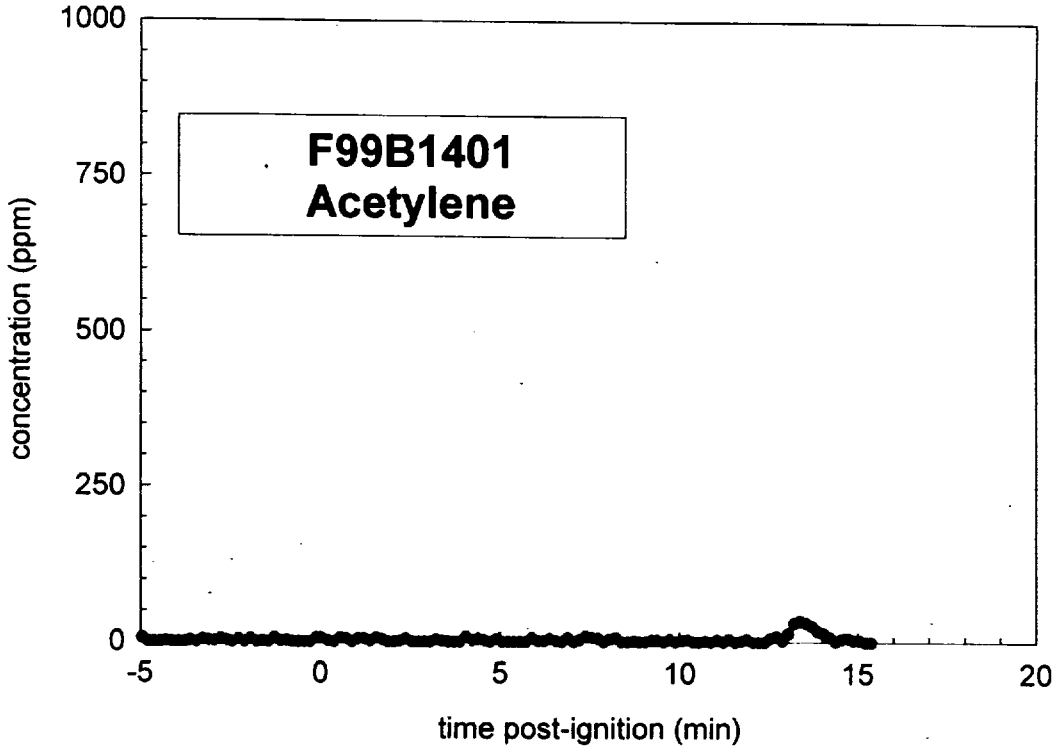


Plot L9. Fire Test F99B1401. Concentration of acetylene ($C_2H_2$) in the passenger compartment determined by FTIR analysis.

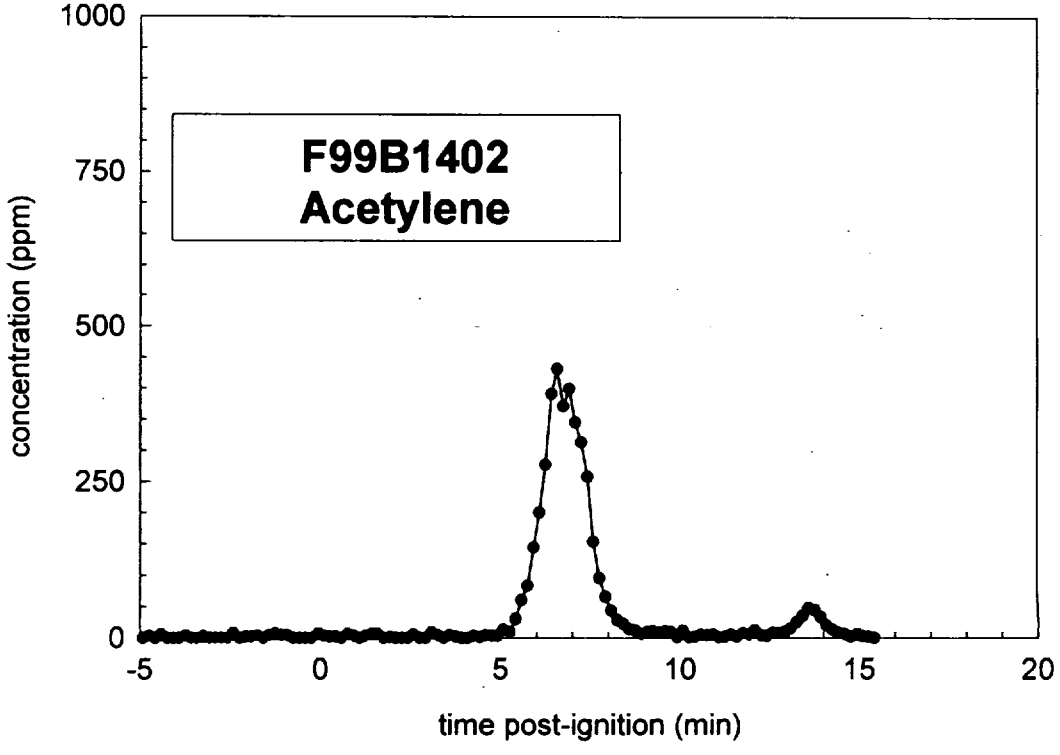


Plot L10. Fire Test F99B1401. Concentration of acetylene ($C_2H_2$) in the passenger compartment determined by FTIR analysis.

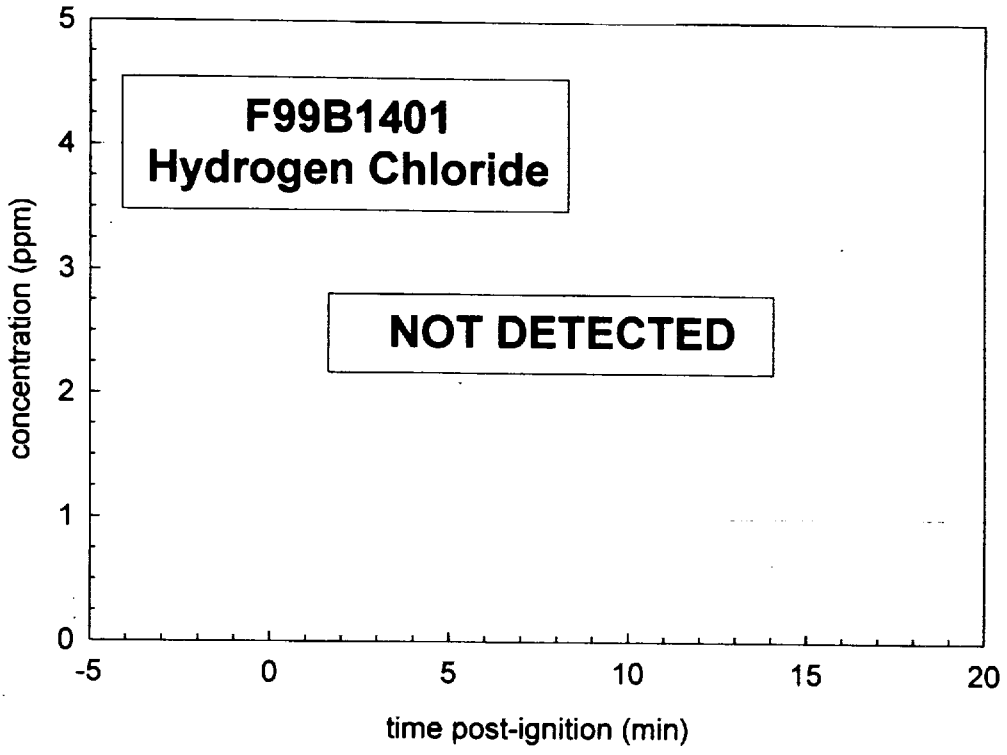


Plot L11. Fire Test F99B1401. Concentration of hydrogen chloride (HCl) in the passenger compartment determined by FTIR analysis.

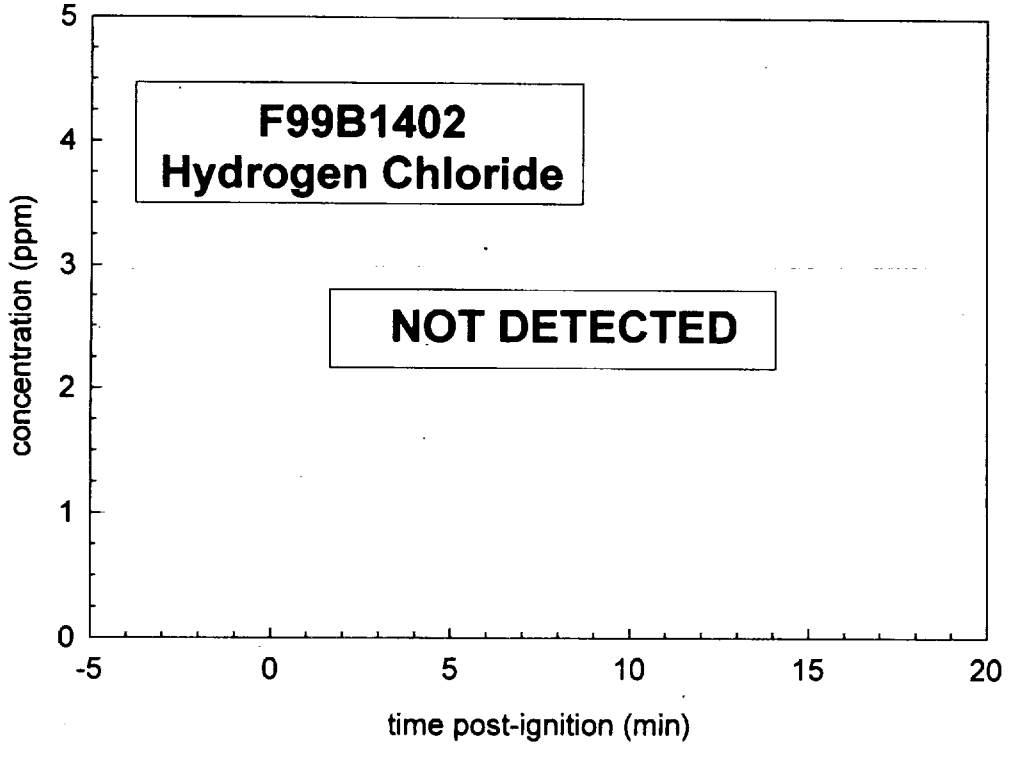


Plot L12. Fire Test F99B1402. Concentration of hydrogen chloride (HCl) in the passenger compartment determined by FTIR analysis.

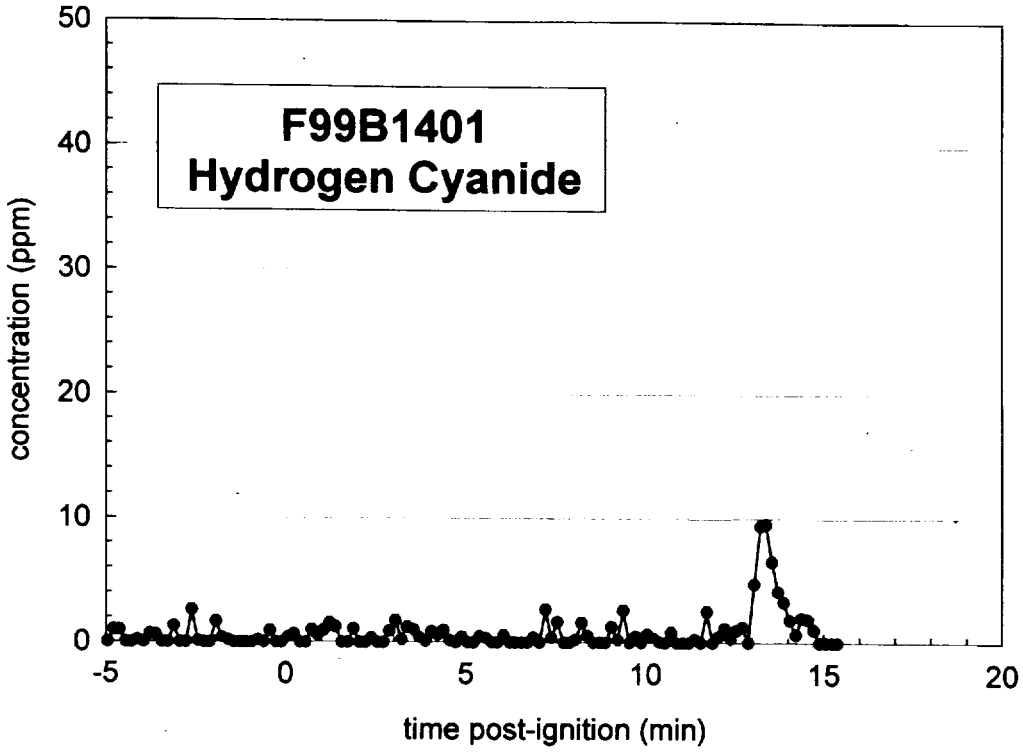


Plot L13. Fire Test F99B1401. Concentration of hydrogen cyanide (HCN) in the passenger compartment determined by FTIR analysis.

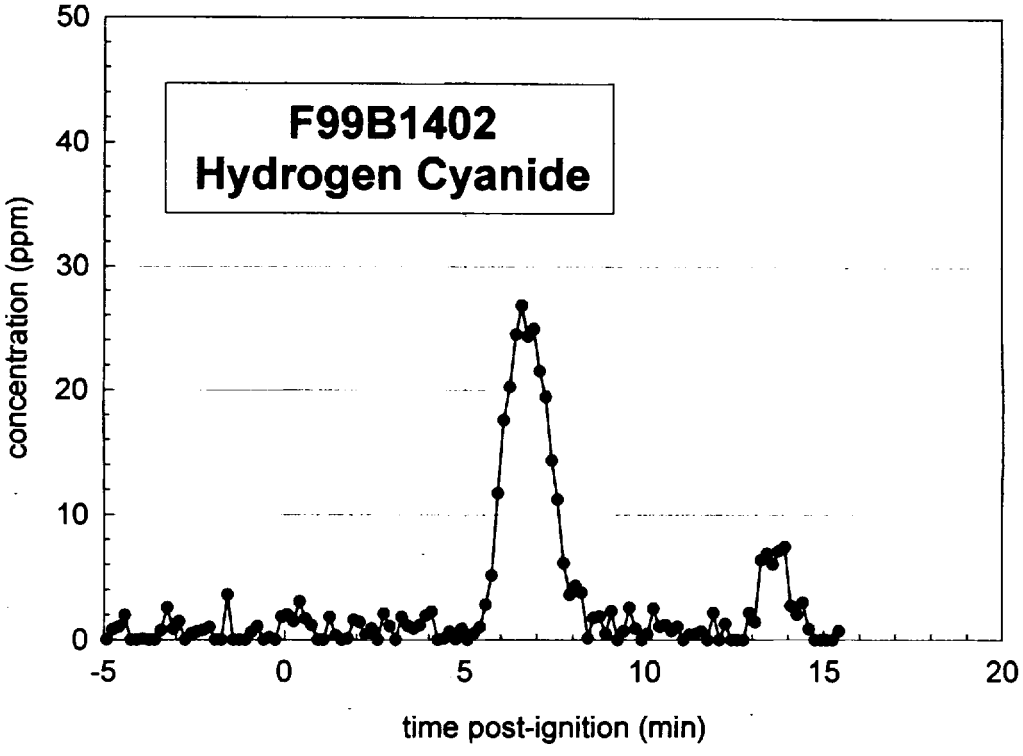


Plot L14. Fire Test F99B1401. Concentration of hydrogen cyanide (HCN) in the passenger compartment determined by FTIR analysis.

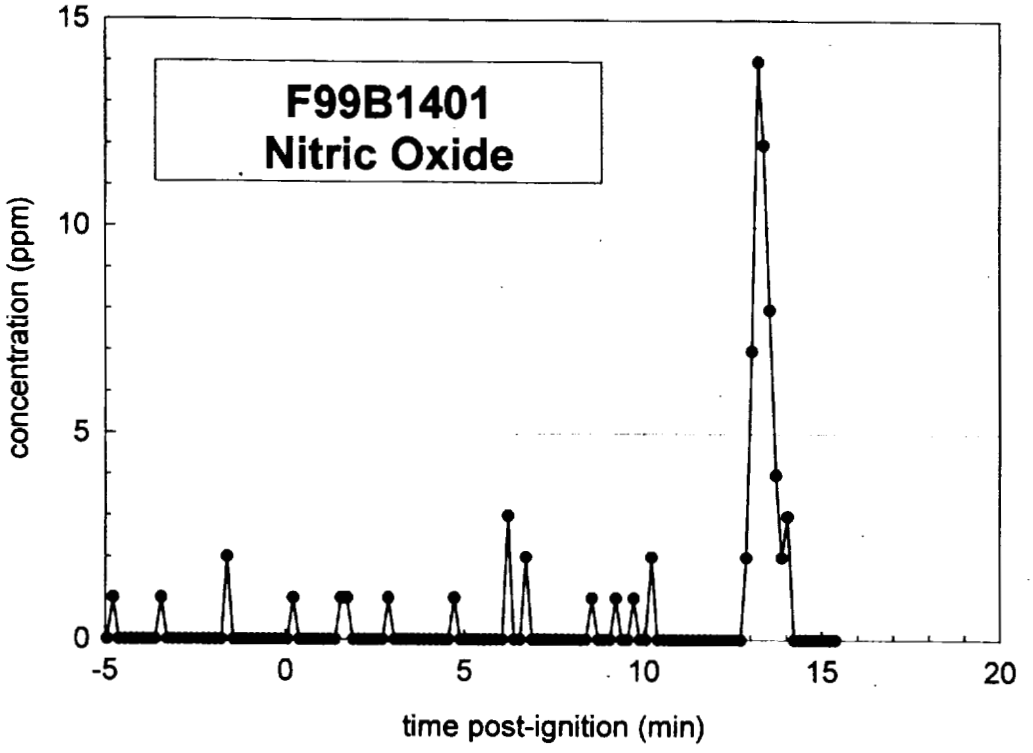


Plot L15. Fire Test F99B1401. Concentration of nitric oxide (NO) in the passenger compartment determined by FTIR analysis.

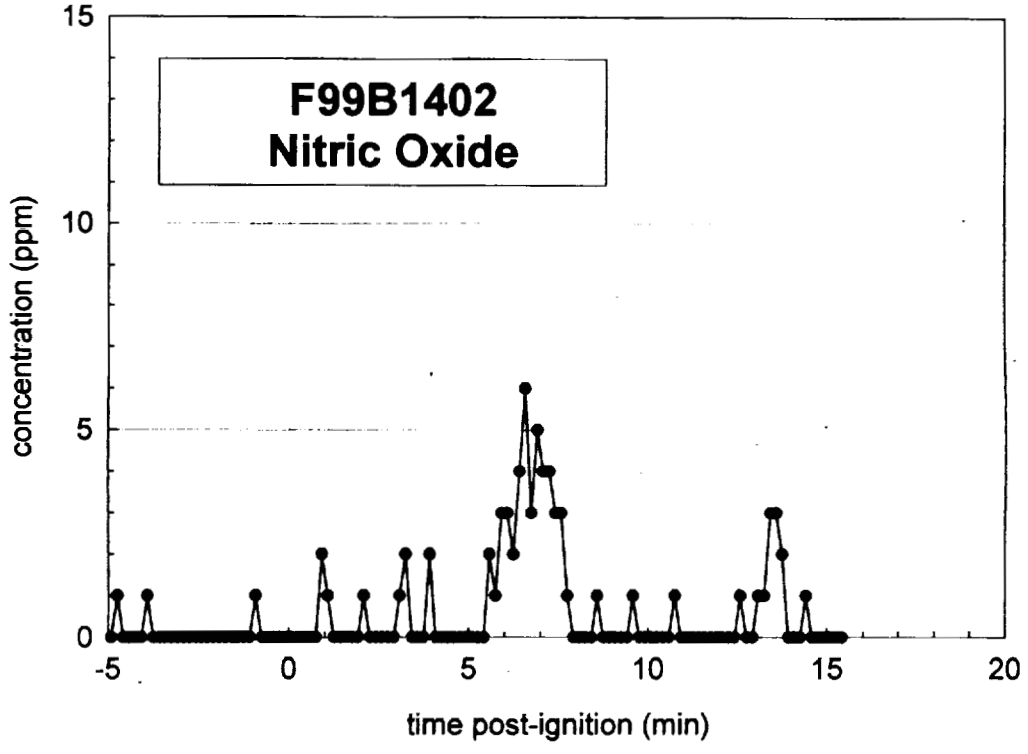


Plot L16. Fire Test F99B1402. Concentration of nitric oxide (NO) in the passenger compartment determined by FTIR analysis.

**Appendix M**

**F99B1401 and F99B1402**
**Fire Products Collector Data**

Scientific and technical personnel from Factory Mutual Research Corporation were primarily responsible for obtaining and analyzing data from the Fire Products Collector (FPC) at the Factory Mutual Test Center.

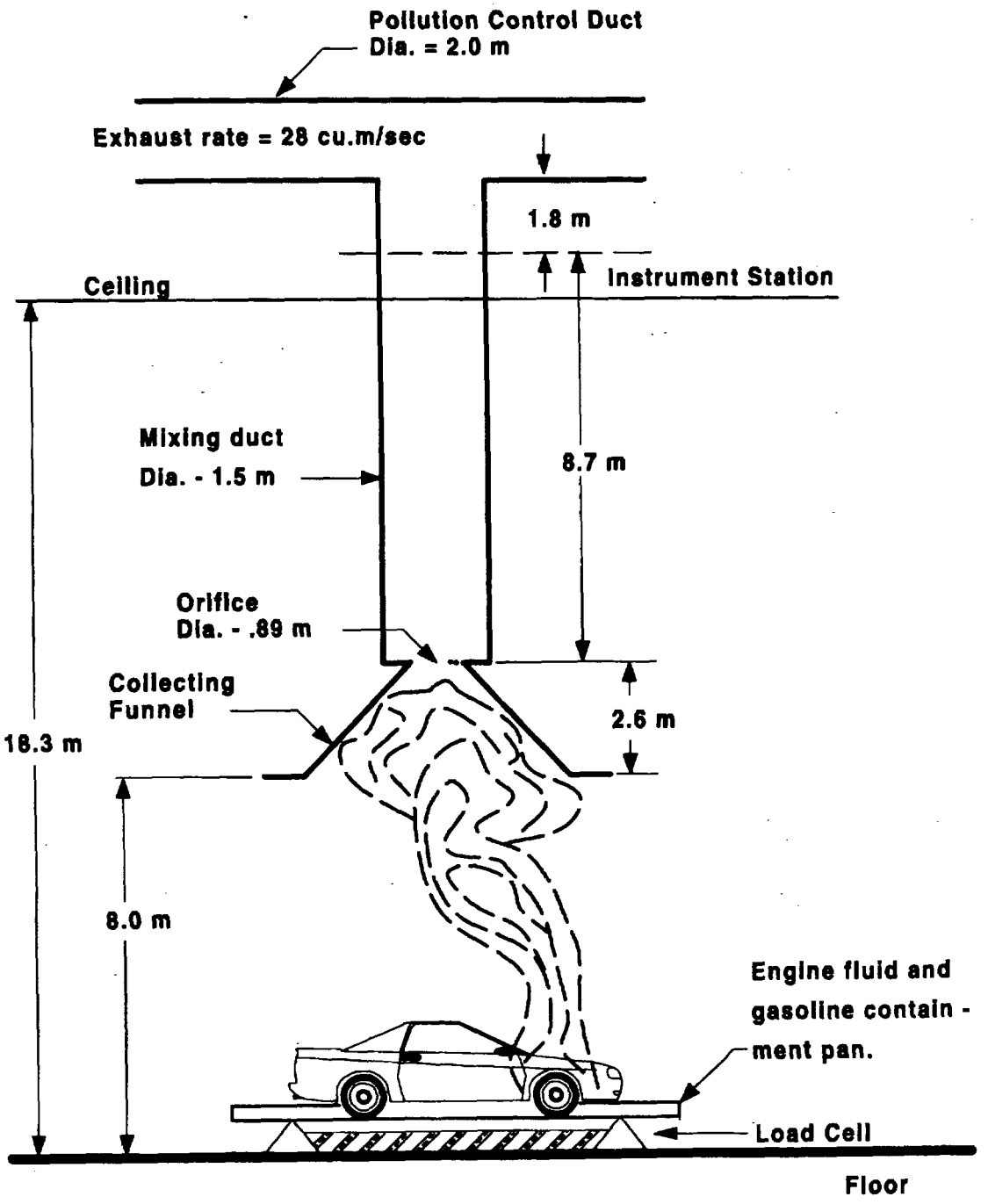


Figure M1. Fire Tests F99B1401 and F99B1402. Diagram of the test vehicle under the fire products collector at the Factory Mutual Test Center.

The Fire Products Collector was used to measure heat and combustion gases generated by the burning vehicles during these tests (Fig. M1). The FPC consisted of a collection funnel (diameter = 6.1 m), an orifice plate (hole = 0.9 m), and a vertical stainless steel sampling duct (diameter = 1.5 m). The sampling duct was connected to the air pollution control system of the Test Center. The blower of the air pollution control system induces gas flow through the sampling duct. Air enters the sampling duct via the orifice plate. The temperature, linear velocity, optical transmission, and chemical composition of the entrained gas were measured in the center of the sampling duct 8.66 m (5.7 duct diameters) downstream from the orifice plate, ensuring a flat velocity profile at the sampling location. The data acquisition system consisted of a Hewlett Packard 2313B analog-to-digital conversion sub-system interfaced to a Hewlett Packard 1000 computer.

Gas temperature in the sampling duct was measured with two Type-K thermocouples (30 gage) with exposed bead-type junctions. The thermocouple leads were housed in stainless steel tubes (o.d. = 6.4 mm). Ambient air temperature in the facility was measured by five Type-K thermocouples attached to the external surface of the duct at 2.44, 5.49, 9.14, 12.8, and 15.9 m above the floor. These thermocouples were shielded from radiation from the fire.

The linear velocity of the gas entrained in the sampling duct was measured with a Pitot ring consisting of four Pitot tubes. A static pressure tap was mounted on the inside wall of the sampling duct. The pressure difference between the Pitot ring and the static wall tap was measured with an electronic manometer (Barocel Model 1173, CGS Scientific Corporation).

The particulate concentration in the entrained air was determined from the optical transmission across the duct measured at 0.4579 μm (blue), 0.6328 μm (red), and 1.06 μm (infrared). The optical path length across the duct was 1.524 m. Gas was withdrawn from the sampling duct through a stainless steel tube (o.d. = 3.9 mm) at a flow rate of $0.17 \times 10^{-3}$ $m^3/s$ for chemical analysis. The gas flowed through a particulate filter, a water condenser, and a drying agent before entering the analyzers. Carbon dioxide ($CO_2$) and carbon monoxide (CO) were measured with two dedicated non-disperse infrared analyzers (Beckman Model 864 Infrared Analyzers). Oxygen ($O_2$) was measured with a paramagnetic oxygen analyzer (Beckman Model 755 Paramagnetic Oxygen Analyzer). Total gaseous hydrocarbons were measured with a flame ionization analyzer (Beckman Model 400 Flame Ionization Analyzer).

The rate of product release was calculated using the following relationship:

$$\left(\frac{dR_j}{dt}\right) = f_j\left(\frac{dV}{dt}\right)\rho_j = f_j\left(\frac{dW}{dt}\right)\left(\frac{\rho_j}{\rho_g}\right) \qquad \text{(M1)}$$

where $d(R_j)/dt$ is the mass release rate of product j in kg/s; $f_j$ is the volume fraction of product j; dV/dt is the total volume flow rate of the gas entrained in the sampling duct in $m^3/s$; dW/dt is the total mass flow rate of the gas entrained in the sampling duct in kg/s; $\rho_j$ is the density of product j in $g/m^3$; and $\rho_g$ is the density of the gas entrained in the concentration measurements. The rate of oxygen consumption was calculated using equation (M1), where the volume fraction of oxygen consumed was substituted for $f_j$.

The volume fraction of smoke particulate was calculated from the following relationship:

$$f_s = \frac{D\lambda \times 10^{-6}}{\Omega} \qquad \text{(M2)}$$

where $f_s$ is the volume fraction of smoke, $\lambda$ is the wavelength of the light source, $\Omega$ is the extinction coefficient of particulate (a value of 0.7 was used in these calculations), and D is the optical density at each of the three wavelengths at which measurements were made:

$$D = \frac{\ln\left(I_0/I\right)}{L} \qquad \text{(M3)}$$

where $I_0$ is the intensity of light transmitted through clean air, I is the intensity of light transmitted through air containing smoke particulate, and L is the optical pathlength, which was equal to 1.524 m. A value of $1.1 \times 10^6$ $g/m^3$ was used for the density of smoke particulate ($\rho_j$) in equation (G1).

The convective heat release rate was calculated using the following relationship:

$$\left(\frac{dE_{conv}}{dt}\right) = \left(\frac{dW}{dt}\right) \times c_p \times \left(T_g - T_a\right) \qquad \text{(M4)}$$

where $d(E_{conv})/dt$ is the convective heat release rate in kW; dW/dt is the mass flow rate of the gas entrained in the sampling duct in kg/s; $c_p$ is the heat capacity of the gas entrained in the sampling

duct at the gas temperature in kJ/(kg×K); $T_g$ is the temperature of the gas entrained in the sampling duct in K; and $T_a$ is the ambient air temperature in K.

The chemical heat release rate was calculated from the release rates of carbon dioxide and carbon monoxide as follows:

$$\left(\frac{dE_{ch}}{dt}\right) = \Delta H^{\bullet}_{CO_2} \times \left(\frac{dR_{CO_2}}{dt}\right) + \Delta H^{\bullet}_{CO} \times \left(\frac{dR_{CO}}{dt}\right) \qquad \text{(M5)}$$

where $d(E_{ch})/dt$ is the chemical heat release rate in kW; $\Delta H^*$ is the net heat of complete combustion per unit mass of carbon dioxide or carbon monoxide released in the fire in kJ/g; and $dR/dt$ is the mass release rate of carbon dioxide or carbon monoxide in kg/s. Values of $\Delta H^*$ for carbon dioxide and carbon monoxide were obtained from the literature [M1 and M2].

The chemical heat release rate also was calculated from the oxygen consumption rate as follows:

$$\left(\frac{dE_{ch}}{dt}\right) = \Delta H^{\bullet}_{O}\left(\frac{dC_O}{dt}\right) \qquad \text{(M6)}$$

where $d(E_{ch})/dt$ is the chemical heat release rate in kW; $\Delta H^*_O$ is the net heat of complete combustion per unit mass of $O_2$ consumed in kJ/g; and $d(C_O)/dt$ is the consumption rate of oxygen in kg/s. The value for $\Delta H^*_O$ was obtained from the literature [M1 and M2].

The radiative heat release rate was the difference between the chemical heat release rate and the convective heat release rate:

$$\left(\frac{dE_{rad}}{dt}\right) = \left(\frac{dE_{ch}}{dt}\right) - \left(\frac{dE_{conv}}{dt}\right) \qquad \text{(M7)}$$

where $d(E_{rad})/dt$ is the radiative heat release rate; and $d(E_{ch})/dt$ is the average chemical heat release rate calculated using equations (M5) and (M6).

The vehicle was placed in a rectangular steel pan (length = 25 ft., width = 15 ft., height = 4 in.) to prevent spilled and leaking automotive fluids from spreading in the test facility. This fluid containment pan was fabricated from two sheets of carbon steel. Angle-braces were welded to

the under-side of the pan to keep it from flexing under the weight of the vehicle. The corners of the support frame rested on load cells. Mass loss was determined from data acquired from the load cells during the test.

The fluid containment pan was lined with a layer of fiberglass-reinforced cement construction board (DuraRock, USG Corporation). A thin layer of sand was used to level the concrete board so that the grade of the surface measured from the center to the edges along the major and minor axes was no greater than 1%. The joints between boards were sealed with latex caulking.

Mass loss from the burning vehicle and any burning fluids retained by the containment pan was measured with a load cell weigh-module system. The fluid containment pan was supported by an I-beam frame a load cell weight-module (KIS Series, BLH Electronics, Inc.) at each corner. These weight-modules contain cylindrical, double cantilever strain gauge transducers that are not generally affected by changes in mass distribution. The weight-module system was calibrated before this test by placing a series of standard weights on the fluid containment pan.

Data from the fire-products collector and load cell weight-module system are shown in Plots O1 through O10.

## REFERENCES


M1. G. Heskestad. A Fire Products Collector for Calorimetry into the MW Range, Technical Report J.I. OC2E1.RA. Factory Mutual Research Corporation, Norwood, MA. June, 1981.

M2. Archibald Tewarson. "Generation of Heat and Chemical Compounds in Fires" Section 3/Chapter 4, SFPE Handbook of Fire Protection Engineering, 2nd Edition, 1995, pp. 3:53-124.

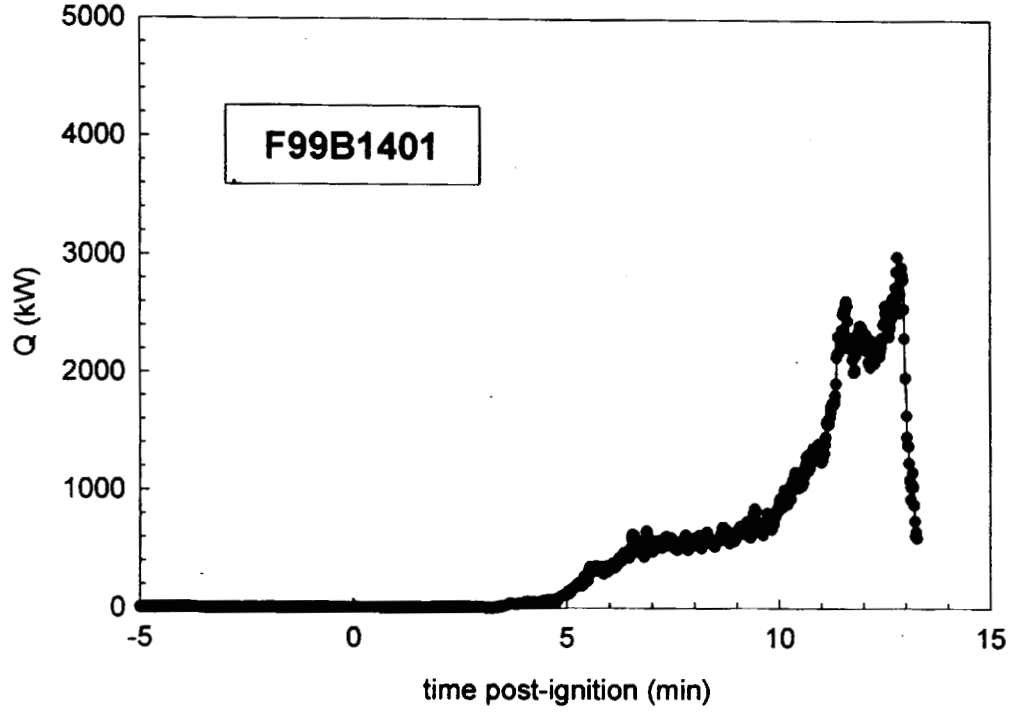


Plot M1. Fire Test F99B1401. Heat release rate measured using the Fire Products Collector.

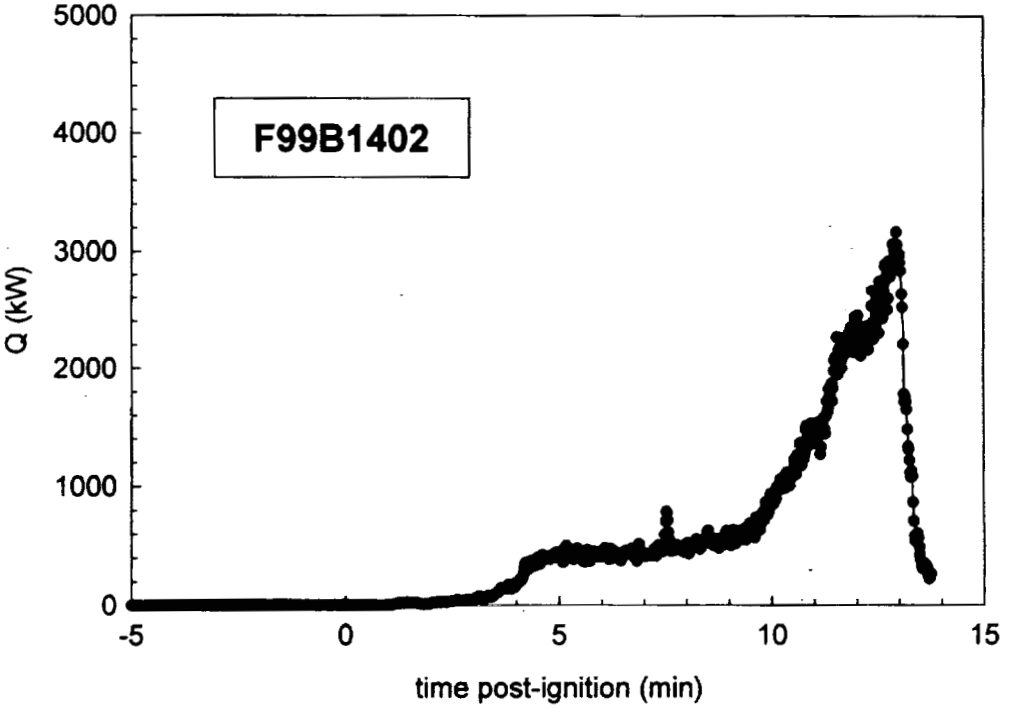


Plot M2. Fire Test F99B1402. Heat release rate measured using the Fire Products Collector.

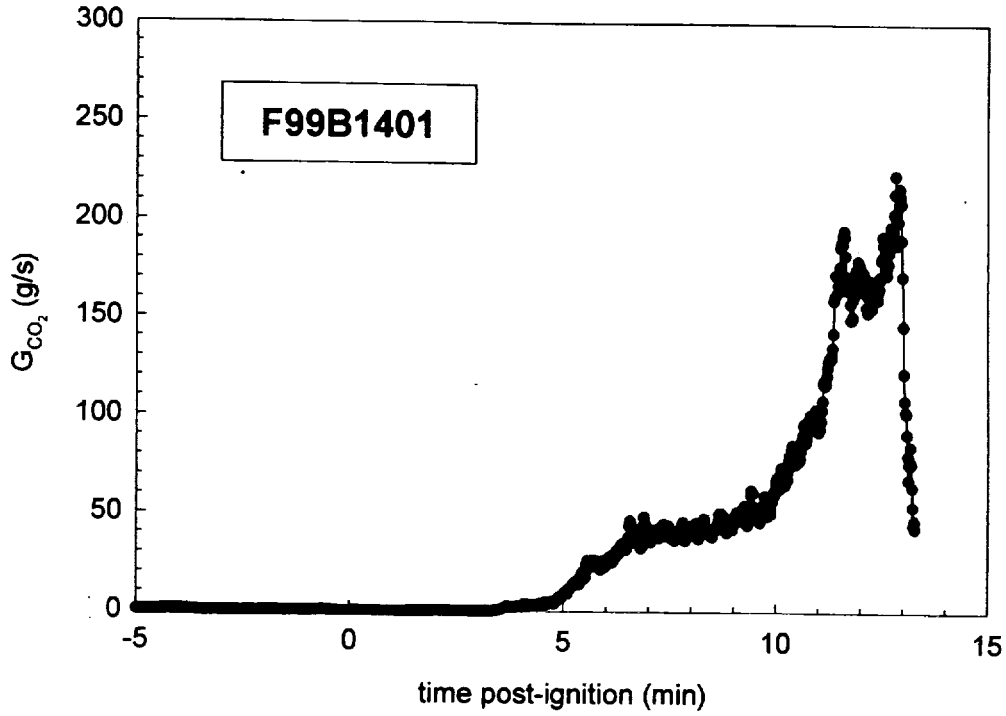


Plot M3. Fire Test F99B1401. Carbon dioxide release rate measured using the Fire Products Collector.

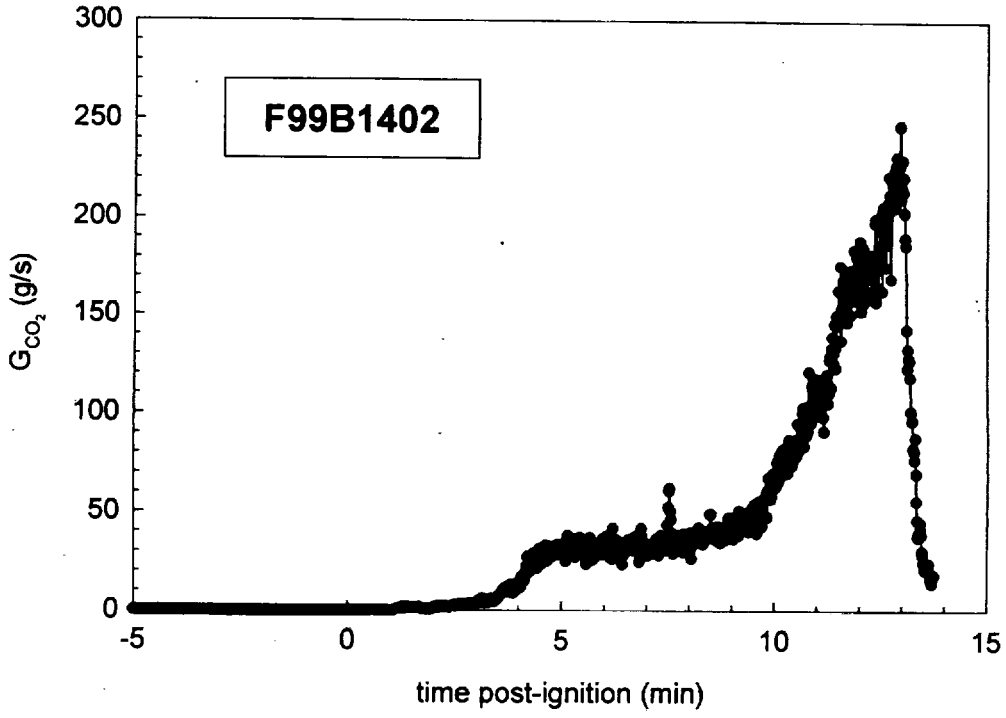


Plot M4. Fire Test F99B1402. Carbon dioxide release rate measured using the Fire Products Collector.

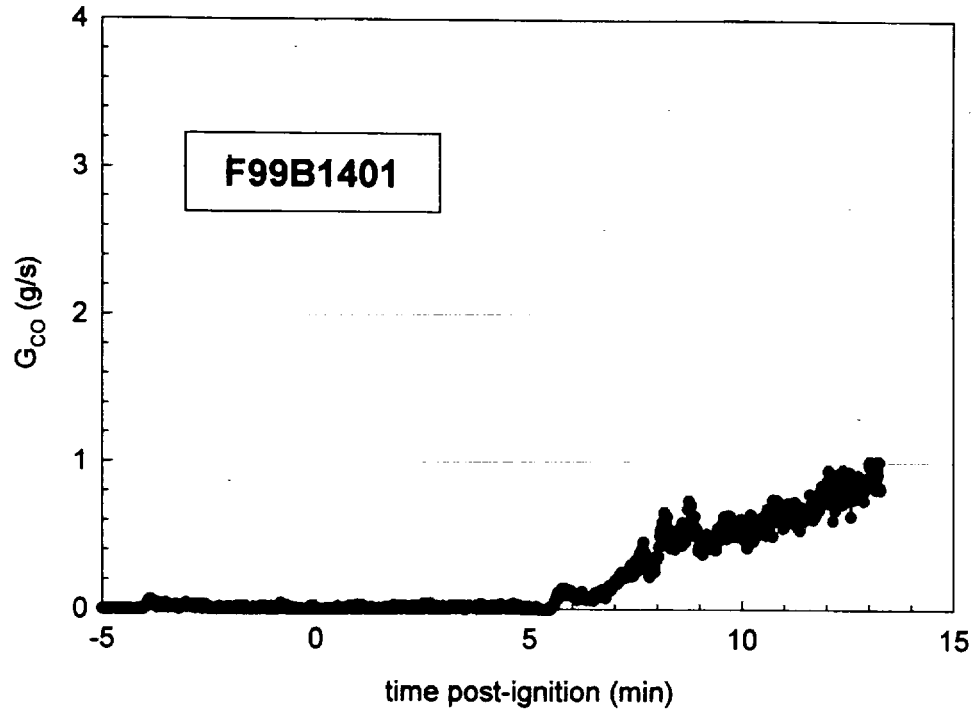


Plot M5. Fire Test F99B1401. Carbon monoxide release rate measured using the Fire Products Collector.

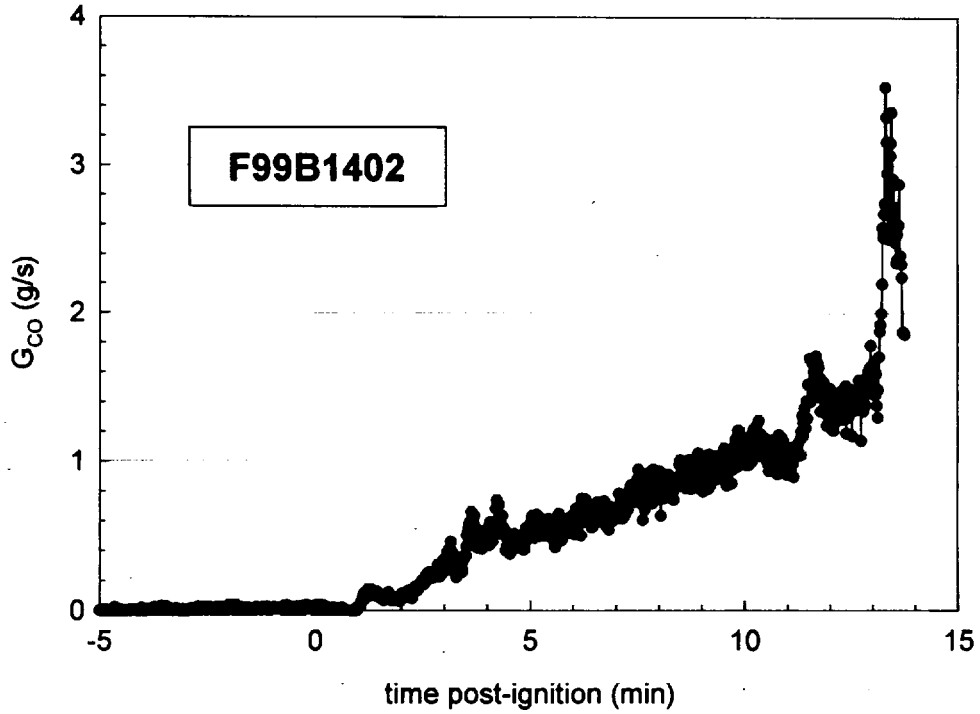


Plot M6. Fire Test F99B1402. Carbon monoxide release rate measured using the Fire Products Collector.

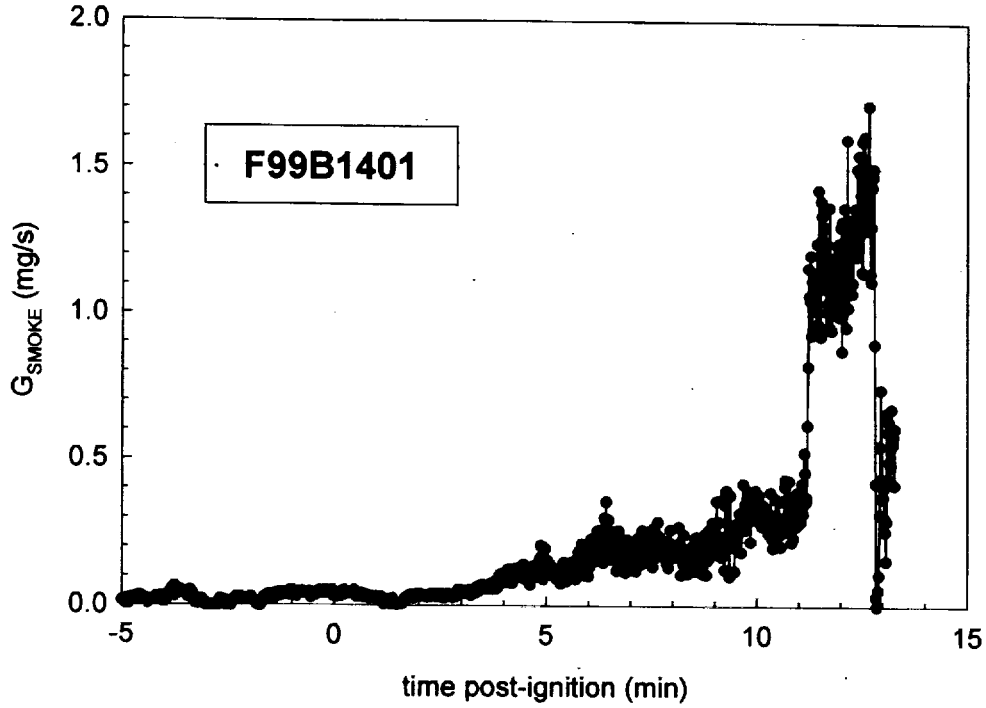


Plot M7. Fire Test F99B1401. Smoke release rate measured using the Fire Products Collector.

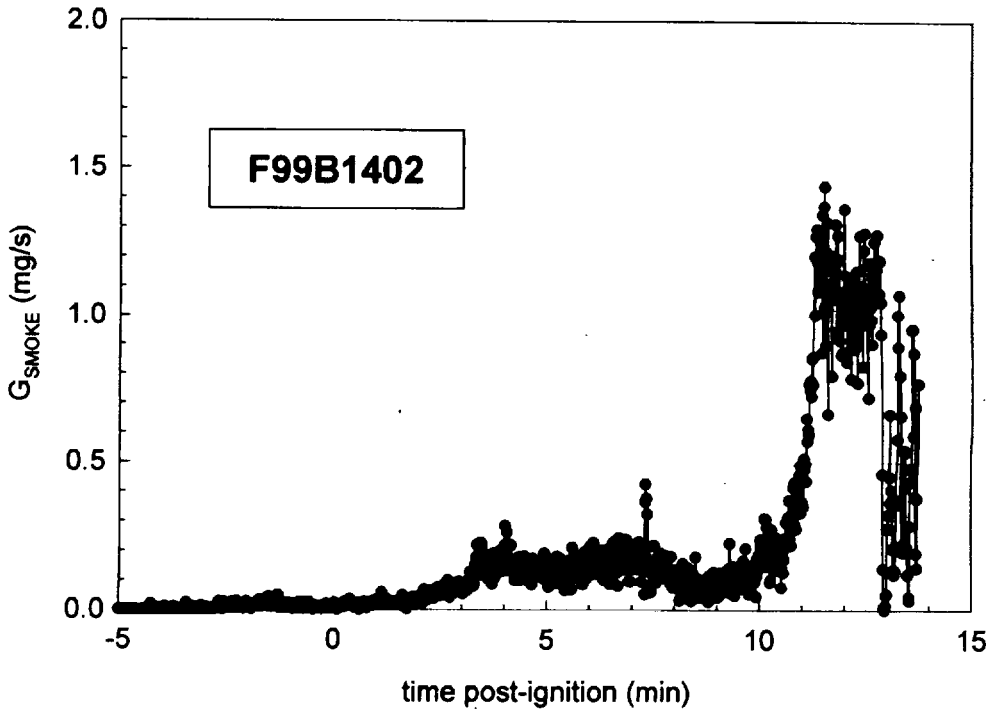


Plot M8. Fire Test F99B1402. Smoke release rate measured using the Fire Products Collector.

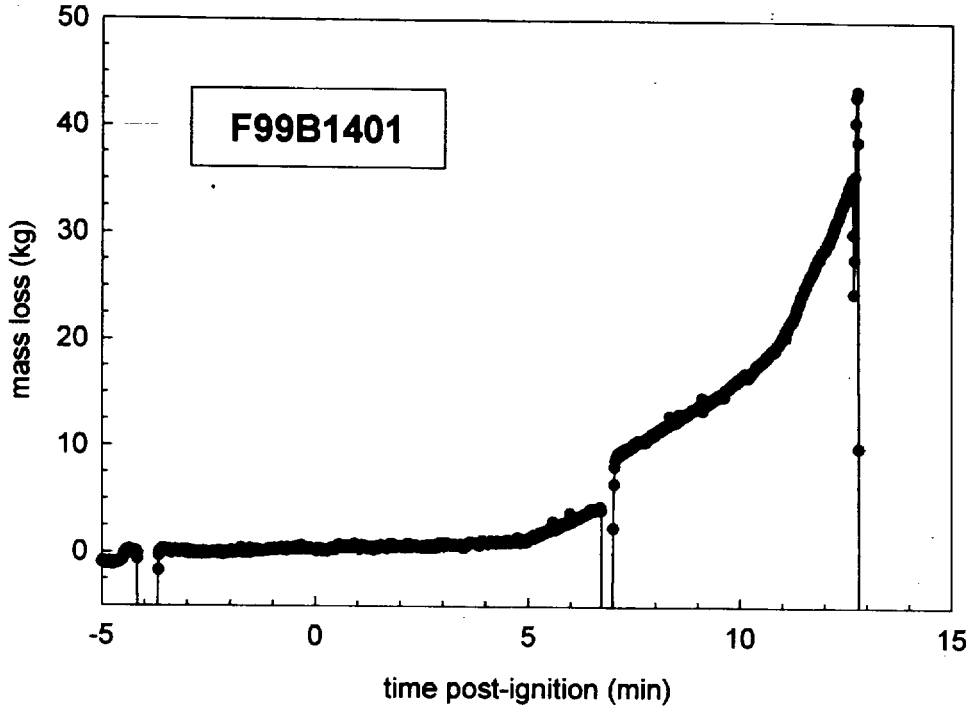


Plot M9. Fire Test F99B1401. Mass Loss from the test vehicle during the fire test.

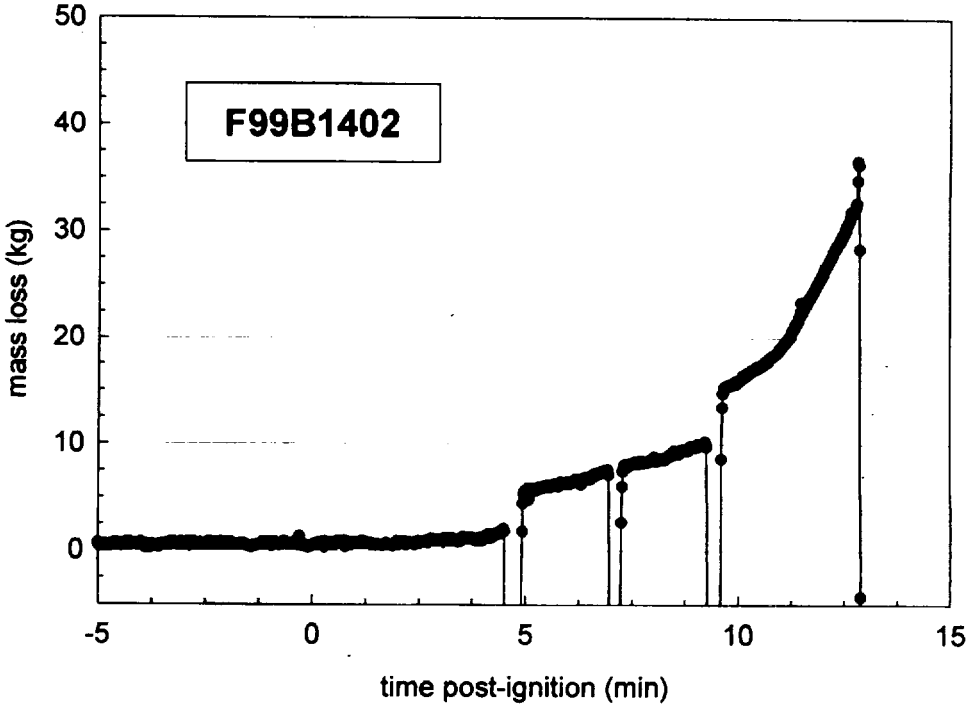


Plot M10. Fire Test F99B1402. Mass Loss from the test vehicle during the fire test.